Inaugural - Dissertation

zur

Erlangung der Doktorwürde

der

Naturwissenschaftlich-Mathematischen

Gesamtfakultät der Ruprecht-Karls-Universität

Heidelberg

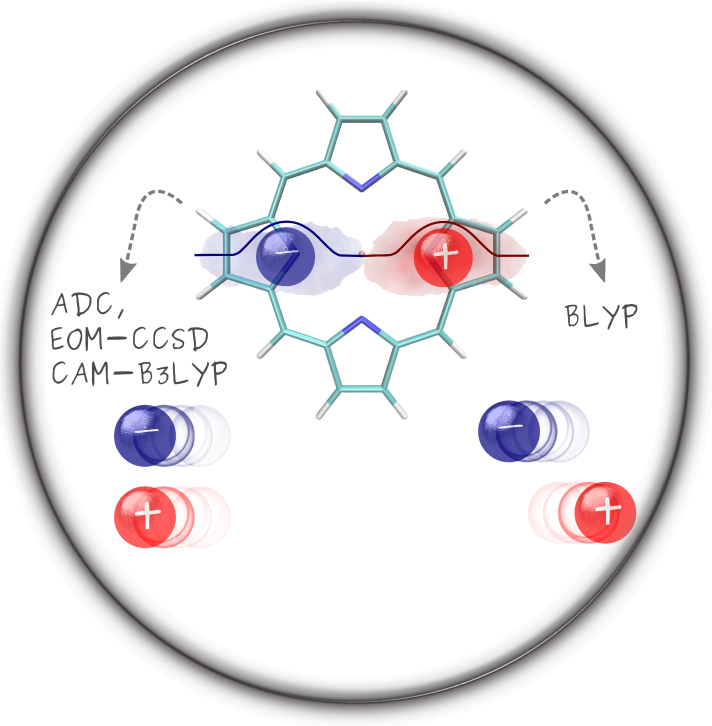

Vorgelegt von
Stefanie Andrea Mewes, Master of Science Chemie
aus Speyer
Kontakt: stefaniemewes@janmewes.de

Datum der Mündlichen Prüfung: 23. Mai 2018

Exciton analysis tools for quantum-chemical investigation of molecular photochemistry

Gutachter:

Prof. Dr. Andreas Dreuw
PD Dr. Alexander Kuleff

March 25, 2018

Für Lotta und Jan

Contents

Preface

Abstract

A chromophore (greek, $\chi\rho\tilde{\omega}\mu\alpha$ "color", $\varphi o\rho\acute{o}\varsigma$, "carrying") is a molecule that appears colorful to the human eye in sunlight. The recognized color is related to the wavelength of light, or in face of particle-wave dualism, to the energy of photons absorbed by the molecule. Light absorption, also called photo-excitation, corresponds to a transition of the molecule from its ground state to an electronically excited state. The energy gained during excitation allows the molecule to undergo manifold chemical and physical processes, giving rise to the presents of a phlethora of chromophores in nature and technology. In order to rationalize these light-induced processes, the involved electronic ground and excited states of a molecule can be investigated by means of quantum-chemical methods. These allow to determine the energy and properties of the molecule in its different electronic states. An important step in the interpretation of the results of such calculations is to determine the character of an excited state, which is directly connected with many properties, such as the interaction with an environment, reaction pathways and deexcitation processes. The aim of this work is to develop new tools for the investigation of excited states, their characters, and quantum-chemical methods for their description.

The central idea is to rationalize excited states in terms of correlated electron-hole quasiparticles, *i.e.* excitons, a concept from solid-state physics. The working hypothesis is to identify the one-particle transition density matrix (1TDM) as an effective electron-hole (*i.e.* exciton) wave function. The character of an excited state can in turn be determined from the calculated exciton properties. These properties are computed by evaluating expectation values of the exciton wave function with respect to operators of interest. In practice, several protocols have been developed, which characterize spatial and statistical properties of the electron-hole quasiparticle. These excited-state descriptors are directly comparable to results from solid-state physics as well as from experiments, emphasizing their physical significance. In contrast to standard approaches, deriving excited-state characters from exciton properties has some immediate advantages. Different types of excited states such as charge-transfer, Rydberg or local, can be directly determined according to a few exciton descriptors. The use of quantitative descriptors is comparably unbiased, since it does not rely on an ambiguous visual interpretation of molecular orbitals (MOs) involved in the electronic transition. Moreover, exciton descriptors allow to investigate excited states that are poorly represented in the MO picture. Since exciton analysis is based on the 1TDM, which is a method-independent quantity, the descriptors allow to investigate quantitative differences between the descriptions of excited states at various levels of theory.

The presented approach is particularly relevant for molecules featuring excited states with exciton character. A particularly important substance class are large π-conjugated organic molecules. Here, delocalized π-electrons play a decisive role and require precise description of correlation effects, posing a challenge for quantum-chemical methods. The scientific interest in large π-conjugated organic molecules is triggered by their special electronic properties, which are applied in organic electronics. In the course of this work, a variety of excited states of extended π-conjugated organic molecules is calculated by means of correlated *ab initio* methods as well as by time-dependent density functional theory (TDDFT) and subjected to exciton analysis. In Chapter 3, exciton sizes are investigated for excited states of poly(*para* phenylene vinylene) (PPV) oligomers and polyacenes. Excited states are found to differ in exciton sizes depending on irreducible representations and multiplicities. In Chapter 4, PPV is thoroughly investigated as a prototypical organic semiconductor to rationalize its exciton properties from a quantum-chemical perspective. The emergence of excitonic states is examined for a series of PPV oligomers with different chain length. It is found that exciton formation takes place for oligomers with four or more building blocks. To gain insight into the spectroscopic properties of the PPV polymer, the largest still computationally feasible representative, the octamer $(PV)_7P$ is studied intensely. A systematic analysis of forty excited states allows to examine their exciton characters in detail. The investigated excitons are found to have well-defined structures that can be rationalized in terms of Frenkel and Wannier exciton models. The results are in good agreement with experimental findings and band-structure calculations of PPV. To investigate the effects of exciton formation for a more chemically diverse set of molecules, a variety of aromats as well as heteroaromats are investigated in Chapter 6. It is found that the first excited state of these π-systems has a uniform exciton character with an exciton size converging towards 7 Å very similar to the trends in PPV. The explicit chemical structures and presence of heteroatoms have surprisingly little influence on this character.

Shifting the focus to methodological aspects, Chapter 6 reveals the influence of exchange-correlation (*xc*) functionals on the description of exciton properties in TDDFT. By comparing exciton sizes and electron-hole correlation coefficients, it is found that there are major differences in the excited-state description for the tested *xc*-functionals. The trends amongst different *xc*-functionals suggest that these deviations are mostly governed by the amount of nonlocal orbital exchange (NLX) in the *xc*-functionals. This finding is of great significance showing that a single parameter can induce a complete change in the electron-hole interaction from repelling (anti-correlated) to strongly attractive

(correlated). A more general investigation of the same effect is presented for Tozer's benchmark set in Chapter 5. This set is composed of a broad selection of molecules featuring different types of excited states and designed to develop diagnostic tools for TDDFT. It is well-known that excited states which involve nonlocal electron transitions, such as charge-transfer, Rydberg or $\pi \rightarrow \pi^*$ states of extended π-systems, show systematic errors in excitation energy for different types of *xc*-functionals. Here, exciton descriptors reveal that these errors are related to substantial differences in the description of the respective excited states by the *xc*-functionals. Since exciton descriptors are able to identify all problematic cases, they are suggested as diagnostic tools for TDDFT.

Ultimately, Chapter 7 focuses on the evaluation of excited-state methods. For this purpose, the selection of methods is extended to include also equation-of-motion coupled-cluster singles doubles (EOM-CCSD) and a diverse set of applications is investigated. Exciton properties calculated with correlated *ab initio* methods (ADC(2), ADC(3) and EOM-CCSD), as well as TDDFT are compared, revealing strengths and weaknesses of the methods in different applications. The most important outcome of investiging exciton properties is that accuracy in terms of excitation energies is not necessary a measure for the quality of description of the underlying wave function and properties of a system. In fact, the best agreement in terms of exciton properties with respect to high level *ab initio* data is obtained with an *xc*-functional that is the least accurate in terms of excitation energies for several examples.

The presented approach is publically available as open-source code package *libwfa* and integrated in the Q-Chem program package.

Zusammenfassung

Ein Chromophor (griechisch, $\chi\rho\tilde{\omega}\mu\alpha$ "Farbe", $\varphi o\rho\acute{o}\varsigma$, "tragend") ist ein Molekül, das dem menschlichen Auge im Sonnenlicht farbig erscheint. Die wahrgenommene Farbe steht in Bezug zur Wellenlänge des Lichts, oder in Anbetracht des Welle-Teilchen Dualismus, zur Energie des vom Molekül absorbierten Photons. Durch die Absorption eines Photons wird ein Molekül "angeregt", das heißt, es geht von seinem Grundzustand in einen elektronisch angeregten Zustand über. Die dabei aufgenommene Energie steht dem Molekül für vielfältige chemische und physikalische Prozesse zur Verfügung, die in Natur und Technik oft wichtige Rollen spielen. Um diese Prozesse zu verstehen, können die beteiligten elektronischen Zustände eines Moleküls mit quantenchemischen Methoden untersucht werden. Diese ermöglichen Energie und Eigenschaften der elektronischen Zustände anhand von Wellenfunktionen und Dichten zu berechnen. Zur Interpretation der Ergebnisse dieser Rechnungen ist die Bestimmung des Charakters eines angeregten Zustandes zentral, da dieser Rückschlüsse auf Eigenschaften wie beispielsweise Umgebungswechselwirkung, mögliche Reaktionspfade und Abregungsprozesse zulässt. Das Ziel dieser Arbeit ist die Entwicklung von neuen Analysemethoden zur Charaktisierung von elektronisch angeregten Zuständen und zur systematischen Untersuchung der zugrundeliegenden quantenchemischen Methoden.

Der Ansatzpunkt der entwickelten Methodik ist die Interpretation von elektronisch angeregten Zuständen als korrelierte Elektron-Loch Quasiteilchen, auch Exzitonen genannt, einem Konzept aus der Festkörperphysik. Die Grundannahme ist dabei, dass Einteilchenübergangsdichtematrizen als Exzitonwellenfunktionen interpretierten werden können. Der Charakter eines angeregten Zustands kann somit aus den Eigenschaften des Exzitons bestimmt werden, welche als Erwartungswerte der Exzitonwellenfunktion berechnen werden können. Konkret werden Protokolle zur Berechnung von räumlichen und statistischen Eigenschaften der Elektron-Loch Quasiteilchen entwickelt. Diese Größen können direkt mit Ergebnissen aus der Festkörperphysik und experimentellen Messungen verglichen werden, was ihre physikalische Bedeutung zeigt. Außerdem ergeben sich einige Vorteile bei der Bestimmung des Charakters angeregter Zustände anhand exzitonischer Eigenschaften. Verschiedene Arten angeregter Zustände wie zum Beispiel charge-transfer, Rydberg, lokal, etc. können durch wenige Deskriptoren eindeutig bestimmt werden. Die Untersuchung quantitativer Deskriptoren ist dabei vergleichsweise objektiv, da sie keine subjektiven Interpretation der am Übergang beteiligten Molekülorbitale (MOs) erfordert. Zudem können auch solche angeregten Zuständen untersucht werden, die im Molekülorbitalbild schlecht repräsentiert werden. Aufgrund der methoden-unabhängigen Definiti-

on der Deskriptoren ist es möglich den Einfluss quantenchemischer Methoden auf die Beschreibung angeregter Zustände quantitativ zu untersuchen.

Die entwickelte Analyse ist besonders relevant für Moleküle, deren angeregte Zustände exzitonischen Charakter haben. Eine Molekülklasse mit diesen Eigenschaften sind große konjugierte π-Systeme. Delokalisierte π-Elektronen spielen hierbei eine entscheidende Rolle und stellen gleichzeitig eine Herausforderung für quantenchemische Methoden dar. Die daraus resultierenden, besonderen elektronischen Eigenschaften großer π-Systeme sind von wissenschaftlichem Interesse und finden im Bereich der organischen Elektronik Anwendung. Diese Arbeit beschäftigt sich mit der quantenchemischen Untersuchung von angeregten Zuständen großer π-konjugierter Moleküle. Diese werden mit korrelierten *ab initio* Methoden und zeitabhängiger Dichtefunktionaltheorie (TDDFT) berechnet und auf exzitonische Eigenschaften untersucht. In Kapitel 3 werden Exzitonengrößen von Poly(*para* phenylen vinylen) (PPV) Oligomeren und Polyacenen untersucht. Hierbei geben die Exzitonengrößen Hinweis auf unterschiedliche exzitonische Eigenschaften der Zustände aus verschiedenen irreduzible Darstellungen oder Multiplizitäten. Kapitel 4 befasst sich mit der Untersuchung des prototypischen PPV, welches eine Schlüsselrolle zum Verständnis von organischen Halbleitermaterialien spielt. Die Entstehung von Exzitonen wird für PPV Oligomere in Abhängigkeit der Molekülgröße untersucht und wird ab vier Untereinheiten deutlich, was einer Kettenlänge von ca. 30 Å entspricht. Um die spektroskopischen Eigenschaften des Polymers aus quantenchemischer Perspektive nachzuvollziehen, wird das Oktamer als größtes Modellsystem intensiv untersucht. Eine systematische Analyse von vierzig angeregten Zuständen ermöglicht die Charaktersierung verschiedener Exzitonen, die mit Frenkel und Wannier Exzitonmodellen interpretiert werden können. Dabei bestätigen die Ergebnisse experimentelle Befunde und die berechnete Bandstruktur von PPV. Eine Betrachtung einer allgemeineren Auswahl an π-konjugierten Systemen wird in Kapitel 6 vorgestellt. Hier werden neben einer Reihe von reinen Aromaten auch Heteroaromaten untersucht. Dabei zeigt sich, dass der erste angeregte Zustand dieser Moleküle einen einheitlichen exzitonischen Charakter mit einer Exzitonengröße von ca. 7 Å besitzt und damit überraschend unabhängig von Details in der chemischen Struktur wie beispielsweise der Verknüpfung von Untereinheiten oder der Einführung von Heteroatomen ist.

Ein methodischer Aspekt von Kapitel 6 befasst sich mit der Beschreibung von Exzitonen durch verschiedene Austausch-Korrelations-Funktionale mittels TDDFT. Der Vergleich von Exzitonengrößen und Elektron-Loch Korrelation zeigt, dass Austausch-Korrelations- (xc) Funktionale einen erheblichen Einfluss auf den Charakter angeregter Zustände haben. Dabei legen die Trends in den Deskriptoren nahe, dass die Ursache in den unterschiedlichen Anteilen

an exaktem Orbitalaustausch in den *xc*-Funktionalen liegt. Der beobachtete Effekt ist drastisch, da eine schlichte Veränderung eines Parameters die physikalischen Eigenschaften des Elektron-Loch Paares vollständig ändern kann in einem Spektrum von sich gegenseitig abstoßend (antikorreliert) bis sich stark anziehend (korreliert). Eine allgemeinere Untersuchung des gleichen Effekts wird in Kapitel 5 für Tozers Datensatz vorgestellt. Dieser enthält eine Auswahl an Molekülen mit unterschiedlichen Arten von angeregten Zuständen wie lokale, charge-transfer, Rydberg und $\pi \rightarrow \pi^*$ Zuständen ausgedehnter π-Systeme und wurde zur Entwicklung diagnostischer Werkzeuge für TDDFT entworfen. Nichtlokale angeregte Zustände weisen bekanntermaßen systematische Abweichungen von experimentellen Anregungsenergien für unterschiedliche *xc*-Funktionale auf. Die Untersuchung der angeregten Zustände mit Exzitondeskriptoren zeigt systematische Unterschiede in deren Beschreibung durch unterschiedliche *xc*-Funktionale, welche die Abweichungen in Anregungsenergien erklären. Da Exzitondeskriptoren in der Lage sind alle problematischen Fälle zu identifizieren und zu charakterisieren, eignen sie sich somit als diagnostische Werkzeuge für TDDFT.

In Kapitel 7 wird die Methodenevaluierung anhand exzitonischer Eigenschaften auf neue Methoden und eine breite Auswahl angeregter Zustände ausgeweitet und zusammenfassend betrachtet. Dabei werden insbesondere die Algebraisch-Diagrammatische Konstruktionsmethode für den Polarisationspropagator (ADC), die Bewegungsgleichungsvariante der Coupled-Cluster Theorie (EOM-CCSD) und TDDFT verglichen, wobei deren jeweilige Stärken und Schwächen in verschiedenen Anwendungen deutlich werden. Während quantenchemische Methoden in der Regel an der Genauigkeit in der Reproduktion von Referenz-Anregungsenergien beurteilt werden, zeigt die Untersuchung von Exzitoneigenschaften, dass dieses Kriterium nicht notwendigerweise die Qualität der zugrundeliegenden Wellenfunktionen und Eigenschaften des Systems abbildet. Tatsächlich werden die besten Übereinstimmungen in exzitonischen Eigenschaften mit *ab initio* Referenzen für ein *xc*-Funktional gefunden, dessen Anregungsenergien in den entspechenden Fällen die geringste Genauigkeit aufweist.

Die entwickelte Analysemethodik ist als open-source Programmpaket *libwfa* veröffentlicht und in Q-Chem integriert.

Abbreviations

1TDM	one-particle transition density matrix
2TDM	two-particle transition density matrix
ADC	algebraic-diagrammatic construction
BSE	Bethe-Salpeter equation
CI	configuration interaction
CIS	configuration interaction singles
CT	charge transfer
DFT	density functional theory
DMABN	4-(*N*,*N*-dimethylamino)benzonitrile
EOM-CCSD	equation-of-motion coupled-cluster singles doubles
ES	excited state
GGA	generalized gradient approximation
GS	ground state
HF	Hartree Fock
KS	Kohn-Sham
LDA	local density approximation
LRC	long-range corrected
MgP	magnesium porphyrin
NLX	nonlocal orbital exchange
NTO	natural transition orbital
MO	molecular orbital
MP	Møller Plesser
PPV	poly(*para* phenylene vinylene)
PT	perturbation theory
rms	root mean square
SE	Schrödinger equation
SI	supplementary information
TDA	Tamm-Dancoff approximation
TDDFT	time-dependent density functional theory
xc	exchange-correlation

Chapter 1

Theory and computational methods

The aim of this chapter is to introduce quantum-chemical methods and concepts that describe molecules in their electronic ground and excited states, which constitutes the basis of this work. The review starts with the description of quantum-chemical systems by means of the Schrödinger equation (SE), followed by a discussion of the Born-Oppenheimer approximation and its implications for molecules. Illustrating ways to find approximate solutions of the electronic SE for the electronic ground state, the concepts of mean-field theory, Hartree-Fock and density functional theory are reviewed. Afterwards configuration interaction (CI) is discussed as approach to account for electron correlation explicitly. As basic method for the calculation of electronically excited-states, configuration interaction singles is presented, which is the simplest truncated CI method. Subsequently, time-dependent density functional theory and the Tamm-Dancoff approximation are introduced. As representative of correlated wave-function-based excited-state methods, the algebraic-diagrammatic construction (ADC) for the polarization propagator method is presented. Ultimately, stategies for the analysis of excited states and electronic transitions are discussed.

Let me start with an overview of central ideas and important methods for describing the electronic structure of a molecular system, in particular its electronic ground and excited states. The equations presented here are fundamental in electronic structure theory and have been reformulated in countless publications. Where no explicit reference is given, the reader is referred to Ref. 1. As general remark for the reader of this work, the term "excited state" always refers to an electronically excited state, if not stated otherwise.

1.1 Molecular Schrödinger equation

A central task in quantum chemistry is to solve the time-independent molecular Schrödinger equation (SE). This equation contains information about stationary states of a system, and allows to characterize them in terms of wave functions and energies. The Schrödinger equation is an eigenvalue equation

$$\hat{H}_{mol}\Psi_{mol} = E_{mol}\Psi_{mol}\,, \tag{1.1}$$

where $\hat{H}_{mol}$ is the Hamiltonian, that is, the total energy operator, Ψ_{mol} the wave function and E_{mol} the energy of the molecular system. Considering different energy terms and the fact that molecules are composed of nuclei (cores, *nuc*) and electrons (*ele*), the molecular Hamiltonian takes the form

$$\hat{H}_{mol} = \hat{T}_{nuc} + \hat{T}_{ele} + \hat{V}_{nuc} + \hat{V}_{ele} - \hat{V}_{nuc-ele}\,, \tag{1.2}$$

where $\hat{T}_{nuc}$ and $\hat{T}_{ele}$ are the kinetic energy operators, $\hat{V}_{nuc}$ and $\hat{V}_{ele}$ are the potential energy operators of nucleus-nucleus and electron-electron interaction, respectively, and $\hat{V}_{nuc-ele}$ describes the electron-nucleus attraction. For a system with N nuclei and n electrons, the operators in eq. (1.2) can be expressed explicitly as

$$\hat{H}_{mol} = -\sum_{A=1}^{N}\frac{1}{2m_A}\nabla_A^2 - \sum_{i=1}^{n}\frac{1}{2}\nabla_i^2 \tag{1.3}$$

$$+\sum_{A=1}^{N}\sum_{B>A}^{N}\frac{Z_A Z_B}{R_A - R_B} + \sum_{i=1}^{n}\sum_{j>i}^{n}\frac{1}{r_i - r_j} \tag{1.4}$$

$$-\sum_{A=1}^{N}\sum_{i=1}^{n}\frac{Z_A}{R_A - r_i} \tag{1.5}$$

where m_A is the mass, Z_A is the charge and R_A is the spatial coordinate of the Ath nucleus, and r_i is the spatial coordinate of the ith electron. Eq. (1.5) is given in atomic units, *i.e.*, $\hbar$, e, m_e and $4\pi\epsilon_0$ are set to one. Since the SE is a

$(N+n)$-body problem, an analytical solution of the SE can only be obtained for hydrogenic systems containing two particles. For any other chemically relevant system, approximations are necessary, and only approximate solutions of the SE can be obtained. In the following, the most important concepts and approximations for solving the molecular SE are reviewed.

1.2 Born-Oppenheimer approximation

The Born-Oppenheimer approximation[2] is based upon the fact that electrons and nuclei possess different masses. Electrons are approximately 1840 times lighter than protons, and thus react much faster to changes in the molecular potential. Hence, the wave function can be approximated as a product of a nuclear and an electronic wave function according to

$$\Psi(r_i; R) = \sum_i \Theta(R)\Psi_i(r_i; R)\,. \tag{1.6}$$

The main concern of this work is to find solutions for the electronic part of the SE. Revisiting the structure of the molecular Hamiltonian in eq. (1.5) and neglecting nuclear motion, the expression can be simplified to obtain an electronic Hamiltonian, in which the nuclear kinetic energy is zero and nuclear coordinates become a set of parameters R

$$\hat{H}_{ele}(r; R) = \hat{T}_{ele}(r) + \hat{V}_{nuc,const.}(R) + \hat{V}_{ele}(r) - \hat{V}_{nuc-ele}(r; R)\,. \tag{1.7}$$

An immediate consequence of the Born-Oppenheimer approximation is the existence of potential energy surfaces, which map the energy of electronic states against the nuclear geometry. Any given change in geometry can be associated with a change of the energy of the system and it is possible to plot *e.g.* two-dimensional representation of the potential energy hypersurface by scanning changes in energy along a chosen coordinate, cf. Fig. 1.1.

The electronic SE has many solutions, which can be categorized according to their energy. The energetically lowest solution is identified as the ground state of a system, while low lying electronically excited states are important for photochemistry and -physics. A transition from the ground state to an excited state typically involves the absorption of a photon, that is, a photo-excitation. This process can be rationalized by the Franck-Condon principle.[3,4] In this picture, the excitation takes place from the ground-state minimum to the excited-state surface at this geometry, and hence, this type of excitation is called vertical, cf. Fig. 1.1. After the initial excitation, the excited molecule can undergo several processes depending on the shape of the energy surface and

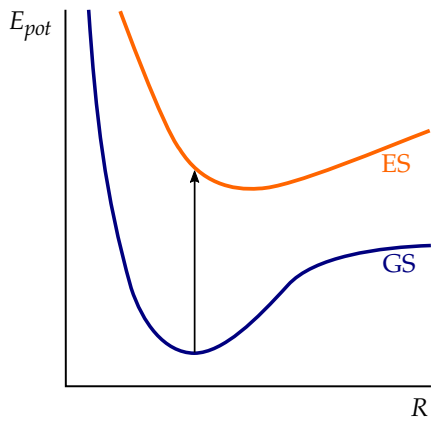

Figure 1.1: 2-D plot of potential energy surface (E_{pot}) of ground (GS) and excited state (ES) against the nuclear coordinate R. The arrow indicates the vertical transition from the ground-state minimum to the excited-state energy surface according to the Franck-Condon principle.

character of the excited state. These processes include energy dissipation via different channels involving electronic and nuclear degrees of freedom, such as internal conversion, inter-system crossing, thermal cooling, fluorescence, phosphorescence, and excited-state absorption. However, these processes will only be considered in very few cases and the main concern of this work is to study the structure of the excited state at the Franck-Condon point, that is, the ground-state optimized geometry.

1.3 Mean-field theory

Mean-field theory transforms an unsoluble many-body problem into a set of coupled one-particle problems. As an ansatz for fermionic systems, a n-electron wave function Φ_{ele} can be expressed anti-symmetrized product of one-electron wave functions $[\{\psi_i(r)\}]$, which is a Slater determinant

$$\Phi_{ele}(r_1, r_2, ..., r_n) = \frac{1}{\sqrt{n!}} \begin{vmatrix} \psi_1(r_1) & \psi_1(r_2) & \cdots & \psi_1(r_n) \\ \psi_2(r_1) & \psi_2(r_2) & \cdots & \psi_2(r_n) \\ \vdots & \vdots & \ddots & \vdots \\ \psi_n(r_1) & \psi_n(r_2) & \cdots & \psi_n(r_n) \end{vmatrix} . \tag{1.8}$$

This ansatz can be plugged into the electronic SE in order to find an approximate solution for the electronic ground state. For this purpose, the one-particle wave functions are optimized according to Ritz's variational principle.[5] This principle states that a trial wave function Ψ' always corresponds to an energy

which is greater or equal to the exact result:

$$\frac{\langle\Psi'|\hat{H}|\Psi'\rangle}{\langle\Psi'|\Psi'\rangle} \geq E_{exact}\,. \tag{1.9}$$

Plugging the wave function ansatz of eq. (1.8) into the electronic SE and imposing the one-electron wave functions to form an orthonormal basis, the following Lagrangian is obtained

$$\mathcal{L}[\{\psi_i\}] = \langle\Phi|\hat{H}_{ele}|\Phi\rangle + \sum_k \lambda(\langle\Phi|\Phi\rangle - 1)\,. \tag{1.10}$$

One important consequence of the mean-field approach is that each electron experiences a mean field of all other electrons and thus, electron-electron interaction is approximated. Two prominent methods are built upon mean-field theory and constitute the basis of modern quantum chemistry, namely Hartree Fock and density functional theory, which will be discussed in the following.

1.4 Hartree Fock method

Hartree Fock[6] is a method to find a solution of the electronic SE for the electronic ground state and is built upon mean-field theory. Evaluating the electronic SE for a single Slater determinant according to the Slater-Condon rules[7,8] allows to formulate an expression for the Hartree-Fock energy

$$E_0^{\mathrm{HF}} = \langle\Phi|\hat{H}|\Phi\rangle = \sum_i^{occ}\langle\psi_i|\hat{h}|\psi_i\rangle + \frac{1}{2}\sum_{ij}^{occ}\left(\langle ij|ij\rangle - \langle ij|ji\rangle\right) \tag{1.11}$$

$$= \sum_i^{occ} h_i + \frac{1}{2}\sum_{ij}^{occ}\left(J_{ij} - K_{ij}\right)\,. \tag{1.12}$$

with

$$\langle\psi_i|\hat{h}|\psi_i\rangle = \int \psi_i^*(r)\left[-\frac{1}{2}\nabla^2 - \sum_A \frac{Z_A}{|r-R_A|}\right]\psi_i(r)dr$$

$$\langle ij|ij\rangle = \iint \frac{\psi_i^*(r)\psi_j^*(r')\psi_j(r')\psi_i(r)}{|r-r'|}drdr'\,.$$

The HF energy has three components. The first h_i only depends on one particle and contains the kinetic energy and Coulomb interaction with the nuclei. The second and third terms, J_{ij} and K_{ij}, depend on two particles and describe the electron-electron Coulomb and exchange interaction, respectively. To avoid double counting, these terms are multiplied by $\frac{1}{2}$ in the HF energy equation (eq. (1.12)). Plugging eq. (1.12) into eq. (1.10), a Lagrangian for HF can be

obtained as

$$\mathcal{L}^{\mathrm{HF}} = \sum_{i}^{occ} h_i + \frac{1}{2}\sum_{ij}^{occ}(J_{ij} - K_{ij}) - \sum_{ij}\lambda_{ij}(\langle\psi_i|\psi_j\rangle - 1)\,. \tag{1.13}$$

Taking the derivative of this Lagrangian with respect to $\langle\psi_i|$

$$\frac{\partial\mathcal{L}^{\mathrm{HF}}}{\partial\psi_i^*} = \left[\hat{h} + \frac{1}{2}\sum_j\left(\hat{J}_j[\psi] - \hat{K}_j[\psi]\right)\right]\psi_i(r) - \sum_j\lambda_{ij}\psi_j(r) \tag{1.14}$$

and setting this equation to zero, yields the Hartree-Fock equations

$$\mathcal{L}^{\mathrm{HF}}([\psi])\psi_i(r) = \sum_j\lambda_{ij}\psi_i(r)\,; \tag{1.15}$$

$$\hat{F}[\psi]\psi_i(r) = \varepsilon_i\psi_i(r)\,, i = 1, ..., n\,. \tag{1.16}$$

Summing over all electrons i, eq. (1.16) can be expressed in matrix form as

$$\mathbf{F}[C^n]\mathbf{C}^{(n+1)} = \varepsilon\mathbf{S}\mathbf{C}^{(n+1)}\,. \tag{1.17}$$

The Fock equations are a set of non-linear differential equations, that is, the operator $\mathbf{F}[C^n]$ already depends on the solution. To find an optimal solution, the one-electron wave functions are optimized iteratively in a self-consistent-field (SCF) procedure. For this purpose, the Fock matrix $\mathbf{F}[C^n]$ is constructed from an approximate solution n to obtain $\mathbf{C}^{(n+1)}$, which is then used to construct a more accurate Fock matrix $\mathbf{F}[C^{(n+1)}]$. This procedure is repeated until self-consistency is reached. The optimized one-electron wave functions correspond to the optimal solution for the given ansatz and basis set.

Solutions of Hartree-Fock calculations have some interesting properties. The eigenvalue ε_i of each one-electron wave function ψ_i is usually referred to as orbital energy. Orbital energies of closed-shell systems can be interpreted according to Koopmans' theorem.[9] Negative (positive) orbital energies of occupied (unoccupied) orbitals correspond to the ionization potential (electron affinity). The HF ground state does not couple to singly excited determinants as described by Brillouin's theorem.

In practice, HF theory is too inaccurate for chemical predictions, since explicit electron-electron interaction is neglected in the mean-field picture. The difference between the HF energy and the exact energy is defined as correlation energy $E_{corr} = E_{exact} - E_{\mathrm{HF}}$. A path to improve HF energies and wave functions systematically is to account for electron correlation explicitly. There are several *ab initio* methods, which improve the HF reference by adding correlation energy terms using different schemes. These are the Møller Plesser[10]

(MP) family, Coupled Cluster (CC) theory and Configuration Interaction (CI) methods, the last of which will be discussed in Sec. 1.6.

1.5 Density functional theory

An alternative approach to HF is formulated in density functional theory (DFT). Instead of solving the complex many-body wave function problem of the SE, the idea is to determine the energy (and properties) of the system based on the three-dimensional electron density

$$E = \int E(\rho)\rho(r)dr \tag{1.18}$$

where ρ is the electron density and $E(\rho)$ is the total energy functional. The electron density can be determined from a known wave function as

$$\rho(r) = \int ... \int \Psi^*(x_1, ..., x_n)\Psi(x_1, ..., x_n)ds_1, ..., dx_n \tag{1.19}$$

with spin-spatial electron coordinates $x_i = (r_x, r_y, r_z, s_i)^T$. The original idea of DFT is, however, to determine ρ directly, that is, without knowing the wave function beforehand.

The Hohenberg-Kohn theorems[11] provide the basis for density functional theory. The first Hohenberg-Kohn theorem proves that a one-to-one mapping exists between the exact electron density ρ and the exact external potential v_{ext}. This exact external potential determines the exact ground-state wave function, and the wave function itself is a functional of the electron density. The second Hohenberg-Kohn theorem ensures a variational principle, that the energy of a trial density is always higher than the energy of the exact density. The energy of a system can thus be written as a functional of the density

$$E^{\mathrm{DFT}}[\rho] = T[\rho] + J[\rho] + E_{xc}[\rho] + v_{ext}[\rho](r)\,, \tag{1.20}$$

where $T[\rho]$ is the kinetic energy (expressed as function of the electron density), $J[\rho]$ is the Coulomb energy describing electron repulsion, $E_{xc}[\rho]$ is the exchange-correlation energy, and v_{ext} is the external potential.

So far, density functional theory is exact. However, no procedure describes how to obtain the exact density directly. A practical solution for this problem was introduced by Kohn and Sham.[12] They suggested to describe the density of a system by a non-interacting system with the same properties. Such a non-interacting system of fermions can be described by a single Slater determinant (giving rise to the formal connection between DFT and HF). By doing this,

the density of a system can be constructed from a set of orbitals, the Kohn-Sham (KS) orbitals. The KS-orbitals themselves can obtained by solving the so-called Kohn-Sham equations,[12] that is, a set of n coupled equations

$$\left(\frac{1}{2}\nabla^2 + v_{\mathit{eff}}(\vec{r}) - \varepsilon_i\right)\psi_i(\vec{r}) = 0\,;\; i = 1, ..., n\,, \tag{1.21}$$

where v_{eff} is the effective (Kohn-Sham) potential, and ε_i is the energy of the ith Kohn-Sham orbital ψ_i. The effective potential is given as

$$v_{\mathit{eff}}(\vec{r}) = v_{ext}(\vec{r}) + \int \frac{\rho(\vec{r'})}{|\vec{r} - \vec{r'}|} d\vec{r'} + \frac{\delta E_{xc}[\rho]}{\delta\rho(\vec{r})}\,, \tag{1.22}$$

where the first term v_{ext} is the external potential containing at least the electron-nuclei attraction, the second term corresponds to the Coulomb potential between electrons, and the third term is the derivative of the exchange-correlation energy with respect to the electron density, that is a functional of the density. For KS-DFT, eq. (1.21) transformes into

$$E^{\mathrm{KS}}[\{\psi_i\}, \rho] = T[\{\psi_i\}] + J[\rho] + v_{ext}[\rho](r) + f_{xc}[\rho](r)\,. \tag{1.23}$$

The last term of eq. (1.23) is the exchange-correlation functional f_{xc} and its structure is unknown. Hence, approximate exchange-correlation (xc) functionals have to be used in practice. The development of xc-functionals is based upon (more or less) empirical approaches, and is an active field of research. Accounting for electron interaction by means of empirical parameters often results in a significantly better accuracy compared to HF. State-of-the-art xc-functionals often yield accuracies comparable to correlated *ab initio* methods at a fraction of the computational cost. However, the empirical character of xc-functionals undermines the reliability of DFT, and thus, benchmarking is very important to examine the applicability and robustness of xc-functionals for different applications.[13]

Since this work is concerned with investigating effects of xc-functionals on the description of excited states (see Chapt. 5−7), the construction principles will be discussed in the following. Exchange-correlation functionals can be classified according to a Jacob's ladder.[14,15] The rungs correspond to different ingredients for the construction of the xc-functionals. These are the local density approximation (LDA), local generalized gradient approximation (GGA), meta-GGA, hybrid and double-hybrid functionals.

In the local density approximation (LDA) the exchange-correlation energy $E_{xc}[\rho]$ is calculated at a given position as a function of the local density at the same position. In local generalized gradient approximation (GGA) functionals

also the local density gradient is taken into account, which corresponds to the first derivative of the density at the given position ($E_{xc}[\rho, \nabla\rho]$). Meta-GGA functionals use the same ingredients as GGAs, and additionally account for the local kinetic energy density at the given position ($E_{xc}[\rho, \nabla\rho, \nabla^2\rho]$). Historically, an ultimate break through in applicability of DFT for the description of molecules was the development of hybrid schemes. Hybrid functionals combine a fraction of exchange energy calculated by pure density functionals with a fraction of Hartree-Fock-type, nonlocal orbital exchange (NLX) calculated for the Kohn-Sham orbitals of the investigated system. For example, in Becke's prominent three-parameter *xc*-functional B3LYP,[16] the exchange-correlation energy takes the form

$$E_{xc}^{\mathrm{B3LYP}} = a_0 E_{x,\mathrm{HF}} + (1-a_0)E_{x,\mathrm{Slater}} + a_x \Delta E_{x,\mathrm{Becke88}} + (1-a_c)E_{c,\mathrm{VWN}} + a_c \Delta E_{c,\mathrm{LYP}}\,, \quad (1.24)$$

where $E_{x,\mathrm{HF}}$ is the NLX energy obtained for the Kohn-Sham orbitals, $E_{x,\mathrm{Slater}}$ is the uniform electron-gas exchange energy,[17] $\Delta E_{x,\mathrm{Becke88}}$ is the generalized gradient approximation for exchange formulated by Becke,[18] $E_{c,\mathrm{VWN}}$ is the correlation energy according to Vosko, Wilk and Nusair,[19] and $\Delta E_{c,\mathrm{LYP}}$ is the correlation energy according to the Lee-Yang-Parr functional.[20] The three parameters a_0, a_x and a_c are optimized for atomization energies. In B3LYP, the NLX energy is constant with $a_0 = 0.21$ independent of the interelectronic distance. The consequences of this choice for excited-state calculations will be discussed in Chapters 5, 6 and 7. Double hybrid functionals extend the hybrid scheme by describing electron correlation explicitly *via* excited determinants (cf. Ref. 21).

In summary, modern density functional theory is an empirically parametrized method, that obtaines reasonably accurate results for a broad range of applications, when employing an appropriate *xc*-functional.[22,23] However, there are some noteworthy issues. The variational principle in DFT is only true for the non-interacting system within the chosen *xc*-functional approximation, and the obtained energy is not necessarily greater than the exact solution of the real system. A fundamental issue is connected to the mathematical structure of exchange-correlation functionals. In HF, the exchange and Coulomb terms cancel out if $i = j$, that is, a particle does not self-interact. In DFT, this cancellation is incomplete due to the *xc*-functional definition, cf. eq. (1.24). Another central issue is connected to the absence of a proper description of long-range electron interaction.[22] This leads to problems in describing London dispersion, extended π-systems, charge-transfer states and bond cleavage. It is important to note that issues in DFT can affect TDDFT in two ways: (*i*) through affect-

ing the ground-state reference and (*ii*) through the linear-response formulation of TDDFT, which can translate them into TDDFT-specific issues.

1.6 Configuration interaction

Configuration interaction[24] is a post-HF *ab initio* method, which constructs excited determinants of ground-state Hartree-Fock references, and uses them to describe electron correlation and excited states. In full configutation interaction (full-CI) the exact ground state wave function can be expressed as

$$\Psi_0^{\mathrm{CI}} = c_0\Phi_0^{\mathrm{HF}} + \sum_{ia} c_i^a\Phi_i^a + \sum_{i<j,a<b} c_{ij}^{ab}\Phi_{ij}^{ab} + ... + \sum_n c_n\Phi_n\,, \tag{1.25}$$

where Φ_0^{HF} is the Hartree-Fock wave function, Φ_i^a are singly excited determinants with particle transitions from ψ_i to ψ_a, Φ_{ij}^{ab} are doubly excited determinants, etc., and c_k are coefficients weighting each contribution. The indices i, j correspond to occupied, and a, b to unoccupied orbitals of the HF reference. Introducing a short-hand notation for different components of the full-CI wave functions, these are categorized according to the type of excitation

$$c_0\Phi_0 = c_0 0 \tag{1.26}$$

$$\sum_{ia} c_i^a\Phi_i^a = c_S S \tag{1.27}$$

$$\sum_{i<j,a<b} c_{ij}^{ab}\Phi_{ij}^{ab} = c_D D\,, \tag{1.28}$$

and so on. To obtain the full-CI energy, eq. (1.25) is plugged into the SE

$$\hat{H}|\Psi_0^{\mathrm{CI}}\rangle = E_{\mathrm{CI}}|\Psi_0^{\mathrm{CI}}\rangle \tag{1.29}$$

and left-multiply with $\langle\Psi_0^{\mathrm{CI}}|$. The task is then to diagonalize the CI matrix. The CI matrix collects interaction between different configurations in terms of expectation values with respect to the Hamiltonian, and has the general structure

$$\begin{pmatrix} \langle 0|\hat{H}|0\rangle & \langle 0|\hat{H}|S\rangle & \langle 0|\hat{H}|D\rangle & \langle 0|\hat{H}|T\rangle & \cdots \\ \langle S|\hat{H}|0\rangle & \langle S|\hat{H}|S\rangle & \langle S|\hat{H}|D\rangle & \langle S|\hat{H}|T\rangle & \cdots \\ \langle D|\hat{H}|0\rangle & \langle D|\hat{H}|S\rangle & \langle D|\hat{H}|D\rangle & \langle D|\hat{H}|T\rangle & \cdots \\ \langle T|\hat{H}|0\rangle & \langle T|\hat{H}|S\rangle & \langle T|\hat{H}|D\rangle & \langle T|\hat{H}|T\rangle & \cdots \\ \vdots & \vdots & \vdots & \vdots & \ddots \end{pmatrix}. \tag{1.30}$$

According to the Slater-Condon rules, the expectation value for a two particle operator is zero if the determinants differ by more than two orbitals. Moreover, Brillouin's theorem states that singly excited determinants do not couple to the electronic ground state. Therefore, the matrix in (1.30) can be reduced to a tridiagonal form

$$\begin{pmatrix} \langle 0|\hat{H}|0\rangle & 0 & \langle 0|\hat{H}|D\rangle & 0 & 0 \\ 0 & \langle S|\hat{H}|S\rangle & \langle S|\hat{H}|D\rangle & \langle S|\hat{H}|T\rangle & 0 \\ \langle D|\hat{H}|0\rangle & \langle D|\hat{H}|S\rangle & \langle D|\hat{H}|D\rangle & \langle D|\hat{H}|T\rangle & \ddots \\ 0 & \langle T|\hat{H}|S\rangle & \langle T|\hat{H}|D\rangle & \langle T|\hat{H}|T\rangle & \ddots \\ 0 & 0 & \ddots & \ddots & \ddots \end{pmatrix} \tag{1.31}$$

A set of eigenfunctions (wave functions) and eigenvalues (energies) can be obtained by diagonalizing the full Hamiltonian matrix. The lowest-energy solution of the full-CI matrix corresponds to the electronic ground state of the system. Higher energy solutions correspond to excited states and will be further discussed in sec. 1.7 for configuration interaction singles.

An expression for the correlation energy of the electronic ground state is yielded by substracting the HF energy from eq. (1.29)

$$(\hat{H} - E_{\mathrm{HF}})|\Psi_0^{\mathrm{CI}}\rangle = (E_{\mathrm{CI}} - E_{\mathrm{HF}}|\Psi_0^{\mathrm{CI}}\rangle\,. \tag{1.32}$$

After imposing an intermediate normalization $\langle\Phi_0^{\mathrm{HF}}|\Psi_0^{\mathrm{CI}}\rangle = 1$, and left-multiplying eq. (1.32) with $\langle\Phi_0^{\mathrm{HF}}|$, the correlation energy can be expressed as

$$\langle\Phi_0^{\mathrm{HF}}|(\hat{H} - E_{\mathrm{HF}})|\Psi_0^{\mathrm{CI}}\rangle = \Delta E_{corr}\,. \tag{1.33}$$

Evaluation of the expectation values by applying Slater-Condon rules and Brilluion's theorem further reduces the expression to

$$\Delta E_{corr} = \langle\Phi_0^{\mathrm{HF}}|(\hat{H} - E_{\mathrm{HF}})|\Phi_0^{\mathrm{HF}}\rangle + \sum_{ij,ab}\langle\Phi_0^{\mathrm{HF}}|(\hat{H} - E_{\mathrm{HF}})|c_{ij}^{ab}\Phi_{ij}^{ab}\rangle \tag{1.34}$$

$$= \sum_{ij,ab} c_{ij}^{ab}\langle ia||jb\rangle\,. \tag{1.35}$$

Apparently, only doubly excited determinants contribute to the correlation energy of the ground state directly, while singly excited determinants do not couple to the HF ground state (Brillouins theorem). However, the coefficients c_{ij}^{ab} depend on the full CI matrix and therefore also on other types of excited determinants, such as triples, etc. In practice, full-CI is only feasible for very small systems. Truncating the full-CI wave function after singly excited deter-

minants yields CIS, after doubly excited determinants CISD, and so on. Since the correlation energy of the ground state is mainly described by doubly excited determinants, CISD is often chosen as reasonable approximation of full-CI for practical applications.

1.7 Configuration interaction singles

In Section 1.6, CI was introduced as a method to describe electron correlation based on excited determinants. The same ansatz also allows to calculate excited states, which correspond to higher-energy solutions of the CI matrix. However, full-CI is too expensive for most practical applications. The simplest truncated variant of CI is the configuration interaction singles (CIS) method,[25] which is the only size-consistent CI scheme. In CIS, an excited-state wave function can be expressed as linear combination of all possible singly excited determinants

$$\Psi^{\mathrm{CIS}} = \sum_{ia} c_i^a \Phi_i^a \,. \tag{1.36}$$

As a consequence of exclusively considering singly excited determinants, CIS can only describe excited states with primary single excitation character. The coefficients c_i^a can be deduced from the normalized eigenvectors of the Hamiltonian matrix, which for a closed-shell system is given as

$$\langle \Phi_i^a | \hat{H} | \Phi_j^b \rangle = (E_{\mathrm{HF}} + \varepsilon_a - \varepsilon_i)\delta_{ij}\delta_{ab} - \langle aj||ib\rangle \,. \tag{1.37}$$

Eigenvalues of this equation are the total energies for excited states in the CIS picture and can be calculated as

$$E^{\mathrm{CIS}} = E^{\mathrm{HF}} + \sum_{ia} c_{ia}^2(\varepsilon_a - \varepsilon_i) - \sum_{ijab} c_{ia}c_{jb}\langle aj||ib\rangle \,. \tag{1.38}$$

In CIS, the energy of an excited state contains three different contributions. The first term is the HF ground-state energy. The second term is a zeroth order guess for the excitation energy accounting for difference in orbital energies weighted by their contribution to the state vector. The third term describes the weighted changes in electronic Coulomb and exchange interaction of the excited electron.

The expression in eq. 1.32 has shown that doubly excited determinants are required to describe the correlation energy of the ground state. To describe electron correlation for singly excited states in an analogous way, it is necessary to consider triply excited determinants. However, such higher excited determinants are not taken into account in CIS, and in the same sense that

HF yields uncorrelated ground-state wave functions, CIS obtains uncorrelated excited-state wave functions.

1.8 Time-dependent density functional theory

Time-dependent density functional theory (TDDFT)[26] is a density-based approach for the computation of excited states of molecular systems. Due to its computational efficiency, it allows even to describe excited states of large chromophores for which high-level *ab initio* methods are not feasible.

TDDFT is built upon a similar set of theorems and approximations as its time-independent counterpart DFT, where the difference is that these theorems and approximations refer to a time-dependent picture. In analogy to the first Hohenberg-Kohn theorem, the Runge-Gross theorem[27] ensures the existance of a one-to-one mapping between the time-dependent density and the time-dependent potential of a real, interacting system evolving from an initial state. This initial state is characterized by an initial wave function, which is a functional of the density.

A generalization of this theorem by van Leeuwen[28] ensures the existence of a time-dependent, non-interacting system described by the density $\rho_S(r,t)$ with the same external potential as a time-dependent real, interacting system. This time-dependent non-interacting system can be represented as single Slater determinant $\Phi(r,t)$ consisting of single-electron orbitals ψ_i

$$\rho_{real}(r,t) = \rho_S(r,t) = \sum_i^n |\psi_i(r,t)|^2 \tag{1.39}$$

The evolution of an initial one-particle wave function ψ_i in time can be propagated as

$$i\frac{\partial}{\partial t}\psi_i(r,t) = \left\{-\frac{1}{2}\nabla_i^2 + v_{ext}(r,t) + J[\rho(r,t)] + \frac{\partial A_{xc}[\rho]}{\partial \rho(r,t)}\right\}\psi_i(r,t)\,, \tag{1.40}$$

which are the time-dependent Kohn-Sham equations. In this expression, $-\frac{1}{2}\nabla_i^2$ is the kinetic energy operator, v_{ext} is the time-dependent external potential describing electron-nucleus interaction, J is the time-dependent Coulomb functional and A_{xc} is the so-called exchange-correlation part of the action integral, cf. Ref. 26 and references therein. In practice, the problem is reduced to a linear-response formulation obtaining a pseudo-eigenvalue equation known as Casida's equation[29]

$$\begin{pmatrix} \mathbf{A} & \mathbf{B} \\ \mathbf{B}^* & \mathbf{A}^* \end{pmatrix}\begin{pmatrix} \mathbf{X} \\ \mathbf{Y} \end{pmatrix} = \omega \begin{pmatrix} \mathbf{1} & \mathbf{0} \\ \mathbf{0} & -\mathbf{1} \end{pmatrix}\begin{pmatrix} \mathbf{X} \\ \mathbf{Y} \end{pmatrix}, \tag{1.41}$$

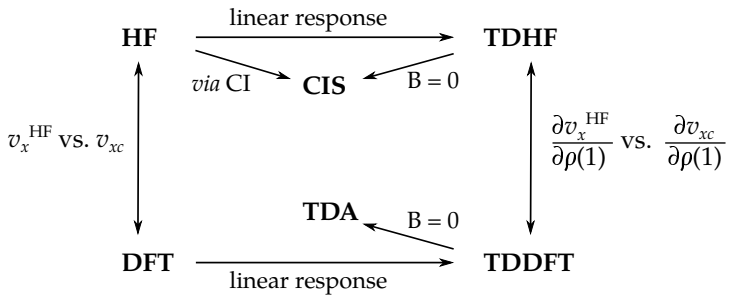

Figure 1.2: Relation between methods: ground-state methods Hartree Fock (HF), density functional theory (DFT), and excited-state methods configuration interaction singles (CIS), time-dependent Hartree Fock (TDHF), time-dependent density functional theory (TDDFT) and Tamm-Dancoff approximation (TDA), adopted from Ref. 26.

where $\mathbf{X}$ and $\mathbf{Y}$ are the excitation and de-excitation amplitudes and ω is the excitation energy. The elements of the $\mathbf{A}$ and $\mathbf{B}$ matrices depend on the xc-functional. In case of a hybrid xc-functional, the elements of the $\mathbf{A}$ matrix are defined as

$$A_{ij,ab} = (\varepsilon_a - \varepsilon_i)\delta_{ij}\delta_{ab} + \langle ia|bj\rangle - c_{\mathrm{HF}}\langle ia|jb\rangle + (1 - c_{\mathrm{HF}})\langle ia|f_{xc}|bj\rangle\,, \quad (1.42)$$

where ε_i and ε_a are the orbital energies of the occupied and virtual orbitals, and i, j and a, b are the indices corresponding to occupied and unoccupied molecular orbitals, respectively. c_{HF} marks the fraction of Hartree-Fock-type nonlocal orbital exchange (NLX) for a standard hybrid functional and f_{xc} is the xc-kernel of the functional. The elements of the $\mathbf{B}$ matrix are given as

$$B_{ij,ab} = \langle ia|jb\rangle - c_{\mathrm{HF}}\langle ia|bj\rangle + (1 - c_{\mathrm{HF}})\langle ia|f_{xc}|jb\rangle\,, \quad (1.43)$$

that is, they correspond to the integrals with permuted indices and describe electronic couplings to de-excitations.

Comparing the structure of the $\mathbf{A}$ matrix (eq. (1.42)) to the matrix elements of the CIS matrix (eq. (1.37)), their construction principle is similar. However, there are two remarkable differences: (*i*) CIS refers to the HF ground state, while TDDFT refers to the DFT ground state; (*ii*) electronic couplings between excited configurations differ in their exchange part, where for CIS the HF-type exact exchange is considered, and for TDDFT this term is substituted by the exchange-correlation functional expression. Furthermore, CIS does not account for couplings to de-excitations as described in the $\mathbf{B}$ matrix for TDDFT (eq. (1.43)). However, such kind of couplings are considered in time-dependent

HF, as depicted in Fig. 1.2.

An anagous method to CIS, the Tamm-Dancoff approximation (TDA)[30] can be constructed by neglecting the **B** matrix and the de-excitation amplitude **Y** of eq. (1.41) in TDDFT. TDA is a linearized, Hermitian version of time-dependent density functional theory, for which the eigenvalue problem takes the form

$$\mathbf{AX} = \omega \mathbf{X}\,. \tag{1.44}$$

Depending on the selected *xc*-functional, the **B** matrix has only minor effect on the results justifying the TDA. TDA calculations are computationally less demanding than standard TDDFT, especially for hybrid and long-range corrected *xc*-functionals.[26] TDA sometimes obtains superior results compared to TDDFT in particular for *xc*-functionals with large amount of nonlocal exchange. Such cases are, *e.g.*, excited states of extended π-systems[31] and triplet excited states, which are prone to be energetically overstabilized by TDDFT.[32,33]

Similar to ground-state DFT, time-dependent density functional theory is a powerful tool to describe excited states of molecular systems. Especially for large chromophores, the computational efficiency is a key ingredient. However, the dependence on empirically fitted *xc*-functionals is a source of significant errors. These errors become apparent for several types of excited states such as charge-transfer states,[34–37] Rydberg states,[38] excited states of large π-conjugated systems,[39–41] and multiply excited states.[42,43]

Charge-transfer states can serve as important test cases to illustrate the underlying issues. First, it is important to realize how electron-electron interaction is described in linear-response TDDFT (eq. (1.41)). In the linear response formalism, a Coulomb integral translates into an exchange-type interaction in the TDDFT energy expression (second term of eq. (1.42)), while an exchange integral translates into Coulomb interaction (third term of eq. (1.42)). For pure GGA functionals without nonlocal orbital exchange the Coulomb repulsion between electrons vanishes, which leads to spurious CT states in the low-energy excited-state regime. In hybrid *xc*-functionals, Coulomb repulsion is reintroduced, but artificially scaled by c_{HF}. While this usually improves the overall description of excited-state spectra, it still leads to a systematic overstabilization of CT states. As will be shown *e.g.* in Chapters 5−7, other types of excited states are critically affected by the same issue, but for less obvious reasons.

One strategy to overcome these issues is to make use of the so-called long-range corrected (LR or LRC) *xc*-functionals.[44–49] In LRC *xc*-functionals the amount of nonlocal exchange depends on the interelectronic distance and the

exchange-correlation energy expression usually takes the form

$$E_{xc}^{\mathrm{LRC}} = E_{c,\mathrm{DFT}} + (1 - a_{\mathrm{HF}})E_{x,\mathrm{DFT}}^{\mathrm{SR}} + a_{\mathrm{HF}}E_{x,\mathrm{HF}}^{\mathrm{SR}} + E_{x,\mathrm{HF}}^{\mathrm{LR}} \,. \tag{1.45}$$

$E_{c,\mathrm{DFT}}$ corresponds to the correlation energy of the chosen xc-functional, while the exchange energy is split into three components corresponding to short-range (SR) DFT and HF-type exchange ($E_{x,\mathrm{DFT}}^{\mathrm{SR}}$ and $E_{x,\mathrm{HF}}$) and long-range (LR) HF-type exchange $E_{x,\mathrm{HF}}^{\mathrm{LR}}$. The separation is realized by means of an Ewald split, which allows to rewrite the electron repulsion operator using standard error function (erf)[45] as

$$\frac{1}{|r_1 - r_2|} = \frac{1 - erf(\mu|r_1 - r_2|)}{|r_1 - r_2|} + \frac{erf(\mu|r_1 - r_2|)}{|r_1 - r_2|} \,. \tag{1.46}$$

The factor μ is the range-separation parameter given in Bohr^{-1} and usually optimized for a certain benchmark set. The first term of eq. (1.46) corresponds to the short-range regime, while the second term defines the long-range part. This formulation connects the favorable description of short-range electron correlation of DFT xc-functionals with the correct asymptotic behaviour of Coulomb interaction for long-range electron separations. A recent approach is to optimize μ for each molecule individually, which is referred to as optimal tuning, cf. Ref. 50.

Despite advances in functional design, TDDFT results have to be checked carefully for each system. While the main criterion for the accuracy of a xc-functional is usually the excitation energy, method assessment should also take diagnostic tools into account, which are capable to detect methodological shortcomings. For this purpose, various descriptors have been designed in recent years,[51–56] and also descriptors developed in this work are suitable to analyze the performance of xc-functionals, cf. Chapters 5−7. The importance of such analyses comes from the fact that benchmarking only according to excitation energies can be in favour of an xc-functional which does not correctly describe the density and properties of the real system, for more details cf. Chapter 7.

1.9 Algebraic diagrammatic construction for the polarization propagator

The algebraic-diagrammatic construction (ADC) scheme for the polarization propagator[57–60] is a correlated *ab initio* method for the description of excited states. Similar to CI, it makes use of n-tuply excited intermediate states, which serve as a basis to expand excited-state wave functions. Instead of an excitation-class based truncation such as in CI, ADC employes Rayleigh-

Schrödinger perturbation theory to identify the terms that need to be included in the ADC matrix for a consistent treatment. ADC is therefore often referred to as the excited-state analog of Møller Plesser[10] (MP) perturbation theory for the ground state.

Taking a look at the origins of ADC,[59,60] it was historically derived from Green's function theory. Another derivation makes use of the intermediate-state representation (ISR) formalism,[61,62] which is considered in the following. As a starting point, a set of excited-state wave functions $|\Psi_J^N\rangle$ is constructed by an excitation operator $\hat{C}$ acting on the exact ground-state wave function Ψ_0

$$\begin{aligned} |\Psi_J\rangle &= \hat{C}_J|\Psi_0\rangle \\ \{\hat{C}_J\} &= \{\hat{a}_a^\dagger\hat{a}_i; \hat{a}_a^\dagger\hat{a}_b^\dagger\hat{a}_i\hat{a}_j; i<j, a<b; ...\}\,, \end{aligned} \tag{1.47}$$

where $\hat{C}$ collects annihilation and creation operators, which correspond to formation of singly, doubly, and higher order multiply excited states. In order to form a proper basis, the intermediate states $\{|\widetilde{\Psi}_J^N\rangle\}$ have to be orthogonal, which is in practice realized by Gram-Schmidt and symmetry orthogonalization. Expressing the shifted hamiltonian in the intermediate-state basis yields the matrix elements of the ADC matrix $\mathbf{M}$ as

$$M_{IJ} = \langle\widetilde{\Psi}_I|\hat{H} - E_0|\widetilde{\Psi}_J\rangle\,, \tag{1.48}$$

where E_0 is the exact ground-state energy. Solving the hermitian eigenvalue problem by diagonalizing the matrix $\mathbf{M}$

$$\mathbf{MX} = \mathbf{X\Omega}\,; \tag{1.49}$$

$$\mathbf{X}^\dagger\mathbf{X} = 1\,, \tag{1.50}$$

yields eigenvalues and eigenvectors, which correspond to excitation energies ω and representation of excited-state wave functions in the IS basis. In practice, the low-lying excited states can usually be obtained by partial diagonalization of the ADC matrix using Davidson or Lanczos algorithms.

Up to this point, ADC is an exact method as no assumptions or approximations have been introduced so far, however, for practical applications this method is not feasible. Employing Rayleigh-Schrödinger perturbation theory, the ADC matrix $\mathbf{M}$ can be expanded as a series

$$\mathbf{M} = \mathbf{M}^{(0)} + \mathbf{M}^{(1)} + \mathbf{M}^{(2)} + \mathbf{M}^{(3)} + ... + \mathbf{M}^{(i)}\,, \tag{1.51}$$

such that the matrix elements can be consistently treated up to a certain order as indicated by the superscript (i). Advantages of employing perturba-

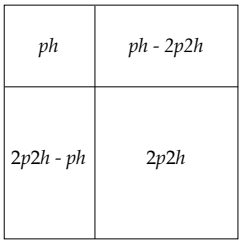

	ph	*ph-2p2h* *2p2h-ph*	*2p2h*
ADC(0)	0	-	-
ADC(1)	1	-	-
ADC(2)	2	1	0
ADC(3)	3	2	1

Figure 1.3: ADC matrix **M**: (a) sketch of different blocks, and (b) level of perturbation-theoretical treatment of these blocks for different ADC variants.

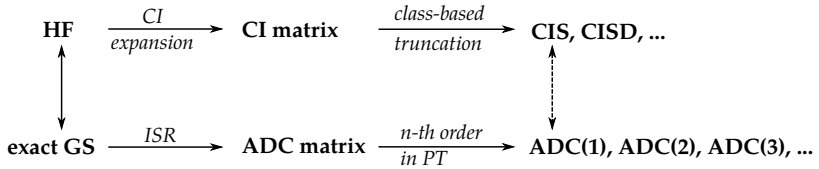

Figure 1.4: Relation of the methods: The main difference between ADC and CI are the principles to reduce the dimensions of the respective matrix. While ADC is built upon a correlated ground-state, CI starts with the uncorrelated HF ground state.

tion theory instead of a excitation-class based truncation scheme in CI is that electron-correlation is treated more consistently while the dimensions of the **M** matrix grow slower as compared to CI or coupled cluster excited-state methods. ADC is therefore a compact, size-consistent method. To illustrate this behaviour in more detail, fig. 1.3 presents the structure of the ADC matrix for different orders of PT. For example, in ADC(3) four blocks are considered: the 1-particle-1-hole (ph) block is treated at third order in PT, the 2-particles-2-holes ($2p2h$) block is treated at first order in PT, and couplings between these blocks are treated at second order in PT. To account for electron correlation in the $2p2h$-block of the CI matrix, an inclusion of triply and quadruply excited determinants would be necessary, hence, the dimensions of the CI matrix grow substantially faster. At first order in perturbation theory ADC(1) is equivalent to CIS: The MP(1) energy expression (which is the ADC ground-state reference) is identical to HF, and in analogy, the ADC(1) energy expression is equal to CIS. Any higher order of ADC corresponds to a successively more accurate treatment electron correlation and excited states compared to CIS, for more details cf. Ref. 59.

In the beginning of this section, the intermediate-state representation was constructed upon the exact ground-state wave function, see eq. (1.47). However, since the exact ground-state wave function is unknown, an approximate

correlated ground-state wave function has to be used in practice. Standard references are Møller Plesser ground-state wave functions constructed at the same level of perturbation theory as the order of ADC. In principle, this restricts the applicability of ADC to systems whose ground states are well-described at the corresponding MP level. Recent developments make use of the possibility to employ other ground-state references. For example, ADC has been successfully adopted for multi-reference ground states by exploiting the spin-flip ansatz.[63]

1.10 Characterization of excited states

Systematic analysis and visualization of excited states is a key step in the interpretation of quantum-chemical results. Visual inspection of molecular orbitals (MOs) that are involved in the electronic transition is the standard way to characterize excited states and electronic transitions in quantum chemistry. But since molecular orbitals describe the electronic ground state of the system, they may not be ideal to represent excited states and electronic transitions. In many cases it can become difficult to draw a conclusive picture about excited states by interpreting MOs, especially if many of them contribute to the excitation vector by similar weights. One way to improve this situation is to move to orbital representations and other properties that are directly connected to excited states. Over the past decades, qualitative and quantitative analysis tools have been developed based on one-particle transition density matrices and one-particle difference density matrices (cf. Refs. 64–66 and references therein). Both quantities serve as bases for compact orbital representations of excited states: the natural transition orbitals[67–69] (cf. sec. 2.8) and natural difference orbitals.[65,66] A variety of excited-state descriptors has been developed mainly with the purpose to characterize the amount of charge transfer and spatial extends of electron and hole distributions in the context of TDDFT diagnosis, cf. Refs 51–53,70–72. This work focuses on the one-particle transition density matrix (1TDM) which is identified as exciton wave function[73] and allows for a clear physical interpretation of derived descriptors. For this purpose, the construction and properties of the one-particle transition density matrix are briefly discussed in the following.

One-particle transition density matrix Many-electron wave functions comprise information about the full n-electron system. If the task is to analyze electronically excited states, the properties of interest are more specifically connected to changes in the electronic structure between the ground and excited state. This information is contained in the one-particle transition density matrix, which is essentially a map of the molecule which indicates how the excited

electron is shifted during excitation. The 1TDM between the ground Ψ^0 and the excited Ψ^I state wave functions is defined as

$$\gamma^{0I}(r_h, r_e) = n \int \Psi^0(r_h, r_2, ..., r_n) \times \Psi^I(r_e, r_2, ..., r_n) dr_2, ...dr_n \,, \tag{1.52}$$

where r_i denotes the spatial and spin coordinates of the i-th electron: $r_i = (\vec{x}_i, s_i)$. Note that in eq. (1.52) and in the following real valued wave functions and orbitals are assumed but an extension to complex quantities is straight forward. The matrix representation with respect to an underlying basis set of spin atomic orbitals (AOs) $\{\chi_\mu(r)\}$ is constructed as

$$D^{0I}_{\mu\nu} = \langle \Psi^0 | \widehat{a}^\dagger_\mu \widehat{a}_\nu | \Psi^I \rangle \,, \tag{1.53}$$

where $\widehat{a}^\dagger_\mu$ and $\widehat{a}_\nu$ are the creation and annihilation operators, respectively. This definition leads to an alternative expression for γ^{0I}

$$\gamma^{0I}(r_h, r_e) = \sum_{\mu\nu} D^{0I}_{\mu\nu} \chi_\mu(r_h) \chi_\nu(r_e) \,, \tag{1.54}$$

which will be used later to derive the exciton wave function and its properties. It is worth noting that switching the bra and ket states amounts to transposing the transition density matrix

$$D^{I0}_{\nu\mu} = \langle \Psi^I | \widehat{a}^\dagger_\nu \widehat{a}_\mu | \Psi^0 \rangle = \langle \Psi^0 | \widehat{a}^\dagger_\mu \widehat{a}_\nu | \Psi^I \rangle = D^{0I}_{\mu\nu} \tag{1.55}$$

$$(\mathbf{D}^{0I})^T = \mathbf{D}^{I0} \,. \tag{1.56}$$

As already mentioned, the 1TDM can be used to construct a compact orbital representation of the electronic transition, the natural transition orbitals. An alternative strategy to further analyze excited states relies on evaluation of 1TDMs in terms of quantitative measures. Such excited-state descriptors have first been derived in the framework of CIS, RPA and TDDFT.[74,75] Specifically, two indices were introduced measuring charge-transfer strengths and electronic coherence.[76] Also a visual representation of the 1TDM itself was introduced. For this purpose, a population analysis with respect to individual atoms is performed creating a probability map for the electron being promoted from one atom to another. These methods have been successfully applied to large π-conjugated systems illustrating their conceptual advantage for interpreting excited states of complex systems, cf. Ref. 77. These ideas have been transferred to higher level *ab initio* methods including CASSCF, MR-CI, ADC(2) and CC2, and inspired the construction of more descriptors for an ever more detailed analysis of excited states.[64] These works have been the starting point and inspiration for the developments presented in the following.

Chapter 2

Exciton analysis

In this chapter, the formalism of exciton analysis is introduced for quantum-chemical calculations. For this purpose, excitons are defined, the concept is transferred to the framework of many-electron wave functions and expectation values of the introduced exciton wave functions are calculated. Definitions and significance of central excited-state descriptors are discussed for exciton sizes, electron and hole sizes, vectorial electron-hole separation and statistical measures quantifying electron-hole correlation effects. An interpretation in terms of natural transition orbitals is given and the definition of exciton wave functions is transferred to time-dependent density functional theory. The chapter closes with a short introduction of electron-hole correlation plots, which allow to visualize excitons, and a definition of total transfer measure. Descriptors that are designed for specific purposes are described in the respective chapters.

Please note that parts of this chapter have already been published in *Physical Reviews A*, volume 90 (**2014**), 052521 (Ref. 73) and in *The Journal of Computational Chemistry*, volume 36, (**2015**), pages 1609 − 1620 (Ref. 78).

2.1 Introduction

A central goal of quantum-chemical calculations is to improve our understanding of investigated molecular systems and their properties. Characterizating electronically excited states according to their excitation energy is a central step in any study. Details about excited-state character are usually extracted from the molecular orbitals (MOs) contributing to the response vector, *i.e.*, they are involved in the electronic transition. A few more properties, *e.g.*, oscillator strengths are frequently considered. Determining the excitation character is important for several reasons. Knowing the type of excitation such as local, Rydberg, charge-transfer, etc. allows one to judge whether a method is reliable for the description of the state, to predict interaction with the molecular environment, to consider excited-state couplings, and many more. In summary, there is a high motivation to determine excitation character as precise as possible. For large molecules, however, the MO picture reaches its limits in terms of interpretive power. In such systems, MOs can be spatially delocalized and excitations can involve many orbital transitions with significant weights. In such a scenario, not only the shapes of the MOs but also their superpositions are important, however, phase information and couplings between MOs are difficult to extract. Furthermore, it is difficult to compare differences between excited-state methods, since the MOs depend on the precise wave function expansion. It is therefore desirable to develop alternative concepts to examine excited states and their properties. In solid-state physics, excited states are rationalized as coupled electron-hole pairs, which arise from transitions between different bands in extended periodic systems. These so-called excitons are directly connected to experimental observables, *e.g.* the exciton binding energy characterizes the amount of energy necessary for charge separation in semiconductors.

Transferring the concept of excitons to the framework of many-body wave functions opens new ways to interpret computational results. Moreover, it allows to bridge the gap between the quasi-particle and MO pictures. An exciton theory for many-body wave functions should (*i*) be well-defined independent of the wave function model and give a result for the exact solution, (*ii*) apply to a wide range of wave function properties, (*iii*) be invariant to redundant orbital rotations, and (*iv*) neither depend on atom-centered basis function nor require a partitioning of the wave function into atom or fragment centered contributions. In the following sections, such an exciton theory is introduced based upon the assumption that the one-electron transition density matrix (1TDM) can be interpreted as an effective two-body exciton wave function describing the correlated *electron-hole* quasiparticles. After reviewing some details about

excitons in solid-state theory, a closer look is taken at the derivation and evaluation of exciton properties in quantum-chemical calculations (see Ref. 73). After that, exciton descriptors are introduced and their interpretive power is discussed (see also Refs. 73,78,79).

2.2 Excitons in solid-state theory

Excitons describe excited states in solid-state theory in terms of correlated electron-hole pairs. A classification of excitons is given according to the character of the bands involved in the electronic transition, where two corner cases are defined, *i.e.*, Wannier-Mott and Frenkel excitons.[80,81] In the first case, the electron is promoted from a delocalized band to another delocalized band, and the resulting exciton is characterized by a large size and small binding energy. In the second case, the promotion takes place between local bands, and the resulting Frenkel excitons are characterized by small sizes and large binding energies. In practice, these models are corner cases, and a variety of excitons with mixed contributions from different bands exist.

A useful strategy to extract information about the nature of excitons is to decompose the exciton wave function into two parts

$$\chi_{exc}(r_h, r_e) \approx \phi_{sep}(r_{eh})\phi_{CM}(R)\,, \tag{2.1}$$

where ϕ_{sep} describes the intrinsic *electron-hole* wave function and ϕ_{CM} is the center-of-mass wave function of the neutral quasi-particle pair. This decomposition allows to determine exciton sizes as well as to find the exciton in Cartesian space. Later this decomposition scheme will be employed to characterize excitons in PPV oligomers and other π-conjugated systems (cf. Chapt. 4 and 6).

2.3 Exciton wave function

As described above, some properties of excited states (*e.g.* exciton sizes and binding energies) are best understood in terms of a two-body exciton wave function describing the correlated motion of *hole* and *electron* quasi-particles (cf. Figure 2.1). Such a wave function appears directly within the solid-state physics approach of using many-body Green's function theory[82–87] while it is usually not considered in the context of quantum chemistry methodology. In the following, a connection of the two theories is presented.

Starting with solid-state physics theory, the Bethe-Salpeter equation (BSE) of the exciton is the standard way of solving the electronic excitation problem

within Green's function theory.[82,83,85] The solution of the BSE can be expressed as frequency (ω) dependent two-body correlation function[83]

$$L(r_1, r_1'; r_2, r_2'; \omega) = i \sum_{I \neq 0} \left[\frac{\chi^I(r_1, r_1')\, \chi^I(r_2', r_2)}{\omega + \Delta E^I} - \frac{\chi^I(r_2, r_2')\, \chi^I(r_1', r_1)}{\omega - \Delta E^I} \right], \quad (2.2)$$

which is closely related to the polarization propagator.[57] Here, ΔE^I denotes the excitation energy of state I and χ^I is the *electron-hole* amplitude. This latter function is commonly regarded as the wave function of the *electron-hole* pair[83–86] and it is precisely the quantity of interest in this work. It usually takes the form[83–85]

$$\chi^I(r_e, r_h) = \sum_{vc} A^I_{vc} \psi^{QP}_v(r_h) \psi^{QP}_c(r_e) \quad (2.3)$$

connecting the valence (ψ^{QP}_v) and conduction (ψ^{QP}_c) quasi-particle states.[88] A rigorous connection between the BSE and explicit many-body theories, and thus between the quasi-particle and MO pictures can be provided by considering the general form of the *electron-hole* amplitudes[83]

$$\chi^I(r_e, r_h) = -\left\langle \Phi^0 | \widehat{\psi}^\dagger(r_h) \widehat{\psi}(r_e) | \Phi^I \right\rangle \quad (2.4)$$

where the field operators $\widehat{\psi}(r)$ can be expressed in the AO basis as

$$\widehat{\psi}(r) = \sum_\mu \widehat{a}_\mu \chi_\mu(r)\,. \quad (2.5)$$

Inserting eq. (2.5) into eq. (2.4) already provides the relation of interest

$$\chi^I(r_e, r_h) = -\sum_{\mu\nu} \langle \Phi^0 | \widehat{a}^\dagger_\mu \widehat{a}_\nu | \Phi^I \rangle \chi_\mu(r_h) \chi_\nu(r_e) = -\gamma^{0I}(r_h, r_e)\ . \quad (2.6)$$

The exciton wave function as defined within Green's function theory is simply the 1TDM as obtained from quantum-chemical calculations. If χ^I is computed by exactly solving the BSE, it contains the same information as the 1TDM between the exact many-body wave functions. This provides a rigorous starting point for further investigations. Specifically, in the notation used here and in previous work,[65] the exciton wave function is defined as

$$\chi_{exc}(r_h, r_e) := \gamma^{0I}(r_h, r_e) = -\chi^I(r_e, r_h)\ , \quad (2.7)$$

i.e. there is a change in sign and an exchange of the *electron* and *hole* coordinates when compared to Ref. 83 (and the superscript I is dropped for brevity).

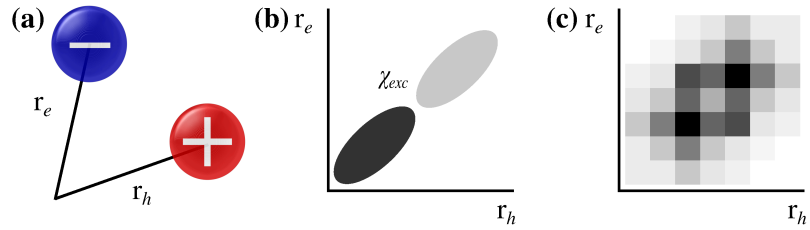

Figure 2.1: Representations of an exciton wave function: (a) the *hole* and *electron* quasi-particles positioned at r_h and r_e, (b) the correlated exciton wave function χ_{exc} plotted against these coordinates, and (c) visualization of χ_{exc} in terms of an *electron-hole* correlation plot.

γ^{0I} certainly possesses the required formal properties of a wave function of two distinguishable particles (*i.e.* being square integrable and continuously differentiable) and allows for computation of operator expectation values. The expectation value of an arbitrary operator $\widehat{O}$ with respect to the exciton wave function is

$$\left\langle \widehat{O} \right\rangle_{exc} = \frac{\langle \chi_{exc} | \widehat{O} | \chi_{exc} \rangle}{\langle \chi_{exc} | \chi_{exc} \rangle} \,. \tag{2.8}$$

To evaluate this expression, a similar strategy is used as by Tamura et al.[89] for the computation of energy transfer couplings: after writing down the equations in their explicit form, they are reformulated in terms of orbital integrals. The denominator of eq. (2.8) contains the squared norm of the exciton wave function Ω, a quantity, which has been used to measure the single excitation character of a transition.[65,90] By inserting the definition for χ_{exc} given in eq. (2.7) Ω can be rewritten as

$$\Omega = \langle \chi_{exc} | \chi_{exc} \rangle = \iint \gamma^{0I}(r_h, r_e)^2 dr_h dr_e \,. \tag{2.9}$$

This quantity can be reexpressed[65] in terms of matrix elements according to eq. (1.54) (and using eq. (1.56) for notational brevity)

$$\Omega = \mathrm{tr}\left((\mathbf{D}^{0I})^{\mathrm{T}} \mathbf{S} \mathbf{D}^{0I} \mathbf{S} \right) = \mathrm{tr}\left(\mathbf{D}^{I0} \mathbf{S} \mathbf{D}^{0I} \mathbf{S} \right) \,. \tag{2.10}$$

Here $\mathbf{S}$ denotes the AO overlap matrix with elements

$$S_{\mu\nu} = \int \chi_\mu(r) \chi_\nu(r) dr \,. \tag{2.11}$$

Furthermore, the numerator of eq. (2.8) can be treated in a similar fashion

$$\left\langle \widehat{O} \right\rangle_{exc} = \frac{1}{\Omega} \iint \gamma^{0I}(r_h, r_e) \widehat{O} \gamma^{0I}(r_h, r_e) dr_h dr_e \tag{2.12}$$

which after inserting eq. (1.54) leads to

$$\left\langle \widehat{O} \right\rangle_{exc} = \frac{1}{\Omega} \sum_{\mu\nu} \sum_{\xi\zeta} D_{\mu\nu} D_{\xi\zeta} \iint \chi_\mu(r_h) \chi_\nu(r_e) \widehat{O} \chi_\xi(r_h) \chi_\zeta(r_e) dr_h dr_e \,. \quad (2.13)$$

Hence, the task reduces to a contraction of AO integrals with the density matrices. Once the AO integrals of $\widehat{O}$ are computed, evaluating eq. (2.13) is straightforward. The relation can be simplified in cases where the operator is a product of two one-particle operators, each acting on only one of the electrons, *i.e.*, $\widehat{O} = \widehat{P}(r_h)\widehat{Q}(r_e)$. Then eq. (2.13) yields

$$\begin{aligned} \left\langle \widehat{P}(r_h)\widehat{Q}(r_e) \right\rangle_{exc} = \frac{1}{\Omega} \sum_{\mu\nu} \sum_{\xi\zeta} D_{\mu\nu} D_{\xi\zeta} \\ \times \iint \chi_\mu(r_h) \chi_\nu(r_e) \widehat{P}(r_h) \widehat{Q}(r_e) \chi_\xi(r_h) \chi_\zeta(r_e) dr_h dr_e \,, \end{aligned} \quad (2.14)$$

which can be decomposed with respect to r_h and r_e

$$= \frac{1}{\Omega} \sum_{\mu\nu} \sum_{\xi\zeta} D_{\mu\nu} D_{\xi\zeta} \int \chi_\mu(r_h) \widehat{P}(r_h) \chi_\xi(r_h) dr_h \int \chi_\nu(r_e) \widehat{Q}(r_e) \chi_\zeta(r_e) dr_e. \quad (2.15)$$

In matrix representation this can be rewritten as

$$= \frac{1}{\Omega} \sum_{\mu\nu} \sum_{\xi\zeta} D_{\mu\nu} D_{\xi\zeta} P_{\mu\xi} Q_{\nu\zeta} \quad (2.16)$$

which, in analogy to eq. (2.10) finally leads to (assuming that $\mathbf{Q}$ is a symmetric matrix)

$$\left\langle \widehat{P}(r_h)\widehat{Q}(r_e) \right\rangle_{exc} = \frac{1}{\Omega} \mathrm{tr} \left(\mathbf{D}^{I0} \mathbf{P} \mathbf{D}^{0I} \mathbf{Q} \right). \quad (2.17)$$

For an operator, which does not explicitly act on r_h and r_e, but is a simple function of these coordinates ($\widehat{O} = f(r_h, r_e)$), eq. (2.12) reduces to

$$\langle f(r_h, r_e) \rangle_{exc} = \frac{1}{\Omega} \iint f(r_h, r_e) \gamma^{0I}(r_h, r_e)^2 dr_h dr_e \,. \quad (2.18)$$

Specifically, if f is a polynomial, then $\langle f(r_h, r_e) \rangle_{exc}$ can be interpreted as a multipole moment of the exciton distribution function χ^2_{exc}. These types of expressions are the ones which are employed in the excited-state analysis.

2.4 Exciton size

In the following the exciton wave function will be evaluated with respect to its size,[79] illustrated in Fig. 2.2 (a). The exciton size is defined here as root-mean-

square (rms) separation between the instantaneous *electron* and *hole* positions

$$d_{exc} = \sqrt{\langle |\vec{x}_h - \vec{x}_e|^2 \rangle_{exc}}\,. \tag{2.19}$$

This equation can be expanded as

$$\begin{aligned} d_{exc}^2 &= \langle (\vec{x}_h - \vec{x}_e) \cdot (\vec{x}_h - \vec{x}_e) \rangle_{exc} && (2.20)\\ &= \langle \vec{x}_h \cdot \vec{x}_h \rangle_{exc} - 2\,\langle \vec{x}_h \cdot \vec{x}_e \rangle_{exc} + \langle \vec{x}_e \cdot \vec{x}_e \rangle_{exc}\,. && (2.21) \end{aligned}$$

Evaluating the dot products leads to the nine terms

$$d_{exc}^2 = \sum_{\xi \in \{x,y,z\}} \left(\langle \xi_h^2 \rangle_{exc} - 2\,\langle \xi_h \xi_e \rangle_{exc} + \langle \xi_e^2 \rangle_{exc} \right), \tag{2.22}$$

which are expectation values of one-electron multipole operators. Considering eq. (2.17), these can be evaluated according to

$$\langle \xi_h^k \xi_e^l \rangle_{exc} = \frac{1}{\Omega} \mathrm{tr} \left(\mathbf{D}^{I0} \mathbf{M}_\xi^{(k)} \mathbf{D}^{0I} \mathbf{M}_\xi^{(l)} \right), \tag{2.23}$$

where for example $\mathbf{M}_\xi^{(k)}$ refers to the k-order multipole matrix for coordinate x. Its components are given as

$$M_{\xi,\mu\nu}^{(k)} = \int \chi_\mu(r) \xi^k \chi_\nu(r) dr\,, \tag{2.24}$$

and specifically $\mathbf{M}_\xi^{(0)} = \mathbf{S}$ is the overlap matrix in the AO basis (eq. (2.11)). These matrices are usually available within quantum-chemical programs, such that in practice the task is reduced to a few matrix multiplications. The final

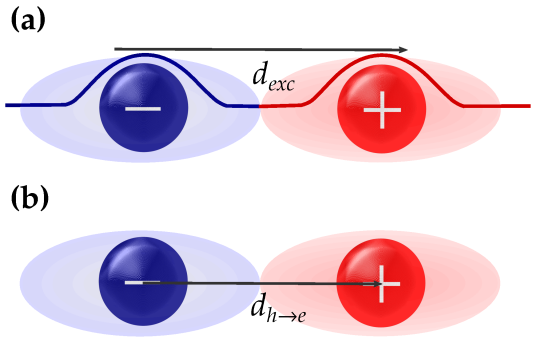

Figure 2.2: (a) Exciton size (d_{exc}) defined by root-mean-square separation of electron and hole, and (b) vectorial *electron-hole* separation ($d_{h\to e}$) defined by the distance between the charge cendroids.

working equation is

$$d_{exc}^2 = \frac{1}{\Omega} \sum_{\xi\in\{x,y,z\}} \Big(\mathrm{tr}\left(\mathbf{D}^{I0}\mathbf{M}_\xi^{(2)}\mathbf{D}^{0I}\mathbf{S}\right) - 2\mathrm{tr}\left(\mathbf{D}^{I0}\mathbf{M}_\xi^{(1)}\mathbf{D}^{0I}\mathbf{M}_\xi^{(1)}\right) + \mathrm{tr}\left(\mathbf{D}^{I0}\mathbf{S}\mathbf{D}^{0I}\mathbf{M}_\xi^{(2)}\right)\Big) . \quad (2.25)$$

The first and third terms in this sum refer to the quadrupole moments of the *hole* $\mathbf{D}^{0I}\mathbf{S}\mathbf{D}^{I0}$ and *electron* $\mathbf{D}^{I0}\mathbf{S}\mathbf{D}^{0I}$ densities (see also Ref. 65). The second term contains mixed dipole contributions deriving from correlated motion of *hole* and *electron*. Decomposing the two-particle problem into matrices of one-particle operators derives from the specific definition of d_{exc} as rms separation, a simplification which is also used in the Boys orbital localization scheme.[91]

Approximate exciton size An evaluation of eq. (2.25) is straight forward if the 1TDM and multipole matrices are available. However, this information is usually not part of the standard output of quantum-chemical programs and the formula has to be implemented.[73] To enable an *a posteriori* evaluation, an approximate version of d_{exc} is derived, which requires only the charge-transfer numbers and the coordinates of the nuclei as input. Starting with the definition of the exciton size (cf. eq. (2.19)) given as

$$d_{exc}^2 = \frac{1}{\Omega} \iint \gamma^{0I}(r_h, r_e)(\vec{x}_h - \vec{x}_e)^2 \gamma^{0I}(r_h, r_e) dr_h dr_e \,, \quad (2.26)$$

the double integral is divided into separate regions pertaining to different atoms M and N,

$$d_{exc}^2 = \frac{1}{\Omega} \sum_{M,N} \int_M \int_N \gamma^{0I}(r_h, r_e) \underbrace{(\vec{x}_h - \vec{x}_e)^2}_{\approx d_{MN}^2} \gamma^{0I}(r_h, r_e) dr_h dr_e \,. \quad (2.27)$$

Subsequently, the $(\vec{x}_h - \vec{x}_e)^2$ term is approximated by the squared distance between the positions of the respective nuclei d_{MN}^2. The constant term d_{MN}^2 is taken out of the integral

$$d_{exc}^2 \approx \frac{1}{\Omega} d_{MN}^2 \sum_{M,N} \int_M \int_N \gamma^{0I}(r_h, r_e) \gamma^{0I}(r_h, r_e) dr_h dr_e \quad (2.28)$$

leaving the CT number Ω_{MN} according to eq. (2.47). This suggests the definition of an approximate exciton size

$$\widetilde{d}_{exc} = \sqrt{\frac{1}{\Omega} \sum_{M,N} \Omega_{MN} d_{MN}^2} \,. \quad (2.29)$$

In contrast to the full implementation, $\widetilde{d}_{exc}$ neglects the spatial extent of the orbitals involved and it is therefore expected that $\widetilde{d}_{exc} \leq d_{exc}$. A detailed evaluation of the accuracy of $\widetilde{d}_{exc}$ for PPV oligomers is presented in Chapter 3. Albeit similar equations have been suggested by other researchers,[77,92–94] only the present approach is embedded in a clear approximation hierarchy and the formalism is applicable to arbitrary wave function models.

Vectorial electron-hole separation An alternative for the characterization of the electron-hole distance is a vectorial measure of the separation of the electron and hole charge cendroids, see Fig. 2.2 (b). This quantity is called vectorial electron-hole distance[78] $d_{h\to e}$ and defined as

$$d_{h\to e} = |\langle \vec{x}_e - \vec{x}_h \rangle_{exc}| \tag{2.30}$$

$$= |\langle \vec{x}_e \rangle_{exc} - \langle \vec{x}_h \rangle_{exc}| \,. \tag{2.31}$$

In contrast to the definition of d_{exc}, the vectorial electron-hole distance $d_{h\to e}$ is computed only from dipole moments of the exciton wave function and neglegts the spatial extention and correlation $d_{h\to e}$ between electron and hole distributions. Expressing eq. (2.31) in terms of matrix elements yields the following form

$$d_{h\to e} = \frac{1}{\Omega} \sum_{\xi\in\{x,y,z\}} \left(\mathrm{tr}\left(\mathbf{D}^{I0}\mathbf{S}\mathbf{D}^{0I}\mathbf{M}_\xi^{(1)}\right) - \mathrm{tr}\left(\mathbf{D}^{I0}\mathbf{M}_\xi^{(1)}\mathbf{D}^{0I}\mathbf{S}\right)\right). \tag{2.32}$$

The descriptor is well-suited to identify direct charge transfer. Moreover, the comparison of $d_{h\to e}$ and d_{exc} can reveal interesting features for the assignment of excited-state characters, as will be demonstrated in Chapters 5 and 7.

2.5 Electron and hole sizes

The spatial extents of electron and hole distributions in a molecular system can be quantified by evaluating the exciton wave function with respect to either the *hole* or *electron* multipole moments. As a measure for *electron* and *hole* sizes, root-mean-square deviations of their centers-of-masses are evaluated as

$$\sigma_h = \sqrt{\langle \vec{x}_h^2 \rangle_{exc} - \langle \vec{x}_h \rangle_{exc}^2} \tag{2.33}$$

or

$$\sigma_e = \sqrt{\langle \vec{x}_e^2 \rangle_{exc} - \langle \vec{x}_e \rangle_{exc}^2} \,. \tag{2.34}$$

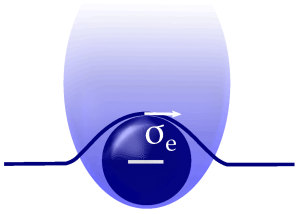

Figure 2.3: Electron size of Rydberg-type electron distribution.

By inserting the respective multipole matrix elements, the working equation of σ_h is obtained as

$$\sigma_h^2 = \sum_{\xi \in \{x,y,z\}} \frac{\mathrm{tr}\left(\mathbf{D}^{I0}\mathbf{M}_\xi^{(2)}\mathbf{D}^{0I}\mathbf{S}\right)}{\Omega} - \left(\frac{\mathrm{tr}\left(\mathbf{D}^{I0}\mathbf{M}_\xi^{(1)}\mathbf{D}^{0I}\mathbf{S}\right)}{\Omega}\right)^2 , \tag{2.35}$$

and for σ_e the analogous equation takes the form

$$\sigma_h^2 = \sum_{\xi \in \{x,y,z\}} \frac{\mathrm{tr}\left(\mathbf{D}^{I0}\mathbf{S}\mathbf{D}^{0I}\mathbf{M}_\xi^{(2)}\right)}{\Omega} - \left(\frac{\mathrm{tr}\left(\mathbf{D}^{I0}\mathbf{S}\mathbf{D}^{0I}\mathbf{M}_\xi^{(1)}\right)}{\Omega}\right)^2 . \tag{2.36}$$

Here, the quadrupole and dipole moments of the exciton wave function are evaluated yielding an average size of the distribution of the *hole* or *electron* quasiparticle around their centres of masses. The descriptors provide a measure of how compact or diffuse the respective distribution is, which in turn allows to characterize excited states of certain types, *e.g.* Rydberg, core-excited or delocalized $\pi \rightarrow \pi^*$ excited states, cf. Refs 78,95,96. As an example for the electron size measure, a diffuse Rydberg-type electron distribution is shown in Fig. 2.3.

2.6 Linear electron-hole correlation

Another class of descriptors is designed to characterize *electron-hole* correlation, *i.e.* interdependent spatial distribution of electron and hole. The first descriptor of this class is defined as the covariance between the joint *electron* and *hole* positions given as

$$\mathrm{COV}(r_h, r_e) = \langle \vec{x}_h \cdot \vec{x}_e \rangle_{exc} - \langle \vec{x}_h \rangle_{exc} \cdot \langle \vec{x}_e \rangle_{exc} . \tag{2.37}$$

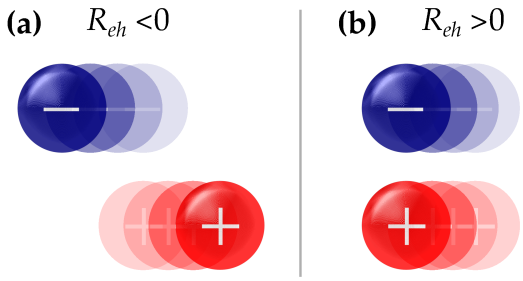

Figure 2.4: (a) Negative and (b) positive correlation between *electron* and *hole* quasiparticles.

Negative values in COV indicate that the *electron* and *hole* quasi-particles dynamically avoid each other in space, cf. Fig.2.4 (a). An example for this case is a charge-resonance state, see *e.g.* excited states of bianthryl in Fig. 3 of Ref. 78. A value of zero indicates no linear *electron-hole* correlation, which is usually assumed when MOs are analyzed. Positive values in COV hint towards the formation of excitons, *i.e.* a joint motion of a bound *electron-hole* pair in space, cf. Fig.2.4 (b). The value range of COV depends on the electron and hole sizes, which makes a comparison meaningful only for excited states belonging to the same system. For comparing the "pure" *electron-hole* correlation independent from other properties, it is advisable to choose the *electron-hole* correlation coefficient instead, which is defined as

$$R_{eh} = \frac{\mathrm{COV}(r_h, r_e)}{\sigma_h \sigma_e} \,. \tag{2.38}$$

R_{eh} is the normed covariance with respect to the *electron* and *hole* sizes. Its values range between $\{-1, ..., 0, ..., +1\}$ and their interpretation is analogous to the previous for COV. Due to the better comparability, R_{eh} is usually the measure of choice to analyze *electron-hole* correlation effects in molecular systems.

An important aspect of correlation analysis is that it only accounts for linear correlation. This is motivated by the connection to the exciton picture (*i.e.* considering only one electron-hole pair). In the case of doubly or multiply excited states monitoring higher order correlation effects becomes necessary constituting a logical extension of the presented descriptors. However, the development of such descriptors is beyond the scope of this work.

2.7 Dependencies of descriptors

In view of their common foundation, the exciton descriptors have some notable dependencies that are relevant to link individual descriptors to a global picture. For example, exciton size definition incorporates electron-hole correlation terms, but also depends on *electron* and *hole* sizes and their vectorial center-of-mass distance:

$$d_{exc} = \sqrt{d_{h\to e}^2 + \sigma_h^2 + \sigma_e^2 - 2 \times \mathrm{COV}(r_h, r_e)}\,. \tag{2.39}$$

This relation has some implications for the characterization of different types of states. For example, in the case of Rydberg states, exciton sizes are enhanced compared to locally excited states of the same system, because they have large *electron* sizes.[96] In the case of excitonic $\pi\pi^*$ states in large conjugated systems, exciton sizes are comparably small due to large *electron-hole* correlation effects.[97]

Concerning the relationship between exciton size and vectorial *electron-hole* distance, the following relation holds

$$d_{h\to e} \leq d_{exc}\,, \tag{2.40}$$

that is, the vectorial *electron-hole* separation is always smaller or equal to the exciton size. This relation is especially interesting when charge transfer and charge resonance excitations are investigated, cf. Chapter 5.

2.8 Interpreting exciton properties from a NTO perspective

To connect exciton properties to an orbital picture, the most intuitive choice is to employ natural transition orbitals (NTOs). NTOs are the most compact orbital representation of the *electron-hole* transition[67–69] and are constructed based on the 1TDM by performing a singluar value decomposition given as

$$\mathbf{D}^{0I} = \mathbf{U}\ \mathrm{diag}(\sqrt{\lambda_1}, \sqrt{\lambda_2}, ...)\mathbf{V}^{\mathrm{T}}\,. \tag{2.41}$$

The matrices $\mathbf{U}$ and $\mathbf{V}$ contain the hole/electron NTO pairs ϕ^{0I} and ϕ^{I0}, and λ_i are the weighted coefficients representing the probability of an electron transition between the NTOs consituting a pair. The exciton wave function

can be rewritten in a diagonal form yielding[78]

$$\chi_{exc}(r_h, r_e) = \sum_i \sqrt{\lambda_i}\phi_i^{0I}(r_h)\phi_i^{I0}(r_e)\,. \tag{2.42}$$

Revisiting the general expression of evaluation of the multipole operators (2.23) and plugging in the definition for χ_{exc} in the NTO basis, the following is obtained

$$\langle x_h^k x_e^l\rangle_{exc} = \frac{1}{\Omega}\sum_{i,j}\sqrt{\lambda_i\lambda_j}\langle\phi_i^{0I}(r_h)|x_h^k|\phi_j^{0I}(r_h)\rangle\langle\phi_i^{I0}(r_e)|x_e^l|\phi_j^{I0}(r_e)\rangle\,. \tag{2.43}$$

Inserting the multipole integrals $\mathbf{M}$ with respect to the electron and hole NTOs into eq. (2.43) yields

$$\langle x_h^k x_e^l\rangle_{exc} = \frac{1}{\Omega}\sum_{i,j}\sqrt{\lambda_i\lambda_j}\mathbf{M}_{\xi,ij}^{0I,k}\mathbf{M}_{\xi,ij}^{I0,l}\,. \tag{2.44}$$

Next, the equation is split into diagonal and off-diagonal terms

$$\langle x_h^k x_e^l\rangle_{exc} = \frac{1}{\Omega}\left(\sum_i \lambda_i\mathbf{M}_{\xi,ii}^{0I,k}\mathbf{M}_{\xi,ii}^{I0,l} + \sum_{i\neq j}\sqrt{\lambda_i\lambda_j}\mathbf{M}_{\xi,ij}^{0I,k}\mathbf{M}_{\xi,ij}^{I0,l}\right). \tag{2.45}$$

In the present form, it is possible to differentiate between components that belong to a simply weighted contribution of individual NTO pairs (non-vanishing coefficients on the main diagonal, first term), and components that originate from mixed contributions between NTOs that do not belong to the same pair (second term). While the situation is very simple if the electron-hole pair can be described by only one NTO pair (all λ are zero except for one), all other scenarios require thoughtful analysis of the involved NTO pairs, and the situation becomes even more involved if off-diagonal contributions are present.

2.9 Exciton analysis in TDDFT

In time-dependent density functional theory, the computation of wave functions is subsidised by the computation of the densities corresponding to the respective states under investigation as discussed in Section 1.8. Hence the exciton wave function has to be redefined employing the 1TDM obtained from TDDFT calculations. In TDDFT, the 1TDM is usually constructed from the excitation and de-excitation amplitudes X_{ia}^I and Y_{ia}^I of the Ith excited state

and the exciton wave function is given as

$$\chi_{exc}^{\mathrm{TDDFT}}(r_h, r_e) = \sum_{i}^{occ} \sum_{a}^{virt} \left[X_{ia}^{I} \phi_i(r_h) \phi_a(r_e) + Y_{ia}^{I} \phi_a(r_h) \phi_i(r_e) \right], \tag{2.46}$$

where ϕ_i and ϕ_a are the occupied and virtual molecular orbitals, and r_h and r_e denote the coordinates of the *electron* and *hole* quasi-particles. The form of eq. (2.46) is used in the current implementation in Q-Chem 4.3,[98] however there exist different formalisms suggesting the use of additional scaling factors.[29,99,100] In the case of the Tamm-Dancoff approximation (TDA)[30] the same formalism is applied, but the Y_{ia}^{I} terms vanish.

The analysis of exciton properties computed with time-dependent density functional theory allows not only to investigate excited states of molecular systems, but also to assess methodological performance by comparing exciton properties for different *xc*-functionals to those obtained with *ab initio* methods. In Chapters 5 and 6, the performance of different types of *xc*-functionals was investigated for various molecular systems. In Chapter 7 benchmarking with exciton properties was discussed revealing that coinciding excitation energies not necessarily correspond to identical description of state characters. For more details, see for example the respective chapters.

2.10 Visualizing exciton wave functions using *electron-hole* correlation plots

A visual representation of the exciton wave function can reveal interesting information about its shape and properties. Such a representation can be obtained by constructing *electron-hole* correlation plots. The plotting procedure was introduced by Luzanov[75] and is reviewed here due to its frequent use throughout this work. Prior to the evaluation of the transition density matrix, fragments of the system need to be chosen. These fragments can contain single atoms or groups of atoms, which form a subunit of the system. Subsequently, a partial integration over the square of γ^{0I} is performed, while the *hole* coordinate is restricted to one fragment A and the *electron* to a fragment B:

$$\Omega_{AB} = \int_A \int_B \gamma^{0I}(r_h, r_e)^2 \, dr_e dr_h \,. \tag{2.47}$$

The resulting charge-transfer numbers[75] afford the probability to find the *hole* on fragment A, while the *electron* is located at B. Subjecting eq. (2.47) to a

Mulliken population analysis leads to the working equation[65]

$$\Omega_{AB} = \frac{1}{2} \sum_{\mu \in A} \sum_{\nu \in B} \left[(\mathbf{D}^{0I}\mathbf{S})_{\mu\nu} (\mathbf{S}\mathbf{D}^{0I})_{\mu\nu} + D^{0I}_{\mu\nu} (\mathbf{S}\mathbf{D}^{0I}\mathbf{S})_{\mu\nu} \right], \tag{2.48}$$

where $\mathbf{S}$ is the overlap matrix between the basis functions. A visualization of the Ω_{AB} matrix in terms of a pseudo-color matrix yields *electron-hole* correlation plots that provide a coarse-grained representation of the exciton wave function, an example of which is shown in Figure 2.1(c). Local excitation contributions are mapped on the main diagonal going from the lower left to the upper right, while off-diagonal contributions indicate charge transfer between fragments A and B. The relative probability is typically visualized in grey scale, where black corresponds to the highest probability and white to zero. Although this is a flexible and rather intuitive tool, it has the drawback of requiring an *a priori* definition of the fragmentation. Furthermore, one can expect the same, significant basis-set dependence for eq. (2.48) that has been reported for standard Mulliken population analysis, cf. Ref. 101.

2.11 Total charge transfer

In many cases it is desirable to deduce more compact, skalar descriptors from the Ω_{AB} matrix[64,102] and in this work the total charge transfer is quantified for several systems. Generally, the descriptor is defined as

$$\omega_{\mathrm{CT}} = \frac{1}{\Omega} \sum_{A} \sum_{B \notin A} \Omega_{AB} \,. \tag{2.49}$$

ω_{CT} ranges from 0 to 1, where 0 corresponds to a local excitation or Frenkel exciton (with respect to the defined fragmentation scheme) and 1 denotes a completely charge-separated state. Like the underlying Ω_{AB} values, ω_{CT} is sensitive to both, the fragmentation scheme and basis set.

The charge-transfer measure is used in this work to cross-validate results of exciton sizes and opens a route to compare 1TDM analysis to other schemes based on 1DDMs or related quantities describing changes in electron density upon excitation in future investigations.

Chapter 3

Exciton size analysis of many-body wave functions

In the course of this work, the first derived exciton property was the exciton size. In this chapter, its application to many-body wave functions from ADC(2) calculations is discussed in detail. A broad selection of examples highlights different aspects of the developed methodology: Starting with an analytical example, a validity check of the developed protocol is presented, delivering expectation values for different types of excited states. Subsequently, two representatives of stacked π-systems, an ethylene-tetrafluoroethylene complex and a pyridine dimer are analyzed with emphasis on differentiating between different types of excited states, such as local, charge transfer, Rydberg, charge resonance, etc. It is found that for charge separated states exciton sizes closely correspond to the intermolecular distances, while they reflect the size of a local excitation on one monomer in the case of locally excited states. Exciton sizes furthermore provide useful information in the case of state mixing, which occurs in symmetric dimers and leads to resonance states. For two examples from the class of large conjugated π-systems, that are, poly(*para* phenylene vinylene) and polyacene compounds, energetically low-lying excitonic states are analyzed in terms of exciton sizes, structures and dynamic charge separation.

Please note that parts of this chapter have already been published by Prof. Dr. Andreas Dreuw, Dr. Felix Plasser, Dr. Michael Wormit and myself in *Physical Reviews A*, volume 90 (**2014**), 052521 (Ref. 73).

3.1 Introduction

In this work, exciton sizes are considered as root-mean-square separation between electron and hole and evaluated for many-body wave functions. Since it was the first developed protocol to examine exciton properties, exciton sizes are closely examined in the following in order to highlight the validity and capabilities of the approach. Let me start the discussion with general properties of exciton sizes and their implications for the analysis of excited states, cf. eq. (2.39). Firstly, exciton sizes characterize the structure of excitons by measuring the dynamic spatial separation of electron and hole. In contrast to measuring the vectorial electron-hole separation, exciton sizes do not only quantify permanent charge-transfer character of excited states, but also account for dynamic electron-hole correlation. This is especially important for identifying excitonic excited states for which permanent charge-transfer is absent. For excited states with exciton character, exciton sizes allow for a first guess of exciton binding energies, which - according to band-structure theory - are inversely related to each other: Small exciton sizes are connected to large binding energies, and vice versa. Secondly, the compactness of electron and hole distributions is also reflected in exciton sizes. It is therefore possible to differentiate between locally and Rydberg excited states of a molecule, since the latter have comparably larger exciton sizes due to their significantly larger and diffuse distribution of the excited electron. Thirdly, exciton sizes are sensitive towards linear electron-hole correlation effects. These effects describe the electron and hole interaction which can range between repulsive, absent or attactive depending on the type of excited state. This information is particularly valuable for examining the domains of applicability of time-dependent density functional theory (TDDFT). The potential of exciton sizes as diagnostic tool for TDDFT is rooted in the capability to measure, both, static and dynamic charge-transfer effects. However, more details about this topic will be discussed later and in Chapters 5−7.

Four molecular systems highlight different aspects of exciton size analysis, see Fig. 3.1. Firstly, it is demonstrated that for simple charge-transfer states between two chromophores the exciton size is equal to their spatial distance. For this purpose, an analytic model, and an ethylene - tetrafluoroethylene complex ([Et$\cdots$TFE]) at varying intermolecular distances are considered. Secondly, the symmetric pyridine dimer is selected as a representative stacked π-system. In this case the differentiation between excitonic and charge resonance states in terms of the completely delocalized MOs will be illustrated (cf. Refs 64,103,104) and state mixing, charge separation, and excimeric effects are discussed. Thirdly, excitons in poly(*para* phenylene vinylene) (PPV),

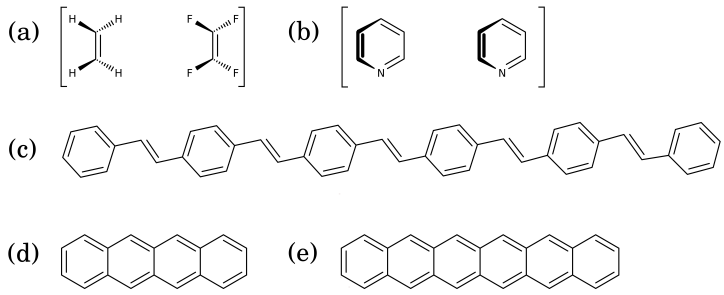

Figure 3.1: Molecular systems considered in this chapter: (a) [ethylene tetrafluoroethylene], (b) pyridine dimer, (c) $(PV)_5P$, (d) tetracene and (e) hexacene.[107]

a representative conjugated organic polymer, will be analyzed by comparing previously computed *electron-hole* correlation plots[105] with exciton sizes. Finally, polyacenes are selected as challenging test case for quantifying hidden excited-state charge-transfer character.[41,106]

3.2 Computational details

If not stated otherwise, all calculations were performed using the algebraic diagrammatic construction scheme for the polarization propagator[57] evaluated at second order in many-body perturbation theory (ADC(2))[58] using a developmental version of the Q-Chem 4.1 program package.[60,98,108] For the ethylene-tetrafluoroethylene complex and the pyridine dimer Dunning's cc-pVDZ basis set[109] was used. For computational efficiency in the cases of PPV and polyacene excited states the smaller Ahlrichs SV basis set[110] was used as it was shown by previous studies that an unpolarized basis set is sufficient to provide a qualitatively correct description of these systems.[105,111] *Electron-hole* correlation plots of the Ω_{AB} matrices (see Sec. 2.10) were created using an external program package.[64,112]

3.3 Applications

In this section a hierarchy of model systems is analyzed highlighting the power of the protocol to compute exciton sizes for a variety of applications (Fig. 3.1). First, the case of local and charge-transfer excitations in a dimer model system is discussed formally in some detail. Specific results are given for the simple case where the excitation process only consists of moving one point charge across a distance d to show that in this case $d_{exc} = d$. This relation is tested practically for the lowest CT state of a complex between ethylene (Et) and

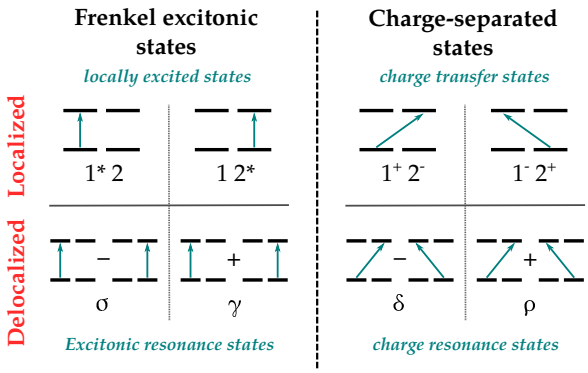

Figure 3.2: Eight limiting cases for excitation patterns emerging in the case of two chromophores with two orbitals each. Adapted from Ref. 64.

tetrafluorethylene (TFE). As a somewhat more extended example the stacked pyridine dimer at varying intermolecular separations is investigated. In this case the different behaviour between excitonic and charge resonance states and mixing between them is analyzed. After these proof-of-principle investigations two examples highlight the potential of the developed methods in the case of conjugated organic molecules are presented. On the one hand the structure of different excitons in PPV is analyzed. On the other hand the excited states of polyacenes are investigated with the aim of elucidating otherwise hidden charge-transfer contributions in their excited states.

3.3.1 Dimer model

In this section the formal structure of the exciton analysis is discussed in some detail using an idealized dimer model. For this purpose, a system of two chromophores **1** and **2** is considered, each possessing two active orbitals (see also Refs 64,103,104). Chromophore **1** contains the initial orbital i (occupied in the ground state) and the final orbital f (unoccupied in the ground state) while the orbitals on **2** are denoted i' and f'. The eight limiting cases arising for singly excited states in such a situation are depicted in Fig. 3.2. On the one hand, four linearly independent states may be constructed as local excitations on each chromophore ($|\mathbf{1}^*\mathbf{2}\rangle = |i \to f\rangle$ and $|\mathbf{12}^*\rangle = |i' \to f'\rangle$) and charge-transfer states between them ($|\mathbf{1}^+\mathbf{2}^-\rangle = |i \to f'\rangle$ and $|\mathbf{1}^-\mathbf{2}^+\rangle = |i' \to f\rangle$). On the other hand, delocalized linear combinations of these may be constructed under resonance conditions leading to Frenkel excitonic (or excitonic resonance, σ and γ) and charge-resonance states (δ and ρ). The transition density matrices $\mathbf{D}^{0I}$ for these states are shown in Tab. 3.1 for local states and in Tab. 3.2 for delocalized states, along with their ω_{CT} and d_{exc} values which are discussed

Table 3.1: Transition density matrices[a] $\mathbf{D}^{0I}$, charge-transfer measures ω_{CT}, and exciton size d_{exc} of the idealized locally excited states $|\mathbf{1}^*\mathbf{2}\rangle$ and $|\mathbf{12}^*\rangle$ and charge-transfer states $|\mathbf{1}^-\mathbf{2}^+\rangle$ and $|\mathbf{1}^+\mathbf{2}^-\rangle$ evaluated under the assumption of a unit overlap matrix.

state	$\|\mathbf{1}^*\mathbf{2}\rangle$	$\|\mathbf{12}^*\rangle$	$\|\mathbf{1}^-\mathbf{2}^+\rangle$	$\|\mathbf{1}^+\mathbf{2}^-\rangle$
$\mathbf{D}^{0I}$	$\begin{pmatrix} 0 & 1 & 0 & 0 \\ 0 & 0 & 0 & 0 \\ 0 & 0 & 0 & 0 \\ 0 & 0 & 0 & 0 \end{pmatrix}$	$\begin{pmatrix} 0 & 0 & 0 & 0 \\ 0 & 0 & 0 & 0 \\ 0 & 0 & 0 & 1 \\ 0 & 0 & 0 & 0 \end{pmatrix}$	$\begin{pmatrix} 0 & 0 & 0 & 0 \\ 0 & 0 & 0 & 0 \\ 0 & 1 & 0 & 0 \\ 0 & 0 & 0 & 0 \end{pmatrix}$	$\begin{pmatrix} 0 & 0 & 0 & 1 \\ 0 & 0 & 0 & 0 \\ 0 & 0 & 0 & 0 \\ 0 & 0 & 0 & 0 \end{pmatrix}$
ω_{CT}	0	0	1	1
d_{exc}[b]	0	0	d	d

[a] Arranged according to (i, f, i', f')
[b] Evaluated specifically for the case of two point-like orbitals separated by a distance d.

later. The non-zero entries of $\mathbf{D}^{0I}$ simply represent the individual orbital transitions as shown in Fig. 3.2. The ω_{CT} values can be extracted immediately from Tab. 3.1 and 3.2 by considering that only the off-diagonal 2×2 blocks contribute to this quantity. The locally excited and excitonic resonance states possess $\omega_{\mathrm{CT}} = 0$, while this value is one for the charge-transfer and charge-resonance states (see also Ref. 64). Let me now analytically evaluate eq. (2.25) to compute d_{exc}. First, the relevant equations will be evaluated in general, and then with respect to a model system of point-like orbitals. Starting with the $|\mathbf{1}^*\mathbf{2}\rangle$ state, the case of a local excitation on one molecule can be illustrated:

$$d^2_{exc}(|\mathbf{1}^*\mathbf{2}\rangle) = \sum_{\xi\in\{x,y,z\}} \left(M^{(2)}_{\xi,ii} + M^{(2)}_{\xi,ff} - 2 \cdot M^{(1)}_{\xi,ii} M^{(1)}_{\xi,ff} \right) \tag{3.1}$$

This equation has a simple interpretation if one assumes both orbitals to be centered at the origin ($M^{(1)}_{\xi,ii} = M^{(1)}_{\xi,ff} = 0$) and to have the same spatial extent ($M^{(2)}_{\xi,ii} = M^{(2)}_{\xi,ff} = \sigma_d^2$). Then $d_{exc}(|\mathbf{1}^*\mathbf{2}\rangle) = \sigma_d\sqrt{6}$ is simply proportional to this extent. For a charge-transfer state, *e.g.* $|\mathbf{1}^-\mathbf{2}^+\rangle$ an analogous equation but with respect to an altered set of orbitals is obtained:

$$d^2_{exc}(|\mathbf{1}^-\mathbf{2}^+\rangle) = \sum_{\xi\in\{x,y,z\}} \left(M^{(2)}_{\xi,ff} + M^{(2)}_{\xi,i'i'} - 2 \cdot M^{(1)}_{\xi,i'i'} M^{(1)}_{\xi,ff} \right). \tag{3.2}$$

The equations for the delocalized states are longer but also easy to set up. For example, for the excitonic state σ one obtains

$$\begin{aligned} d^2_{exc}(\sigma) = \frac{1}{2} \sum_{\xi\in\{x,y,z\}} \Big(& M^{(2)}_{\xi,ii} + M^{(2)}_{\xi,ff} + M^{(2)}_{\xi,i'i'} + M^{(2)}_{\xi,f'f'} \\ & - 2 \left(M^{(1)}_{\xi,ii} M^{(1)}_{\xi,ff} + M^{(1)}_{\xi,i'i'} M^{(1)}_{\xi,f'f'} - 2 \cdot M^{(1)}_{\xi,ii'} M^{(1)}_{\xi,ff'} \right) \Big) \end{aligned} \tag{3.3}$$

Table 3.2: Transition density matrices[a] $\mathbf{D}^{0I}$, charge-transfer measures ω_{CT}, and exciton size d_{exc} of the idealized Frenkel excitonic resonance states σ and γ and charge resonance states δ and ρ evaluated under the assumption of a unit overlap matrix.

state	σ	γ	δ	ρ
$\mathbf{D}^{0I} \cdot \sqrt{2}$	$\begin{pmatrix} 0 & 1 & 0 & 0 \\ 0 & 0 & 0 & 0 \\ 0 & 0 & 0 & -1 \\ 0 & 0 & 0 & 0 \end{pmatrix}$	$\begin{pmatrix} 0 & 1 & 0 & 0 \\ 0 & 0 & 0 & 0 \\ 0 & 0 & 0 & 1 \\ 0 & 0 & 0 & 0 \end{pmatrix}$	$\begin{pmatrix} 0 & 0 & 0 & 1 \\ 0 & 0 & 0 & 0 \\ 0 & 1 & 0 & 0 \\ 0 & 0 & 0 & 0 \end{pmatrix}$	$\begin{pmatrix} 0 & 0 & 0 & 1 \\ 0 & 0 & 0 & 0 \\ 0 & -1 & 0 & 0 \\ 0 & 0 & 0 & 0 \end{pmatrix}$
ω_{CT}	0	0	1	1
d_{exc}[b]	0	0	d	d

[a] Arranged according to (i, f, i', f')
[b] Evaluated specifically for the case of two point-like orbitals separated by a distance d.

which includes also some matrix elements with mixed indices. A similar situation arises for the charge-resonance states, *e.g.* for δ the exciton size takes the form

$$d^2_{exc}(\delta) = \frac{1}{2} \sum_{\xi \in \{x,y,z\}} \Big(M^{(2)}_{\xi,ii} + M^{(2)}_{\xi,ff} + M^{(2)}_{\xi,i'i'} + M^{(2)}_{\xi,f'f'} - 2 \left(M^{(1)}_{\xi,ii} M^{(1)}_{\xi,f'f'} + M^{(1)}_{\xi,ff} M^{(1)}_{\xi,i'i'} + 2 \cdot M^{(1)}_{\xi,ii'} M^{(1)}_{\xi,ff'} \right) \Big). \quad (3.4)$$

A general interpretation of the above equations can be given in the limit that the involved orbitals are points in space and that i and f, as well as, i' and f' are located at the same positions, respectively. Furthermore, without loss of generality, i and f are placed at the origin of the three-dimensional coordinate system while i' and f' are at a distance d in x-direction. This leads to the multipole matrices

$$\mathbf{M}^{(k)}_x = \mathrm{diag}(0, 0, d^k, d^k) : k \geq 1 \quad (3.5)$$

while the ones with respect to the y and z coordinates vanish. The results obtained in this way are marked as d_{exc} in Tab. 3.1 and 3.2. For locally excited states and coupled local excitations (Frenkel excitons) it holds that $d_{exc} = 0$ Å while for the charge separated states $d_{exc} = d$. In other words d_{exc} corresponds to the natural definition of a charge-transfer distance. In the remaining sections, this concept will be applied to increasingly complex cases.

3.3.2 Ethylene tetrafluoroethylene

The stacked ethylene-tetrafluoroethylene [Et$\cdots$TFE] complex (Fig. 3.1 (a)) is a prototype system for intermolecular charge transfer.[36] In this work this system serves as a first proof-of-principle application of the developed approach. For this purpose, Et and TFE are set up in a parallel face-to-face arrangement using

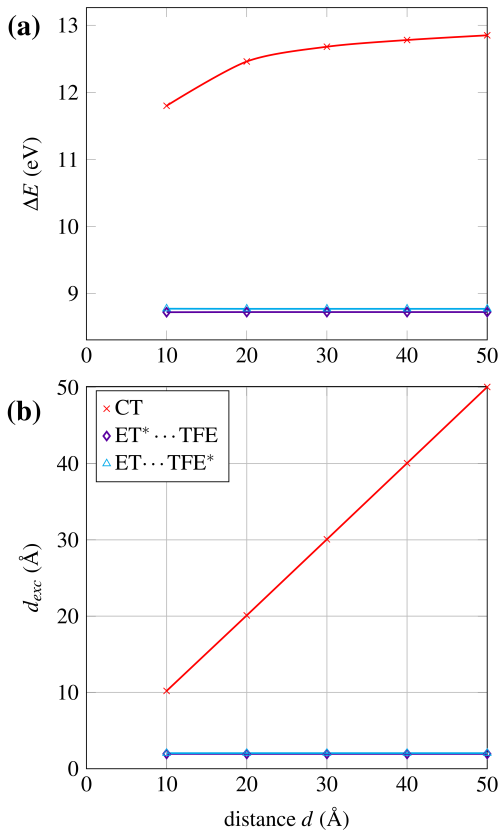

Figure 3.3: (a) Excitation energies of charge-transfer and locally excited $\pi\pi^*$ states of [Et$\cdots$TFE] and (b) exciton sizes (d_{exc}, Å) examined for varied molecular distances d (Å) at the ADC(2)/cc-pVDZ level of theory. Legend in (b) also applies to (a).

varying molecular distances between 10 and 50 Å. For comparing properties of local and charge-transfer (CT) excited states, the two lowest lying local $\pi\pi^*$ excitations on each molecule (denoted [Et$^*\cdots$TFE] and [Et$\cdots$TFE*]) and the CT state from Et to TFE [Et$^+\cdots$TFE$^-$] are investigated at the ADC(2)/cc-pVDZ level of theory.

Excitation energies and exciton sizes d_{exc} of these three states are presented in Fig. 3.3. For the local states (positioned at S_2 and S_3) the excitation energies remain constant at about 8.73 and 8.77 eV for the range considered. In contrast, the excitation energy of the CT state increases strongly according to the expected $1/d$ behaviour (where d is the intermolecular separation) as a consequence of the electrostatic attraction between *electron* and *hole*. Accordingly the relative position of this state is raised: While it is the S_9 state at $d = 10$ Å, it becomes the S_{14} state at $d = 50$ Å. Similarly to excitation ener-

gies also exciton sizes of the local states remain constant at $d_{exc} = 1.94$ and 2.04 Å for [Et$^* \cdots$TFE] and [Et$\cdots$TFE*], respectively (Fig. 3.3(b)). These values are identical to the ones obtained for the $\pi\pi^*$ excited states of isolated Et and TFE molecules. For the CT state there is a close correspondence between d and d_{exc} and only a minor difference remains due to the non-vanishing size of the molecules making d_{exc} slightly larger. For example at a distance of $d = 10$ Å the exciton size is 10.20 Å. In summary, the results are consistent with the theoretical considerations of the previous section and highlight the suitability of d_{exc} for quantifying charge transfer.

3.3.3 Pyridine dimer

Complexes of aromatic and heteroaromatic molecules are highly interesting models for biological chromophores with particular relevance to DNA.[113] The excited states of these systems are characterized by excitonic delocalization and charge transfer, and at smaller intermolecular separations exciplex interactions come into play.[114,115] However, analyzing these processes is challenging, in particular when several transitions between delocalized orbitals are involved.[64,104] The pyridine dimer[116,117] is chosen as a prototypical example: two pyridine molecules are positioned in a face-to-face arrangement, with the nitrogen atoms located on top of each other yielding C_{2v} symmetry for the total system. Due to this symmetric arrangement, all states and MOs are evenly delocalized over the system and no net charge transfer or dipole moments are present. While this is a challenging situation for standard analysis methods,[104,118] the states can be readily characterized using charge-transfer measures ω_{CT} and exciton sizes d_{exc}.

Tab. 3.3 summarizes properties of the 15 lowest lying singlet states of the pyridine dimer at 5 Å distance. The twelve lowest lying states are excitonic resonance states of $n\pi^*$ and $\pi\pi^*$ nature. These states arise as the σ and γ linear combinations (cf. Fig. 3.2) of the six low lying states of the pyridine monomer.[66,119] In all these cases ω_{CT} is very close to zero and the exciton size is about 2.5 Å. After these twelve excitonic states, the two charge separated states ($\omega_{\mathrm{CT}} \approx 0.99$) $4^1\mathrm{B}_1$ and $5^1\mathrm{A}_1$ follow. Their exciton sizes ($d_{exc} \approx 5.6$ Å) reflect extended *electron-hole* separation of these states spanning the intermolecular separation of 5.0 Å. These are the δ and ρ charge resonance states deriving from the same orbitals as the $1^1\mathrm{B}_1$ and $2^1\mathrm{A}_1$, σ and γ excitonic states, forming together a complete set of four delocalized states as described in Fig. 3.2. The last state considered is the $5^1\mathrm{B}_1$ state. This state is local in the sense that $\omega_{\mathrm{CT}} \approx 0.0$, but Tab. 3.3 reveals that its exciton size is somewhat increased compared to the previous cases ($d_{exc} = 3.81$ Å). The reason for this is the Rydberg character of this state, *i.e.* the diffuse *particle* orbital leads to an

Table 3.3: Excitation energies (ΔE, eV), oscillator strengths (f), charge-transfer measures (ω_{CT}), exciton sizes (d_{exc}, Å) and type assignment of the 15 lowest energy singlet nπ^*, $\pi\pi^*$, CT and Rydberg states of the pyridine dimer at an intermolecular separation of 5 Å at the ADC(2)/cc-pVDZ level of theory.

state	ΔE	f	ω_{CT}	d_{exc}	type
$1^1\mathrm{B}_1$	5.13	0.00	0.000	2.55	$n\pi^*$
$2^1\mathrm{A}_1$	5.13	0.00	0.000	2.55	$n\pi^*$
$1^1\mathrm{A}_2$	5.37	0.00	0.000	2.57	$n\pi^*$
$1^1\mathrm{B}_2$	5.37	0.00	0.000	2.57	$n\pi^*$
$2^1\mathrm{A}_2$	5.44	0.00	0.001	2.43	$\pi\pi^*$
$2^1\mathrm{B}_2$	5.45	0.04	0.000	2.43	$\pi\pi^*$
$2^1\mathrm{B}_1$	6.92	0.00	0.002	2.54	$\pi\pi^*$
$3^1\mathrm{A}_1$	6.95	0.04	0.000	2.53	$\pi\pi^*$
$3^1\mathrm{A}_2$	7.67	0.00	0.006	2.51	$\pi\pi^*$
$3^1\mathrm{B}_1$	7.78	0.00	0.005	2.57	$\pi\pi^*$
$3^1\mathrm{B}_2$	7.84	1.10	0.000	2.49	$\pi\pi^*$
$4^1\mathrm{A}_1$	7.92	0.92	0.008	2.72	$\pi\pi^*$
$4^1\mathrm{B}_1$	8.00	0.00	0.990	5.65	$n\pi^*$
$5^1\mathrm{A}_1$	8.00	0.02	0.984	5.63	$n\pi^*$
$5^1\mathrm{B}_1$	8.19	0.00	0.011	3.81	Rydberg

increase in exciton size.

Tab. 3.3 is used as a starting point for a scan of intermolecular separations between 2.5 and 9 Å. To reduce the complexity of the information only states of B_1 symmetry will be considered, as this irreducible representation contains both, the lowest lying excitonic and charge-resonance states. In Fig. 3.4 the relative energies, exciton sizes d_{exc}, and the ω_{CT} values of these states are plotted against the intermolecular distance d. Above distances of 6.0 Å (*i.e.* on the right hand side of Fig. 3.4) the first three excited states ($1^1\mathrm{B}_1 - 3^1\mathrm{B}_1$) are excitonic combinations of $n\pi^*$ and $\pi\pi^*$ states while $4^1\mathrm{B}_1$ is a Rydberg state and none of these states show any charge separation ($\omega_{\mathrm{CT}} = 0$). The $n\pi^*$ charge resonance state ($\omega_{\mathrm{CT}} = 1$) is the highest lying state presented here ($5^1\mathrm{B}_1$). This latter state exhibits the expected $1/d$ dependence of the total energy and a linear growth of d_{exc} comparable to the CT state $[\mathrm{Et}^+ \cdots \mathrm{TFE}^-]$ described previously. For the other states these values remain constant possessing similar values as in Tab. 3.3. In Fig. 3.4, coming from the right, the first state crossing occurs at about 5.75 Å affecting the Rydberg and the charge resonance state. This goes along with an abrupt exchange of the excited state characters of the $4^1\mathrm{B}_1$ and $5^1\mathrm{B}_1$ states as seen in Fig. 3.4 (b) and (c). Below about 5 Å direct orbital interactions come into play[104] and the clear distinction between excitonic and charge-resonance states is no longer possible. In Fig. 3.4 this effect can be

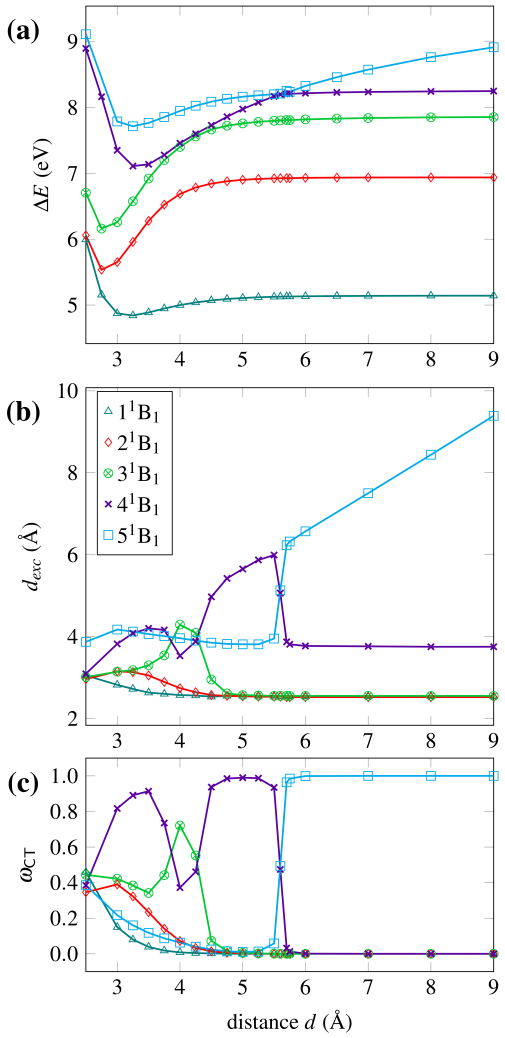

Figure 3.4: (a) Total energy relative to the ground state at infinite separation (E, eV), (b) exciton size (d_{exc}, Å), (c) charge-transfer measures (ω_{CT}) for the five energetically lowest lying $^1B_1$ states of pyridine dimer calculated at the ADC(2)/cc-pVDZ level for varied molecular distances d (Å). Legend in (b) applies to all plots in this figure.

seen by the fact that starting at around this separation the d_{exc} and ω_{CT} values of the individual states diverge from the idealized results described above. This effect is enhanced for the 3^1B_1 and the 4^1B_1 states which lie close in energy over an extended geometric range around $d = 4$ Å. Substantial coupling between these states leads to strong modulations of the d_{exc} and ω_{CT} values. At intermolecular separations below 3.5 Å excimeric effects play the dominant role. In particular the $\pi\pi^*$ states (2^1B_1 and 3^1B_1) exhibit deep potential wells at intermolecular separations below 3.0 Å. It should be noted that a quantitatively correct description of these minima cannot be guaranteed using the present computational protocol owing to potential multi-reference effects and basis set superposition error,[115] but a semi-quantitative analysis of the wave functions is certainly of highest interest. As discussed previously,[64,113,115] the energetic stabilization goes along with a significant change in wave function character, which is reflected by the fact that at smaller separations the charge-transfer measures (ω_{CT}) of all states approach a value of 0.5. This means that the differentiation between excitonic and charge separated states disappears and the resulting exciplex states are of a homogeneous and coherent nature. An analogous trend is observed for d_{exc}, which converges to about 3.0 Å for all the valence states. Only the Rydberg state (4^1B_1) retains its distinctly higher value of 3.87 Å.

In summary, the presented analysis strategy revealed a detailed picture about excited-state characters in stacked systems. It provided new quantitative information, which remained hidden when simpler analysis strategies were applied.

3.3.4 Poly(para phenylene vinylene)

Over the last decades the study of poly(*para* phenylene vinylene) has provided fundamental insight into the working principles of π-conjugated polymers used in organic electronics.[81,120,121] However, a number of questions remain open and especially the magnitude of the exciton binding energy is still discussed controversially.[122–127] Aside from the large system sizes the main barrier for computational studies lies in the fact that even when accurate excitation energies are available, an analysis of excitonic correlation effects is by far not trivial and outside the scope of standard quantum chemical approaches. One strategy used to overcome these problems is analysis of the 1TDM revealing otherwise hidden excitonic properties.[77,102,105] In this work, a more refined picture is presented by considering quantitative information through the analysis of exciton sizes.

For the description of PPV, the strategies explored in Refs 64,105 are revisited. The main tools in these investigations were the charge-transfer numbers

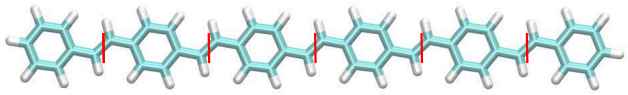

Figure 3.5: Fragmentation scheme for *electron-hole* correlation plots Ω_{AB} of $(PV)_5P$.[131]

Ω_{AB} (cf. sec. 2.10 and in particular eq. (2.48)),[64,75] which allow to visualize the correlated *electron-hole* distribution (cf. Refs 102,128–130). This analysis requires a fragmentation of the molecule into subunits, which is chosen according to "chemically intuitive" units, *e.g.* Fig 3.5. The Ω_{AB} numbers then encode the joint probability of finding the *hole* and *electron* at fragments A and B, respectively. An *electron-hole* correlation plot visualizes these probabilities and presents a coarse representation of the correlated *electron-hole* wave function (cf. Fig. 2.1 (c)). In these representations, the *hole* and *electron* positions are plotted along the horizontal and vertical axis, respectively. Elements on the main diagonal represent local excitations within one fragment, whereas charge-transfer contributions between two fragments appear as off-diagonal elements. While the CT numbers can be useful to represent excitonic structures in π-conjugated organic polymers, there are several downsides: (*i*) the results depend on the fragment definitions, (*ii*) on population analysis scheme, and (*iii*) the plots are only easily interpreted for linear molecules. Exciton sizes d_{exc} provide a more compact and clearly defined measure of *electron-hole* separation and can deliver useful additional information. A hexamer fragment of poly(*para* phenylene vinylene) termed $(PV)_5P$ was considered as a model for the spectroscopic unit in the polymer. To perform the CT number analysis, the molecule was split into six quasi-equivalent fragments by cutting through carbon-carbon double bonds (Fig. 3.5, see also Refs 64,105). The resulting correlation plots and additional information about the lowest four singlet and triplet excited states of $(PV)_5P$ are presented in Tab. 3.4.

A first visual inspection of the correlation plots for the singlet excited states directly suggests the existence of two distinct excitation patterns: The first three states ($S_1 - S_3$) resemble a series of particle-in-a-box-like excitations with increasing number of nodes subdividing the π-system into regular units (see also Ref. 92). By contrast, the S_4 state (3^1A_g) has much more pronounced off-diagonal contributions highlighting its enhanced intrinsic charge-transfer character. The same trend can also be seen in the ω_{CT} values (counting the fraction of charge separated configurations in the excited state, eq. (2.49)). For the first three states ω_{CT} lies between 0.61 and 0.51 decreasing for the higher excited states, while the value of $\omega_{CT} = 0.75$ for S_4 indicates a considerable

Table 3.4: Excitation energies (ΔE, eV), exciton sizes (d_{exc}, Å), charge-transfer measures (ω_{CT}) and *electron-hole* correlation plots Ω_{AB} of the first four singlet and triplet excited states of $(\mathrm{PV})_5\mathrm{P}$ computed at the ADC(2)/SV level.

(a) Singlets				
	$S_1(1^1B_u)$	$S_2(2^1A_g)$	$S_3(2^1B_u)$	$S_4(3^1A_g)$
ΔE	3.45	3.96	4.46	4.50
d_{exc}	6.49	5.92	5.19	10.45
ω_{CT}	0.61	0.59	0.51	0.75
Ω_{AB}				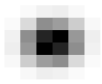
(b) Triplets				
	$T_1(1^3B_u)$	$T_2(1^3S_g)$	$T_3(2^3B_u)$	$T_4(2^3S_g)$
ΔE	2.28	2.49	2.78	3.12
d_{exc}	4.53	4.14	3.79	3.47
ω_{CT}	0.38	0.36	0.34	0.32
Ω_{AB}				

charge separation (according to the chosen fragmentation scheme).

Tab. 3.4 presents the exciton size d_{exc}, which allows for a quantitative comparison among the excited states. The sizes for the first three states are somewhat smaller than the length of the PV repeat unit (6.71 Å) while they are significantly larger than the diameter of a single phenyl ring (2.86 Å) (see Ref. 93 for a related analysis in poly(*para* phenylene)). These values are reflected in the *electron-hole* correlation plots Ω_{AB}, which show that excitations occur either locally or between adjacent fragments. With an increase of nodes perpendicular to the π-system, the *electron-hole* distance d_{exc} drops from 6.49 to 5.19 Å, which suggests that excitons become more tightly bound for higher momentum particle-in-a-box states (a similar trend is observed in Ref. 77). In comparison to the $S_1 - S_3$ states, the *electron-hole* separation of S_4 is much larger with $d_{exc} = 10.45$ Å. Previous studies[64,105] suggested that the S_4 state belongs to a distinct PPV band and the difference in d_{exc} is in agreement with this idea (see also Ref. 132 for a discussion of the different possible states).

The four triplet states show similar exciton structures as compared to the $(S_1 - S_3)$ singlets. The *electron-hole* correlation plots illustrate that the exciton wave functions have similarities to the particle-in-a-box model. However, in contrast to the singlet states, the triplets show a reduced CT character (see also Ref. 77). Accordingly, the mean *electron-hole* distances are significantly smaller and lie between 4.53 and 3.47 Å. These findings nicely reflect the contrasting exchange-correlation effects expected for singlet and triplet excitons[81] as only

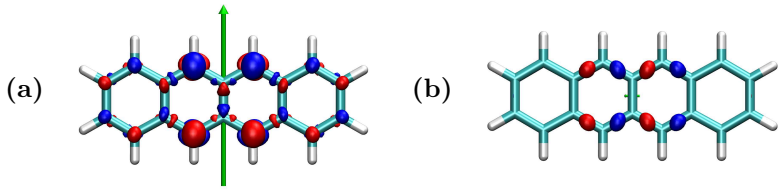

Figure 3.6: Transition densities (with isovalue 0.003 e) and transition moments shown as green arrows with volume proportional to the oscillator strength for (a) $^1\mathrm{L}_a$, and (b) $^1\mathrm{L}_b$ of tetracene.[131]

the former are affected by exchange repulsion between the *electron* and the *hole*.

3.3.5 Polyacenes

Polyacenes are a promising substance class for applications in organic electronics due to their unique electronic structure properties. However, the description of their electronic states is quite challenging.[40,41,111,133–137] In particular, in the case of the larger polyacenes open-shell character in the ground state[133] and doubly excited character in some of the excited states come into play.[134] Furthermore, there are specific problems for TDDFT even at smaller system sizes.[40,41] In the light of these considerations, a more detailed comprehension of polyacene excited states is certainly of highest interest. This work is specifically concerned with tetracene and hexacene, which have comparatively large π-systems but are still amenable to a single-reference approach.[133]

The two lowest spectroscopically relevant states, usually termed $^1\mathrm{L}_a(1^1\mathrm{B}_{2u})$ and $^1\mathrm{L}_b(1^1\mathrm{B}_{3u})$, are computed at the ADC(2) level, which has been tested previously for this purpose, cf. Ref. 134. To analyze the general character of these states, the transition densities and moments are considered in the case of tetracene (Fig. 3.6). In this representation it becomes apparent that the $^1\mathrm{L}_a$ state is polarized along the short axis (the transition moment points in this direction) and possesses a large oscillator strength ($f = 0.113$). By contrast, the $^1\mathrm{L}_b$ state is polarized along the long axis and is almost dark ($f = 0.002$). The transition density is located on the carbon atoms for the $^1\mathrm{L}_a$ state while it is centered around the bonds in the $^1\mathrm{L}_b$ case (see also Ref. 41).

To get more insight into the wave functions of these states a similar strategy as in Section 3.3.4 is adopted, that is, a decomposition in terms of charge-transfer numbers as well as the computation of d_{exc}. However, in contrast to $(\mathrm{PV})_5\mathrm{P}$ setting up the fragmentation scheme required for the charge-transfer analysis is not quite as unambiguous. The choice finally adopted is presented in Fig. 3.7. Unfortunately, it is not possible to set up chemically equivalent

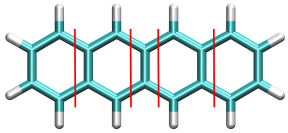

Figure 3.7: Fragmentation scheme for *electron-hole* correlation plots Ω_{AB} for tetracene. Hexacene is fragmented in analogy.[131]

fragments in this way and the obtained results should be analyzed with care. By contrast, there is no such arbitrariness in the computation of d_{exc}, which highlights the power of this approach. The results of this investigation are presented in Tab. 3.5. For both systems the $^1\mathrm{L}_a$ state is significantly lower in energy than the $^1\mathrm{L}_b$ state and possesses by far the larger oscillator strength. An inspection of the *electron-hole* correlation plots (Ω_{AB}) reveals clear differences between the states. The $^1\mathrm{L}_a$ state possesses enhanced charge separation (strong contributions on the upper left and lower right corners) and notably no contribution on the central fragment. By contrast, the $^1\mathrm{L}_b$ states possess enhanced contributions on the main diagonal (going from lower left to upper right), which derive from configurations where the *electron* and *hole* are on the same fragment. While the construction and interpretation of these correlation plots is quite involved, d_{exc} provides a more compact and simple descriptor of the dynamical charge transfer in these systems. Two trends can be observed immediately: Firstly, d_{exc} increases when going from tetracene to hexacene, meaning that there is a significant change in electronic structure between these molecules, which probably derives from confinement effects. Secondly, in both cases the charge separation for the $^1\mathrm{L}_a$ state is significantly larger when compared to the $^1\mathrm{L}_b$ state. Interestingly, it has been known for a long time that

Table 3.5: Excitation energies (ΔE, eV), oscillator strengths (f_{osc}), exciton sizes (d_{exc}, Å) and *electron-hole* correlation plots (Ω_{AB}) of tetracene and hexacene excited states computed at the ADC(2)/SV level of theory.

	Tetracene		**Hexacene**	
	$^1\mathrm{L}_a$	$^1\mathrm{L}_b$	$^1\mathrm{L}_a$	$^1\mathrm{L}_b$
ΔE	3.20	3.67	2.18	3.23
f_{osc}	0.113	0.002	0.093	0.006
d_{exc}	4.60	4.02	5.60	4.76
Ω_{AB}	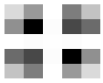	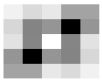		

the $^1\mathrm{L}_a$ state of polyacenes is not described well by local density functionals.[40]

This phenomenon, which has been attributed to hidden charge transfer, has since been difficult to understand in a quantitative sense.[41,106] However, the presented results show that d_{exc} does indeed find enhanced charge transfer for this state. Combined with the results of the previous sections, discussing charge separation in dimers, these findings suggest that d_{exc} carries potential as a new charge-transfer diagnostic for TDDFT (see Refs 51–54,71 for alternative strategies). The presented formalism can also be combined with TDDFT and a more detailed analysis of the excited states of acenes is presented in Chapter 5. Furthermore, the potential of d_{exc} as a diagnostic tool for direct charge-transfer and charge-resonance states is discussed.

3.4 Conclusion

The performance and predictive power of the developed exciton size d_{exc} protocol was investigated for a diverse set of applications. Quantifying exciton sizes provided insight into excited states of dimers and aggregates as well as of extended π-conjugated systems. Three examples of the first class were chosen featuring excited states with divers properties: (*i*) an analytical dimer model of two separated chromophores, (*ii*) the ethylene tetrafluoroethylene system, and (*iii*) the pyridine dimer. In the case of charge-transfer and charge-resonance states an almost perfect correspondence between exciton sizes and intermolecular separation was found, while for local and Frenkel excitonic states exciton sizes depend on the excited-state properties of the respective monomers. For pyridine dimer, exciton sizes were used to rationalize state mixing, orbital interactions, and excimeric effects, and revealed that Rydberg states possess high d_{exc} values.

As representatives for extended π-systems, two prototypical compounds, PPV and oligoacenes, were analyzed in terms of exciton sizes and related 1TDM-based properties. In both cases, a wealth of information was obtained with exciton analysis, which would have remained hidden if only the Hartree-Fock orbitals were analyzed. The findings of this chapter generally stand in good agreement with results and hypotheses by other researchers, cf. 40,41,64, 77,105,106,134. Specifically, the exciton size measure proved beneficial with respect to the analysis of dynamic charge-separation effects, *i.e.*, excitonic effects providing a more compact quantitative measure when compared to previously used *electron-hole* correlation plots.[102,105] In this context, the exciton size provided a quantitative description of *electron-hole* correlation effects, which has potential as diagnostic tool for charge-transfer interactions in time-dependent density functional methods (cf. Refs 51–54,71). The analysis of charge-transfer interactions in TDDFT calculations is analyzed in more detail in Chapt. 5, 6.

Chapter 4

Excitons in poly(*para* phenylene vinylene): A quantum-chemical perspective based on high-level *ab initio* calculations

This chapter focuses on the investigation of excited states of poly(*para* phenylene vinylene) (PPV), a prototypical π-conjugated system for which excitonic effects play a fundamental role. A high-level benchmark based on ADC(3) results confirms that the more efficient ADC(2) method is generally adequate for calculating singly excited states, but also reveals the existence of low-energy doubly excited states. For a series of oligomers with increasing lengths it is shown how confinement effects dominate excited state of small oligomers, while delocalized exciton bands emerge for larger systems. For the largest studied oligomer, $(PV)_7P$, the first twenty singlet and triplet excited states are characterized and compared to Wannier and Frenkel models. Different Wannier bands appear following a general trend that exciton sizes are lowered with increasing quasi-momentum for each band. Ultimately, triplet excitons of oligomers with different sizes are compared to their singlet counterparts. It is found that the absence of exchange repulsion results in more tightly bound triplet excitons.

Please note that parts of this chapter have already been published by Prof. Dr. Andreas Dreuw, Dr. Felix Plasser, Dr. Jan-Michael Mewes and myself in *the Journal of Physical Chemistry and Chemical Physics*, volume 18 (**2016**), pages 2548 – 2563 (Ref. 138).

4.1 Introduction

Poly(*para* phenylene vinylene) (PPV)[122,123,139–141] is an organic π-conjugated system, which plays a key role in the rapidly advancing scientific field of organic electronics due to its electronic structure.[120,121,123,130,142–145] Its simple molecular structure consisting of the two monomers phenylene and vinylene renders this molecule an ideal prototype to explore the relation between molecular structure and electronic properties. The theoretical investigation of this polymer is, however, challenging due to its large size and the involvement of complex electron correlation effects. Despite the large number of studies, there is not even qualitative consensus about the nature of the excitons. Estimates of the binding energy lie in the range from almost free charge carriers at 0.1 eV to strongly bound states at 1.0 eV.[124,125,146–148]

A wide range of computational studies of PPV have been performed in recent years covering such diverse methods as solid-state physics models,[81,147,149] semi-empirical methods,[102,120,150–152] density matrix renormalization group theory solving a Pariser-Parr-Pople model,[153,154] time-dependent density functional theory,[94,155,156] many-body Green's function theory,[84,157] correlated *ab initio* methods[105,158,159] and non-adiabatic dynamics.[160,161] These studies have elucidated the properties of this polymer from different, sometimes contradictory viewpoints. The reconciliation of these different viewpoints is arguably one of the most pressing issues in this field and could move our understanding of these systems forward considerably. The major dividing line may be drawn between the solid-state physics inspired methods and the quantum chemical methods. The former are formulated in terms of a correlated quasi-particle *electron-hole* wave function and possess the advantage of a direct connection to the picture of charge carriers, which are invoked for the understanding of electronic devices. The latter take full account of the molecular details, but are based on molecular orbitals and hence lack the direct connection to charge carriers.

In the following, a selection of quantum-chemical studies, that are best suited for a comparison with this work, are briefly summarized. As a consequence of the large system size, the first computational studies were performed using approximate, semi-empirical methods[102,120,150–152,162] such as the collective-electronic oscillator (CEO) and the Zerner's intermediate neglect of differential overlap (ZINDO) methods. These led to a coarse picture of excitonic wave functions and assignment of different bands in the excitation spectrum of PPV. Further studies reported the application of linear-response time-dependent density functional theory (TDDFT) to oligomers of PPV.[94,155,156] This method has the ability to describe excited states of fairly large systems

with twenty repeat units and more. However, this comes at the cost of a strong dependency of the results on the *xc*-functional. It was illustrated that excitons can be tuned from completely unbound electron-hole pairs to tightly bound quasi-particles by employing different *xc*-functionals.[156,163] Accurate multi-reference *ab initio* methods such as complete active space self-consistent field (CASSCF) and complete active space perturbation theory to second order (CASPT2) have only been applied to the smallest PPV oligomer, stilbene, for which the computational demand is feasible.[164,165] Although these high-level *ab initio* methods yield accurate results for small systems, a transfer of these results to extended polymers is difficult. Due to its lower computational cost, symmetry-adapted cluster-configuration interaction (SAC-CI) can afford the computation of small oligomers with up to four units.[159] In this respect, the algebraic-diagrammatic construction for the polarization propagator of second order (ADC(2)) constitutes a great improvement[105] as it allows for a description of oligomers with up to eight phenyl rings, which closely resemble the polymer with respect to its electronic properties.[162] The calculated vertical excitation energies are in good agreement with experimental data. Furthermore, it was found that defects in the oligomer chain invoked by a break in the conjugated system lead to exciton localization. In addition, the one-particle transition density matrix has been visualized to interpret the excited states in terms of an *electron-hole* picture.

In this chapter, high-level *ab initio* calculations are combined with elaborate exciton analysis tools to take advantage of, both, the molecular and quasi-particle viewpoints of excitation processes. This is realized by subjecting the computed excited-state wave functions to exciton analysis[64,65,73,78] following previous ideas in literature.[77,92,102,151] A key quantity in this analysis is the interpretation of the one-particle transition density matrix as an effective exciton wave function. The major objectives of this chapter are (*i*) to provide a high-level *ab initio* benchmark for vertical excitation energies and exciton properties on third-order level of perturbation theory (*ii*) to emulate the emergence of exciton properties for sufficiently large π-systems, and (*iii*) to systematically characterize exciton bands, both qualitatively and quantitatively.

4.2 Phenomenological models for exciton wave functions

Since high-level *ab initio* methods become prohibitively expensive for large system sizes, it is interesting to test whether reasonable results for extended systems can be obtained with more phenomenological exciton models. While

this question is only qualitatively assessed in this work, a similar methodology can in the future be used to evaluate, re-parametrize or adjust existing empirical models allowing for accurate multi-scale descriptions of large systems.

A number of excellent discussions of excitons in polymers is available in literature[93,132,144,166,167] and therefore only the concepts that are immediately relevant to this work are reviewed in the following. The central idea is to move away from the molecular-orbital picture to the quasi-particle exciton representation. This is achieved mathematically by a coordinate transformation of the exciton wave function (Fig. 2.1) into the *electron-hole* separation (or relative) coordinate $r_{he} = r_e - r_h$ and the center-of-mass (CM) coordinate $R = (r_h + r_e)/2$. Furthermore, it is assumed that these two variables are separable and the wave function can be rewritten, at least approximately, into a product of the form

$$\chi_{exc}(r_h, r_e) \approx \phi_{sep}(r_{he})\phi_{CM}(R), \tag{4.1}$$

where ϕ_{sep} describes the intrinsic *electron-hole* wave function and ϕ_{CM} the center-of-mass wave function. $\phi_{sep}(r_{he})$ describes the relative motions of two oppositely charged particles. Its solutions in a homogeneous medium will therefore possess the same shape as the wave functions of a simple hydrogen atom, only that a different effective mass and dielectric susceptibility have to be inserted. By contrast, $\phi_{CM}(R)$ describes a neutral particle, which is not subjected to any Coulomb potential. In a periodic system this yields a plane-wave solution, while in a confined molecular system a *particle-in-a-box* picture is adequate, and for more complex branched systems an exciton scattering approach[166] has been developed.

Following the above considerations, the Wannier-Mott picture of excitons in polymers can defined. In this concept, the radial wave functions $\phi_{sep}(r_{he})$ are assumed to resemble hydrogenic s, p, d etc. orbitals only that they extend in a one-dimensional space. These wave functions are indexed by a principle quantum number n. Specifically, the exciton size of the Wannier B_u excitons is expected to scale linearly with n according to[81]

$$d_{exc,n} \approx n \times d_{exc,1} \tag{4.2}$$

where $d_{exc,1}$ is the size for the primary ($n = 1$) exciton. Furthermore, the center-of-mass wave functions $\phi_{CM}(R)$ are described by the quasi-momentum quantum number j. These can be identified with *particle-in-a-box*-like wave functions possessing $j - 1$ nodal planes. In the following, Wannier excitons can be characterized by the quantum numbers n and j using the notation $W(n, j)$.

The Wannier picture assumes the presence of freely moving quasi-particles.

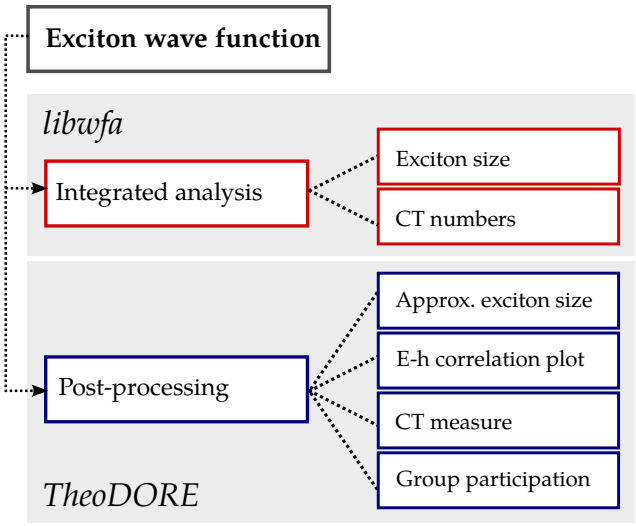

Figure 4.1: Wave function analysis software used in this chapter: the libwfa library and the TheoDORE program package.

More localized states can be rationalized using the Frenkel exciton model. This model is based on entirely different assumptions, and is discussed for PPV in detail in Ref. 168: In the Frenkel picture, the system is divided into individual sites i, and these give rise to locally excited states $|i\rangle$ that are each confined to the respective site. The excited states of the whole system are obtained as eigenstates of the Hamiltonian

$$\widehat{H}_{Frenkel} = \sum_i \varepsilon_i \, |i\rangle \, \langle i| + \sum_{ij} c_{ij} \, |i\rangle \, \langle j| \tag{4.3}$$

where ε_i are the site excitation energies and c_{ij} are the electronic couplings or transfer integrals, which are usually assumed to derive from Coulomb interactions. To understand this equation, it may be helpful to realize that the resulting Hamiltonian matrix $\langle i| \, \widehat{H}_{Frenkel} \, |j\rangle$ possesses the same structure as a matrix in Hückel theory considering only nearest neighbour couplings. Furthermore, considering close-lying ε_i values and small couplings c_{ij}, it is clear that the resulting excitation energies are closely spaced.

4.3 Computational details

All calculations were performed using variants of the algebraic diagrammatic construction (ADC) scheme for the polarization propagator.[57,58] ADC(2) and ADC(3/2) calculations were performed employing the Q-Chem 4.2 package in

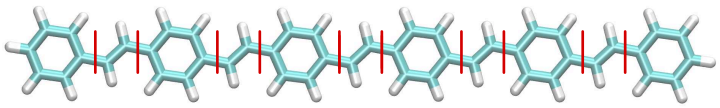

Figure 4.2: Fragmentation scheme to compute *electron-hole* correlation plots and ω_{CT} values shown for $(\mathrm{PV})_5\mathrm{P}$.[131]

a developmental version.[59,60,98,169] The abbreviation ADC(3/2) indicates that although excited-state vectors are computed at the third order of perturbation theory, the corresponding densities are computed using these vectors in combination with the second-order intermediate-state basis, cf. sec. 1.9. For these calculations, an efficient calculation of properties is possible through the intermediate state representation (ISR).[170] For larger systems and basis sets, the Turbomole 6.3.1 program package[171] was used, which affords an efficient implementation of ADC(2) exploiting the resolution-of-the-identity (RI) approximation (RI-ADC(2)).[172–174] The calculations were performed using the Ahlrichs basis sets SV, SV(P), and TZVP[110,175] to examine basis-set effects. For all calculations planar geometries were taken from Ref. 105 and C_{2h} symmetry was used throughout. In the case of the ADC calculations in Q-Chem, the wave function analysis library (libwfa)[65,73,78] was applied to directly analyze the 1TDMs as given by the ISR to compute the exciton size and charge-transfer numbers. This information was, however, not accessible in the RI-ADC computations in Turbomole. Therefore, the response vectors were read instead and processed externally by the TheoDORE 1.0 analysis package.[176] In all cases, post-processing of the results and the creation of *electron-hole* correlation plots was carried out using TheoDORE.[176] The different software used to compute the various wave function properties is summarized in Fig. 4.1. While TheoDORE is publicly available as a stand-alone package, libwfa is distributed as a part of Q-Chem 4.3. The fragmentation scheme used to compute *electron-hole* correlation plots and ω_{CT} numbers is shown in Fig. 4.2. The oligomers were cut into fragments that alternatively represent phenylene rings or vinylene groups yielding, *e.g.*, 11 fragments in the case of $(\mathrm{PV})_5\mathrm{P}$.

4.3.1 Total charge transfer

As opposed to the general definition given in eq. (2.49), the total charge transfer is calculated in this chapter according to

$$\omega_{\mathrm{CT}} = \frac{1}{\Omega} \sum_{A} \sum_{B \notin \{A-1, A, A+1\}} \Omega_{AB} \tag{4.4}$$

which means that only charge transfer between at least second-nearest neighbours is taken into account. This is motivated by the small sizes of the chosen fragments.

4.3.2 Functional group contribution

The functional group contribution may be regarded as a specific fragmentation scheme, where the fragments are identified as the functional groups. This is particularly interesting as PPV is composed of two distinct monomer building blocks, the phenyl ring (P) and the vinylene group (V). In the fragmentation scheme, the P and V contributions are separated and the partial summation

$$\omega_P = \frac{1}{2\Omega} \sum_{P \in \mathcal{P}} \sum_{A} (\Omega_{AP} + \Omega_{PA}) \tag{4.5}$$

is performed, where P runs over the set of phenyl rings $\mathcal{P}$ while A runs over all fragments. ω_P, ranging from 0 to 1, counts the total participation of all phenylene groups to both, *electron* and *hole* of an excitation. Technically, this summation is realized by dividing the system into two formal fragments, one related to all phenyl rings and one to all vinylene groups and counting the excitation contributions that go from and to these fragments.

4.4 Results and discussion

In this section a detailed analysis of the excited states of poly(*para* phenylene vinylene) oligomers is presented. Firstly, a high-level benchmark of the excitation energies is presented and the role of double excitations is addressed. Secondly, the low-lying excited states of oligomers from two to eight phenyl rings are discussed. These oligomers emulate spectroscopic units, which help to explain the properties of the polymer.[121,140,177] In these cases a detailed analysis of the different excited states is carried out. Special attention is devoted to the emergence of exciton bands, which are illustrated by employing visual representations, as well as numerical descriptors of the excitations. Thirdly, a large-scale analysis including twenty singlet and twenty triplet excited states of $(PV)_7P$ is performed and the results are interpreted within the exciton models discussed above (Section 4.2). Ultimately, triplet excitons are investigated for oligomers of small to large chains in analogy to their singlet counterparts.

4.4.1 High-level benchmark of singly and doubly excited states

The discussion starts with high-level benchmark calculations performed at the ADC(3) level of theory.[169,178,179] ADC(3) is a polarization-propagator based excited-state method that consistently treats terms to the polarization propagator up to the third order in perturbation theory, cf. sec. 1.9. It provides a very accurate, third-order description of singly excited states, which are the primary focus of this chapter. Also the description of doubly excited states is reasonably accurate and correct to first order of perturbation theory.[59] ADC(2) on the contrary treats all terms at one order of perturbation theory lower than ADC(3). To keep the computational cost at an affordable level, the ADC(3) computations are limited to the smallest three oligomers investigated, *i.e.*, stilbene to $(PV)_3P$.

Vertical excitation energies, oscillator strengths as well as additional excited-state descriptors computed at the ADC(3)/SV(P) level are presented in Tab. 4.1 and compared to the analogous ADC(2)/SV(P) results. In this analysis the double excitation character is of particular interest and two different values are used for its quantification. On the one hand, the Ω value, defined as the squared norm of the 1TDM,[65,90] is used providing a universal method-independent measure for single excitation character. On the other hand, the weight of the single excitation amplitudes t_1 is used, which is straightforward to extract from a computation but possesses a meaning only within a chosen computational protocol. Fortunately, as seen in Tab. 4.1, the numbers are very similar with the only exception that t_1 is always slightly larger than Ω.

For the smallest oligomer PVP (*i.e.* stilbene, $n = 1$) the excitation energies of the first three excited states are shifted down by about -0.2 eV when going from ADC(2) to ADC(3). Furthermore, there is a notable transfer of oscillator strength: While the 1^1B_u state is by far the brightest state in the ADC(2) calculation, there is an even distribution of oscillator strength between the 1^1B_u and 2^1B_u states for ADC(3). The remaining values for the first three states shown in Tab. 4.1 are rather similar for both methods, and this is also true for the *electron-hole* correlation plots shown in Fig. 4.4.1. After these three singly excited states, there are a number of low-energy doubly excited states found with ADC(3), which are missing in the ADC(2) spectrum. A doubly excited state (3^1A_g, $\Omega = 0.19$) is found at 4.66 eV with ADC(3). The excitation energy of this state stands in agreement with both, the experimental value of 4.84 eV, which was predicted by two-photon absorption,[180] and calculations on the CASPT2 level of theory with a vertical excitation energy of 4.95 eV.[165] Since the analysis protocols of the 1TDM are not applicable to doubly excited

Table 4.1: Vertical excitation energies (ΔE, eV) and oscillator strengths (f) and a selection of excited-state descriptors for $(PV)_nP$ singlet states with $n = 1$ to 3 calculated at the ADC(2)/SV(P) and ADC(3)/SV(P) levels of theory.

n	method	state	ΔE	f	Ω	t_1	ω_{CT}	d_{exc}
1	ADC(3)	1^1B_u	4.449	0.514	0.80	0.86	0.09	3.61
	ADC(2)	1^1B_u	4.543	1.082	0.85	0.91	0.14	4.01
	ADC(3)	2^1A_g	4.544	0	0.75	0.81	0.06	3.28
	ADC(2)	2^1A_g	4.844	0	0.83	0.90	0.06	3.33
	ADC(3)	2^1B_u	4.629	0.610	0.81	0.87	0.10	3.67
	ADC(2)	2^1B_u	4.854	0.089	0.83	0.90	0.08	3.41
	ADC(3)	3^1A_g	4.659	0	0.19	0.20	(0.29)	(4.59)
	ADC(2)	–						
	ADC(3)	3^1B_u	5.652	0.010	0.23	0.24	(0.04)	(3.88)
	ADC(2)	–						
	ADC(3)	5^1A_g	6.108	0	0.82	0.87	0.07	3.51
	ADC(2)	3^1A_g	6.106	0	0.83	0.89	0.24	4.52
	ADC(3)	6^1A_g	6.336	0	0.77	0.81	0.14	3.90
	ADC(2)	–						
2	ADC(3)	2^1A_g	3.758	0	0.16	0.17	(0.45)	(6.28)
	ADC(2)	–						
	ADC(3)	1^1B_u	3.819	1.982	0.83	0.90	0.22	4.81
	ADC(2)	1^1B_u	3.814	2.068	0.83	0.90	0.26	5.16
	ADC(3)	2^1B_u	4.251	0.115	0.74	0.80	0.10	3.70
	ADC(2)	2^1B_u	4.526	0.033	0.82	0.89	0.10	3.72
	ADC(3)	3^1A_g	4.498	0	0.75	0.81	0.08	3.55
	ADC(2)	2^1A_g	4.780	0	0.83	0.90	0.09	3.72
	ADC(3)	5^1A_g	4.992	0	0.85	0.90	0.14	4.00
	ADC(2)	3^1A_g	4.967	0	0.83	0.89	0.30	5.35
3	ADC(3)	2^1A_g	3.460	0	0.14	0.15	(0.51)	(7.34)
	ADC(2)	–						
	ADC(3)	1^1B_u	3.504	2.963	0.83	0.90	0.26	5.43
	ADC(2)	1^1B_u	3.487	2.959	0.82	0.90	0.32	5.86
	ADC(3)	2^1B_u	3.886	0.001	0.16	0.16	(0.45)	(6.32)
	ADC(2)	–						
	ADC(3)	3^1A_g	4.184	0	0.75	0.81	0.11	3.92
	ADC(2)	2^1A_g	4.310	0	0.84	0.90	0.23	4.90
	ADC(3)	3^1B_u	4.224	0.079	0.74	0.80	0.10	3.84
	ADC(2)	2^1B_u	4.495	0.029	0.82	0.89	0.11	3.93
	ADC(3)	6^1A_g	4.389	0	0.81	0.87	0.17	4.40
	ADC(2)	3^1A_g	4.516	0	0.82	0.89	0.17	4.57

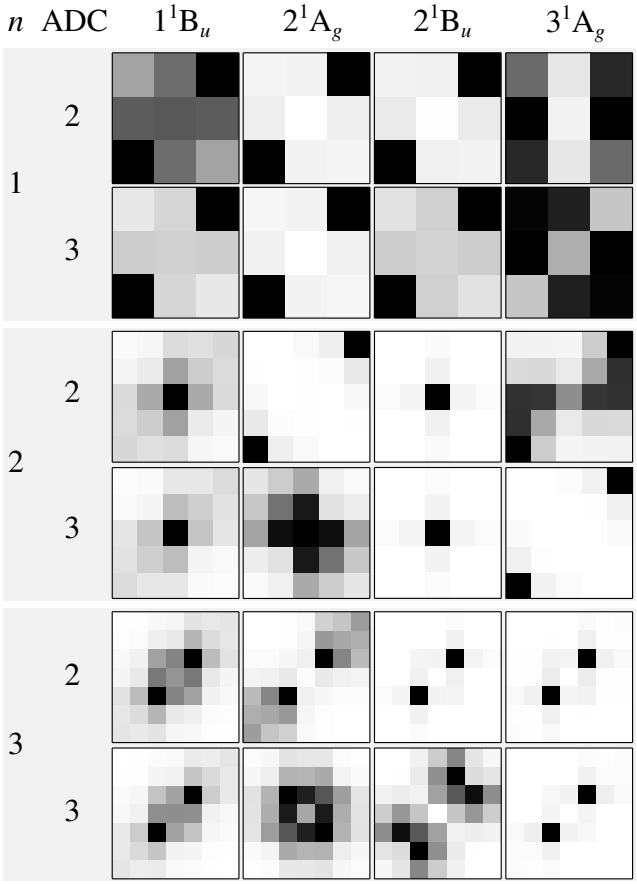

Figure 4.3: *Electron-hole* correlation plots of the first four electronically excited states of $(PV)_nP$ oligomers with $n = 1, 2, 3$ calculated at the ADC(2)/SV(P) and ADC(3)/SV(P) levels of theory. Only the plots corresponding to singly excited states are shown in the case of ADC(3) and the state nomenclature refers to the ADC(2) states.

Table 4.2: Vertical excitation energies (eV) of the first optically allowed 1^1B_u state of $(PV)_nP$ oligomers with $n = 1, ..., 4$.

state	method	$n = 1$	$n = 2$	$n = 3$	$n = 4$
1^1B_u	exp.	4.15[a]	3.50[b]	3.20[b]	3.05[b]
	exp.[c]	4.19	3.69	3.47	3.35
	ADC(2)/SV(P)	4.54	3.81	3.49	3.32
	ADC(3)/SV(P)	4.45	3.82	3.50	-
	SAC-CI/6-31G(d)[d]	4.21	3.57	3.18	3.09

Data taken from [a]Ref. 184, [b] Ref. 185, [c] Ref. 186, [d] Ref. 159.

states and their character is not discussed further here. However, it should be noted that analysis methods of two-body densities have been indeed introduced in literature.[181–183] By contrast, at the ADC(2) level the 3^1A_g state is located at 6.10 eV and possesses single excitation character. It is the counterpart of the fifth totally symmetric state 5^1A_g at the ADC(3) level. While the amount of single excitation character of this state is the same for both methods, the exciton properties differ significantly. Inspecting the *electron-hole* correlation plot for the 5^1A_g state (see Fig. 4.4.1), dominant contributions on the phenyl rings are found, but also charge transfer between the rings and towards the vinylene group is present.

Going to the second oligomer $(PV)_2P$, the differences between ADC(2) and ADC(3) are more pronounced: For ADC(3) already the first excited state (2^1A_g) is a dark doubly excited state ($f = 0$, $\Omega = 0.16$). The assumption that this state indeed lies below the bright 1^1B_u state is contradictory to the observation of luminescence in PPV oligomers. However, geometric and environmental effects as well as methodological uncertainty can easily cause a shift by a few tenths of eV which would again establish the bright state as the lowest-energy state. The remaining states are only slightly displaced in energy and the oscillator strengths are almost unaltered. In the case of 1^1B_u a slight lowering of ω_{CT} and d_{exc} is observed for ADC(3) indicating a small reduction in charge-transfer character. Furthermore, the Ω values of the 2^1B_u and 3^1A_g states are lowered to about 0.75, which indicate an enhanced admixture of double excitation character.

In the case of $(PV)_3P$ the lowest excited state at the ADC(3) level is again a doubly excited 2^1A_g state and as well a doubly excited 2^1B_u state comes into play. By contrast, the bright 1^1B_u state is more or less unaltered with only a small blue shift and a slightly diminished CT character as indicated by ω_{CT} and d_{exc}.

The computed results and experimental data is compared for the 1^1B_u state for oligomers with up to five phenyl rings (cf. Tab. 4.2). There exist some

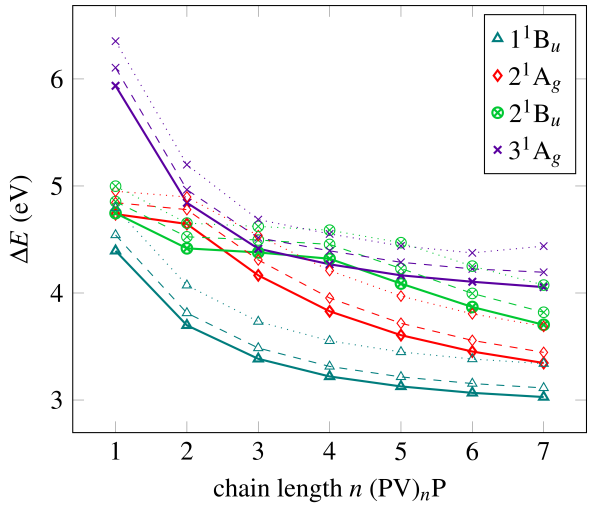

Figure 4.4: Vertical excitation energies (ΔE, eV) of poly(*para* phenylene vinylene) oligomers of increasing chain length computed at the RI-ADC(2)/SV (dotted lines), RI-ADC(2)/SV(P) (dashed lines) and RI-ADC(2)/TZVP (solid lines) levels of theory.

controversial experimental values from Hohlneicher et al.,[184] Woo et al.[185] and Gierschner et al.,[186] which deviate increasingly as a function of chain length. The results of this work agree very well with the data from Gierschner et al., while previous SAC-CI calculations[159] agree much better with the first series by the other researchers. As will be shown below, excitation energies are somewhat lowered with larger basis sets shifting the results more towards Refs. 184,185. Despite some deviations, experimental data confirms the accuracy of ADC(2) for these systems as far as energies, oscillator strengths, and wave functions of singly excited states are concerned. The ADC(3) results, however, give rise to a new perspective onto low-energy doubly excited states. The presence of such states is not necessarily surprising considering their importance for other related systems, *e.g.* polyenes[187,188] or polyacenes.[134] To our knowledge, however, they have only received little attention so far. It would be of particular interest to explore whether these states have a connection to singlet fission observed in PPV,[189,190] *i.e.* the generation of two charge carrier pairs from one photon. However, this question has to be postponed to future studies.

4.4.2 Excitons in PPV oligomers of increasing size

After establishing ADC(2) as reliable method for computing primarily singly excited states in PPV, excited states of PPV oligomers of varying size will now be analyzed. Excitation energies of the first four singlet excited states of

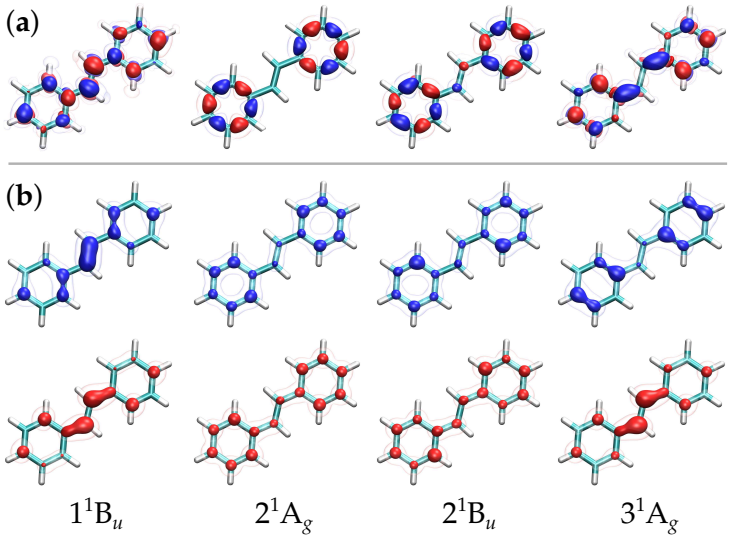

Figure 4.5: (a) Transition, (b) *hole* and *electron* densities of first four excited states of stilbene calculated at the ADC(2)/SV(P) level of theory. Isovalues are 0.003 and 0.001 e, negative (*hole*) densities in blue, positive (*electron*) densities in red.[131]

oligomers with $(PV)_nP$ chains from $n = 1$ to 7 are presented in Fig. 4.4 at the RI-ADC(2) level in combination with three basis sets SV, SV(P) and TZVP. In all cases the lowest excited state is the 1^1B_u state which is significantly lowered in energy for increasing length of the π-conjugated system, *e.g.* from approximately 4.5 to 3.0 eV in the TZVP basis. This lowering in energy can be rationalized by considering the diminished gap between the frontier molecular orbitals, or by a reduction in kinetic energy[154] deriving from delocalization. For all systems except for the $(PV)_2P$ oligomer, the second lowest state is the 2^1A_g, and similarly to the 1^1B_u state a significant decrease in excitation energy and a convergence for larger chains is observed. The 2^1B_u energies decrease unsteadily, being similar to the 2^1A_g ones first, and clearly above them for larger oligomers. The highest-energy state in this series is the 3^1A_g state for all oligomers. It has an excitation energy of $\Delta E = 6.38$ eV for PVP in the TZVP basis, and the energy curve significant drops until $(PV)_3P$, and stays rather flat for larger oligomers. The shape of the energy curve is somewhat similar to the 1^1B_u energy curve. Reducing the number of basis functions does not change the qualitative trends of the curves, but systematically raises the excitation energies. The SV(P) curves (dashed lines) lie about +0.12 eV higher than the TZVP reference, while the SV curves (dotted lines) are shifted by about +0.32 eV. These results stand in agreement with the findings of Ref. 105.

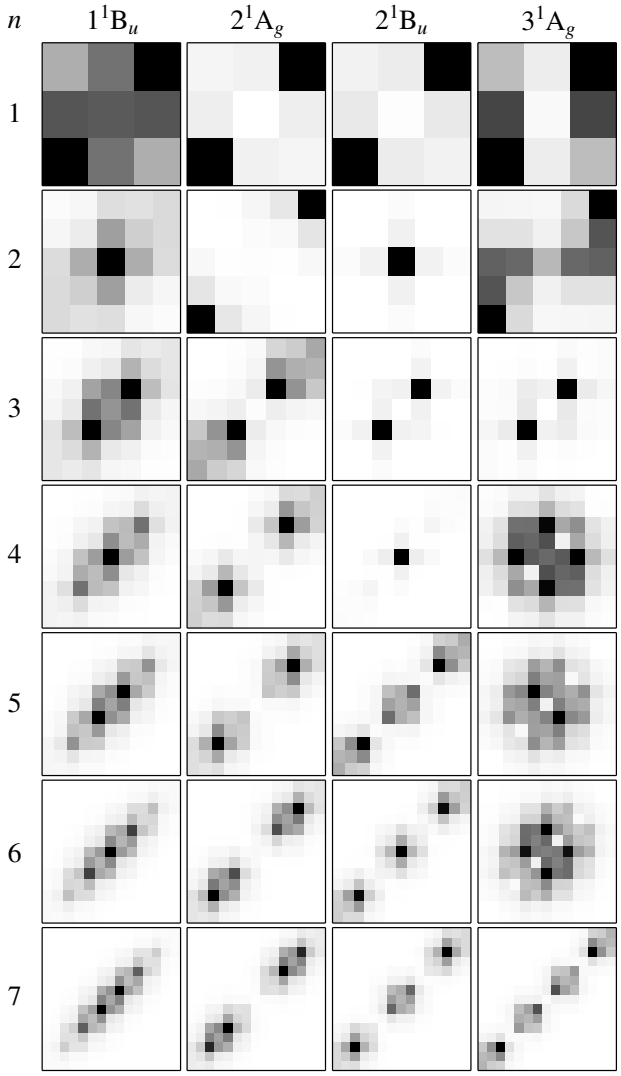

Figure 4.6: *Electron-hole* correlation plots of the first four excited states of PPV oligomers computed at the RI-ADC(2)/TZVP level of theory.

The characters of the singlet states involved for the different oligomers can be interpreted by analyzing the *electron-hole* correlation plots of the Ω_{AB} matrices (cf. Fig. 2.1 (c)). The first four singlet excited states of each oligomer are analyzed, see Fig. 4.6. In this figure the excited states are ordered according to their symmetry, which does not necessarily coincide with an arrangement of increasing excitation energies. In the case of the smallest system, stilbene or PVP, the *electron-hole* correlation plots contain a 3 x 3 matrix where the main diagonal goes from the lower left to the upper right. On the main diagonal the first and third element represent the probability for local excitations at the phenyl rings and the central element displays this probability for the vinylene group. Charge transfer between these functional groups is indicated in the respective off-diagonal fields. In the first row going from left to right, the $1^1\mathrm{B}_u$ state is delocalized over the entire PVP molecule and both, charge transfer and local excitation character are present. The $2^1\mathrm{B}_u$ and $2^1\mathrm{A}_g$ states, in contrast, show predominantly local excitation character. The two states represent a pair of excitonic resonance states (see *e.g.* Ref. 73) consisting of one positive and one negative linear combination of locally excited states at the phenyl rings. The fourth state of stilbene is the $3^1\mathrm{A}_g$ state and possesses a different excitation pattern compared to the previous ones. In this case, local contributions at the phenyl rings are found as well as charge-transfer contributions between each phenyl ring and the vinylene group.

To relate the *electron-hole* correlation plots to more common representations of excited states, the transition densities as well as the *electron* and *hole* densities[65,66] for the four states of stilbene are plotted in Fig. 4.5. The transition density is the diagonal part of the 1TDM, where the *electron* and *hole* are at the same location in space ($r_h = r_e$). This, in turn, means that the main diagonals in the *electron-hole* correlation plots are a coarse representation of the transition densities. Inspecting the plots in Fig.s 4.5 and 4.6, a close correspondence between the different representations can be found. In particular, it is observed that in all cases there are important contributions on the phenyl rings while only the first state ($1^1\mathrm{B}_u$) possesses significant vinylene participation. The *electron* and *hole* densities correspond to partial summations of the Ω-matrices over individual rows or columns, respectively. Also in this case a correspondence between the representations can be observed and it is possible to get an impression about the state character. If the *electron* and *hole* densities are rather similar, charge transfer is only involved to a smaller extent (*e.g.* $2^1\mathrm{A}_g$ and $2^1\mathrm{B}_u$), while large differences in their spatial distribution indicate a more pronounced charge transfer (*e.g.* $1^1\mathrm{B}_u$ and $3^1\mathrm{A}_g$). The advantage of the *electron-hole* correlation plot is, however, that it collects all the presented aspects in one representation, and also contains crucial information

about dynamic charge transfer.

Going to the second row in Fig. 4.6, the matrix is increased by one phenylene and one vinylene to 5×5. The first 1^1B_u state is slightly delocalized over the entire system with a dominant contribution on the central phenylene unit. Some charge transfer occurs, mostly between direct and second-nearest neighbours. In contrast, the second and third state of this system have dominantly local nature, concentrated on the terminal and central phenyl rings, respectively. The fourth excited state 3^1A_g shows enhanced charge-transfer character, where mostly the terminal phenyl rings are involved. The asymmetric pattern with respect to the main diagonal arises from a directed transfer of electron density from the terminal phenyl rings to the inner vinylene and phenylene groups.

In $(PV)_3P$, the first two states are delocalized similar to the 1^1B_u states of the smaller systems and *electron* and *hole* are not separated by more than three functional units. However, a new feature is observed for the 2^1A_g state: A nodal plane perpendicular to the main diagonal is found. This phenomenon, which will appear more prominently for the larger oligomers, is interpreted as a *particle-in-a-box*-like state of higher quasi-momentum. The third and fourth state of the $(PV)_3P$ molecule are again a pair of excitonic resonance states at the central two phenyl rings and the two states are quasi-degenerate.

For $(PV)_4P$, the first two states are again delocalized and the third state is a local excitation at the central phenyl ring. Interestingly for the fourth state 3^1A_g, a new excitation pattern is found. In this case, major CT contributions over larger separations play a dominant role. On the main diagonal there are only three small contributions of the phenyl groups around the center. Such kind of distinct intrinsic *electron-hole* structure was earlier assigned to a distinct Wannier exciton band[73,105] and in the above-defined nomenclature it corresponds to a $W(2,1)$ state. In accordance with predictions of Mukamel et al.[162] at this chain length some of the bulk properties start to become apparent.

Going to larger chains with $n > 4$, the exciton wave function patterns reappear and enhanced electronic coherence is present. The exclusively local states are no longer observed for $n \geq 5$ and in the case of $(PV)_7P$ also the charge-separated state disappears and only four similar looking Wannier states, $W(1,j)$ with j between 1 and 4 remain. The other types of states are located at higher relative energies as will be examined in Section 4.4.3.

While the previous analysis gave an intuitive visual representation of the excited states, let me now proceed to a more compact quantitative analysis. For this purpose different excited-state descriptors will be applied to the same set of computations (see Chapter 2 and Section 4.3 for definitions of descriptors). The exciton sizes ($\widetilde{d}_{exc}$) are presented in Fig. 4.7 (a). In case of the 1^1B_u, 2^1A_g

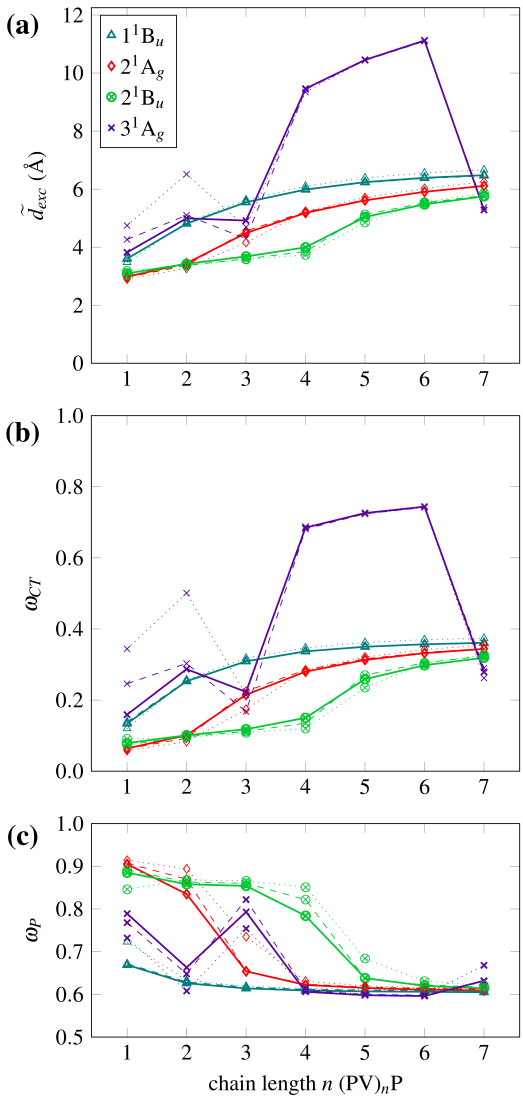

Figure 4.7: (a) Approximate exciton sizes ($\widetilde{d}_{exc}$, Å), (b) charge-transfer measures (ω_{CT}) and (c) functional group contribution ω_P of excited states of poly(*para* phenylene vinylene) oligomers of increasing chain length computed at the RI-ADC(2)/TZVP (solid lines) RI-ADC(2)/SV(P) (dashed lines) and RI-ADC(2)/SV (dotted lines) levels of theory.

and 2^1B_u states these increase steadily with growing system size until they converge against values between 5 and 6 Å. As a common trend, it is observed that the exciton sizes decrease with more nodes perpendicular to the main diagonal as seen in Fig. 4.6, *i.e.* with a higher translational quantum number j. Contrary to the three lower-energy states, the 3^1A_g states show larger fluctuations in exciton sizes with a minimal value of 4.92 Å for $(PV)_3P$ and a large jump to 9.46 Å for $(PV)_4P$ until the value once again drops to 5.28 Å for $(PV)_7P$. These variations follow the changes in state character as presented in Fig. 4.6. The charge-separated 3^1A_g states of $W(2,1)$ character found for $n = 4, 5, 6$ possess large exciton sizes of about 10 Å while the lowering in the case of $n = 7$ coincides with the appearance of the $W(1,4)$ exciton. A more detailed understanding of the variations in state characters could be gained by computing higher excited states, which is postponed the next section. An important conclusion of Fig. 4.7 (a) is that the exciton size saturates at about 6 Å and does not increase further with increasing system size. A similar trend was found for a variety of polymers in a related study, only that a somewhat larger saturation size was found with the chosen computational protocol.[191]

The charge-transfer measures shown in Fig. 4.7 (b) are largely consistent with the exciton sizes with some small differences observed only on closer inspection. For example for large oligomers, the three lower energy states 1^1B_u, 2^1A_g and 2^1B_u converge to almost the same value of $\omega_{\mathrm{CT}} \approx 0.33$ while a clear separation exists between them with respect to the d_{exc} values. The general consistency between the $\widetilde{d}_{exc}$ and ω_{CT} values facilitates the interpretation of the results by transmitting a clear connection between pictorial representations and quantitative analysis of the exciton wave functions. However, the close correspondence between these values shows that in future studies, it may suffice to compute exciton sizes.

Ultimately, the functional group contribution as defined in eq. (4.5) is discussed, see Fig. 4.7 (c). This descriptor accounts for the fraction of excitation that takes place at all phenylene groups of the system, *e.g.* a high value in ω_P indicates that the excitation mostly occurs at the phenyl rings. In the case of the 1^1B_u states, it is almost constant with values sightly above 0.6. For the other states, the values vary depending on the exciton wave function character as examined in the *electron-hole* correlation plots. If the states are predominantly locally confined at the phenyl rings, they possess high ω_P values ≥ 0.8. However, the values become smaller with increasing chain length indicating that a delocalization over adjacent vinylene groups becomes more important. Interestingly, the charge-transfer 3^1A_g states for $(PV)_nP$ with $n = 5, 6$ show the same amount of phenylene contribution as the other exciton states, although they are assumed to belong to a different band. Summarizing the findings,

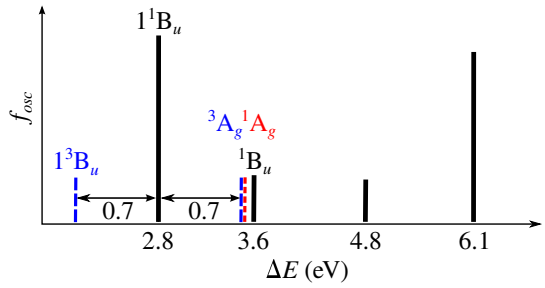

Figure 4.8: Schematic excitation spectrum and dark states of PPV deduced from experiment.[192–196] Peaks visible in the absorption spectrum are indicated by solid black lines, dark states are indicated by dashed lines, where red corresponds to singlet and blue to triplet states.

major differences in ω_P can be associated with Frenkel ($\omega_P \geq 0.8$) or Wannier nature of the states where different Wannier bands exhibit similar behaviour in terms of ω_P.

To estimate basis-set effects on the excited-state descriptors, the values are recalculated at the RI-ADC(2)/SV(P) and RI-ADC(2)/SV levels of theory and the results are shown in Fig. 4.7 as dashed and dotted lines, respectively. The results are largely consistent with the TZVP results for the large oligomers. However for the smallest three oligomers, significant deviations from the TZVP reference are found for the 3^1A_g state hinting on differences in the state character in this case. For the RI-ADC(2)/SV(P) results the mean absolute error for $\widetilde{d}_{exc}$ is 0.16 Å (mean error −0.09 Å) and for ω_{CT} it amounts 0.01 (mean error 0.00).

Summarizing the results of this section, it was found that for large π-conjugated systems a band picture emerges featuring different types of excitons, while for smaller oligomers excited states are spatially confined.

4.4.3 Systematic study of $(PV)_7P$ excitons

In the previous section, various exciton patterns are revealed for the low-lying excited states of different oligomers. To understand their significance in more detail, it is necessary to arrange them in a more systematic way. For this purpose, the largest compound presented above, $(PV)_7P$, is chosen and its higher excited states are studied. The first twenty singlet and twenty triplet states are computed at the RI-ADC(2)/TZVP level of theory and analyzed using the methods discussed previously. Furthermore, the results are analyzed with respect to the phenomenological models discussed in Section 4.2.

To relate the results of this study to experimentally determined properties

Table 4.3: Vertical excitation energies (ΔE, eV), oscillator strengths (f), weight of the single excitation amplitudes (t_1), charge transfer (ω_{CT}), exciton size ($\widetilde{d}_{exc}$), phenyl group participation (ω_P), and type assignments computed for $(\mathrm{PV})_7\mathrm{P}$ singlet excited states at the RI-ADC(2)/TZVP level of theory.

	state	ΔE	f[1]	t_1	ω_{CT}	$\widetilde{d}_{exc}$	ω_P	type[2]
1	$1^1\mathrm{B}_u$	3.028	6.212	0.93	0.36	6.48	0.61	W(1,1)
2	$2^1\mathrm{A}_g$	3.346	0	0.93	0.34	6.11	0.61	W(1,2)
3	$2^1\mathrm{B}_u$	3.703	0.654	0.93	0.32	5.75	0.61	W(1,3)
4	$3^1\mathrm{A}_g$	4.055	0	0.93	0.28	5.28	0.63	W(1,4)
5	$4^1\mathrm{A}_g$	4.070	0	0.90	0.75	11.59	0.60	W(2,1)
6	$3^1\mathrm{B}_u$	4.254	0.000	0.90	0.69	10.01	0.61	W(2,2)
7	$4^1\mathrm{B}_u$	4.309	0.101	0.92	0.16	4.16	0.78	F
8	$5^1\mathrm{B}_u$	4.344	0.033	0.91	0.15	4.39	0.84	F
9	$5^1\mathrm{A}_g$	4.356	0	0.91	0.14	4.10	0.84	F
10	$6^1\mathrm{A}_g$	4.361	0	0.91	0.14	4.08	0.84	F
11	$6^1\mathrm{B}_u$	4.390	0.026	0.91	0.15	4.29	0.84	F
12	$7^1\mathrm{A}_g$	4.399	0	0.91	0.17	4.46	0.83	F
13	$7^1\mathrm{B}_u$	4.498	0.173	0.92	0.23	4.82	0.70	W(1,5)
14	$8^1\mathrm{A}_g$	4.511	0	0.90	0.63	8.89	0.62	W(2,3)
15	$9^1\mathrm{A}_g$	4.670	0	0.92	0.11	3.68	0.86	F
16	$8^1\mathrm{B}_u$	4.688	0.013	0.92	0.13	3.92	0.87	F
17	$9^1\mathrm{B}_u$	4.771	0.005	0.90	0.62	8.19	0.61	W(2,4)
18	$10^1\mathrm{A}_g$	4.829	0	0.93	0.23	4.67	0.66	W(1,6)
19	$10^1\mathrm{B}_u$	4.866	0.224	0.90	0.88	20.73	0.60	W(3,1)
20	$11^1\mathrm{A}_g$	5.037	0	0.89	0.60	7.56	0.58	W(2,5)

[1] All bright states shown are polarized along the chain axis.

[2] Assignment as Wannier exciton $W(n, j)$ or Frenkel exciton F, see Section 4.2.

Table 4.4: Vertical excitation energies (ΔE, eV), weight of the single excitation amplitudes (t_1), charge transfer (ω_{CT}), exciton size ($\widetilde{d}_{exc}$), phenylene group participation (ω_P), and type assignments computed for $(\mathrm{PV})_7\mathrm{P}$ triplet excited states at the RI-ADC(2)/TZVP level of theory.

	state	ΔE	t_1	ω_{CT}	$\widetilde{d}_{exc}$	ω_P	type[1]
1	$1^3\mathrm{B}_u$	2.123	0.98	0.22	4.98	0.55	$W(1,1)$
2	$1^3\mathrm{A}_g$	2.248	0.98	0.20	4.63	0.55	$W(1,2)$
3	$2^3\mathrm{B}_u$	2.429	0.98	0.17	4.25	0.55	$W(1,3)$
4	$2^3\mathrm{A}_g$	2.652	0.98	0.14	3.90	0.54	$W(1,4)$
5	$3^3\mathrm{B}_u$	2.903	0.98	0.12	3.57	0.53	$W(1,5)$
6	$3^3\mathrm{A}_g$	3.166	0.98	0.09	3.26	0.50	$W(1,6)$
7	$4^3\mathrm{B}_u$	3.418	0.98	0.07	3.00	0.42	$W(1,7)$
8	$4^3\mathrm{A}_g$	3.869	0.98	0.05	2.98	0.83	$W(1,8)$
9	$5^3\mathrm{B}_u$	4.070	0.98	0.03	2.68	0.74	$W(1,9)$
10	$5^3\mathrm{A}_g$	4.174	0.96	0.82	13.17	0.60	$W(2,1)$
11	$6^3\mathrm{A}_g$	4.268	0.98	0.06	3.00	0.77	$W(1,10)$
12	$6^3\mathrm{B}_u$	4.282	0.97	0.15	4.51	0.85	F
13	$7^3\mathrm{A}_g$	4.296	0.98	0.13	4.18	0.86	F
14	$7^3\mathrm{B}_u$	4.301	0.97	0.15	4.39	0.85	F
15	$8^3\mathrm{B}_u$	4.348	0.98	0.14	4.30	0.85	F
16	$8^3\mathrm{A}_g$	4.351	0.98	0.10	3.59	0.86	F
17	$9^3\mathrm{A}_g$	4.371	0.98	0.09	3.48	0.80	F
18	$9^3\mathrm{B}_u$	4.389	0.96	0.71	10.88	0.63	$W(2,2)$
19	$10^3\mathrm{B}_u$	4.504	0.99	0.03	2.51	0.75	F
20	$10^3\mathrm{A}_g$	4.594	0.98	0.22	5.67	0.80	F

[1]Assignment as Wannier exciton $W(n,j)$ or Frenkel exciton F, see Section 4.2.

of excited states of PPV, the latter are briefly summarized, cf. Fig. 4.8. The absorption spectrum of PPV is dominated by two absorption peaks with high oscillator strength.[192] They lie at 2.8 and 6.1 eV and are polarized parallel to the chain axis. Two weaker absorptions are found at around 3.6 and 4.8 eV, where the prior has a less well-defined polarization but the latter is polarized perpendicular to the chain axis.[192,193] Electroabsorption[192] and two-photon absorption[194] spectroscopy revealed information about three additional states. One dipole-forbidden state can be found at about 0.7 eV above the lowest dipole-allowed state, which is approximately at 3.5 eV. Furthermore there are two triplet states, one is approximately 0.7 eV below the lowest bright state[195] and another one 0.7 eV above.[196] This latter state is quasi-degenerate to the dipole-forbidden state and these two states are referred to as the singlet and triplet charge-transfer states.[154,197]

An analysis of the computed singlet excited states is shown in Tab. 4.3 presenting vertical excitation energies as well as various data about the excited states. Excitation energies range from 3.03 eV up to 5.04 eV with a very dense region of states around 4.3 eV. Only states of B_u symmetry possess non-vanishing oscillator strength due to dipole selection rules. In all of these cases, the transition moment lies in the molecular plane pointing along the chain axis. The brightest state with $f = 6.2$ is the 1^1B_u state at 3.03 eV. This value is somewhat higher than the lowest bright peak in the experimental absorption spectrum with 2.8 eV.[146,192,193,198] The second largest oscillator strength is found for 2^1B_u, which is the $j = 3$ state of the same exciton band. This state could certainly be responsible for the shoulder to the main peak at around 3.7 eV,[192,193] cf. Fig. 4.8. The remaining states have rather small oscillator strengths below 0.25 and may be hidden in the experimental spectrum. The higher energy peaks detected by experiment are most likely beyond the states computed here and, in particular, no off-axis polarized state is found as was reported for the band at 4.7 eV.[193] The 10^1B_u state at 4.87 eV, which is the $W(3,1)$ exciton, matches from an energetic viewpoint but due to its rather small oscillator strength of 0.224 and its polarization along the main axis it remains unsure whether it should be assigned to the experimental peak. The experimentally characterized, dipole-forbidden state can be identified as the 4^1A_g at 4.07 eV, which is blue-shifted compared to the experimental value of ≈ 3.5 eV.

Collected data of the triplet states is summarized in Tab. 4.4. In their case, excitation energies are shifted to smaller values compared to the singlets and range from 2.12 eV up to 4.59 eV. Similar to the singlets, there is a dense region of states around 4.3 eV. The two triplet states that have been reported from experiment can both be identified with calculated states: The lowest-

energy triplet 1^3B_u state lies at 2.12 eV which stands in agreement with the measured value of 2.1 eV. Moreover, the second state with an excitation energy of 4.17 eV is the 5^3A_g state, which is again blue-shifted w.r.t. experiment by about 0.7 eV. The 4^1A_g and 5^3A_g states are quasi-degenerate as expected as they both belong to the $n = 2$ branch of Wannier excitons. As discussed later for the *electron-hole* correlation plots, they possess odd-parity wave functions with respect to the *electron-hole* separation coordinate. This pair of states is referred to as the singlet-triplet charge-transfer states and are proposed to play an important role in the formation of free charge carriers.[154] Comparing excitation energies of the lowest-lying singlet and triplet states, a gap of 0.91 eV is found similar to values that have been reported for this gap at the polymer limit.[140]

Moving to visual representations, the excited states are divided into local and delocalized states, or in other words Frenkel and Wannier excitons, based on the information in Tabs 4.3 and 4.4. Frenkel excitons are distinguished by small exciton sizes and charge transfer combined with enhanced participation of the phenyl rings. In the case of $(PV)_7P$, eight local states of this type should be present, *i.e.*, one for each phenyl ring. Inspecting the singlet excited states these can be identified as the states featuring $\omega_{\mathrm{CT}} < 0.23$, $\widetilde{d}_{exc} < 4.50$ Å, and $\omega_P > 0.75$. The situation is less clear in the triplet case as there is some mixing between the Frenkel and the more compact Wannier states. Nevertheless eight states are identified as Frenkel excitons (these are marked *F* in Tab. 4.4). The *electron-hole* correlation plots for the singlet and triplet Frenkel excitons are presented in Fig. 4.9. Due to the C_{2h} symmetry of $(PV)_7P$, the excitations are always distributed over pairs of rings separated by an equal distance from the center of the molecule. In Fig. 4.9 these are arranged by showing the states with excitations on the central phenyl rings on top and moving to the outer part below. The excitation patterns and excitation energies are similar for singlet and triplet states. This agreement supports the idea that the interactions are dominated by Coulomb coupling, which acts independently of the spin. A determination of the couplings (c_{ij} in eq. (4.3)) is not straightforward in this complex system, but a glance at the energy scale shows that these are probably not much larger than 0.01 eV. As a final note, it should be pointed out that these states lie significantly below the bright band at 6 eV that is usually assigned with Frenkel character.[102,193,198] A comparison to these higher-lying Frenkel states could be of interest but is out of the scope of this investigation.

The structures of the delocalized Wannier excitons are more complex and, as explained in Section 4.2, it is favorable to discriminate between two independent phenomena: (*i*) the intrinsic structure of the *electron-hole* pair, which is determined by the relative motions of the *electron* and *hole*, and (*ii*) the

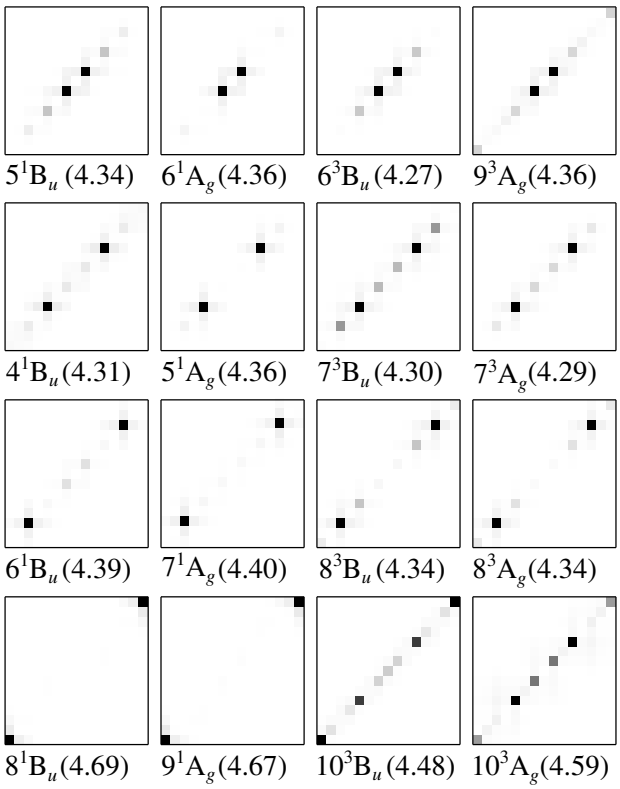

Figure 4.9: *Electron-hole* correlation plots of the singlet and triplet Frenkel-type excitonic states for $(PV)_7P$ (excitation energies in eV in parentheses).

combined exciton quasi-particle. For this purpose, a two-index nomenclature $W(n, j)$ is adopted where n is the quantum number of the intrinsic wave function and j indicates the quasi-momentum of the *particle-in-a-box*-like state. The intrinsic quantum number correlates with the number of nodal planes in parallel to the main diagonal (going from lower left to upper right). Each of these main types gives rise to a series of *particle-in-a-box*-like states with different j, which are in turn characterized by the number of nodal planes perpendicular to the main diagonal.

The discussion starts with the singlet excitons shown in Fig. 4.10 (top). In this case examples for n ranging from 1 to 3 are obtained within the first twenty states. Six $W(1, j)$ excitons starting at 3.03 eV can be found while the $W(2, j)$ series starts at 4.07 eV and consists of five states in the examined energy range. Besides these, there is one $W(3, j)$ exciton at 4.87 eV. The idealized $W(2, j)$ wave functions possess odd-parity with respect to the *electron-hole* separation. Accordingly, the probability of the *electron* and *hole* occupying the same position tends toward zero, which in turn means that the transition density vanishes everywhere in space and that the Ω_{AA} elements vanish almost completely. As a consequence of the vanishing transition density,[65] none of these states possesses any noticeable oscillator strength.[102] By contrast, all the $W(1, j)$ and $W(3, j)$ excitons of B_u symmetry exhibit oscillator strengths above 0.15. In the case of triplet Wannier-type excitons, only two series are found within the first twenty states, $W(1, j)$ and $W(2, j)$. The $W(1, j)$ series starts at 2.13 eV and consists of ten states. In this series the lower-energy states present the clear *particle-in-a-box*-like picture found in the singlet case while the higher-energy states possess reduced CT character and start to resemble Frenkel states. The fact that these triplet states are positioned at lower energy and possess reduced charge-transfer character when compared to the singlets stands in agreement with the expected effects of missing exchange repulsion.[81] In contrast to the $W(1, j)$ excitons the triplet $W(2, j)$ series starts at 4.17 eV and rather resembles the properties of the singlet case (with the exception that only two states of this type are computed here).

After the visual classification of the state characters, a quantitative analysis is performed to further refine the description of the states. For this purpose, the exciton sizes $\widetilde{d}_{exc}$, charge-transfer measures ω_{CT} and functional group participation ω_P of the various singlet and triplet states are plotted against the excitation energies in Fig. 4.11. The Frenkel excitons are found clustered around an excitation energy of about 4.3 eV. They are characterized by small ω_{CT} values (below 0.23) and exciton sizes ranging between 2.51 and 4.51 Å. Comparing these values to molecular and fragment sizes, they lie between the size of an individual phenyl ring and a PV subunit, both indicated by dotted

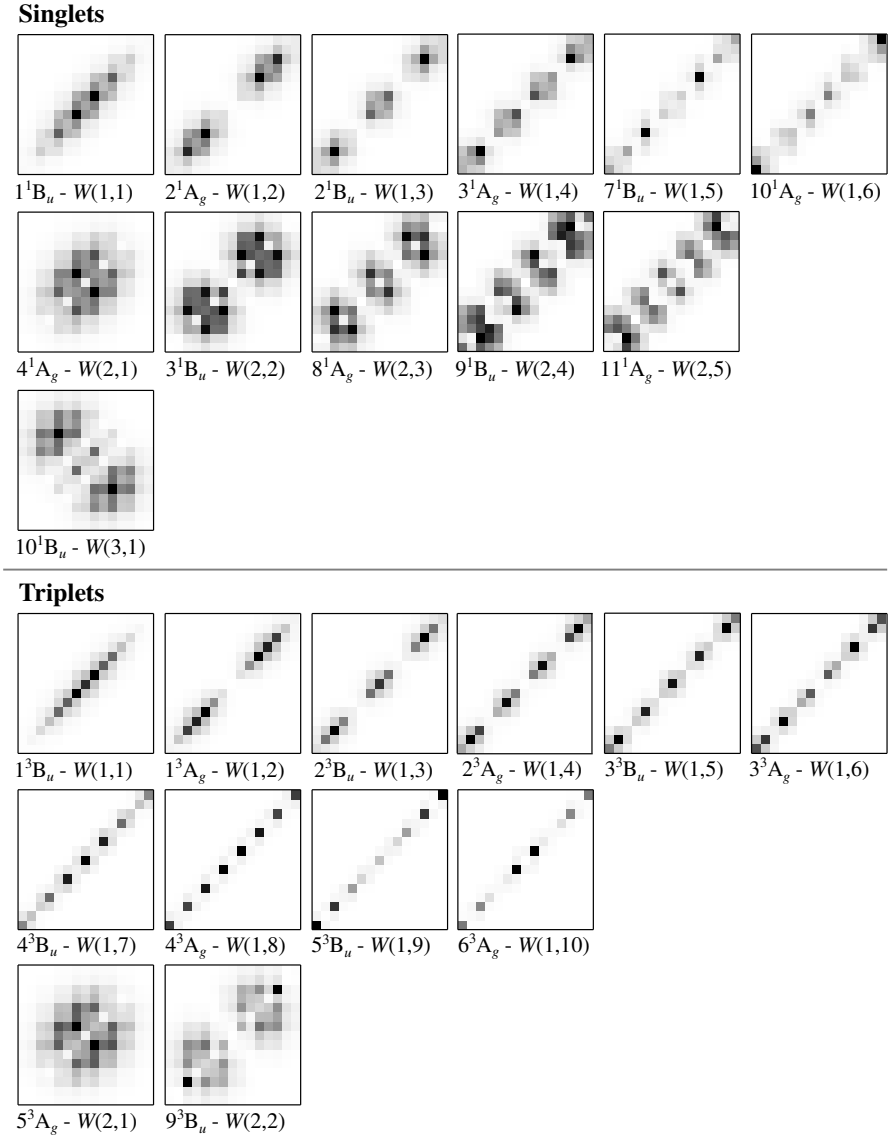

Figure 4.10: *Electron-hole* correlation plots of Wannier-type singlet and triplet excitons of $(PV)_7P$, as well as, assignment of principle n and *center-of-mass* quantum numbers j, written $W(n, j)$.

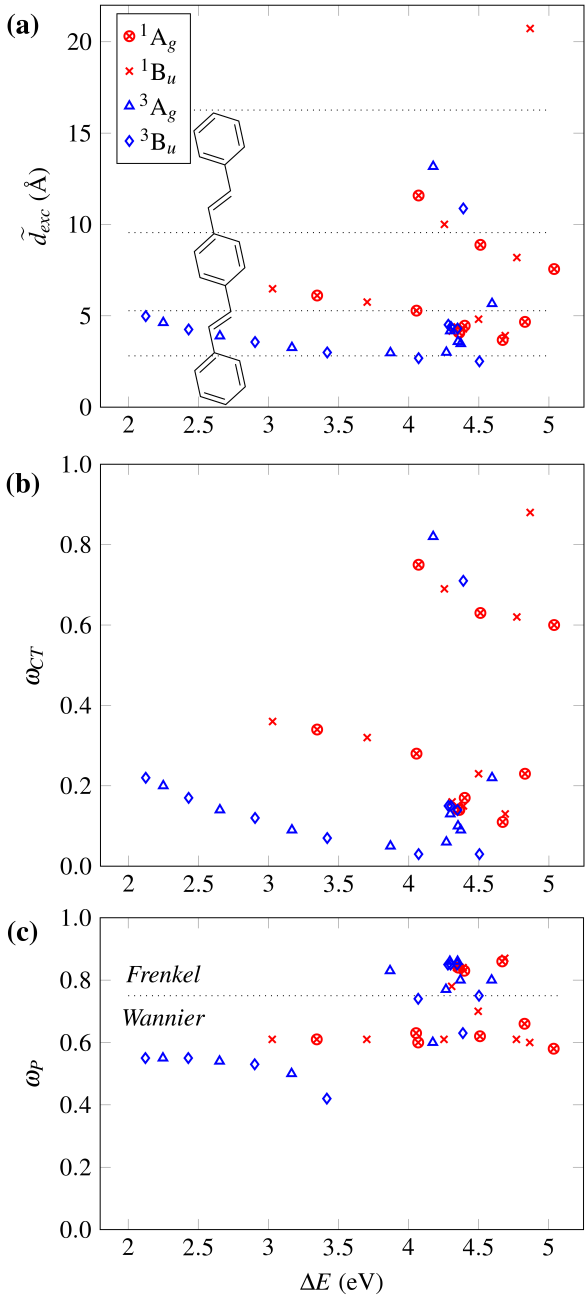

Figure 4.11: Analysis of excited states of $(PV)_7P$: (a) Exciton sizes ($\widetilde{d}_{exc}$, Å), (b) charge-transfer measures (ω_{CT}), and (c) functional group participation (ω_P) of singlet and triplet excitons plotted against vertical excitation energy at the RI-ADC(2)/TZVP level of theory. The inset in (a) shows the size of a PPV oligomer for comparison. The legend in (a) applies to all plots in this figure.

lines in Fig. 4.11 (a). Charge-transfer measures of the Frenkel states are below 0.23 for all states resembling the ω_{CT} values of locally confined excitations in the oligomer series in Sec. 4.4.2. The Wannier excitons present a different picture showing a large dispersion of the excitation energies with varying quasi-momentum and strong variations in the $\widetilde{d}_{exc}$ and ω_{CT} measures. Different series of data points are, however, clearly apparent and a more detailed examination shows that they indeed correspond to the previously defined exciton types. For the singlet $W(1,j)$ series marked in red, [x, $\otimes$] in Fig. 4.11, exciton sizes start at 6.48 Å, which is somewhat larger than a PV subunit, slowly decreasing towards 4.67 Å. The corresponding charge-transfer measures lie between 0.36 and 0.23. In contrast, the $W(2,j)$ series starts at exciton sizes of 11.59 Å, about the size of a PVPV fragment, decreasing to 7.56 Å. The $W(2,1)$ exciton is almost double the size of $W(1,1)$, in agreement with eq. (4.2).[81] In Fig. 4.11 (a) there is an isolated data point at $\widetilde{d}_{exc} = 20.73$ Å. It belongs to the $W(3,1)$ exciton, which also possesses the large ω_{CT} value of 0.88. The triplet excitons are marked in blue [$\diamond$, $\triangle$] in Fig. 4.11. The $W(1,j)$ series starts slightly above 2 eV with the $W(1,1)$ exciton possessing an exciton size of 4.98 Å. The series slowly decreases towards a size of 3.00 Å. The second triplet exciton series $W(2,j)$ starts at exciton sizes more than twice as large as the $W(1,j)$ excitons with 13.17 Å and contains a second state at 10.88 Å. A general trend found in Fig. 4.11 is that excitons become more tightly bound with increasing quasi-momentum (see also Ref. 77). This shows that the intrinsic wave function is not completely separated from the combined quasi-particle motion. It will certainly be of interest to determine whether similar effects are found for other systems.

In band models three different types of excitons are usually considered to be responsible for the excitation spectrum of PPV. These are constructed from two different types of bands, one has delocalized orbital contributions over phenylene and vinylene groups (d and d^*) and one has localized orbitals confined at the phenyl rings with zero orbital contributions at the bridging C-atoms connected to the vinylene groups (l and l^*). The first exciton is a Wannier-type exciton with a transition between delocalized bands ($d \rightarrow d^*$), the second is an intermediate species with transitions between different band types ($l \rightarrow d^*$ and $d \rightarrow l^*$) and the third is a Frenkel-type exciton with a transition between localized bands ($l \rightarrow l^*$).[81,102] In the present quantum-chemical framework, the contributing molecular orbitals are computed without *a priori* assumptions and therefore it is interesting to examine the participation of the two functional groups to different excitonic states identified earlier. For this purpose, the ω_P value as defined in eq. (4.5) is employed, which counts the probability of *electron* or *hole* to be found at a phenyl ring plotted in Fig. 4.11 (c).

The results show that Wannier excitons are in general composed of an even mixture of phenylene and vinylene orbital contributions with ω_P values ranging between 0.42 and 0.66. For example the 1^1B_u state has an ω_P value of 0.61 and the 1^3B_u state a somewhat smaller value of 0.55. This observation is truly independent from the quantum numbers n or j. This stands in good agreement with the picture of delocalized bands responsible for the $d \rightarrow d^*$ transitions. In contrast, Frenkel states show much larger ω_P values of ≈ 0.85 indicating that these are primarily localized on the phenylene groups. However, it should be noted that there are indeed resonances with the vinylene groups, which contribute about 15% of the excitation. The delocalization effect may in fact be responsible for the small excitation energies of these states compared to isolated benzene rings. In the whole set of excited states there are not any states with more than 50% vinylene contribution. In fact, the states with large vinylene group contributions are always at least delocalized over the adjacent phenylene carbon atoms.

4.4.4 Triplet excitons in PPV oligomers

Triplet excitons are structurally different from singlet excitons as the *electron* and *hole* do not experience an exchange repulsion.[81] In Sec. 4.4.2, the emergence of excitonic states for increasing chain lengths were already discussed for singlet excited states, yet it is interesting to investigate how the exchange repulsion influences the exciton formation as well as the exciton properties. Triplet excitons, furthermore, are interesting excited-state species in organic electronics as the lowest triplet state is usually energetically below the first bright singlet state, and hence a potential candidate for intersystem crossing and intermediate state for decay channels to the electronic ground state.

In analogy to Sec. 4.4.2, the first four triplet excited states of a set of PPV oligomers $(PV)_nP$ with $n = 1 - 7$ are investigated focussing on the results for TZVP basis set (cf. Fig. 4.12). The triplet excited states are on average shifted by about -1 eV compared to their singlet counterparts. In contrast to the singlet excited states, however, excitation energies smoothly converge against state-specific values within each state symmetry and the order of the states is pertained throughout the complete data set. Only some states show excitation energies above 3.5 eV and are potential candidates for being locally excited states. For completeness, it is noted that the t_1 values (not shown, see ESI of Ref. 138) are all close to 1 indicating a predominant single excitation character for all triplet excited states.

Proceeding to the charge-transfer numbers ω_{CT} shown in Fig. 4.12 (c), very low values below 0.23 are found with a maximum of 0.22 for the 1^3B_u state of $(PV)_7P$. Similar to the singlet states, a decrease in charge-transfer character is

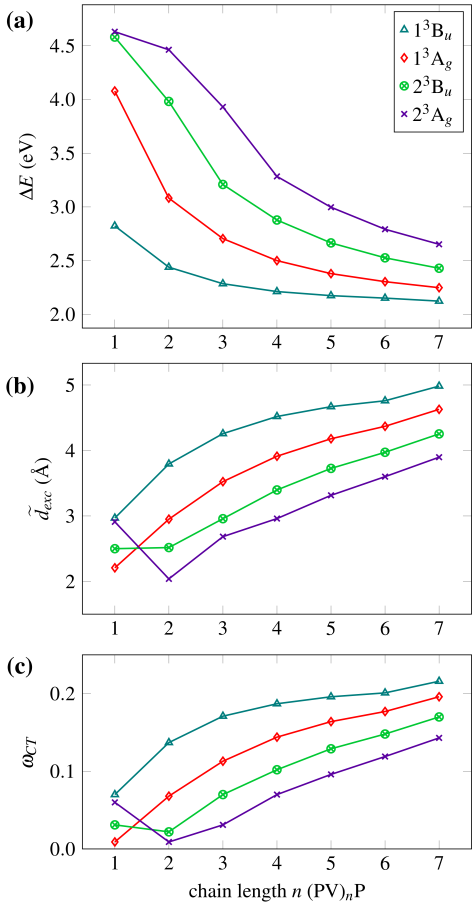

Figure 4.12: (a) Vertical excitation energies (ΔE, eV), (b) approximate exciton sizes ($\widetilde{d}_{exc}$, Å), and (c) charge-transfer measures (ω_{CT}) of poly(*para* phenylene vinylene) oligomers plotted against chain length n computed at the RI-ADC(2)/TZVP level of theory. Legend in (a) applies to all plots in this figure.

observed for higher excited states of the same oligomer. This trend is confirmed by the exciton sizes, which are plotted in Fig. 4.12 (b). Generally, the triplet exciton sizes range between 2 and 5 Å, and for longer chains the values increase. Except for the first PVP oligomer, a clear pattern emerges where for each oligomer exciton sizes can be sorted according to $1^3\mathrm{B}_u < 1^3\mathrm{A}_g < 2^3\mathrm{B}_u < 2^3\mathrm{A}_g$, which is the reverse order of the state energies. Earlier, this behaviour has been found for the excited states of $(\mathrm{PV})_7\mathrm{P}$ for Wannier excitons with increasing quasi-momenti, a trend which is again confirmed by visual analysis in the next step.

A visual analysis of the triplet exciton wave functions (shown in Fig. 4.13) reveals that exciton formation is favoured compared to the formation of charge-

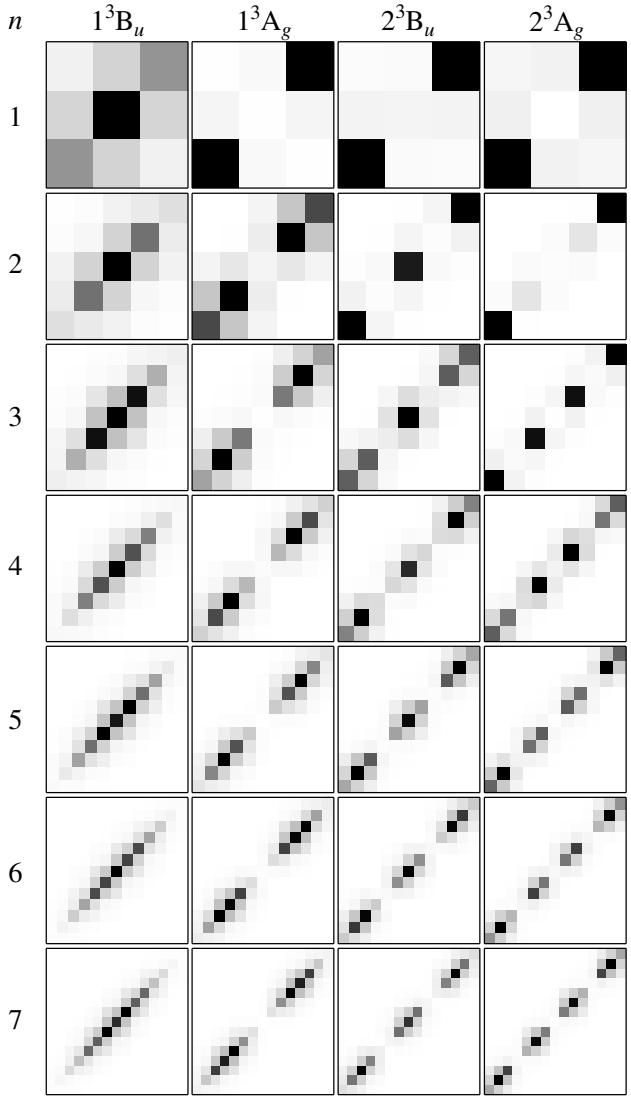

Figure 4.13: *Electron-hole* correlation plots Ω_{AB} of the first four triplet excited states of poly(*para* phenylene vinylene) oligomers computed at the RI-ADC(2)/TZVP level of theory.

separated states, which were somewhat likely to find in small systems the case of singlet excited states (see Fig. 4.6 for comparison). Moreover, triplet exciton wave functions do not spread out as much from the main diagonal of the Ω_{AB} plots as compared to their the singlet counterparts. This means that the *electron-hole* pairs are more localized in space and hence more tightly bound.

In summary, for the same excitation pattern, the triplet excitons form electron-hole pairs which are closely confined in space, *i.e.* tighter bound than their singlet counterparts. This behaviour is present in all descriptors analyzed here. Hence, the results from *ab initio* calculations confirm the predictions from solid-state theory.[81]

4.5 Conclusion

In this chapter, high-level *ab initio* calculations of the excited states of poly(*para* phenylene vinylene) oligomers were presented and interpreted using specialized wave function analysis protocols. The results have shown a good agreement with experimental findings and essential excitonic properties were reproduced. Furthermore, a variety of details about the exciton wave functions were examined in qualitative and quantitative analyses.

High-level benchmark computations employing the ADC(3) method were presented for the smallest three oligomers. Aside from verifying the accuracy of the ADC(2) method with respect to energies, oscillator strengths, and wave functions of primarily singly excited states, the importance of low-energy doubly excited states was highlighted. Albeit the doubly excited states have received little attention so far, they are presumably of high importance as they represent ideal doorway states for singlet fission as observed in PPV.[189,190]

The influence of increasing the size of the π-conjugated system on the excited states was investigated. For this purpose, a set of eight oligomers was constructed ranging from two to eight phenyl rings. While for the smaller oligomers, confinement effects dominated, delocalization and the formation of exciton bands was observed for the larger cases. These changes were illustrated in a pictorial representation, using *electron-hole* correlation plots, as well as quantified through excited-state descriptors.

The largest compound octa(*para* phenylene vinylene), $(PV)_7P$, was analyzed in detail investigating the first twenty singlet and twenty triplet excited states. A detailed examination of exciton wave functions revealed the presence of different exciton bands which were identified as Wannier or Frenkel excitons. For Wannier excitons, bands of varying quasi-momentum were identified. A comparison of singlet and triplet excitons revealed that the latter exhibited more tightly bound *electron-hole* pairs leading to significantly lower

excitation energies which matches experimental findings. A characterization in terms of the participation of the phenylene and vinylene functional groups was provided. The results of this study highlighted some new aspects, which were previously not at the center of attention, pertaining to (*i*) the systematic lowering of *electron-hole* separation distances with increasing quasi-momentum for Wannier excitons, (*ii*) the importance of low-energy doubly excited states, and (*iii*) the presence of a band of dark low-energy Frenkel excitons around 4.5 eV. Understanding these points and determining whether (*i*) and (*ii*) are general phenomena in conjugated organic polymers will require extended studies in the future. Furthermore, it will be beneficial to examine the effects of structural fluctuations and of dielectric screening, which is expected to be strong and variable in bulk PPV.[81] These questions will be addressed in forthcoming work employing ADC in combination with equilibrium and non-equilibrium polarizable continuum models[199] and appropriate structural sampling.

Chapter 5

Exciton analysis in time-dependent density functional theory: How functionals shape excited-state characters

Time-dependent density functional theory (TDDFT) is a widely applied excited-state method which affords an efficient computation of excited states of even large molecules. However, its reliability suffers from the absence of an exact exchange-correlation (*xc*) functional, which gives rise to significant errors. Consequently, benchmarking of *xc*-functionals against experimental and/or high-level computational data is an important step to find an adequate *xc*-functional that properly describes the investigated system. From a more general point of view, it is important to identify systematic errors and understand their origins. To gain insight into methodological shortcomings, results from TDDFT calculations are subjected to exciton analysis: State characters are determined, categorized as local, extended $\pi\pi^*$, Rydberg or charge transfer, and compared revealing substantial differences amongst the *xc*-functionals. Furthermore, strong effects of the choice of the *xc*-functional on the physical nature of excited states are found in the case of acenes. A strong influence of nonlocal orbital exchange on electron-hole correlation effects is proposed to cause significant errors in the description of excited states of large π-conjugated organic systems for certain *xc*-functionals.

Please note that parts of this chapter have already been published by Prof. Dr. Andreas Dreuw, Dr. Felix Plasser and myself in *the Journal of Chemical Physics*, volume 143 (**2015**), number 171101 (ref. 163).

5.1 Introduction

Linear-response time-dependent density functional theory (TDDFT) is certainly one of the most widely-used quantum-chemical methods for excited-state calculations of medium-size and large molecules.[26,27,29] At the same time, the failure of TDDFT to correctly describe charge-transfer (CT) states is well-known.[34–37] Also Rydberg states, excited states of extended π-conjugated systems[39,40] and multiply-excited states[42,43] cause difficulties. To solve conceptual shortcomings, great effort has been made to search for improved functionals that reliably describe CT states, and in particular long-range corrected (LRC) functionals featuring varying amounts of nonlocal exchange were developed for this purpose. The first LRC functional proposed by Yanai et al.[47] was a Coulomb-attenuated variant of the prominent Becke-3-Lee-Yang-Parr functional[16,20] (CAM-B3LYP), which contains nonlocal orbital exchange from 19 % at short range up to 65 % at long range.

The search for tools to diagnose the failures of TDDFT in combination with different functionals is an ongoing challenge and several descriptors measuring orbital overlaps[51–53] and centroid distances[55,71,94] have been proposed. However, some cases like extended symmetric π-conjugated systems, *e.g.* acenes, cause significant but hard-to-detect errors.[39–41] For these systems the overlap of the canonical orbitals is not a good predictor of the performance of TDDFT[41,106,137,200] and a more complex dynamical view has to be adopted.

In recent work,[65,66,73,78] my co-workers and I established a series of excited-state descriptors based on the physical picture of an exciton wave function, which is constructed from the one-particle transition density matrix (1TDM) (see also Refs 64,75,102). Information about the spatial distributions of *electron* and *hole* over the molecular system as well as statistical descriptors provide a solid basis for analyzing excited states. This opens a route to assign excited-state characters without the need for orbital inspection, which is beneficial for identifying problematic cases. Furthermore, the effect of a chosen exchange-correlation (xc) functional on an excited state can be investigated in detail. High-level benchmarks are accessible as the same descriptors can be computed for any method providing 1TDMs. This allows detailed benchmarking of TDDFT results going beyond a simple comparison of energies.

5.2 Results and discussion

First the relation between rms exciton sizes d_{exc} and charge centroid distances $d_{h\to e}$ will be examined for Tozer's benchmark set[51] (molecules shown in Fig. 5.1) as presented in Figure 5.2. In these and all following computations,

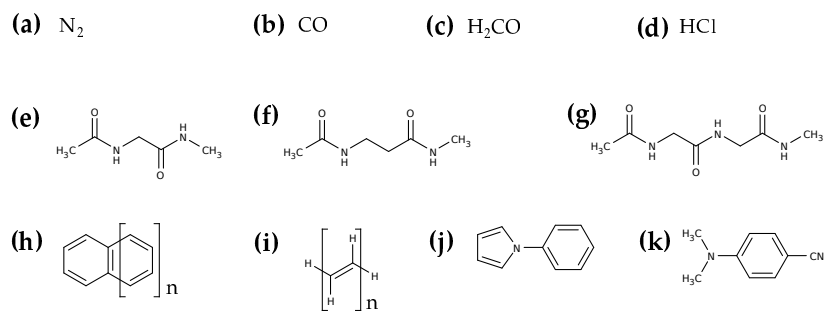

Figure 5.1: Tozer's benchmark set[51] investigated in this chapter: (a) nitrogene, (b) carbon monoxide, (c) formaldehyde, (d) hydrogen chloride, (e) dipeptide, (f) β-dipeptide, (g) tripeptide, (h) acenes ($n = 1 - 5$), (i) polyacetylene oligomers ($n = 2 - 5$), (j) *N*-phenylpyrrole, (k) 4-(*N*,*N*-dimethylamino)benzonitrile (DMABN).[107]

three functionals of different classes are applied: PBE[201] is employed as a representative of the local generalized gradient approximation (GGA), B3LYP[16,20] as hybrid, and CAM-B3LYP as long-range corrected functional. The exciton descriptors are plotted against the error in excitation energy compared to experimental data, where the same geometries, basis sets, and reference data are used as in Ref. 51. Starting with exciton sizes computed by TDA/PBE, four different groups can be identified. First, locally excited states with well-described excitation energies and small exciton sizes appear in the upper left corner of Figure 5.2 (a) marked in black. Second on the main diagonal, charge-transfer states with strongly underestimated excitation energies are found, where the error in excitation energies seems to scale linearly with the exciton size (also marked in black). To highlight some notoriously difficult cases, the exciton sizes for acenes and polyacetylenes are marked in red. As their energies are rather well-described using the Tamm-Dancoff approximation,[31] they appear at small deviations in ΔE_{exp} but possess large exciton sizes with a linear dependency between molecular size and exciton size. In addition, the Rydberg states are marked in blue. They have rather large exciton sizes due to their diffuse electron sizes σ_e. At the same time, their description is somewhat poorer compared to the previous group and they show a systematic underestimation of excitation energies on the order of 2 eV.

Going to the charge centroid separation $d_{h\to e}$ plotted in Figure 5.2 (d), the overall distribution of the black data group is preserved. The interpretation of this finding is simple: Locally excited states show only small *electron-hole* separations, however, some values above zero may occur as in some cases charges are promoted between adjacent functional groups. For the charge-transfer states,

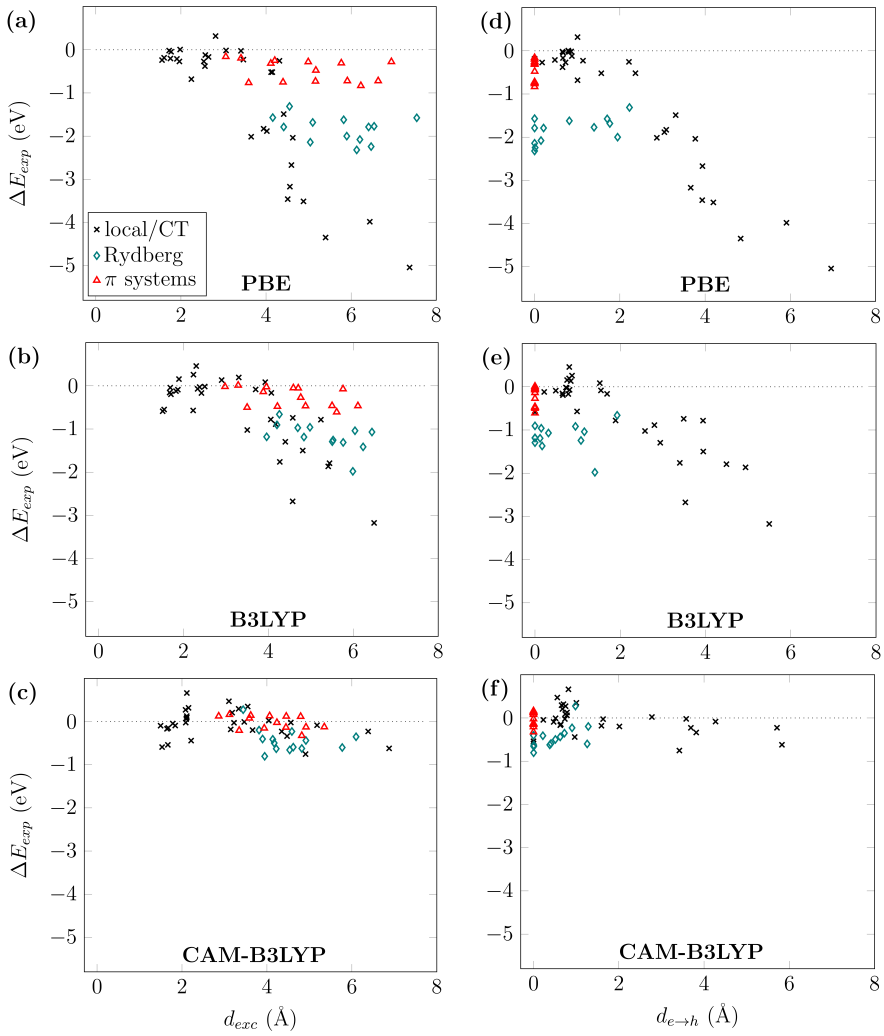

Figure 5.2: Exciton sizes (d_{exc}, Å, first column) and center-of-mass *electron-hole* distances ($d_{h\to e}$, Å, second column) for Tozer's benchmark set[51] plotted against the error in excitation energy with respect to experimental data (ΔE_{exp}, eV). All presented states are singlet excited states and the Tamm-Dancoff approximation was applied. Excited states with local or directed charge-transfer character are marked in black ($\times$), states for extended π systems (polyacenes and polyenes) in red ($\triangle$), and Rydberg states in blue ($\diamond$).

the values of $d_{h\to e}$ and d_{exc} are quite similar as expected from eq. (2.39) in the case for insignificant electron and hole sizes, as well as correlation effects. For the two other groups, the large conjugated systems and the Rydberg states, the situation differs dramatically. With a few exceptions for some Rydberg states, the static *electron-hole* separation $d_{h\to e}$ is zero, which means that no static charge transfer occurs. In particular in extended π systems, an almost equal and symmetric distribution of *electron* and *hole* densities over the excited molecules and a superposition of their centroids is present. The spatial extent of the charge clouds, as measured by σ_h and σ_e, and correlation effects are responsible for the large exciton sizes. In contrast for the Rydberg states, the dominant factor for large exciton sizes is clearly the *electron* size σ_e.

Proceeding to the B3LYP functional, locally excited states show similar exciton sizes compared to PBE. In contrast, the other states show in average a shift to smaller exciton sizes, especially in the cases of extended π systems and Rydberg states. While the huge errors of the directed charge-transfer states are attenuated at this level, there is only a slight improvement for the extended π system states. For the Rydberg states, the excitation energies are substantially corrected by about +1 eV compared to PBE.

For the CAM-B3LYP functional, the best performance in excitation energies is found, see Figure 5.2 (c). Examining the exciton sizes of the locally excited states, their sizes are found to be preserved independent of the functional choice. This comes along with almost constant excitation energy shifts with respect to experiment. In contrast, as observed before in the case of B3LYP, the states for extended π systems and Rydberg states have a tendency to significantly smaller exciton sizes compared to PBE. To understand this localization effect in more detail, it is worth revisiting eq. (2.40). Especially for the cases where $d_{h\to e}$ is zero, the exciton size depends on the sizes of *electron* σ_e and *hole* σ_h and their covariance. Going from PBE to B3LYP to CAM-B3LYP for these states a general trend is that $\sigma_{e,\mathrm{PBE}} > \sigma_{e,\mathrm{B3LYP}} > \sigma_{e,\mathrm{CAM-B3LYP}}$ and the same is observed for σ_h which is logical considering that a diminished self-interaction error results in more compact *electron-hole* distributions. However, the variations in σ_h and σ_e only explain a small part of the variations in d_{exc} and the covariance becomes the decisive factor for explaining the differences between the functionals. In the case of a positive *electron-hole* correlation, the resulting attraction leads to an additional compression of d_{exc}. In contrast for a negative correlation, the exciton size is enlarged because of the effective repulsion and charge avoidance. To gain deeper insight into this effect, the correlation coefficient R_{eh} will be discussed for acenes.

Let me now examine the linear *electron-hole* correlation effects with respect to the choice of functionals and compare standard linear-response TDDFT

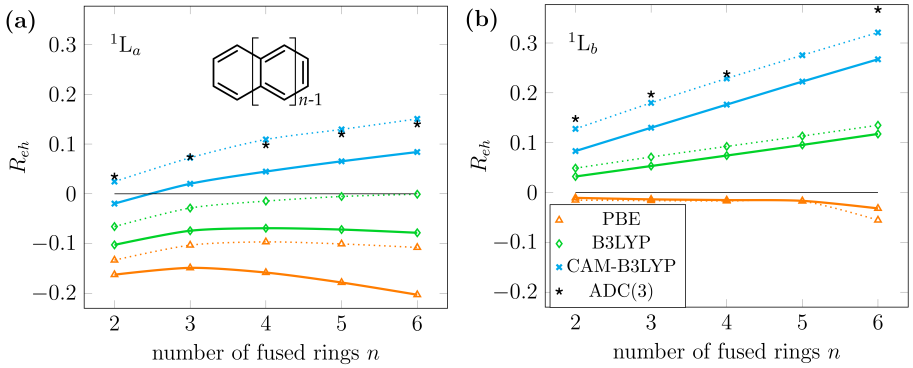

Figure 5.3: Correlation coefficients R_{eh} for (a) ^1L_a and (b) ^1L_b states for the acene series from naphthalene ($n = 2$) to hexacene ($n = 6$) calculated at the TDDFT/cc-pVTZ (solid lines) and TDA/cc-pVTZ (dotted lines) levels of theory employing the PBE, B3LYP and CAM-B3LYP functionals and ADC(3)/SV(P) reference values. Legend in (b) also applies to (a).

with the Tamm-Dancoff approximation. The ^1L_a and ^1L_b states of acenes from naphthalene to hexacene are calculated at the TDDFT/cc-pVTZ and TDA/cc-pVTZ levels of theory employing the PBE, B3LYP and CAM-B3LYP functionals and the correlation coefficient R_{eh} is plotted against the system size in Figure 5.3. First, the ^1L_a states are discussed, see Figure 5.3 (a). For the TDDFT results indicated by solid lines, the correlation coefficient R_{eh} for the PBE functional (orange) is the smallest for all molecules ranging between -0.20 and -0.15 with a trend towards lower values for larger systems. This behaviour can be interpreted with the picture of two charges avoiding each other dynamically. Proceeding to B3LYP (green), the values of R_{eh} become closer to zero staying slightly below -0.05 and are almost constant for the systems larger than naphthalene ($n = 2$). Finally, in the case of CAM-B3LYP (blue) the correlation coefficient starts from approximately zero and constantly increases for larger systems to a value of 0.08 for hexacene. This positive correlation can be understood as the onset of exciton binding. This result sheds new light on the observations by Tretiak *et al.*[156] that bound excitons in large conjugated systems can only be described by long-range corrected functionals.

Going from time-dependent density functional theory to the Tamm-Dancoff approximation (dotted lines), the *electron-hole* correlation behaviour is significantly altered in favour of a stronger *electron-hole* attraction or at least a decrease of their repulsion. In the case of PBE, the average shift is about $+0.06$ still containing significant amount of dynamic *electron-hole* repulsion. For the B3LYP functional an increase of R_{eh} from clearly negative values of -0.05 for naphthalene to zero correlation for tetracene and larger molecules is found. This zero correlation is considered as linearly independent dynamical

motion of *electron* and *hole* which is the standard assumption when inspecting molecular orbitals. Going to the long-range corrected CAM-B3LYP functional, the positive correlation increases almost constantly for all systems and ranges between 0.02 and 0.15 which is significantly higher than for TDDFT.

The values for the ^1L_b states are shown in Figure 5.3 (b) and again the discussion starts with the TDDFT results. For PBE the R_{eh} values are approximately zero for all systems independent of their sizes. In contrast, for B3LYP and CAM-B3LYP positive values are found with a constant increase for larger system sizes. At the same time for CAM-B3LYP the slope of the curve is larger and a stronger trend towards bound excitons is found. Going to the TDA results, essentially the same trends can be observed for all functionals. However, an almost constant shift towards higher correlation values is observed with a shift of +0.02 for B3LYP and an even larger shift of +0.05 for CAM-B3LYP. For a more extended discussion about the effect of varying exact exchange in the TDA and TDDFT methods, cf. Ref. 32. The R_{eh} values were recomputed at the *ab initio* level using the algebraic-diagrammatic construction method for the polarization propagator to third order (ADC(3)/SV(P))[169] showing excellent agreement with the TDA/CAM-B3LYP level.

In view of *electron-hole* correlation effects within the ^1L_a and ^1L_b states, the problems encountered to calculate excitation energies for the two states at the TDDFT level can be easily explained. For the ^1L_a state, a long-range corrected hybrid functional is absolutely necessary to correctly describe a bound exciton. In contrast, the physically correct picture for the ^1L_b state emerges already for B3LYP and in the case of PBE at least no dynamical *electron-hole* repulsion is found. This explains the increased sensitivity of the ^1L_a state with respect to the choice of functional.[31,41] The level of theory and the choice of the exchange-correlation functional are very critical to obtain a physically reasonable description. In this respect there is a decisive difference between TDDFT and TDA, that Peach *et al.* related to the singlet-triplet instability issue.[32,33]

5.3 Conclusion

A series of excited-state descriptors based on the concept of excitons has been combined with time-dependent density functional theory. These descriptors allow to determine diverse excited-state properties such as static *electron-hole* separations, exciton sizes and correlation coefficients affording a detailed description of excited states. Tozer's benchmark set was studied to illustrate how excited states can be characterized distinguishing different types, *e.g.* Rydberg, charge-transfer, locally excited and charge-resonance states. Furthermore, the

influence of exchange-correlation functionals on the description of excited states was analyzed by monitoring variations in exciton properties.

Correlation coefficients are a powerful tool to describe *electron-hole* correlation effects in excited states of acenes which have shown to be crucial for understanding the performance of different *xc*-functionals. The erroneous description of excitation energies with the local GGA functional PBE was associated with repulsive *electron-hole* interactions. In contrast, the long-range corrected CAM-B3LYP functional does not only obtain much better excitation energies, but also bound excitonic states with attractive *electron-hole* interactions. This effect is even enhanced when the Tamm-Dancoff approximation is applied, and the poorer results from full time-dependent density functional theory can be traced back to more weakly bound *electron-hole* pairs.

The results illustrate that exciton properties are useful for evaluating exchange-correlation functional performance in time-dependent density functional theory. Exciton analysis has potential for diagnosing methodological shortcomings and should be able to provide useful information for *xc*-functional design in the future. As the employed exciton descriptors can also be used in combination with *ab-initio* methods,[73,78] they open a route for improved benchmarking as will be discussed in Chapter 7.

Chapter 6

Universal exciton size in organic polymers is determined by nonlocal orbital exchange in TDDFT

In this chapter, the reasons why certain *xc*-functionals in time-dependent density functional theory have problems to correctly describe excited states of extended π-systems are investigated in detail. A diverse set of large π-conjugated organic systems is studied employing a variety of *xc*-functionals. The results reveal that the exciton size of the lowest singlet excited state is a universal, system-independent quantity of approximately 7 Å. Moreover, the explicit exciton size as well as the overall description of the exciton is almost exclusively governed by the amount of nonlocal orbital exchange in the *xc*-functionals. This behaviour is traced back to the lack of Coulomb attraction between electron and hole quasiparticles in pure TDDFT, which is reintroduced only with admixing nonlocal orbital exchange. This study confirms the utility of exciton descriptors for assessing *xc*-functional performance as proposed in the previous chapter.

Please note that parts of this chapter have already been published by Prof. Dr. Andreas Dreuw, Dr. Felix Plasser and myself in *The Journal of Physical Chemistry Letters*, volume 8 (**2017**), number 6, pages 1205–1210 (Ref. 97).

6.1 Introduction

Quantum-chemical methods applied on modern computer architectures allow for investigating excited states of ever larger molecules.[26,27,29] Despite the rapid developments on the computational side, analysis of excited-state properties of these large systems is in practice often limited to visual inspection of frontier orbitals. As an example, for a $\pi \rightarrow \pi^*$ excitation it seems at first sufficient to analyze the highest occupied (HOMO) and the lowest unoccupied molecular orbitals (LUMO) as they usually represent large parts of the excitation process. In extended π-systems, however, *electron-hole* correlation effects gain substantial importance and the assumption underlying MO theory that the excited electron is decoupled from the excitation hole is no longer true.[163] Moreover, it becomes crucial to adopt a picture of coupled *electron-hole* pairs *i.e.* excitons, a concept which is central to the description of excited states in solid-state physics.

In the following, evidence is provided for the necessity to move to a correlated *electron-hole* description for investigating excitons in the context of quantum-chemical calculations of large molecular systems.[65,73,163] Specifically, the onset of excitonic properties is studied for π-conjugated systems of varying size to illustrate how excitonic effects emerge. This aspect is of high importance in the discussion of localization effects in finite π-systems, a topic that is intensely debated.[202–206] While previous work was focused on a qualitative rationalization of excitonic effects,[92,137,156,207] a quantitative perspective is adopted here which allows to decompose excitonic effects in large conjugated π-systems on different levels. Furthermore, a hierarchy of exchange-correlation (xc) functionals is investigated in terms of their ability to describe excitonic properties, *i.e.* the *electron-hole* interaction, which turns out to crucially depend on the amount of nonlocal orbital exchange.

6.2 Theory

In linear-response time-dependent density functional theory (TDDFT),[26,29] Casida's pseudo-eigenvalue equation is solved

$$\begin{pmatrix} \mathbf{A} & \mathbf{B} \\ \mathbf{B}^* & \mathbf{A}^* \end{pmatrix} \begin{pmatrix} \mathbf{X} \\ \mathbf{Y} \end{pmatrix} = \omega \begin{pmatrix} \mathbf{1} & \mathbf{0} \\ \mathbf{0} & -\mathbf{1} \end{pmatrix} \begin{pmatrix} \mathbf{X} \\ \mathbf{Y} \end{pmatrix}, \tag{6.1}$$

where ω is the excitation energy, and $\mathbf{X}$ and $\mathbf{Y}$ are the excitation and de-excitation amplitudes. The elements of the $\mathbf{A}$ matrix in the case of a hybrid

functional are given as

$$A_{ia,jb} = (\varepsilon_a - \varepsilon_i)\delta_{ij}\delta_{ab} + \langle ia|bj\rangle - c_{\mathrm{HF}}\langle ia|jb\rangle + (1 - c_{\mathrm{HF}})\langle ia|f_{xc}|bj\rangle, \quad (6.2)$$

and the elements of the **B** matrix possess a similar structure with permuted indices. The indices i, j and a, b pertain to occupied and virtual orbitals, respectively. The ε_i and ε_a values denote the orbital energies, c_{HF} marks the fraction of nonlocal orbital exchange, and f_{xc} is the xc-kernel of the employed functional. Connecting this equation to the quasi-particle picture,[85] occupied orbitals involved in electronic excitation are relabeled as "hole" and virtual orbitals as "electron". In this picture, the second term in eq. (6.2) $\langle ia|bj\rangle$, which is the response of (*i.e.* originates from) the Coulomb interaction in DFT takes the form of an exchange repulsion between the electron and hole in TDDFT. The third term $c_{\mathrm{HF}}\langle ia|jb\rangle$, the response of the nonlocal exchange interaction takes the form of a Coulomb attraction. Hence, in TDDFT c_{HF} can be interpreted as charge screening parameter, cf. Ref. 208. In the case of $c_{\mathrm{HF}} = 1$ the *electron-hole* pair experiences the full Coulomb attraction, while it is screened for lower values and disappears for $c_{\mathrm{HF}} = 0$. The fourth term depends specifically on the xc-functional and has no such simple interpretation. If range-separated xc-functionals are used, eq. (6.2) becomes somewhat more involved. In a nutshell, the more nonlocal orbital exchange is employed, the stronger becomes the *electron-hole* Coulomb attraction.

A new perspective on the results of eq. (6.1) can be obtained employing exciton analysis.[64,65,73,78] For this purpose, an effective exciton wave function is constructed using the excitation and de-excitation amplitudes

$$\chi_{exc}(r_h, r_e) = \sum_{i}^{occ}\sum_{a}^{virt}\big[X_{ia}\phi_i(r_h)\phi_a(r_e) + Y_{ia}\phi_a(r_h)\phi_i(r_e)\big]. \quad (6.3)$$

ϕ_i and ϕ_a refer to occupied and virtual molecular orbitals, respectively, and r_h and r_e are the coordinates of the electron and hole quasi-particles.[163] To characterize excitons, the expectation value of an operator $\hat{O}$ can be evaluated as

$$\langle\hat{O}\rangle = \frac{\langle\chi_{exc}|\hat{O}|\chi_{exc}\rangle}{\langle\chi_{exc}|\chi_{exc}\rangle}. \quad (6.4)$$

To measure the spatial extent of the hole generated during excitation, the hole size is computed as

$$\sigma_h = \sqrt{\langle r_h^2\rangle - \langle r_h\rangle^2}. \quad (6.5)$$

The exciton size depends on the joint *electron-hole* position, and is analyzed

as the root-mean-square (rms) *electron-hole* distance

$$d_{exc} = \sqrt{\langle |r_e - r_h|^2 \rangle}. \tag{6.6}$$

Furthermore, linear *electron-hole* correlation effects are investigated employing a correlation coefficient similar to Pearson correlation as

$$R_{eh} = \frac{\mathrm{COV}(r_h, r_e)}{\sigma_h \sigma_e} \tag{6.7}$$

with the covariance defined as

$$\mathrm{COV}(r_h, r_e) = \langle r_h \cdot r_e \rangle - \langle r_h \rangle \cdot \langle r_e \rangle. \tag{6.8}$$

R_{eh} ranges from -1 to $+1$, where negative values correspond to anti-correlation, *i.e.* a dynamical avoidance of electron and hole in space, 0 indicates no linear *electron-hole* correlation (which is the standard assumption in the MO-based picture), and positive values correspond to a joint *electron-hole* movement, *i.e.* exciton formation. To rationalize excitonic effects, the exciton wave function can be decomposed as

$$\chi_{exc}(r_h, r_e) \approx \phi_{he}(r_{he}) \phi_{CM}(R), \tag{6.9}$$

where $\phi_{he}(r_{he})$ describes the intrinsic *electron-hole* structure, which is similar to a hydrogen atom but with different effective masses, and $\phi_{CM}(R)$ describes the center-of-mass (CM) movement of the neutral exciton within the molecular potential.[93,138] To visualize the decomposed exciton wave function in terms of the joint *electron-hole* distribution in space the so-called *electron-hole* correlation plots are employed (cf. Refs. 65,75,138). The probability of an electron being promoted from one molecular site to another is encoded in grey scale.

6.3 Computational details

All calculations are performed with Q-Chem 4.3.[98] For the TDDFT calculations, the geometries are optimized in the corresponding ground state for each *xc*-functional using Alrichs' SV(P) basis set.[110] Seven *xc*-functionals are selected with different amounts of nonlocal orbital exchange (NLX): (a) PBE[201] as representative of local generalized-gradient-approximation-type functionals without nonlocal orbital exchange; (b) three different global hybrid functionals including: B3LYP (21 %),[16,20] PBE0 (25 %),[209] and M06-2X (54 %);[210] (c) three different long-range corrected (LRC) functionals CAM-B3LYP[47] (19−65 %), ωPBE (0−100 %),[211] and ωB97 (0−100 %)[49] (fraction of NLX in parenthesis).

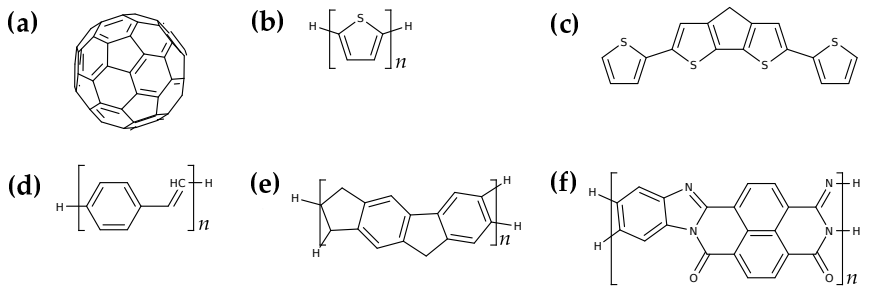

Figure 6.1: Conjugated π-systems investigated in this chapter: (a) fullarene C_{60}, (b) polythiophene ($n = 4, 6, 8$) (c) 4TB, (d) poly(*para* phenylene vinylene) ($n = 3, 5, 7$), (e) ladder-type poly(*para* phenylene) ($n = 1 - 4, 6, 8$), (f) benzimidazo-benzophenanthroline polymer ($n = 3 - 6$).[107]

If not stated otherwise, the Tamm-Dancoff approximation[30] was employed. For the configuration interaction singles (CIS) calculations, the geometries are optimized at the Hartree Fock (HF) level of theory and for the algebraic-diagrammatic construction for the polarization propagator (ADC(2)) calculations,[57–59] the geometries are optimized with ωB97. Conjugation lengths are determined by measuring the distance of the outermost atoms for each system for the B3LYP-optimized geometry and are presented in the supporting information. This quantity is not a unique measure for the extent of the π-system, nevertheless it is accurate enough for a rough estimate for the HOMO and LUMO sizes, since they are in all cases completely delocalized over the entire molecules. *Electron-hole* correlation plots are created using TheoDORE 1.1.4[176] with fragments representing individual phenyl rings as defined in Fig. 6.3.

6.4 Results and discussion

In the following, the first excited state of a set of prototypical, large π-conjugated molecules is investigated employing exciton analysis. These π-systems are the fullerene C_{60}, and oligomers of polythiophene (T), poly(*para* phenylene vinylene) (PPV), ladder-type poly(*para* phenylene) (LPPP) and poly(benzimidazo-benzophenanthroline) (BBL) as shown in Fig. 6.1.

In Fig. 6.2 (a) the exciton size for all molecules is plotted against the conjugation length. The first remarkable observation is a uniform exciton size scaling, *i.e.* the growth of exciton size with the conjugation length, cf. Refs 191,212. This uniform scaling is surprisingly independent from the molecular details of this diverse set of π-conjugated oligomers. However, large differences are observed between the computational methods. While with PBE (0 %

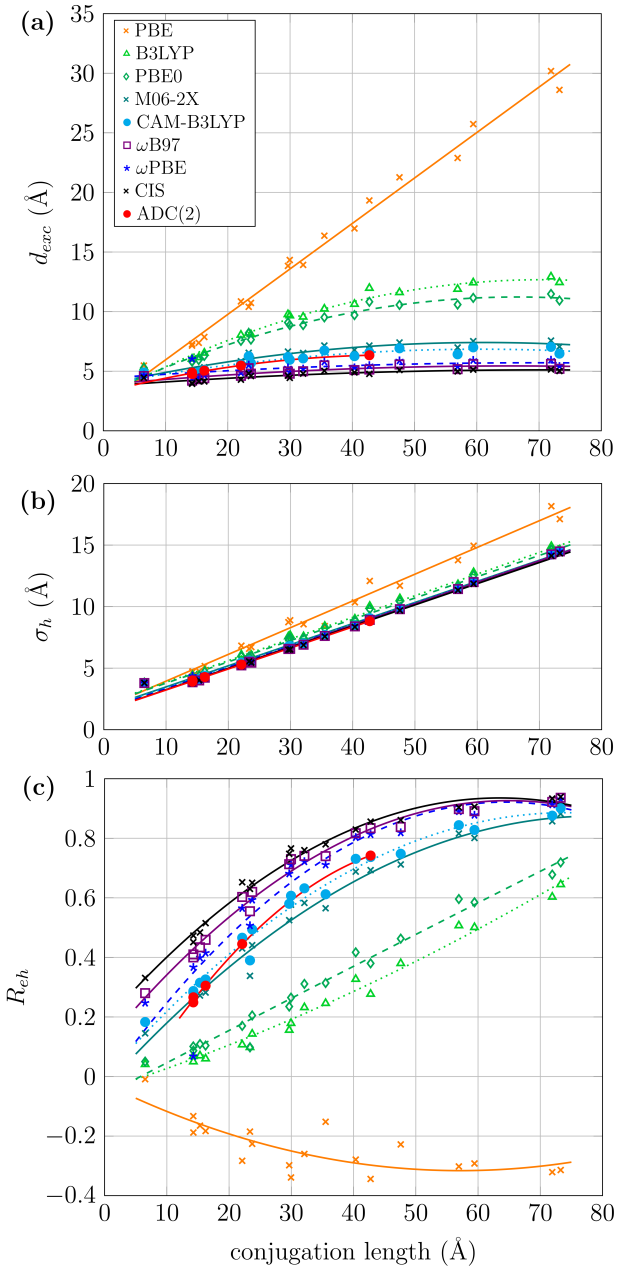

Figure 6.2: (a) Exciton sizes (d_{exc}, Å), (b) hole sizes (σ_h, Å), and (c) correlation coefficients R_{eh} for the first excited singlet state of each molecule plotted against conjugation length. Legend in (a) also applies to (b) and (c).

NLX) the exciton sizes increase linearly with values of about half of the conjugation lengths, for all other *xc*-functionals which include nonlocal orbital exchange, d_{exc} converges to functional-dependent values for long chains. For B3LYP (21 % NLX), a maximum of approx. 13.0 Å is found, while for PBE0 (25 % NLX) d_{exc} converges against 11.5 Å. With 54 % of nonlocal orbital exchange included, the exciton size with M06-2X is about 7.5 Å, and 7.0 Å for the long-range corrected CAM-B3LYP (19−65 % NLX). For the LRC functionals ωPBE and ωB97, which admix up to 100 % nonlocal orbital exchange at large electron-electron separations, the exciton size converges to 5 Å. To put these results into perspective, the exciton sizes are calculated with the *ab initio* methods CIS and ADC(2). The CIS exciton sizes mark a lower limit below the LRC functionals with a maximum of 5.0 Å, while ADC(2) closely resembles CAM-B3LYP with 7.0 Å. For semi-empirical methods, an even lower exciton size of 4 Å is found for ladder-type *para* phenylene oligomers.[207] Generally, the results confirm exciton size trends of Refs 102,191,213,214. As opposed to Ref. 212, there is no indefinite linear increase in d_{exc}, but the exciton size quickly levels off. In conclusion, the asymptotic exciton size limit in TDDFT depends almost exclusively on the amount of nonlocal orbital exchange included in the *xc*-functional. This nicely falls into place considering that this value determines the strength of the Coulomb interaction between electron and hole, cf. eq. (6.2).

The results for the hole sizes σ_h are shown in Fig. 6.2 (b) and electron sizes follow similar trends (see in Fig. 2 in SI of Ref. 97). In contrast to the exciton sizes d_{exc}, the electron and hole sizes increase linearly for all *xc*-functionals. To rationalize the discrepancy between d_{exc} and σ_h, it is instructive to examine linear correlation effects between electron and hole (R_{eh}) plotted in Fig. 6.2 (c). For the pure GGA functional PBE, correlation coefficients are negative throughout all systems investigated. This indicates that electron and hole quasi-particles dynamically avoid each other in space, which is rather typical for charge-transfer states than for bound excitons.[78,163] For all other *xc*-functionals that include nonlocal orbital exchange, *electron-hole* correlation coefficients are positive. This corresponds to a correlated motion of electron and hole in space, *i.e.* exciton formation. For the two hybrid functionals B3LYP and PBE0, the *electron-hole* correlation grows linearly with the system size with maxima for the largest conjugated system of 0.65 (B3LYP) and 0.72 (PBE0). For all LRC functionals and M06-2X, there is a strong increase between 5 to 40 Å, after which the value is already close to 1. The CAM-B3LYP results again closely resemble the ADC(2) results. These trends illustrate how exciton formation emerges for medium to large sized systems, whereas there is an intermediate range in which scattering prevents the excitons to form standing waves within

the molecular potentials.[92] The key message of the results is that the exciton structure can be manipulated from anti-correlated *electron-hole* pairs to strongly bound excitons just by tuning the c_{HF} parameter in eq. (6.2).

To further analyze the connection between correlation coefficient R_{eh}, exciton size d_{exc} and hole size σ_h, it is worth to examine their mathematical dependencies. The exciton size can be rewritten as[78]

$$d_{exc} = \sqrt{d_{h\to e}^2 + \sigma_h^2 + \sigma_e^2 - 2 \times \mathrm{COV}(r_h, r_e)}. \tag{6.10}$$

In the case of extended π-conjugated polymers, it can be assumed that the vectorial *electron-hole* distance $d_{h\to e}$ is approximately zero, and that electron and hole sizes are approximately the same ($\sigma_h \approx \sigma_e$). Considering this, eq. (6.10) can be simplified to obtain

$$d_{exc} \approx \sigma_h \sqrt{2(1 - R_{eh})}. \tag{6.11}$$

Eq. (6.11) allows to predict expectation values for different scenarios. For an uncorrelated electon-hole pair, the exciton size amounts to $\sqrt{2}\sigma_h$. For positive or negative correlation, it can vary between 0 and $2\sigma_h$, respectively. Revisiting Fig. 6.2, these trends are reproduced as *e.g.* in the case of PBE, the exciton size is always above $\sqrt{2}\sigma_h$, whereas it is always below this value for all other *xc*-functionals.

For drawing a connection between correlation effects of R_{eh} and excitonic structure, exciton wave functions of 8LPPP are visualized in terms of *electron-hole* correlation plots for all *xc*-functionals in Fig. 6.3.[65,75,102] For the PBE functional, the elements on the main diagonal (going from lower left to upper right) indicate a probability of almost zero, while the off-diagonal elements show a broad distribution of charge transfer between molecular sites in various distances. This pattern highlights the charge-transfer character of the excited state,[64,73,138] which coincides with a negative correlation coefficient of -0.31. On the contrary, for all the other *xc*-functionals which obtain positive R_{eh} values, *electron-hole* correlation plots are dominated by local excitations and charge transfer between neighboring sites. These patterns correspond to Wannier-type excitons, for which the intrinsic structure of the *electron-hole* pair is hydrogenic (for more details see Ref. 138). The off-diagonal width in the *electron-hole* correlation plots represents the average *electron-hole* distance (*i.e.* exciton size), and is controlled by the amount of nonlocal orbital exchange employed in the respective *xc*-functional in analogy to the values of d_{exc} and R_{eh}. The decomposition of the exciton wave function into an intrinsic part (shown as off-diagonal width of the *electron-hole* distribution) and an extrinsic part (distribution of the neutral exciton within the molecular potential parallel

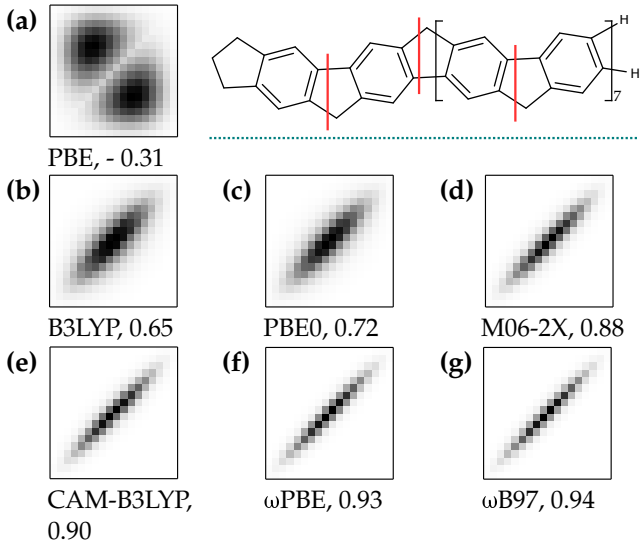

Figure 6.3: *Electron-hole* correlation plots and correlation coefficients R_{eh} of the first excited state of 8LPPP calculated using various *xc*-functionals. The fragmentation scheme is shown as inset.[107] The main diagonal in the *electron-hole* correlation plots[65,75,102] going from the lower left to the upper right element represents the probability of an electron being locally excited within one site while promotion between different sites is indicated as off-diagonal elements.

to main diagonal) allows to rationalize the connection between the exciton and MO pictures, cf. eq. (6.9). The delocalization of the joint *electron-hole* pair over the molecular potential generates a non-zero probability for the exciton to be located anywhere in the entire system. This translates into completely delocalized MOs, which themselves, however, are not capable to highlight the underlying exciton structure dominating the excited-state character. At this point it becomes clear why it is misleading to interpret excited states as weakly bound Wannier excitons with large sizes by arguing that the HOMO and LUMO are delocalized over the entire molecule. An exciton can simply not be characterized in the MO picture. To reveal its intrinsic structure, it is imperative to move to a correlated *electron-hole* representation.

As an alternative computational approach, the standard variant of linear-response TDDFT is employed to compare the performance of TDA and TDDFT for the systems investigated in this work. A reason for studying large systems with the Tamm-Dancoff approximation (TDA) is that it offers a computationally cheaper alternative to full TDDFT.[30] It is usually a good approximation to the full TDDFT scheme, and similar, sometimes even superior results can be obtained concerning excitation energies and properties, *e.g.* oscillator strength, motivating its use in the computations discussed previously. For comparing TDA and TDDFT in terms of exciton properties, exciton sizes and correlation coefficients are evaluated for three representative *xc*-functionals, PBE, PBE0 and ωPBE. Concerning the excitation energies shown in Fig. 6.4 (a), the results obtained by TDA and TDDFT show small deviations which decrease when going from small to larger systems for all *xc*-functionals. In the case of exciton sizes and correlation coefficients presented in Fig. 6.4 (b) and (c), the deviations between TDA and TDDFT results are consistently small, and the most significant deviations are found for PBE. Concerning the discussion of which method should be preferred to calculate excited states of large conjugated systems, this study reveals the treatment in terms of excitonic properties is similar for both methods and the largest differences are found for excitation energies of medium-size systems.

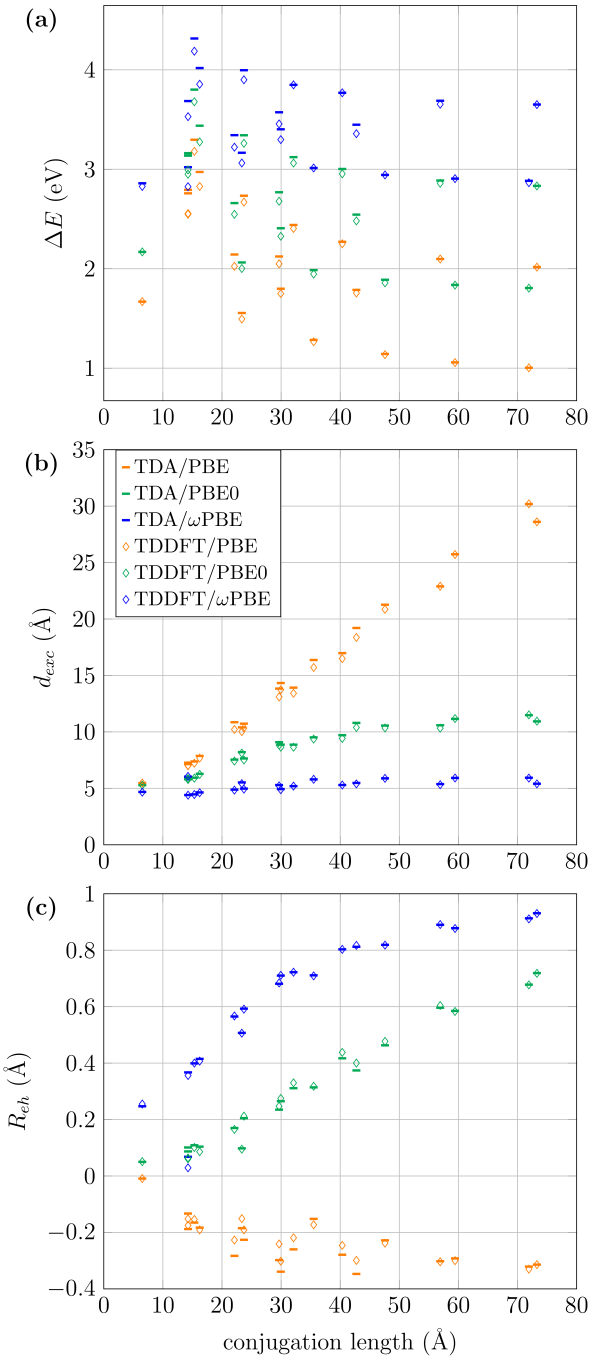

Figure 6.4: Comparison of TDA and TDDFT in terms of (a) excitation energies (ΔE, eV), (b) exciton sizes (d_{exc}, Å) and (c) correlation coefficients (R_{eh}) for the first excited state of the π-conjugated molecules employing PBE, PBE0 and ωPBE. Legend in (b) applies to all plots in this figure.

6.5 Conclusion

Exciton properties of the energetically lowest singlet excited states of a set of extended π-conjugated molecules were investigated with TDDFT in combination with a hierarchy of *xc*-functionals as well as the *ab initio* methods CIS and ADC(2). With the latter, the exciton size converges against 7 Å. In general, the convergence of the exciton size is found to be system-independent, but essentially governed by the amount of nonlocal orbital exchange in TDDFT. This effect is traced back to the *electron-hole* correlation, which is influenced by the *xc*-functional-dependent Coulomb attraction between the electron and hole quasiparticles. The problem of pure TDDFT to describe excited states in extended π-conjugated systems[31,39–41,106,137] hence originates from the inability to describe bound excitonic states.

Chapter 7

Benchmarking excited-state calculations using exciton properties

In this chapter, exciton analysis is employed for the evaluation of *ab initio* and TDDFT excited-state methods. Assessment of the accuracy of excited-state methods, whether for specific application or for establishing new approaches, is an important task in quantum chemistry. In benchmark studies, excitation energies are the central and often only criterion to judge the performance of excited-state methods. However, a detailed comparison of excited-state description is crucial to gain insight into differences of computational models. For this purpose, it is necessary to analyze the underlying wave functions and densities, and consequently, physically relevant quantities. Exciton-related properties provide a concise, quantitative description of excited-state properties, which is independent of computational protocols. Exciton properties are used to examine the performance of several excited-state methods for carefully selected molecules featuring challenging cases, such as Rydberg, doubly excited, extended $\pi \rightarrow \pi^*$ and charge-transfer states. These examples illustrate the utility of different exciton descriptors in assigning state characters and explaining discrepancies among different methods.

Please note that parts of this chapter have already been published by Prof. Dr. Andreas Dreuw, Prof. Dr. Anna I. Krylov, Dr. Felix Plasser and myself in the *Journal of Chemical Theory and Computation*, volume 14 (2018), number 2, pages 710−725 (Ref. 96).

7.1 Introduction

One important task in quantum chemistry[215] is proper benchmarking of approximate computational methods against highly accurate ones.[216–225] Such benchmark studies are motivated by the limited applicability of highly accurate methods to large systems due to unfavorable computational scaling of many-body theories leading to high computational demands.[215] The necessity to employ computationally more efficient but less reliable methods[26,208,226] together with limited experimental data undermine the credibility of computational protocols. In benchmarks of excited-state methods, the main (and often only) criterion is the excitation energy. While the excitation energy is certainly very important, the character of the underlying states should also be correctly described by approximate methods. However, the analysis of the underlying wave functions is often omitted, since it is a non-trivial task to compare orbitals and amplitudes systematically and quantitatively.[227] However, exactly these details are crucial to get insight into the differences in the physical description of excited states, and can be a decisive factor in determining the domains of applicability of approximate models.

In this chapter, a new perspective on benchmarks of excited-state methods is adopted by using exciton analysis.[73] Excited states are interpreted as excitons, *i.e.*, correlated electron-hole pairs. Exciton wave functions can be extracted from quantum-chemical computations via the one-particle transition density matrix (1TDM), which contains information on coupled electron-hole properties of an excited state. A variety of exciton properties can subsequently be extracted and serve as a basis for detailed analyses of excited states.[65,66,73,78] The exciton-based analysis of the electronic transitions provides insight into character of excited electronic states and offers several advantages for benchmarking: Firstly, it is independent from the method-dependent MO picture. Secondly, it can be applied to any excited-state method giving access to the one-particle transition density matrix. Thirdly, it enables explicit benchmarking of electron-hole correlation phenomena, which are directly related to the physical description of the excited state and crucial for the performance of quantum-chemical methods. Fourthly, it facilitates state character assignment, as different types of excited states can be distinguished by the features that are easy to identify (for example, Rydberg states possess large electron sizes, charge-transfer states have large separations between the centroids of holes and electrons). Ultimately, it affords detailed benchmarking of different methods, even when experimental data is absent.

While reduced density matrices and NTOs have been used in electronic structure for quite some time,[67–69,228] using them to compute properties of exci-

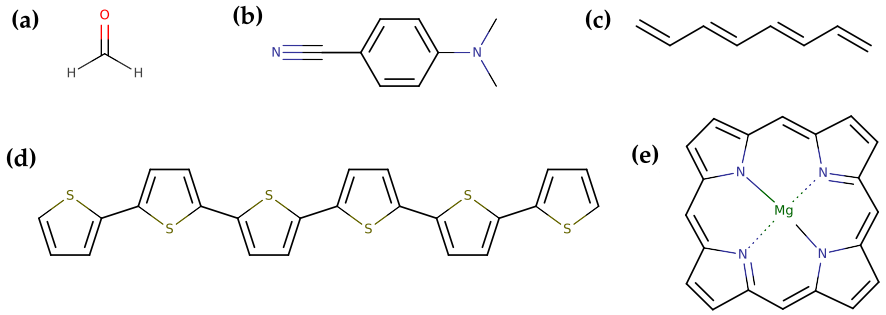

Figure 7.1: Molecules investigated in this chapter: (a) formaldehyde, (b) 4-(*N,N*-dimethylamino)benzonitrile (DMABN), (c) all-*trans* octatetraene, (d) *hexa*(thiophene) (6T), and (e) magnesium porphyrin (MgP).[107]

tons is relatively new.[65,66,73,78] Complementary to the here presented approach, there exists a variety of descriptors based on orbital overlaps,[51,53] changes in the density matrix[54,55] or in the electron density.[52] While these descriptors have been successfully employed for assessing the accuracy of TDDFT calculations,[229,230] they have not yet been generalized to higher-level *ab initio* methods. As an alternative approach for benchmarking, a comparison of entire many-electron wave functions by calculating wave function overlaps was recently introduced.[231] This analysis affords quantification of variations in wave functions with respect to a reference wave function for a wide range of computational methods.

In the following, it is shown that focusing on exciton properties opens a new route for a simple yet detailed benchmarking of excited states. A carefully chosen set of molecules is investigated that features various types of excited states (sec. 7.3). These systems, shown in Fig. 7.1, are formaldehyde, the push-pull system 4-(*N,N*-dimethylamino)benzonitrile (DMABN), all-*trans* octatetraene as a representative for multiply excited states, *hexa*(thiophene) (6T) as a large π-conjugated system with delocalized $\pi\pi^*$ excited states, and magnesium porphyrin (MgP) as large, biologically relevant compound. Two families of *ab initio* methods are compared: the equation-of-motion coupled-cluster singles doubles (EOM-CCSD)[232–236] and the algebraic-diagrammatic construction for the polarization propagator (ADC(n))[57–59] methods. In selected cases, time-dependent density functional theory[26,27,29] is employed in combination with a few, commonly used exchange-correlation functionals.

7.2 Computational details

All calculations were performed with the Q-Chem[98,108] electronic structure package. NTOs were visualized using Jmol.[237]

Formaldehyde. The geometry was optimized at the RI-MP(2)/cc-pVTZ level of theory yielding C_{2v} symmetry. Excited-state calculations were carried out with the ADC[57–59] method for the polarization propagator at the second and third order of perturbation theory as well as with the EOM-CCSD method for excitation energies (EOM-EE-CCSD).[232–234,238] ADC(2) and ADC(3) were used in their standard variants in combination with the Ahlrichs' SV(P) and SVP basis sets, and in the Resolution-of-Identity approximation[239] (RI) in combination with Ahlrichs' SV,[110] SV(P) and SVP, and Dunning's cc-pVDZ, cc-pVTZ, aug-cc-pVDZ, and aug-cc-pVTZ basis sets.[109,240] EOM-CCSD was used in its canonical variant (no RI) for all basis sets.

DMABN. Six structures were considered: the fully relaxed, ground-state geometry (GS) optimized at RIMP(2)/cc-pVDZ level of theory and five excited-state geometries, LE, CT0, CT45, CT90, CTP, optimized with RI-ADC(2)/cc-pVDZ. The LE and CTP structures were fully relaxed. For the CT geometries, constained optimization was carried out with the twisting angle between the benzene ring and the dimethylamino group constrained to 0° (CT0), 45° (CT45), and 90° (CT90). All optimizations were carried out in vacuum. Further details can be found in Ref. 241. Excited-state calculations were performed using ADC(2)/cc-pVDZ, ADC(3)/cc-pVDZ and EOM-CCSD/cc-pVDZ in vacuum in their canonical variants. Calculating solvent effects, a state-specific polarizable continuum model (IEF-PCM)[199] was employed in combination with standard ADC(2)/*SS*-PCM/cc-pVDZ available in Q-Chem 5.0. The solvents cyclohexane (cHex, $\varepsilon = 1.89$, $n^2 = 1.88$) and acetonitrile (MeCN, $\varepsilon = 36.7$, $n^2 = 1.81$) were employed (information about specific input parameters can be found in Ref. 241).

***Hexa*(thiophene).** The ground-state geometry was first optimized using ωB97/SV(P) level of theory and then symmetrized using IQmol (the symmetrization resulted in very small changes in total energy). Excited-state geometry of the S_1 state was optimized using CAM-B3LYP/cc-pVDZ. Excited-state calculations for vertical excitations were carried out at the RI-ADC(2), RI-EOM-CCSD (with core electrons frozen), and CIS *ab initio* levels of theory, and at the full-time-dependent density functional theory[26,27,29] (TDDFT) and Tamm-Dancoff approximation[30] (TDA) levels employing BLYP, B3LYP, CAM-B3LYP exchange-correlation functionals. The three *xc*-functionals feature different amounts of nonlocal orbital exchange: the BLYP functional (0 % of exact exchange) is a representative of local generalized-gradient-approximation-type

(GGA) functionals, the B3LYP functional is a global hybrid functional (21 % of exact exchange),[16,20] and CAM-B3LYP is a long-range corrected method (19−65 % of exact exchange).[47] All calculations were performed using Ahlrichs' SV(P) basis set. In addition, RI-EOM-CCSD calculations with aug-cc-pVDZ were carried out. Adiabatic excitation energies were calculated using TDDFT optimized structure and the RI-ADC(2)/SV(P) and RI-EOM-CCSD/aug-cc-pVDZ levels of theory.

All-*trans* octatetraene. The ground-state geometry was optimized using CCSD(T)/cc-pVTZ level of theory yielding C_{2h} symmetry. This high level of theory is essential to correctly describe the electronic structure of the ground state and to obtain accurate carbon-carbon distances for the conjugated system.[242] Excited-state calculations were carried out with RI-ADC(2), RI-ADC(3), RI-EOM-CCSD and with TDDFT/TDA using BLYP, B3LYP, and CAM-B3LYP *xc*-functionals employing Dunning's cc-pVTZ basis.

Magnesium(II)porphyrin. The ground-state geometry was optimized using RIMP/TZVP level of theory, followed by IQmol symmetrization. Excited-state calculations were performed with RI-ADC(2)/SV(P), RI-EOM-CCSD/-SV(P), RI-EOM-CCSD/cc-pVDZ, RI-EOM-CCSD/cc-pVTZ, ADC(3)/SV(P), and CIS/SV(P) as well as with TDDFT/TDA employing BLYP, B3LYP, and CAM-B3LYP as *xc*-functionals with Ahlrichs' SV(P) and TZVP basis sets.

Cartesian coordinates for all structures are given in SI of Ref. 96. It should be noted that Q-Chem does not follow the standard Mulliken convention[243] for molecular orientation, such that the labels of some irreps are flipped.[244]

All raw numbers shown in figures are given in SI of Ref. 96.

7.3 Results and discussion

In the following, different types of excited states are examined focusing on exciton descriptors that deliver information relevant to each particular case. It is illustrated which descriptors can aid the benchmark procedure and how they can inform the user about methodological aspects.

7.3.1 Valence and Rydberg states in formaldehyde

A popular benchmark molecule,[25,245] formaldehyde demonstrates the utility of exciton descriptors in distinguishing Rydberg and locally excited states.[227] Rydberg states have relatively small hole sizes σ_h and large electron sizes σ_e. In contrast, locally excited states show rather similar electron and hole sizes. Table 7.1 shows excitation energies, term labels, and state characters for six singlet excited states of formaldehyde.[25] The experimental values are compared with

Table 7.1: Excited states of formaldehyde: irreducible representations, characters and excitation energies (eV).

		.	cc-pVTZ			aug-cc-pVTZ		
state	type[a]	exp.[a]	ADC(3)	ADC(2)	EOM.	ADC(3)	ADC(2)	EOM.
1^1A_2	$n \rightarrow \pi^*$	4.1	3.92	4.01	4.07	3.90	3.92	4.02
1^1B_1	$n \rightarrow 3s$	7.13	8.77	7.66	8.35	7.63	6.52	7.24
2^1B_1	$n \rightarrow 3p$	7.98	10.53	9.94	9.36	8.46	7.54	8.12
2^1A_1	$n \rightarrow 3p$	8.14	(9.23)[b]	9.37	9.82	8.62	7.49	8.22
1^1B_2	$\sigma \rightarrow \pi^*$	9.0	9.20	9.29	10.28	9.18	9.18	9.30
3^1A_1	$\pi \rightarrow \pi^*$	10.7	(9.81)[b]	10.22	(10.57)[c]	9.06	(9.48)[d]	9.68

[a] experimental data and state assignment is from Ref. 25.

[b] substantial state mixing and double excitation character.

[c] state has 53% Rydberg character and only 30% $\pi \rightarrow \pi^*$.

[d] state has 64% Rydberg character and only 25% $\pi \rightarrow \pi^*$.

the computational results obtained with ADC(3), ADC(2) and EOM-CCSD in combination with the cc-pVTZ and aug-cc-pVTZ basis sets. As expected, the cc-pVTZ basis is not sufficient for describing Rydberg states, leading to large errors in excitation energies. The results improve considerably in the aug-cc-pVTZ basis set: the state ordering is correct in almost all cases and the errors against the experimental values are substantially smaller. Using specialized basis sets[246] for the description of Rydberg states may further improve the results, however, for the purpose of this study the obtained results suffice. Using this assessment of the accuracy of the methods as a starting point, detailed analysis based on exciton descriptors will be discussed in the following.

Fig. 7.2 shows the ADC(3) results for the first two singlet excited states of each irreducible representation. Two states are highlighted in blue, 1^1A_2 and 2^1A_2, which are discussed in more detail below. Fig. 7.2 (a) shows the changes in excitation energies with respect to the basis sets. The following hierarchy of basis sets is considered (from left to right): first, the polarization of the second-row atoms is included; second, the basis is extended from double-ζ to triple-ζ; third, diffuse functions are included (for both double-ζ and triple-ζ bases). While the excitation energies remain constant for almost all states for the first five basis sets (with a few exceptions), significant changes occur upon the augmentation. This is expected since diffuse functions are mandatory for the correct description of Rydberg states.[227] Although more compact valence states do not requite diffuse functions, they can mix and interact with Rydberg states, especially when the density of states is high[227] as it is the case around 9 eV in formaldehyde. Consequently, locally excited states in this energy range also stabilize in the augmented basis sets (black, dotted lines). This example illustrates that the dependence of excitation energy on the basis set is not sufficient for distinguishing Rydberg and valence states and the utility of exciton

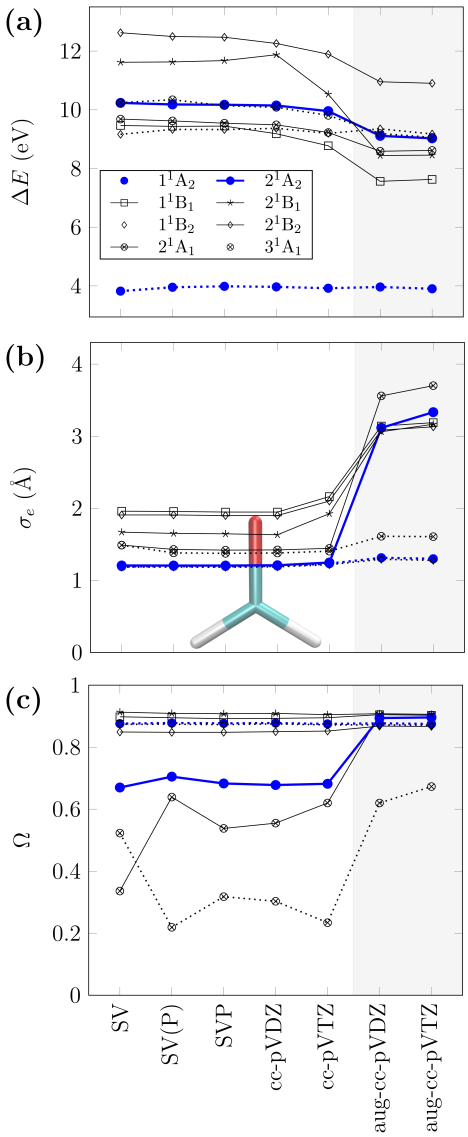

Figure 7.2: Excited states in formaldehyde. (a) Excitation energies (ΔE, eV), (b) electron size (σ_e, Å), and (c) Ω values of the first two excited states of each irreducible representation calculated by ADC(3) with different basis sets. The legend in (a) applies to all diagrams. The inset of the formaldehyde structure in (b) shows the size of the molecule.

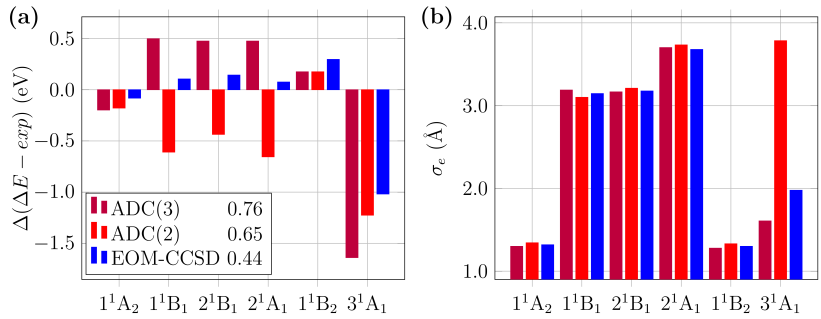

Figure 7.3: Excited states of formaldehyde. (a) Differences between experimental and computed excitation energies ($\Delta(\Delta E - exp)$, eV), and (b) electron sizes (σ_e, Å) of six excited states computed at the ADC(3), ADC(2) and EOM-CCSD levels of theory employing the aug-cc-pVTZ basis set. Root-mean-square deviations (eV) are displayed in legend.

analysis becomes obvious.

Fig. 7.2 (b) and Fig. S1(b) in SI of Ref. 96 illustrate the effect of the basis set on the excited-state wave functions by considering electron and hole sizes, cf. eq. (2.33). While the hole sizes (Fig. S1(b) in SI of Ref. 96) vary between 1.0 and 1.3 Å (and only two excited states show a noticeable increase of ∼0.2 Å upon the inclusion of diffuse functions), the electron sizes change dramatically for the Rydberg states (Fig. 7.2 (b)). This behavior can be contrasted to almost constant values of σ_e of the locally excited states (1^1A_2, 1^1B_2, 3^1A_1). Thus, σ_e is a key descriptor which is able to differentiate between valence and Rydberg states.

Fig 7.2 (c) presents another important property, Ω, which quantifies the amount of single excitation character in the excited-state wave functions. For a primarily singly excited state, $\Omega \approx 1$. In small (not augmented) basis sets, some states (two $^1A_1$ states and 2^1A_2) show significantly smaller values of Ω at the ADC(3) level of theory, which indicates substantial double excitation character. This doubly excited character disappears when diffuse functions are included, suggesting that it is an artifact of using small basis sets (which is similar to a well-known phenomenon of valence-space CASSCF, overestimating doubly excited character).

In the following, exciton characters will be compared for ADC(2), ADC(3) and EOM-CCSD wave functions with the aug-cc-pVTZ basis set. Fig. 7.3 (a) presents the differences between experimental and computed excitation energies for the six excited states discussed above including the ADC(2), ADC(3) and EOM-CCSD levels of theory. The corresponding electron sizes are plotted in Fig. 7.3 (b). The deviations from the experimental values can be systematically

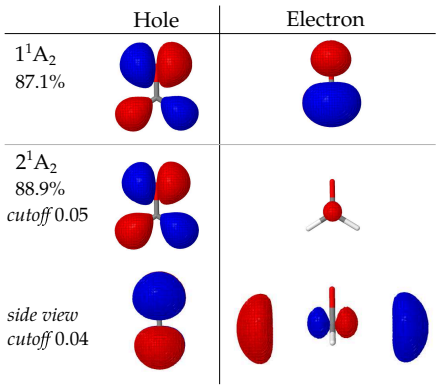

Figure 7.4: Natural transition orbitals of the $1^1A_2(n \rightarrow \pi^*)$ and $2^1A_2(n \rightarrow Ry(3p))$ excited states of formaldehyde calculated at the ADC(3)/aug-cc-pVTZ level of theory. Singular values are given in percentage. For the Rydberg state, two different isovalues are used (0.05 e and 0.04 e).

explained in terms of the state characters. The ADC(2) method underestimates Rydberg excitation energies by about 0.5 eV, whereas ADC(3) overestimates energies of these states by 0.5 eV. EOM-CCSD yields the smallest errors for, both, valence and Rydberg states. An outstanding case is the 3^1A_1 state, for which all computational methods yield large errors in excitation energies. The electron sizes indicate that the state has some Rydberg character at the ADC(2) level, while it appears to be rather local at the other levels of theory. The analysis of single excitation character in Fig 7.2 (c) reveals that this state has some double excitation character. However, it seems that both ADC(3) and EOM-CCSD are underestimating the energy of this state.

A practical issue for which electron sizes are helpful is connected to creating orbital representations of Rydberg states. Fig. 7.4 shows NTOs for the 1^1A_2 $(n \rightarrow \pi^*)$ and 2^1A_2 $(n \rightarrow Ry(3p))$ excited states of formaldehyde. Both states are well described by a single NTO pair (the respective leading σ^2 values are 0.87 and 0.89). The visualization of the hole orbital is straightforward, however, accurate rendering of the electron (particle) orbital requires some care. While valence-like electron NTOs (such as π^* electron orbital of the 1^1A_2 state) can be adequately visualized using the same isovalues as used for the also valence-like hole orbitals, the diffuse Rydberg orbitals need to be rendered with smaller isovalues. When using the same isovalue as for valence orbitals, the isosurface encloses only a small part of the electron density of much more diffuse Rydberg orbitals (this can be easily understood by comparing two normalized gaussians with different exponents, see Fig. S3 in SI of Ref. 96). This can lead to a misleading picture as illustrated by the middle row of Fig. 7.4. Only when the

isovalue is adjusted to a lower value (as in the low row of Fig. 7.4), the true shape of the Rydberg orbital becomes visible. By considering electron sizes, the Rydberg character of a state becomes directly apparent, alerting users that small isovalues are required for rendering NTOs.

7.3.2 Charge-transfer states in DMABN

Charge-transfer states present a challenge for many excited-state methods (cf. sec. 1.8). As a consequence, they are often used in benchmark studies to examine methodological issues.[36,51] In this benchmark set, 4-(*N,N*-dimethylamino)-benzonitrile (DMABN), a substituted benzene ring with a donor and acceptor group in *para* position, is considered as a representative organic push-pull molecule. The photochemistry of DMABN is rather complex. DMABN features dual fluorescence in polar environments,[247] where there are two fluorescence peaks, one at 350 nm (3.54 eV) and another at 475 nm (2.61 eV); the latter peak vanishes in apolar solvents. The origin of dual fluorescence and the solvent-dependent vanishing of the second peak has been attributed to the two singlet excited states that are responsible for the fluorescence. The first state is a locally excited state (LE) of $\pi \rightarrow \pi^*$ character localized on the benzene ring. The second state is a charge-transfer (CT) state, in which an electron is promoted from the electron-donating dimethylamino group towards the benzonitrile group (cf. Fig. S4 of SI of Ref. 96). It should be noted that none of these states is of "pure" LE or CT character, but mixing of different configurations occurs to a various extent. The LE and CT states experience different interactions with a polar solvent and also exhibit different structural relaxation. Detailed discussion on the role of these states in dual fluorescence can be found in Refs. 241,248.

In this work, excited states of DMABN are investigated by means of exciton analysis in order to analyze the properties of LE and CT states in detail. Several geometries from Ref. 241 are used to represent excited-state relaxation (see sec. 7.2). The LE geometry is the fully-relaxed geometry optimized for the LE state. By using the sequence of CT structures, the effect of solvent-dependent structural relaxation is investigated by considering a twist of the two methyl groups with respect to the benzene (these structures with different twisting angles are denoted by CT0, CT45 and CT90). The fully relaxed CT state structure has a pyramidalized dimethylamin group (denoted CTP).

Fig. 7.5 presents the results for the lowest LE and CT states of DMABN at different geometries computed at the ADC(3)/cc-pVDZ, ADC(2)/cc-pVDZ, and EOM-CCSD/cc-pVDZ levels of theory. Fig. 7.5 (a) shows that the LE state is the lowest at the ground-state geometry for all three methods. While ADC(2) and ADC(3) values are on top of each other (4.49 eV and 4.47 eV,

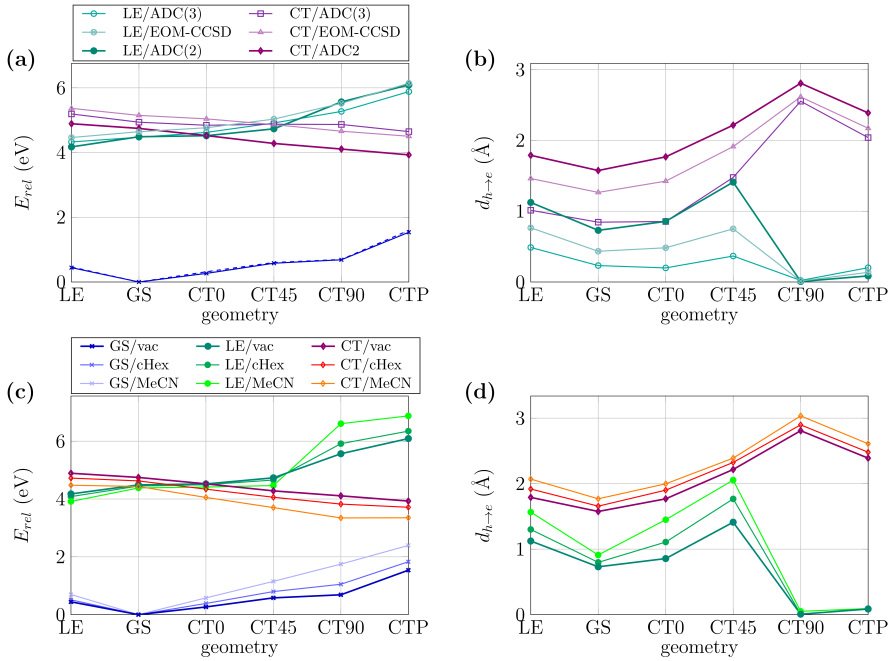

Figure 7.5: Lowest LE and CT states of DMABN at different geometries at the ADC(3)/cc-pVDZ, ADC(2)/cc-pVDZ, and EOM-CCSD/cc-pVDZ levels of theory. (a) Relative excitation energies (E_{rel}, eV). (b) Distances between electron and hole charge centers ($d_{h\to e}$, Å). Legend in (a) also applies to (b). (c) Relative energies (E_{rel}, eV) of the ground (GS) and excited states (LE, CT) calculated at the ADC(2)/cc-pVDZ level of theory in combination with PCM.[241] (d) Solvent effects on electron-hole separation ($d_{h\to e}$, Å). Legend in (c) also applies to (d).

respectively), the EOM-CCSD excitation energy is slightly higher (4.65 eV). For the CT state, the spread in excitation energies is larger: at the ADC(2) level, the CT state lies only 0.26 eV above the LE state, whereas the gap is larger (≈0.5 eV) for ADC(3) and EOM-CCSD (the respective excitation energies are 4.94 and 5.15 eV). At the LE geometry (Fig. 7.5 (a), left side), the LE state is strongly stabilized, while the energy of the CT state is slightly blue-shifted. At the CT geometries (right side of Fig. 7.5 (a)), the excitation energy of the LE state slightly increases. These trends are observed at all levels of theory. At the CT90 geometry, the LE excitation energy computed by ADC(2) jumps up to 5.57 eV in sharp contrast to ADC(3) and EOM-CCSD. At all levels of theory, the CT state exhibits a gradual stabilization along the twisting coordinate. The stabilization is most pronounced at the ADC(2) level. At the CT45 geometry, the excitation energies for the LE and CT state are almost degenerate at the ADC(3) and EOM-CCSD levels. Increasing the angle disrupts the conjugation between the benzene ring and the lone pair orbital at the nitrogen atom, leading to further stabilization of the CT state and destabilization of the LE state.

To rationalize differences between the different levels of theory, excited-state properties are examined. In the context of CT states, the vectorial electron-hole distance $d_{h\to e}$ is the key property. For the LE state, it is expected that the vectorial distance between the electron and hole distribution $d_{h\to e}$, that is, the separation of the charge cendroids (eq. (2.31)) is close to zero since the relevant orbitals reside in the same part of the molecule despite being delocalized (which is the case for the π-orbitals of a benzene ring). In contrast, CT states involve transitions between orbitals located at different parts of the molecule. Consequently, $d_{h\to e}$ values should reflect the distances between the parts of the molecule involved in charge transfer. The data presented in Fig. 7.5 (b) shows that at the GS geometry, the LE and CT states differ in $d_{h\to e}$ by at least 0.6 Å for EOM-CCSD and by more than 0.8 Å for the ADC methods. At the LE-optimized geometry and along the twisting coordinate, the charge separation moderately increases for the LE state and is strongly enhanced for the twisted structures (CT45 and CT90) at all levels of theory. Rationalizing the trends in ADC(2) excitation energies, the $d_{h\to e}$ values reveal major changes in the state character for the LE state: for the CT45 geometry, $d_{h\to e}$ of the LE state is as large as 1.41 Å which is rather typical for a CT state. At the CT90 geometry, $d_{h\to e}$ drops to almost zero. Obviously, the twist of the dimethylamin group beyond 45 degrees breaks the conjugation, and, as a consequence, the LE state localizes on the benzene ring. This effect can also be visualized using NTOs, which are presented in Fig. S4 in the SI of Ref. 96 for three geometries at the EOM-CCSD level of theory.

It is worth noting that electron-hole separation $d_{h\to e}$ increases in the fol-

lowing sequence: ADC(3) < EOM-CCSD < ADC(2). To my knowledge, no systematic analysis of this trend has been reported so far, yet there have been a couple of studies with similar findings suggesting that ADC(2) tends to overestimate charge-transfer character.[241,249,250]

To understand solvent effects on excitation energies and exciton properties, the $d_{h\to e}$ values of the LE and CT states are recalculated employing a polarizable continuum model (PCM) with equilibrium solvation, that is, the solvent field is optimized for the same state as the geometry as described in detail in Ref. 241. Fig. 7.5 (c) shows the results for two solvents, acetonitrile (MeCN), an example of a polar solvent, and cyclo-hexane (cHex), a non-polar solvent. Fig. 7.5 (c) shows the relative energies for the ground and excited states with respect to the ground-state energy at the GS geometry, which is set to zero for each model. At the GS geometry, the CT state is more stabilized by the solvents than the LE state. At the CT-optimized geometries, the ground state is strongly destabilized and its energy rises up by more than 2 eV for the CTP geometry in MeCN. At the same time, the CT energy decreases for the CT-optimized geometries, as shown in the right hand side of Fig. 7.5 (c), and the stabilization is more pronounced in the polar solvent, just as expected. The LE state is slightly destabilized, with only minor influence of the environment for the smaller twisting angles. In contrast, at the CT90 and CTP geometries there are significant changes: the excitation energies steeply increase and the solvent effects become more pronounced. Comparing these trends with the changes in $d_{h\to e}$ presented in Fig. 7.5 (d), it is interesting that the effects generally follow the trends in relative energies but that the magnitude of change in $d_{h\to e}$ does not necessarily linearly correspond to the solvent-induced shifts. While the $d_{h\to e}$ values of the CT state show a constant shift when going from vacuum to cHex to MeCN, irrespectively of the geometry, the LE state shows a very different trend. At the GS geometry, the shifts in $d_{h\to e}$ are almost equal to the ones of the CT state at this geometry. In contrast, the shifts are more than twice as large for the LE, CT0 and CT45 geometries. The dramatic drop in $d_{h\to e}$ at the CT90 geometry, which is attributed to the break in conjugation between the benzene ring and the dimethylamino group, is accompanied by a complete vanishing of solvent effect on the $d_{h\to e}$ values. The solvent-dependent changes in excitation energies of the LE state at the CT90 and CTP geometries are driven by the changes in the ground-state energies at these geometries rather than by changes in the excited-state character.

In conclusion, it was demonstrated how the $d_{h\to e}$ values of the LE and CT states in DMABN are affected by the electronic structure method as well as by different solvent models. Comparing these values with the trends in relative energies allowed to quantify different effects of the solvent models on different

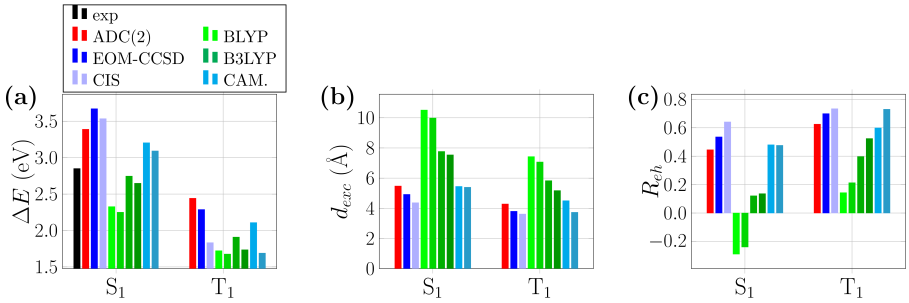

Figure 7.6: Excited states of *hexa*(thiophene). (a) Excitation energies (ΔE, eV), (b) exciton sizes (d_{exc}, Å), and (c) correlation coefficients (R_{eh}) of the first singlet (S_1, 1^1B_u) and triplet (T_1, 1^3B_u) states calculated at various levels of theory employing the SV(P) basis set. The legend in (a) applies to all plots in this figure, CAM. refers to CAM-B3LYP. Light colors for BLYP, B3LYP and CAM-B3LYP correspond to TDA, dark colors to full TDDFT. Experimental spectrum recorded in dioxane.[251,252]

types of states. The examples highlighted the utility of $d_{h\to e}$ in identifying and quantifying permanent charge-transfer character.

7.3.3 Delocalized $\pi\pi^*$ states in *hexa*(thiophene)

Excited states of extended π-systems, such as *hexa*(thiophene) oligomer (6T) tend to form excited states with exciton character.[81,97,120,121,138,156] It is therefore particularly interesting to analyze their excited states by means of exciton descriptors. The theoretical description of transitions with charge-resonance character, as those giving rise to bright states in organic photovoltaic materials, is affected by the same methodological shortcomings as charge-transfer states,[34,36,37] although the origin of the problem is less obvious due to the absence of permanent charge separation.[41,106,137] Two descriptors are relevant is this case: the exciton size and the linear electron-hole correlation. While the former allows to determine the type and character of the exciton, the latter is important to assess the description of electron-hole correlation effects by different quantum-chemical methods.[97,138]

In the following, the first singlet (S_1,1^1B_u) and triplet (T_1,1^3B_u) excited states are considered. The 1^1B_u state is the lowest singlet excited state and carries large oscillator strength. Fig. 7.6 presents an analysis of the states in terms of excitation energies as well as exciton descriptors using R_{eh} and d_{exc}. In terms of excitation energies shown in Fig. 7.6 (a), ADC(2) and EOM-CCSD appear to significantly overestimate the excitation energy of S_1 state, by 0.54 eV and 0.82 eV, respectively (the experimental value is 2.85 eV). Several factors contribute to this rather large discrepancy. Firstly, the experimental spectrum

has been recorded in dioxane, which has a refractive index of 1.42 and stabilizes excited states, thus lowering vertical excitation energies in comparison to gas-phase experiments. Secondly, the selected geometry contributes to the rather large errors. The employed geometry was optimized at the ωB97/SV(P) level. Reoptimizing the structure and calculating vertical excitation energies at the CAM-B3LYP/cc-pVDZ level yields 3.05 eV, which is a significant improvement and a similar effect is expected for ADC(2) and EOM-CCSD. Thirdly, using a more appropriate basis, such as the aug-cc-pVTZ set, is expected to lead to additional lowering of excitation energy by 0.1−0.2 eV.[138,253] While 6T is too large for EOM-CCSD calculations with a triple-zeta basis, EOM-CCSD calculations were performed with aug-cc-pVDZ basis and obtained excitation energy of 3.38 eV (thus, reducing the error down to 0.53 eV). Ultimately, states with large charge-resonance character (such as singlet $\pi \rightarrow \pi^*$ states in conjugated systems) are known to require accurate account of dynamic correlation, and the errors of EOM-CCSD are often close to 0.3 eV and systematic for such states leading to overestimation of excitation energies, cf. Ref. 253. This is reflected in the trends when going from CIS to ADC(2): Increasing the level of treatment of doubly excited determinants yields more accurate excitation energies. While it is clear that the bright B_u state is a singly excited state, doubly excited determinants contribute indirectly, giving rise to a more accurate description of electron correlation. Among TDDFT methods, the B3LYP shows the best agreement with experimental vertical excitation energy (error of −0.10 eV for TDA) in both TDA and full TDDFT variants. The CAM-B3LYP/TDA result is blue-shifted by 0.35 eV, and BLYP/TDA underestimates the excitation energy by −0.52 eV. The blue shift observed with CAM-B3LYP is consistent with the behavior of wave-function methods, whereas seemingly better agreement of BLYP and B3LYP is likely to be an artifact.

For the T_1 state (^3B_u), EOM-CCSD and ADC(2) obtain very similar results: The EOM-CCSD excitation energy for T_1 is 2.29 eV, which is only −0.15 eV below the ADC(2) value of 2.44 eV. In contrast, TDDFT (and CIS) methods for T_1 state obtain much smaller values clustered around 1.7 eV.

Fig. 7.6 (b) and (c) show exciton descriptors, revealing a large spread in exciton sizes and correlation coefficients for the two states. For the S_1 state, EOM-CCSD exciton size is 5 Å, which is very similar to the CAM-B3LYP value. B3LYP and BLYP results have substantially larger values of 8 Å and 10 Å, respectively. These values can be compared to the size of the molecule, which is 22.1 Å. Taking into account that the exciton size is defined as root-mean-square separation of the *electron-hole* distribution, EOM-CCSD, ADC(2) and CAM-B3LYP predict a bound *electron-hole* pair, whereas BLYP and B3LYP describe the exciton as unbound, for a more detailed discussion of these effects

cf. Chapter 6. The exciton size in T_1 is much smaller for all methods, which can be attributed to the absence of exchange repulsion.

The *electron-hole* correlation coefficients (Fig. 7.6 (c)) illuminate the observed wide spread in exciton sizes for the S_1 state: While for the *ab initio* methods and CAM-B3LYP R_{eh} is positive with values above 0.46, BLYP result has a negative *electron-hole* correlation (-0.29), and B3LYP has small positive value ($+0.12$). A negative value in R_{eh} corresponds to a dynamical avoidance of the electron and hole in space, which is physically incorrect according to the *ab initio* references and contradicts the picture of bound excitons. A related study on *tetra*(thiophene) has shown that the excitation energies of the first bright excited state strongly depend on the amount of nonlocal exact exchange and that spurious charge-transfer states appear for *xc*-functionals without or with low percentage of nonlocal orbital exchange.[35] The same phenomenon is at play in π-conjugated systems and is related to methodological issues in the description of excitonic properties.[97] The results of *hexa*(thiophene) present another example of misleading error cancellation, illustrating that seemingly accurate excitation energies obtained by B3LYP correspond to erroneous description of the exciton.

In the triplet state, all methods yield R_{eh} larger that the respective S_1 values. The increase in *electron-hole* correlation can be rationalized in terms of exchange interaction: While electron and hole experience a short-range exchange repulsion in the case of singlet excitons, in triplet excitons this repulsion is absent due to the different multiplicity, allowing the hole and electron to co-localize in space. This phenomenon, clearly seen in d_{exc} and R_{eh}, is a short-range effect and largely determined by the response of the Hartree potential. Consequently, it is well captured by TDDFT with all *xc*-functionals.

Concerning the applicability of the Tamm-Dancoff approximation in extended π-systems, Fig. 7.6 (a) also compares the S_1 excitation energies computed employing the TDA (light colors) and full TDDFT (dark colors) in combination with BLYP, B3LYP and CAM-B3LYP. While for the BLYP and B3LYP functionals deviations from the experimental excitation energy are smaller for TDA, full TDDFT seems to perform better for CAM-B3LYP ($+0.24$ eV versus $+0.35$ eV).

7.3.4 Doubly excited states in octatetraene

All-*trans* polyenes, prototypical linear π-conjugated systems, play key roles in many biologically relevant systems, for example, in carotenoids. Despite their simple molecular structure, excited states of polyenes are challenging for theoretical description due to low-lying doubly excited configurations.[42,90,187] A plethora of studies investigated different aspects of the excited states of

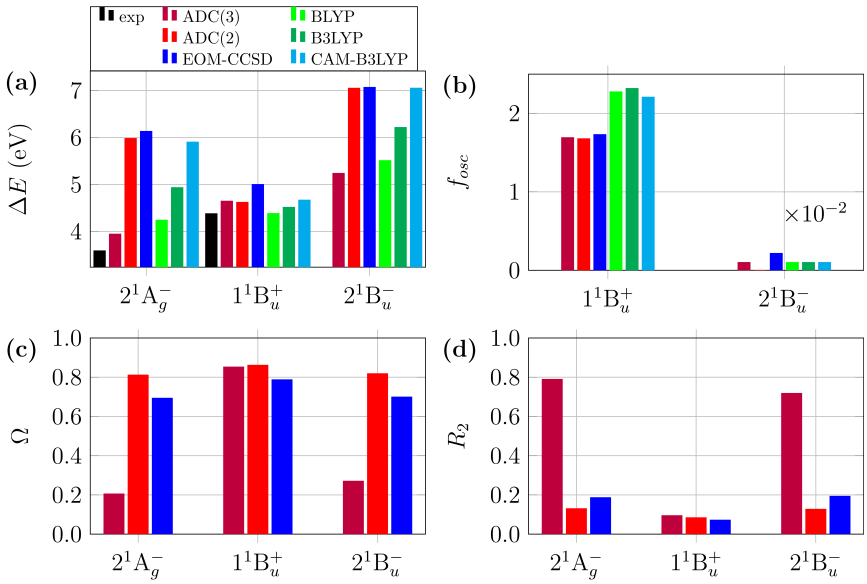

Figure 7.7: Excited states of all-*trans* octatetraene. (a) Excitation energies (ΔE, eV), (b) oscillator strengths (f_{osc}), (c) Ω values (Ω), and (d) squared doubles amplitudes (R_2) of the $2^1A_g^-$, $1^1B_u^+$, and $2^1B_u^-$ states calculated with ADC(2), ADC(3), EOM-CCSD, BLYP/TDA, B3LYP/TDA and CAM-B3LYP/TDA employing the cc-pVTZ basis set. The legend in (a) applies to all diagrams. Experimental data are from Ref. 187.

polyenes.[39,42,187,242,254–260] In this benchmark set, octatetraene is selected to identify double, or, more generally, multiple excitation character in excited states according to exciton properties, and to compare excited states and their properties at different levels of theory. In many biologically relevant applications, excited-state calculations are only feasible using very efficient but approximate TDDFT approach. An intense search for an appropriate exchange-correlation functional revealed that BLYP was capable of obtaining the experimentally observed state order, *i.e.*, that the dark A_g state is the lowest excited state for all compounds larger than hexatriene. Therefore the BLYP functional is included in the benchmark study, along with its hybrid counterpart, B3LYP, and a long-range corrected functional, CAM-B3LYP. However, it is well known that linear-response TDDFT performs poorly for doubly excited states.[42,43] It would therefore be interesting to compare these methods with alternative approaches, *e.g.* dressed TDDFT or spin-flip TDDFT,[261,262] cf. *e.g.* Ref. 208 and references therein, however, this is beyond the scope of the present work. The excited states are classified in terms of their irreducible representation as A_g, A_u, B_g and B_u and marked with + or − depending on their character, *i.e.*, + denotes ionic resonance structures and − denotes neutral (covalent) ones (cf. Ref. 259 and references therein). Fig. 7.7 presents the results for

the $2^1A_g^-$, the $1^1B_u^+$, and the $1^1B_u^-$ excited states of octatetraene. Fig. 7.7 (a) shows a large spread in the excitation energies computed by different methods. ADC(3) shows the best agreement with the experimental data,[187] with deviations of +0.36 eV and +0.27 eV for $2^1A_g^-$ and for $1^1B_u^+$, respectively. ADC(3) is the only *ab initio* method that reproduces the experimental state ordering. ADC(2) and EOM-CCSD show substantial deviations for the $2^1A_g^-$ state (+2.39 eV for ADC(2) and +2.54 eV for EOM-CCSD). For the $1^1B_u^+$ state, the errors are much smaller: +0.24 eV and +0.62 eV for ADC(2) and EOM-CCSD, respectively. Increasing the basis set up to aug-cc-pVTZ lowers the EOM-CCSD excitation energies by about 0.1 eV yielding 6.055 and 4.896 eV for the $2^1A_g^-$ and $1^1B_u^+$ states, respectively. Thus, even with a larger basis EOM-CCSD still places the dark A_g state above the bright B_u state vertically.

Exciton analysis provides information to rationalize these large discrepancies between the methods. The key quantity is the amount of single and double (or multiple) excitation character. Fig. 7.7 (c) and (d) show two measures, the squared norm of the exciton wave function Ω and the squared value of the doubles amplitudes R_2 in the excited states. An advantage of using Ω is that the respective values are orbital invariant and well-defined independently from the computational protocol, which affords a more precise comparison than using R_2. The ADC(3) values clearly indicate a predominant double excitation character in the $2^1A_g^-$ and $2^1B_u^-$ excited states. ADC(2) fails to capture this effect even qualitatively: all three states have Ω values larger than 0.8, completely missing out differences in state character and confirming the results of Ref. 169. Despite relatively large errors in excitation energies, the EOM-CCSD Ω values indicate that EOM-CCSD captures a small difference in excitation character in accordance with the trends observed at the ADC(3) level. The R_2 values follow similar trend as the Ω values. In face of the differences in state characters, it is not surprising that the ADC(3) method, which describes doubly excited determinants at first order in perturbation theory, performs much better than ADC(2), which describes these determinants only at zeroth order, cf. sec 1.9. In EOM-CCSD ansatz, the double excitations are included explicitly, but their primary role is to describe dynamical correlation for singly excited configurations. Thus, when excited states have predominantly doubly excited character, there are no higher-level configurations to correlate these states. An explicit inclusion of double excitations in EOM-CCSD is responsible for its superiority relative to to ADC(2). Further discussion on doubly excited states can be found in Ref. 187.

The performance of TDDFT is discussed in the following, cf. Fig. 7.7 (a). At the first glance, BLYP shows the best agreement with the experimental data and the ADC(3) results. While CAM-B3LYP closely follows ADC(2) and

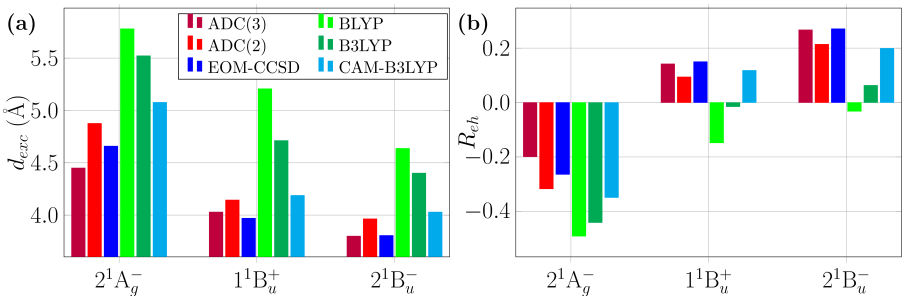

Figure 7.8: Excited states of all-*trans* octatetraene. (a) Exciton sizes (d_{exc}, Å) and (b) correlation coefficients (R_{eh}) of the $2^1A_g^-$, $1^1B_u^+$, and $2^1B_u^-$ excited states calculated with ADC(2), ADC(3), EOM-CCSD, BLYP/TDA, B3LYP/TDA and CAM-B3LYP/TDA employing cc-pVTZ basis set. The legend in (a) applies to both diagrams.

EOM-CCSD, the excitation energies obtained with B3LYP are almost exactly in between BLYP and CAM-B3LYP for all three states. As TDDFT only includes singly excited determinants, Ω=1 for all TDDFT states, which means that doubly (or multiply) excited character cannot be described.[39] To rationalize the differences and similarities of the computational results regarding the excited-state wave functions, Fig. 7.8 shows exciton sizes and correlation coefficients. It should be noted that these descriptors only characterize the part of the excited state that is described by single electron transitions, since it is based on the one-particle transition density matrix. For example, the predominantly doubly excited state $2^1A_g^-$ has Ω=0.2 at the ADC(3) level. This means that only 20% of the excited state can be described within the exciton model. Consequently, exciton sizes and correlation coefficients in Fig. 7.8 have limited significance for the $2^1A_g^-$ and $2^1B_u^-$ states. For the predominantly singly excited state $1^1B_u^+$, all wave-function based methods are in good agreement with an exciton size of about 4 Å and a slightly positive correlation coefficient of +0.1. Among TDDFT methods, CAM-B3LYP shows the best agreement with these values. In contrast, for BLYP, d_{exc} is much larger (5.21 Å) and R_{eh} is negative (−0.148). Other states (those with substantial single excitation character) are described consistently within the wave-function based methods, suggesting the major differences in excitation energies originates from the doubly or multiply excited determinants. It would be interesting to further characterize this phenomenon, however, more advanced techniques need to be employed, cf. Ref. 183, which is beyond the scope of this work. Using ADC(3) as a reference, the best agreement in exciton properties is observed for the EOM-CCSD results, while the largest discrepancies are found for the $2^1A_g^-$ state with ADC(2). In contrast to the good agreement in excitation energies, the exciton sizes obtained with BLYP deviate the most from the ADC(3) values. A systematic

decrease in differences from the ADC(3) results is observed when going from BLYP to B3LYP to CAM-B3LYP, which effectively corresponds to an increase of nonlocal orbital exchange.[97,208]

Fig. 7.8 (b) plots *electron-hole* correlation coefficient R_{eh}, showing a qualitative agreement among all wave function based methods. An opposite trend is observed concerning the deviations from the ADC(3) reference: When the correlation is smaller, then the exciton size increases with respect to the reference. While for the predominantly doubly excited state, the *electron-hole* correlation is negative, *i.e.*, the electron and hole dynamically avoid each other in space, the R_{eh} values for the second and third state are slightly positive.

In summary, the low-lying excited states of octatetraene are characterized in terms of double excitation character and exciton properties confirming the findings of Ref. 187. Interestingly, in the doubly excited $2^1A_g^-$ state, there is a negative correlation between electron and hole. CAM-B3LYP is the only *xc*-functional that reproduces exciton properties of *ab initio* references, while its performance in excitation energies is rather poor in contrast to, *e.g.*, BLYP. Ref. 39 has pointed out that excited states in polyenes require a more accurate treatment of electron correlation than provided by pure local gradient-corrected functionals. The presented results confirm this conclusion suggesting that long-range corrections are unlikely to compensate the errors for polyenes and related molecules inherited from the simpler *xc*-functionals.

7.3.5 Magnesium(II)porphyrin

Porphyrins are an important class of molecules present in active centers of biologically and physiologically relevant molecules. Magnesium(II)porphyrin is a model for chlorophyll, which has been an object of intense studies ever since its discovery in 1940. Using this molecule as a representative of a large molecular class with rich photochemistry, it is illustrated how benchmarking and interpretation of the excited states can benefit from exciton analysis.

The excited-state absorption spectrum of magnesium(II)porphyrin (MgP) is rationalized using a four-orbital model by Gouterman,[263–265] which explains the origin of the Q and B bands. While drawing a full picture of all relevant excited states is beyond the scope of this work, the focus is on the first bright excited state related to the low-intensity Q band and on the interpretation of the four doubly degenerate, bright states in comparison to Gouterman's model.

The discussion is started with the benchmark data set for the first bright excited state shown in Table 7.2. Comparing the excitation energies obtained with the different computational methods with the experimental value of 2.07 eV,[263] the ADC(3) method shows the best agreement (excitation energy of 1.996 eV). The second smallest error obtained with BLYP is already substantially larger

Table 7.2: Excitation energies (ΔE, eV), oscillator strengths (f), single excitation character (Ω), exciton sizes (d_{exc}, Å), hole and electron sizes (σ_h and σ_e, Å) and linear correlation coefficients (R_{eh}) of the first excited Q state of magnesium(II)porphyrin calculated at various levels of theory employing Ahlrichs SV(P)[110] basis set if not stated otherwise.

method	ΔE	f	Ω	d_{exc}	σ_h	σ_e	R_{eh}
exp.	2.07[a]						
ADC(3)	1.996	0.008	0.728	4.58	3.50	3.65	0.179
ADC(2)	2.382	0.007	0.757	4.64	3.38	3.67	0.169
EOM-CCSD[b]	2.344	0.001	0.759	4.58	3.45	3.65	0.167
EOM-CCSD[b,c]	2.345	0.007	0.736	4.62	3.46	3.64	0.158
EOM-CCSD[b,d]	2.302	0.007	0.741	4.65	3.49	3.67	0.158
BLYP	2.265	0	1	5.17	3.46	3.70	−0.048
B3LYP	2.388	0.001	1	5.03	3.47	3.68	0.012
CAM-B3LYP	2.423	0.004	1	4.81	3.48	3.65	0.090
CIS	2.432	0.038	1	4.68	3.55	3.67	0.160

[a] From Ref. 263.

[b] Symmetrized geometry.

[c] Dunning's cc-pVDZ basis set.

[d] Dunning's cc-pVTZ basis set.

with 2.265 eV. All other methods exhibit a uniform blue shift of about 0.3 eV (or even +0.4 eV for CAM-B3LYP). It is worth noting that EOM-CCSD and ADC(2) excitation energies are close (2.344 eV and 2.382 eV, respectively) and also B3LYP is close to these values (2.388 eV). For EOM-CCSD, the effects of the basis set are investigated. While the value obtained with Dunning's double-ζ basis is within 0.001 eV from the value obtained with Ahlrichs' SV(P) basis, using triple-ζ basis leads to an improved agreement with the experiment (2.30 eV).

Despite the discrepancies in the excitation energies, the overall description of the first excited state in terms of the exciton properties is consistent among the wave function-based methods (ADC(3), ADC(2) and EOM-CCSD), and in particular ADC(3) and EOM-CCSD obtain similar values. The ADC(2) descriptors show larger differences, but are nevertheless in a good overall agreement.

Considering differences between the tested TDDFT methods, the most interesting trend can be attributed to a stepwise introduction of nonlocal orbial exchange. In the BLYP functional nonlocal orbital exchange is absent, while a constant fraction of 21 % is included for B3LYP, and a range-separation function admixes nonlocal orbital exchange between 19 % and 65 % in CAM-B3LYP. While the best results for the excitation energy appears to be obtained with BLYP, it is noteworthy that the electron-hole correlation is negative ($R_{eh} = -0.048$) as opposed to the ADC(3) results, which suggest that

Table 7.3: Characterization of the four doubly degenerate, bright excited states of MgP in terms of excitation energies (ΔE, eV), oscillator strengths (f_{osc}), exciton sizes (d_{exc}, Å), hole and electron sizes (σ_h, σ_e,Å) and correlation coefficients (R_{eh}) calculated by CIS and TDDFT with the BLYP, B3LYP, and CAM-B3LYP functionals employing Ahlrichs' TZVP basis set.

method	state	ΔE	f_{osc}	d_{exc}	σ_h	σ_e	R_{eh}
exp.	Q	2.07[a]					
BLYP	S_1	2.271	0	5.20	3.47	3.72	−0.046
B3LYP	S_1	2.393	0	5.05	3.48	3.70	0.011
CAM-B3LYP	S_1	2.430	0.001	4.83	3.48	3.66	0.088
ADC(2)[b]	1^1B_{2u}	2.382	0.007	4.64	3.38	3.67	0.136
CIS	S_1	2.465	0.020	4.71	3.56	3.68	0.155
exp.	B	3.05[a]					
BLYP	S_3	3.156	0.016	5.55	3.77	3.71	−0.101
B3LYP	S_4	3.676	0.110	5.14	3.70	3.70	0.038
CAM-B3LYP	S_3	4.098	1.123	4.65	3.43	3.79	0.172
ADC(2)[b]	2^1B_{2u}	3.487	1.357	4.88	3.40	3.76	0.075
CIS	S_3	4.578	2.698	4.88	3.38	3.80	0.079
exp.	N	3.97[a]					
BLYP	S_{10}	3.441	0.064	5.47	3.75	3.77	−0.059
B3LYP	S_8	3.947	0.593	5.04	3.45	3.82	0.042
CAM-B3LYP	S_7	4.402	0.992	4.93	3.60	3.71	0.092
ADC(2)[b]	3^1B_{2u}	3.993	0.007	4.89	3.62	3.68	0.105
CIS	S_7	5.274	0.323	4.44	3.79	3.80	0.314
BLYP	S_{15}	3.973	1.583	5.60	3.72	4.00	−0.052
B3LYP	S_{13}	4.340	1.722	5.63	4.05	3.79	−0.031
CAM-B3LYP	S_{12}	4.994	0.798	5.28	4.07	3.67	0.072
ADC(2)[b]	4^1B_{2u}	4.625	0.478	5.26	4.06	3.66	0.075
CIS	S_{16}	6.235	0.729	4.92	3.94	3.66	0.163

[a] From Ref. 263.

[b] Symmetric structure, SV(P) basis.

electron-hole correlation should be positive. Increasing the amount of exact exchange, which corresponds to introducing the electron-hole attraction in the framework of TDDFT,[97,208] improves the description of the electron-hole correlation yielding positive values of R_{eh}. But while the R_{eh} value is improved when going from BLYP to B3LYP to CAM-B3LYP, the excitation energies become worse, approaching the typical error of CIS.

As the next step, the first four doubly degenerate $\pi\pi^*$ states of MgP are analyzed employing TDDFT and a triple-ζ basis set and it is attempted to reconstruct Gouterman's model. The TDDFT results and experimental data,[263] as well as ADC(2)/SV(P) references are presented in Table 7.3 (only the results for one state from each degenerate pair is presented as the second state has identical properties). Following the trends described for the S_1 state, the results illustrate impressively how difficult it is to describe excited states of large conjugated systems, highlighting a true dilemma. While BLYP deliv-

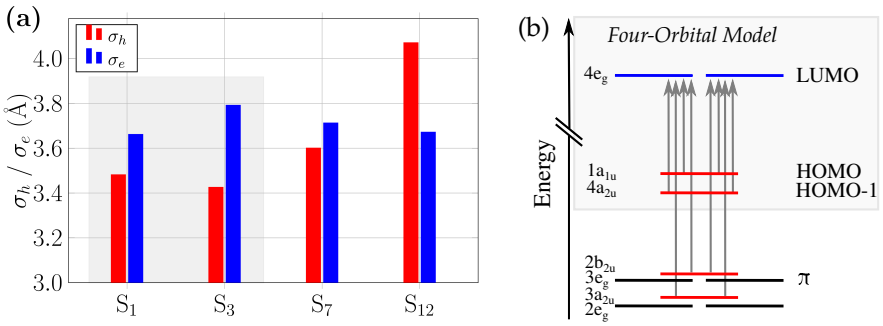

Figure 7.9: Gouterman's model: (a) hole and electron sizes (σ_h and σ_e, Å) of four doubly degenerate excited states calculated at the CAM-B3LYP/TZVP level of theory, (b) sketch of orbitals and transitions involved in the absorption spectrum of MgP including the classic Four-Orbital model (grey), adopted from Ref. 266.

ers reasonable excitation energies, the negative correlation between hole and electron reflects a qualitatively wrong description of the corresponding exciton. Adding exact exchange as, *e.g.*, in CAM-B3LYP improves exciton properties, yielding the expected positive electron-hole correlation similar to the ADC(2) reference, but at the price of increased errors in excitation energies, which are overestimated by $0.36 - 1.00$ eV.

Fig. 7.9 (a) visualizes the hole and electron sizes of the four bright states computed with CAM-B3LYP/TZVP. While electron sizes (blue) are quite similar with a mean value of 3.71 ± 0.06 Å, hole sizes (red) show larger variation around the mean value of 3.65 ± 0.29 Å. Nearly constant σ_e values are consistent with the Four-Orbital model of Gouterman in which the two degenerate LUMOs act as final orbitals in all bright states.[263] At the same time, variations in σ_h indicate the different types of initial orbitals. These observations are confirmed by an inspection of the NTOs shown in Fig. S8 in the SI of Ref. 96. All final (electron) orbitals have the same shape with only minor differences in amplitudes. S_1 and S_3 contain admixture of the same initial orbitals (50 % and 36 %, respectively), in agreement with the Four-Orbital model. For the S_{12} state, the hole orbitals are localized on the porphyrin ring with amplitudes in the largest possible distance to each other which results in the largest σ_h. The metal center is not involved in the excitation process as the NTOs illustrate.

Summarizing the magnesium porphyrin results, ADC(3) yields the best agreement with the experimental value of the S_1 excitation energy. The EOM-CCSD excitation energy is blue-shifted by ∼0.25 eV, but the respective exciton properties are in excellent agreement with ADC(3). TDDFT results depend strongly on the amount of nonlocal orbital exchange as defined in the

xc-functionals. The increased fraction of nonlocal orbital exchange improves exciton description, but leads to larger errors in the excitation energies. The NTO analysis of the four bright states responsible for the visible MgP spectrum confirm Gouterman's classic model.

7.4 Conclusion

This work presented a new strategy for benchmarking excited-state calculations that went beyond excitation energies by employing exciton analyses. The utility of exciton analyses in benchmarking was illustrated for a comprehensive set of examples ranging from small to large molecules with different types of excited states. The study considered correlated *ab initio* methods, EOM-CCSD, ADC(2) and ADC(3), as well as time-dependent density functional theory in combination with three *xc*-functionals (BLYP, B3LYP and CAM-B3LYP).

It was illustrated that electron sizes provide a convenient tool for differentiating between Rydberg and valence excited states. The distance between charge cendroids ($d_{h\to e}$) of electron and hole were used to quantify the amount of permanent charge transfer. Computing electron-hole correlation illuminated the nature of excitons and revealed important methodological aspects, such as a qualitatively different description of singlets and triplets by TDDFT. The analysis of exciton properties in large π-conjugated systems highlighted the limitations of energy-based benchmarking: it was shown that for TDDFT methods the best agreement in terms of excitation energies corresponded to a rather poor (and even qualitatively incorrect) exciton description, while improving the exciton description by increasing the fraction of exact exchange led to increased errors in excitation energies.

Exciton properties facilitated the assignment of state characters and delivered important information about *electron-hole* correlation effects, thus establishing a new criterion for benchmarking. Importantly, the analysis based on density matrix and exciton properties enabled unambigous comparisons of different many-body wave functions and between wave function-based and DFT methods. While this chapter was focussed on comparisons between single-reference methods, it should be noted that analysis of exciton properties has been recently implemented[267] within the framework of multireference methods, CASSCF and CASPT2. This allows for comparisons between single- and multi-reference methods in the future.

Chapter 8

Conclusion

I presented the development and application of analysis tools for the systematic quantum-chemical investigation of electronically excited states and excited-state methods. The central idea underlying the methodology is to describe excited states in terms of correlated electron-hole pairs called excitons. The developed tools were shown to afford a precise, quantitative description of excited states in terms of spatial and statistical properties. As such, they provide a basis for exploring molecular photochemistry and benchmarking of quantum-chemical excited-state methods. To highlight the utility and outreach of the developed approach, I presented a diverse set of applications in combination with various quantum-chemical methods with focus on organic molecules as summarized in the following.

A particularly relevant application for the developed approach are molecules that form excitons upon excitation. As prominent representatives I selected large π-conjugated organic molecules. While already the computation of electronic ground and excited states of these molecules poses a challenge for quantum-chemical methods due to strong electron correlation effects, the interpretation of exciton-related phenomena is notoriously difficult in the molecular orbital picture. This problem is mitigated by moving to the exciton picture as I demonstrated for several examples throughout this work. One of these examples is poly(*para* phenylene vinylene) (PPV), a prototypical semiconductor relevant in organic electronics, which I investigated in Chapters 3 and 4. For this purpose, excited states of PPV oligomers were computed with the correlated excited-state methods ADC(2) and ADC(3) and subjected to exciton analysis. This revealed a detailed picture about the emergence of excitons and their properties in PPV. Exciton formation in PPV oligomers was found to depend on the chain length. For small oligomers, confinement effects are dominant leading to locally excited and charge-transfer states. For oligomers with a size of approximatly 30 Å or larger, exciton formation was observed. These

excitons were found to have defined structures, that is, electron and hole quasiparticles experience interaction with each other and the molecular potential that result in certain patterns of wave functions. In the case of Wannier excitons, these wave functions have similarity with particle-in-a-box and hydrogen wave functions. As another aspect of Chapter 4, I devised a quantum-chemical perspective on the band structure of PPV. For this purpose, twenty singlet and twenty triplet excited states of the octamer $(PV)_7P$ were computed. The found excitons were categorized according to their wave functions and properties, and interpreted in terms of Wannier and Frenkel models. In that way, I could reconstruct the band structure of PPV in good agreement with experimental data and solid-state physics approaches. In accordance with band-structure calculations, triplet excitons were found to be spatially more confined as compared to their singlet counterparts, suggesting that they are more tightly bound due to the absence of spin repulsion.

In Chapter 6, I extended the selection of molecules to include various aromats and heteroaromats with chain lengths of up to 80 Å. Excited states were calculated using time-dependent density functional theory (TDDFT) in combination of various exchange-correlation (*xc*-) functionals. For this diverse set of molecules, exciton formation was again found to mainly depend on the chain length, while the explicit chemical structure plays a surprisingly unimportant role. Accordingly, the exciton character of the first excited state of these systems was found to be very similar to PPV, with a uniform exciton size converging against 7 Å and positively correlated electron and hole quasiparticles.

Another central aspect of this work was the assessment of the domains of applicability of computational methods by means of exciton analysis. As the available quantum-chemical methods substantially differ in computational demand and accuracy, an essential step in, both, development of new methods and practical application is to carefully examine the performance of a chosen method by comparison to higher level calculations. Since exciton analysis is based on the method-independent 1TDM, it allows to compare the description of excited states calculated at different levels of theory in a quantitative way.

Following this line of thought, I investigated the performance of TDDFT and the Tamm-Dancoff approximation (TDA) for different *xc*-functionals in Chapters 5 and 6. A important difference in these *xc*-functionals is the amount of nonlocal orbital exchange (NLX). The influence of *xc*-functionals on excitation energies is known to be strong for excited states involving nonlocal electron transitions such as charge-transfer, Rydberg or extended $\pi \rightarrow \pi^*$ excited states. Here, this influence is reinvestigated using Tozer's benchmark set in order to test the suitability of the developed tools for diagnosing TDDFT shortcomings. This set is chosen such that the description of excited states is particularly

challenging for TDDFT. Using the developed excited-state descriptors, the different types of excited states and variations in their character could be easily traced and problematic cases identified. This revealed major differences in the description of excited states with different *xc*-functionals, which stand in line with systematic errors in excitation energies. They furthermore illustrate that NLX does not only become a decisive factor when describing charge-transfer states, but also more general when long-range electron interactions become important. To shed light on the trends of L_a and L_b excited states of oligoacenes, electron-hole correlation effects were investigated in dependence of the system size. It was found that the L_a state is much more sensitive towards the *xc*-functional choice and application of the TDA. This was traced back to the description of its electron-hole interaction, which completely changes from repulsive (PBE) to attractive (CAM-B3LYP) depending on the *xc*-functional. In conclusion, exciton descriptors were able to identify all types of problematic states and allowed to quantify differences in their description depending on the *xc*-functionals.

Returning to Chapter 6, I furthermore investigated how the description of excited states with exciton character differs between *xc*-functionals and as a function of NLX. The trends in exciton sizes and electron-hole correlation coefficients for organic π-conjugated molecules of different chain length revealed that the pure GGA functional PBE is unable to describe bound excitons. This was traced back to the absence of NLX, which results in repulsive electron-hole interaction and spurious charge-transfer character of the first excited state of the π-conjugated molecules. For global hybrid functionals, such as B3LYP, PBE0 and M06-2X, exciton sizes were found to increase linearly with the system size, whereas the slope is proportional to the fraction of NLX. Only long-range corrected *xc*-functionals (CAM-B3LYP, ωB97 and ωPBE) reproduced the asymptotic trend in exciton sizes in agreement with *ab initio* reference data. In summary, the results from Chapters 5 and 6 clearly demonstrated that the choice of *xc*-functional and in particular the amount of NLX has a dramatic influence on excited-state properties.

Ultimately, I employed the developed tools to study the performance of different high level *ab initio* methods and aspects of benchmarking in Chapter 7. For this purpose, the excited-state methods ADC(2), ADC(3), equation-of-motion coupled-cluster (EOM-CCSD), configuration interaction singles (CIS), TDDFT and TDA in combination with a few *xc*-functionals were considered. In benchmarks, the performance of excited-state methods is usually assessed by their ability to reproduce reference excitation energies. However, this investigation revealed that this criterion does not necessarily reflect the quality of description of the underlying wave functions and densities. For example

for octatetraene, both, ADC(3) and BLYP provide reasonably accurate excitation energies in agreement with the experimental state ordering. However, in contrast to ADC(3), which provides an adequate and balanced description of excited states with substantial double excitation character, the commonly used BLYP functional fails to describe many relevant excited-state properties as indicated by several descriptors. Its good performance in terms of excitation energies is therefore likely a result of fortuitious error compensation. For excited states of magnesium porphyrin, correlated *ab initio* methods provide reasonably accurate excitation energies and a uniform description of excited-state properties in accordance with Gouterman's model. For TDDFT calculations, the situation was found to be difficult. While BLYP and B3LYP provide rather accurate excitation energies, the excited-state properties significantly deviate from *ab initio* references. In contrast, the long-range corrected functional CAM-B3LYP performes worst in terms of excitation energies, but best in terms of excited-state properties. These results clearly show that in order to identify suitable *xc*-functionals, it is mandatory to consider not only excitation energies but also excited-state properties. Furthermore, it would be interesting to survey a broader selection of *xc*-functionals and the influence of optimal tuning.

Other aspects studied in Chapter 7 are the effect of nuclear relaxation as well as the influence of the environment onto excited states. These are often of particular relevance for the investigation of photochemical processes. For this purpose, excited states of the push-pull system 4-(*N,N*-dimethylamino)-benzonitrile were calculated with high level *ab initio* methods along nuclear relaxation pathways and in different environments represented with a polarizable continuum model. Excited states were analyzed in terms of their charge-transfer character, which helped to explain the respective excited-state potential energy curves. Excited-state descriptors were furthermore shown to be particularly useful to keep track of excited states as these significantly change in energy and properties along relaxation pathways. This is an important step in determining the molecular mechanism underlying dual fluorescence in DMABN.

An interesting aspect for future investigations is to examine the effects of thermal fluctuations onto exciton properties. For this purpose, exciton analysis could be applied to geometries sampled from molecular dynamics simulations. While such investigations could be readily conducted with available methods, it is furthermore desirable to combine exciton analysis with more computational methods in order to increase the scope of benchmarking and applications. Some interfaces to other methods already exist, for example to the GW+Bethe-Salpeter method.[268] Furthermore, exciton analysis has been recently adopted

for multi-reference methods, such as complete active space self-consistent field (CASSCF) and the complete active space second-order perturbation theory (CASPT2) methods.[267] A detailed comparison of these methods to the ones studied in this work would be certainly of high interest.

Further developments in exciton analysis may concern the derivation of new descriptors. A quantity of high interest is the exciton binding energy, which characterizes the energy that is necessary to dissociate bound excitons into separate charges. This property is directly related to the work principles of organic photovoltaics and organic light emitting devices. Going beyond the exciton picture, which describes only singly excited states, it would be desirable to explore two-electron-two-hole properties as collected by the two-particle transition density matrix and related concepts of biexcitons. In the face of the advent of data-driven investigations of excited states, a future application of exciton descriptors could be automatized character assignment. While one attempt of creating a scheme for this purpose has been reported already,[268] a robust scheme for classifying excited states still needs to be elaborated. Such a methodology could also be developed under the premise to automatically identify problematic cases and alert the user.

Bibliography

[1] A. Szabo and N. S. Ostlund. *Modern Quantum Chemistry - Introduction to Advanced Electronic Structure Theory*. ISBN-13: 978-0-486-69186-2. Dover Publications, INC., Mineola, New York (**1996**).

[2] M. Born and R. Oppenheimer. "Zur Quantentheorie der Molekeln". *Ann. Phys.*, 389 (1927) pages 457–484. doi:10.1002/andp.19273892002.

[3] J. Franck and E. G. Dymond. "Elementary processes of photochemical reactions". *Trans. Faraday Soc.*, 21 (1926) pages 536–542. doi:10.1039/TF9262100536.

[4] E. U. Condon. "Nuclear Motions Associated with Electron Transitions in Diatomic Molecules". *Phys. Rev.*, 32 (1928) pages 858–872. doi:10.1103/PhysRev.32.858.

[5] W. Ritz. "Über eine neue Methode zur Lösung gewisser Variationsprobleme der mathematischen Physik". *Journal für reine und angewandte Mathematik*, 135 (1909) pages 1–61. doi:10.1515/crll.1909.135.1.

[6] J. C. Slater. "A Simplification of the Hartree-Fock Method". *Phys. Rev.*, 81 (1951) pages 385–390. doi:10.1103/PhysRev.81.385.

[7] J. C. Slater. "The Theory of Complex Spectra". *Phys. Rev.*, 34 (1929) pages 1293–1322. doi:10.1103/PhysRev.34.1293.

[8] E. U. Condon. "The Theory of Complex Spectra". *Phys. Rev.*, 36 (1930) pages 1121–1133. doi:10.1103/PhysRev.36.1121.

[9] T. Koopmans. "Über die Zuordnung von Wellenfunktionen und Eigenwerten zu den Einzelnen Elektronen Eines Atoms". *Physica*, 1 (1934) pages 104–113. doi:10.1016/S0031-8914(34)90011-2.

[10] C. Møller and M. S. Plesset. "Note on an Approximation Treatment for Many-Electron Systems". *Phys. Rev.*, 46 (1934) pages 618–622. doi:10.1103/PhysRev.46.618.

[11] P. Hohenberg and W. Kohn. "Inhomogeneous Electron Gas". *Phys. Rev.*, 136 (1964) pages B864–B871. doi:10.1103/PhysRev.136.B864.

[12] W. Kohn and L. J. Sham. "Self-Consistent Equations Including Exchange and Correlation Effects". *Phys. Rev.*, 140 (1965) pages A1133–A1138. doi:10.1103/PhysRev.140.A1133.

[13] L. Goerigk, A. Hansen, C. Bauer, S. Ehrlich, A. Najibi and S. Grimme. "A look at the density functional theory zoo with the advanced GMTKN55 database for general main group thermochemistry, kinetics and noncovalent

interactions". *Phys. Chem. Chem. Phys.*, 19 (2017) pages 32184–32215. doi: 10.1039/C7CP04913G.

[14] J. P. Perdew and K. Schmidt. "Jacobs ladder of density functional approximations for the exchange-correlation energy". *AIP Conference Proceedings*, 577 (2001) pages 1–20. doi:10.1063/1.1390175.

[15] R. Car. "Fixing Jacob's ladder". *Nat. Chem.*, 8 (2016) pages 820–821. doi: 10.1038/nchem.2605.

[16] A. D. Becke. "Density-functional thermochemistry. III. The role of exact exchange". *J. Chem. Phys.*, 98 (1993) pages 5648–5652. doi:10.1063/1.464913.

[17] P. Hohenberg and W. Kohn. "Inhomogeneous Electron Gas". *Phys. Rev.*, 136 (1964) pages B864–B871. doi:10.1103/PhysRev.136.B864.

[18] A. D. Becke. "Density-functional exchange-energy approximation with correct asymptotic behaviour". *Phys. Rev. A*, 38 (1988) pages 3098–3100. doi: 10.1103/PhysRevA.38.3098.

[19] S. H. Vosko, L. Wilk and M. Nusair. "Accurate spin-dependent electron liquid correlation energies for local spin density calculations: a critical analysis". *Can. J. Phys*, 58 (1980) pages 1200–1211. doi:10.1139/p80-159.

[20] C. Lee, W. Yang and R. G. Parr. "Development of the Colle-Salvetti correlation-energy formula into a functional of the electron density". *Phys. Rev. B*, 37 (1988) pages 785–789. doi:10.1103/PhysRevB.37.785.

[21] S. Grimme and F. Neese. "Double-hybrid density functional theory for excited electronic states of molecules". *J. Chem. Phys.*, 127 (2007) page 154116. doi: 10.1063/1.2772854.

[22] J. R. Reimers, Z.-L. Cai, A. Bilić and N. S. Hush. "The Appropriateness of Density-Functional Theory for the Calculation of Molecular Electronics Properties". *Annals of the New York Academy of Sciences*, 1006 (2003) pages 235–251. doi:10.1196/annals.1292.017.

[23] J. P. Perdew, A. Ruzsinszky, L. A. Constantin, J. Sun and G. I. Csonka. "Some Fundamental Issues in Ground-State Density Functional Theory: A Guide for the Perplexed". *J. Chem. Theory Comput.*, 5 (2009) pages 902–908. doi:10.1021/ct800531s.

[24] R. K. Nesbet. "Configuration Interaction in Orbital Theories". *Proc. Roy. Soc. A*, 230 (1955) pages 312–321.

[25] J. B. Foresman, M. Head-Gordon, J. A. Pople and M. J. Frisch. "Toward a systematic molecular orbital theory for excited states". *J. Phys. Chem.*, 96 (1992) pages 135–149. doi:10.1021/j100180a030.

[26] A. Dreuw and M. Head-Gordon. "Single-Reference Ab Initio Methods for the Calculation of Excited States of Large Molecules". *Chem. Rev.*, 105 (2005) pages 4009–4037. doi:10.1021/cr0505627.

[27] E. Runge and E. K. U. Gross. "Density-Funtional Theory for Time-Dependent Systems". *Phys. Rev. Lett.*, 52 (1984) pages 977–1000. doi: 10.1103/PhysRevLett.52.997.

[28] R. van Leeuwen. "Mapping from Densities to Potentials in Time-Dependent Density-Functional Theory". *Phys. Rev. Lett.*, 82 (1999) pages 3863–3866. doi: 10.1103/PhysRevLett.82.3863.

[29] M. E. Casida. *Recent Advances in Density Functional Methods Part I.* World Scientific, Singapore (**1995**).

[30] S. Hirata and M. Head-Gordon. "Time-dependent density functional theory within the Tamm-Dancoff approximation". *Chem. Phys. Lett.*, 314 (1999) pages 291–299. doi:10.1016/S0009-2614(99)01149-5.

[31] Y.-L. Wang and G.-S. Wu. "Improving the TDDFT Calculation of Low-Lying Excited States for Polycyclic Aromatic Hydrocarbones Using the Tamm-Dancoff Approximation". *Int. J. Quantum Chem.*, 108 (2008) pages 430–439. doi:0.1002/qua.21510.

[32] M. J. G. Peach, M. J. Williamson and D. J. Tozer. "Influence of Triplet Instabilities in TDDFT". *J. Chem. Theory Comput.*, 7 (2011) pages 3578–3585. doi:10.1021/ct200651r.

[33] M. J. G. Peach, N. Warner and D. J. Tozer. "On the Triplet Instability in TDDFT". *Mol. Phys.*, 111 (2013) pages 1271–1274. doi:10.1080/00268976.2013.777481.

[34] A. Dreuw and M. Head-Gordon. "Failure of Time-Dependent Density Functional Theory for Long-Range Charge-Transfer Excited States: The Zincbacteriochlorin-Bacteriochlorin and Bacteriochlorophyll-Spheroidene Complexes". *J. Am. Chem. Soc.*, 126 (2004) pages 4007–4016. doi:10.1021/ja039556n.

[35] R. J. Magyar and S. Tretiak. "Dependence of Spurious Charge-Transfer Excited States on Orbital Exchange in TDDFT: Large Molecules and Clusters". *J. Chem. Theory Comput.*, 3 (2007) pages 976–987. doi:10.1021/ct600282k.

[36] A. Dreuw, J. L. Weisman and M. Head-Gordon. "Long-range charge-transfer excited states in time-dependent density functional theory require non-local exchange". *J. Chem. Phys.*, 119 (2003) page 2943. doi:10.1063/1.1590951.

[37] W. Hieringer and A. Görling. "Failure of time-dependent density functional methods for excitations in spatially separated systems". *Chem. Phys. Lett.*, 419 (2006) pages 557–562. doi:10.1016/j.cplett.2005.11.112.

[38] M. W. Casida, C. Jamorski, K. C. Casida and D. R. Salahub. "Molecular excitation energies to high-lying bound states from time-dependent density-functional response theory: Characterization and correction of the time-dependent local density approximation ionization threshold". *J. Chem. Phys.*, 108 (1998). doi:10.1063/1.475855.

[39] Z. L. Cai, K. Sendt and J. R. Reimers. "Failure of density-functional theory and time-dependent density-functional theory for large extended π systems". *J. Chem. Phys.*, 117 (2002) page 5543. doi:10.1063/1.1501131.

[40] S. Grimme and M. Parac. "Substantial Errors from Time-Dependent Density Functional Theory for the Calculation of Excited States of Large π Systems". *ChemPhysChem*, 4 (2003) pages 292–295. doi:10.1002/cphc.200390047.

[41] R. Richard and J. Herbert. "Time-Dependent Density-Functional Description of the ^1L_a State in Polycyclic Aromatic Hydrocarbons: Charge-Transfer Character in Disguise?" *J. Chem. Theory Comput.*, 7 (2011) pages 1296–1306. doi:10.1021/ct100607w.

[42] R. J. Cave, F. Zhang, N. T. Maitra and K. Burke. "A dressed TDDFT treatment of the 2^1A_g states of butadiene and hexatriene". *Chem. Phys. Lett.*, 389 (2004) pages 39–42. doi:10.1016/j.cplett.2004.03.051.

[43] N. T. Maitra, F. Zhang, R. J. Cave and K. Burke. "Double excitations within time-dependent density functional theory linear response". *J. Chem. Phys.*, 120 (2004) pages 5932–5937. doi:10.1063/1.1651060.

[44] H. Iikura, T. Tsuneda, T. Yanai and K. Hirao. "A long-range correction scheme for generalized-gradient-approximation exchange functionals". *J. Chem. Phys.*, 115 (2001) pages 3540–3544. doi:10.1063/1.1383587.

[45] Y. Tawada, T. Tsuneda, S. Yanagisawa, T. Yanai and K. Hirao. "A long-range-corrected time-dependent density functional theory". *J. Chem. Phys.*, 120 (2004) pages 8425–8433. doi:10.1063/1.1688752.

[46] M. Kamiya, H. Sekino, T. Tsuneda and K. Hirao. "Nonlinear optical property calculations by the long-range-corrected coupled-perturbed Kohn-Sham method". *J. Chem. Phys.*, 122 (2005) 234111. doi:10.1063/1.1935514.

[47] T. Yanai, D. P. Tew and N. C. Handy. "A new hybrid exchange-correlation functional using the Coulomb-attenuating method (CAM-B3LYP)". *Chem. Phys. Lett.*, 393 (2004) pages 51–57. doi:10.1016/j.cplett.2004.06.011.

[48] O. A. Vydrov and G. E. Scuseria. "Assessment of a long-range corrected hybrid functional". *J. Chem. Phys.*, 125 (2006) 234109. doi:10.1063/1.2409292.

[49] J.-D. Chai and M. Head-Gordon. "Systematic optimization of long-range corrected hybrid density functionals". *J. Chem. Phys.*, 128 (2008) page 084106. doi:10.1063/1.2834918.

[50] L. Kronik, T. Stein, S. Refaely-Abramson and R. Baer. "Excitation Gaps of Finite-Sized Systems from Optimally Tuned Range-Separated Hybrid Functionals". *J. Chem. Theor. Comput.*, 8 (2012) pages 1515–1531. doi: 10.1021/ct2009363.

[51] M. J. G. Peach, P. Benfield, T. Helgaker and D. J. Tozer. "Excitation energies in density functional theory: An evaluation and a diagnostic test". *J. Chem. Phys.*, 128 (2008) page 044118. doi:10.1063/1.2831900.

[52] T. Le Bahers, C. Adamo and I. Ciofini. "A Qualitative Index of Spatial Extent in Charge-Transfer Excitations". *J. Chem. Theory Comput.*, 7 (2011) pages 2498–2506. doi:10.1021/ct200308m.

[53] C. A. Guido, P. Cortona, B. Mennucci and C. Adamo. "On the Metric of Charge Transfer Molecular Excitations: A Simple Chemical Descriptor". *J. Chem. Theory Comput.*, 9 (2013) pages 3118–3126. doi:10.1021/Ct400337e.

[54] T. Etienne, X. Assfeld and A. Monari. "New Insight into the Topology of Excited States through Detachment / Attachment Density Matrices-Based Centroids of Charge". *J. Chem. Theory Comput.*, 10 (2014) pages 3906–3914. doi:10.1021/ct500400s.

[55] T. Etienne, X. Assfeld and A. Monari. "Toward a Quantitative Assessment of Electronic Transitions' Charge Transfer Character". *J. Chem. Theory Comput.*, 10 (2014) pages 3896–3905. doi:10.1021/ct5003994.

[56] M. Campetella, F. Maschietto, M. J. Frisch, G. Scalmani, I. Ciofini and C. Adamo. "Charge Transfer Excitations in TDDFT: A Ghost-Hunter Index". *J. Comput. Chem.*, 38 (2017) pages 2151–2156. doi:10.1002/jcc.24862.

[57] J. Schirmer. "A new approximation scheme for the polarization propagator". *Phys. Rev. A*, 26 (1982) pages 2395–2416. doi:10.1103/PhysRevA.26.2395.

[58] A. B. Trofimov and J. Schirmer. "An efficient polarization propagator approach to valence electron excitation spectra". *J. Phys. B*, 28 (1995) pages 2299–2324. doi:10.1088/0953-4075/28/12/003.

[59] A. Dreuw and M. Wormit. "The algebraic diagrammatic construction scheme for the polarization propagator for the calculation of excited states". *WIREs Comput. Mol. Sci.*, 5 (2015) pages 82–95. doi:10.1002/wcms.1206.

[60] M. Wormit, D. R. Rehn, P. H. Harbach, J. Wenzel, C. M. Krauter, E. Epifanovsky and A. Dreuw. "Investigating Excited Electronic Stated using the Algebraic Diagrammatic Construction (ADC) Approach of the Polarisation Propagator". *Mol. Phys.*, 112 (2014) pages 774–784. doi: 10.1080/00268976.2013.859313.

[61] F. Mertins and J. Schirmer. "Algebraic propagator approaches and intermediate-state representations. I. The biorthogonal and unitary coupled-cluster methods". *Phys. Rev. A*, 53 (1996) pages 2140–2152. doi: 10.1103/PhysRevA.53.2140.

[62] J. Schirmer. "Closed-form intermediate representations of many-body propagators and resolvent matrices". *Phys. Rev. A*, 43 (1991) pages 4647–4659. doi:10.1103/PhysRevA.43.4647.

[63] D. Lefrancois, M. Wormit and A. Dreuw. "Adapting algebraic diagrammatic construction schemes for the polarization propagator to problems with multi-reference electronic ground states exploiting the spin-flip ansatz". *J Chem. Phys.*, 143 (2015) page 124107. doi:10.1063/1.4931653.

[64] F. Plasser and H. Lischka. "Analysis of excitonic and charge transfer interactions from quantum chemical calculations". *J. Chem. Theory Comput.*, 8 (2012) pages 2777–2789. doi:10.1021/ct300307c.

[65] F. Plasser, M. Wormit and A. Dreuw. "New tools for the systematic analysis and visualization of electronic excitations. Part I: Formalism". *J. Chem. Phys.*, 141 (2014) page 024106. doi:10.1063/1.4885819.

[66] F. Plasser, S. Bäppler, M. Wormit and A. Dreuw. "Visualization and systematic analysis of electronic excitations using density matrices. Part II." *J. Chem. Phys.*, 141 (2014) page 024107. doi:10.1063/1.4885820.

[67] A. V. Luzanov, A. A. Sukhorukov and V. É. Umanskii. "Application of transition density matrix for analysis of excited states". *Theor. Exp. Chem.*, 10 (1976) pages 354–361. doi:10.1007/BF00526670.

[68] R. L. Martin. "Natural transition orbitals". *J. Chem. Phys.*, 118 (2003) pages 4775–4777. doi:10.1063/1.1558471.

[69] I. Mayer. "Using singular value decomposition for a compact representation and improved interpretation of the CIS wave function". *Chem. Phys. Lett.*, 437 (2007) pages 284–286. doi:10.1016/j.cplett.2007.02.038.

[70] D. Jacquemin, T. Le Bahers, C. Adamo and I. Ciofini. "What is the "best" atomic charge model to describe through-space charge-transfer excitations?" *Phys. Chem. Chem. Phys.*, 14 (2012) pages 5383–5388. doi: 10.1039/C2CP40261K.

[71] C. A. Guido, P. Cortona and C. Adamo. "Effective electron displacements: A tool for time-dependent density functional theory computational spectroscopy." *J. Chem. Phys.*, 140 (2014) page 104101. doi:10.1063/1.4867007.

[72] E. Ronca, M. Pastore, L. Belpassi, F. D. Angelis, C. Angeli, R. Cimiraglia and F. Tarantelli. "Charge-displacement analysis for excited states". *J. Chem. Phys.*, 140 (2014) page 054110. doi:10.1063/1.4863411.

[73] S. A. Bäppler, F. Plasser, M. Wormit and A. Dreuw. "Exciton analysis of many-body wavefunctions: Bridging the gap between the quasi-particle and molecular orbital pictures". *Phys. Rev. A*, 90 (2014) page 052521. doi:10.1103/PhysRevA.90.052521.

[74] A. V. Luzanov, A. A. Sukhorukov and V. É. Umanskii. "Application of transition density matrix for analysis of excited states". *Theor. Exp. Chem.*, 10 (1976) pages 354–361. doi:10.1007/BF00526670.

[75] A. V. Luzanov and O. A. Zhikol. "Electron Invariants and Excited State Structural Analysis for Electronic Transitions Within CIS, RPA, and TDDFT Models". *Int. J. Quant. Chem.*, 110 (2010) pages 902–924. doi:10.1002/qua.22041.

[76] A. V. Luzanov and O. V. Prezhdo. "Irreducible Charge Density Matrices for Analysis of Many-Electron Wave Functions". *Int. J. Quant. Chem.*, 102 (2005) pages 582–601. doi:10.1002/qua.20438.

[77] A. V. Luzanov. "Analysis of the exciton states of polyconjugated systems by the transition density matrix method". *J. Struct. Chem.*, 43 (2002) pages 711–720. doi:10.1023/A:1022884018770.

[78] F. Plasser, B. Thomitzni, S. A. Bäppler, J. Wenzel, D. R. Rehn, M. Wormit and A. Dreuw. "Statistical Analysis of Electronic Excitation Processes: Location, Compactness, and Electron-Hole Correlation". *J. Comput. Chem.*, 36 (2015) pages 1609–1620. doi:10.1002/jcc.23975.

[79] S. A. Bäppler. *Analysis of Excitons in Conjugated Organic Polymers*. Master's thesis, Ruprecht-Karls-University Heidelberg (**2014**).

[80] J. Frenkel. "On the transformation of light into heat in solids. I". *Phys. Rev.*, 37 (1931) pages 17–44. doi:10.1103/PhysRev.37.17.

[81] N. Kirova. "Understanding excitons in optically active polymers". *Polym. Int.*, 57 (2008) pages 678–688. doi:10.1002/pi.2391.

[82] G. Strinati. "Effects of dynamical screening on resonances at inner-shell thresholds in semiconductors". *Phys. Rev. B*, 29 (1984) pages 5718–5726. doi:10.1103/PhysRevB.29.5718.

[83] M. Rohlfing and S. G. Louie. "Electron-hole excitations and optical spectra from first principles". *Phys. Rev. B*, 62 (2000) pages 4927–4944. doi:10.1103/PhysRevB.62.4927.

[84] J.-W. van der Horst, P. A. Bobbert, M. A. J. Michels and H. Bässler. "Calculation of excitonic properties of conjugated polymers using the Bethe-Salpeter equation". *J. Chem. Phys.*, 114 (2001) page 6950. doi:10.1063/1.1356015.

[85] G. Onida, L. Reining and A. Rubio. "Electronic excitations: density-functional versus many-body Green's-function approaches". *Rev. Mod. Phys.*, 74 (2002) pages 601–659. doi:10.1103/RevModPhys.74.601.

[86] T. G. Pedersen and T. B. Lynge. "Ab initio tight-binding study of exciton optical and electro-optic properties of conjugated polymers". *Comput. Mater. Sci.*, 27 (2003) pages 123–127. doi:10.1016/S0927-0256(02)00435-4.

[87] C. Faber, I. Duchemin, T. Deutsch and X. Blase. "Many-body Green's function study of coumarins for dye-sensitized solar cells". *Phys. Rev. B*, 86 (2012) page 155315. doi:10.1103/PhysRevB.86.155315.

[88] Note that in eq. (2.3) two distinct sets of valence and conduction states appear while in eq. (1.54) both indices run over the whole set of atomic orbitals. The former simplification follows from the specific form of eq. (2.2) and the Tamm-Dancoff approximation (see also Ref. 83).

[89] H. Tamura, J. M. Mallet, M. Oheim and I. Burghardt. "Ab Initio Study of Excitation Energy Transfer between Quantum Dots and Dye Molecules". *J. Phys. Chem. C*, 113 (2009) pages 7548–7552. doi:10.1021/jp811042t.

[90] S. Matsika, X. Feng, A. V. Luzanov and A. I. Krylov. "What We Can Learn from the Norms of One-Particle Density Matrices, and What We Can't: Some Results for Interstate Properties in Model Singlet Fission Systems." *J. Phys. Chem. A*, 118 (2014) pages 11943–11955. doi:10.1021/jp506090g.

[91] S. F. Boys. *Quantum theory of atoms, molecules and the solid state.* Academic Press, New York (**1968**).

[92] J. Rissler. "Effective conjugation length of π-conjugated systems". *Chem. Phys. Lett.*, 394 (2004) pages 92–96. doi:10.1016/j.cplett.2004.07.058.

[93] W. Barford and N. Paiboonvorachat. "Excitons in conjugated polymers: Wavefunctions, symmetries, and quantum numbers". *J. Chem. Phys.*, 129 (2008) 164716. doi:10.1063/1.3001584.

[94] H. Ma, T. Qin and A. Troisi. "Electronic Excited States in Amorphous MEH-PPV Polymers from Large-Scale First Principles Calculations". *J. Chem. Theory Comput.*, 10 (2014) pages 1272–1282. doi:10.1021/ct4010799.

[95] J. Wenzel and A. Dreuw. "Physical Properties, Exciton Analysis, and Visualization of Core-Excited States: An Intermediate State Representation Approach". *J. Chem. Theory Comput.*, 12 (2016) pages 1314–1330. doi: 10.1021/acs.jctc.5b01161.

[96] S. A. Mewes, F. Plasser, A. I. Krylov and A. Dreuw. "Benchmarking excited-state calculations using exciton properties". *J. Chem. Theory Comput.*, 14 (2018) pages 710–725. doi:10.1021/acs.jctc.7b01145.

[97] S. A. Mewes, F. Plasser and A. Dreuw. "Universal Exciton Size in Organic Polymers is Determined by Nonlocal Orbital Exchange in Time-Dependent Density Functional Theory". *J. Phys. Chem. Lett.*, 8 (2017) pages 1205–1210. doi: 10.1021/acs.jpclett.7b00157.

[98] Y. Shao, L. F. Molnar, Y. Jung, J. Kussmann, C. Ochsenfeld, S. T. Brown, A. T. Gilbert, L. V. Slipchenko, S. V. Levchenko, O. D. P. *et al.* "Advances in quantum chemical methods and algorithms in the Q-Chem 3.0 program package". *Phys. Chem. Chem. Phys.*, 8 (2006) page 3172. doi: 10.1039/B517914A.

[99] B. F. E. Curchod, U. Rothlisberger and I. Tavernelli. "Trajectory-based nonadiabatic dynamics with time-dependent density functional theory". *Chem. Phys. Chem.*, 14 (2013) pages 1314–40. doi:10.1002/cphc.201200941.

[100] F. Plasser, R. Crespo-Otero, M. Pederzoli, J. Pittner, H. Lischka and M. Barbatti. "Surface Hopping Dynamics with Correlated Single-Reference Methods: 9H-Adenine as a Case Study". *J. Chem. Theory Comput.*, 10 (2014) pages 1395–1405. doi:10.1021/ct4011079.

[101] A. E. Reed, R. B. Weinstock and F. Weinhold. "Natural population analysis". *J. Chem. Phys.*, 82 (1985) pages 735–746. doi:10.1063/1.449486.

[102] S. Tretiak and S. Mukamel. "Density Matrix Analysis and Simulation of Electronic Excitations in Conjugated and Aggregated Molecules". *Chem. Rev.*, 102 (2002) pages 3171–3212. doi:10.1021/cr010125.

[103] G. D. Scholes and K. P. Ghiggino. "Electronic Interactions and Interchromophore Excitation Transfer". *J. Phys. Chem.*, 98 (1994) pages 4580–4590. doi:10.1021/j100068a017.

[104] A. L. L. East and E. C. Lim. "Naphthalene dimer: Electronic states, excimers, and triplet decay". *J. Chem. Phys.*, 113 (2000) pages 8981–8994. doi:10.1063/1.1319345.

[105] A. N. Panda, F. Plasser, A. J. A. Aquino, I. Burghardt and H. Lischka. "Electronically Excited States in Poly(p-phenylenevinylene): Vertical Excitations and Torsional Potentials from High-Level Ab Initio Calculations". *J. Phys. Chem. A*, 117 (2013) pages 2181–2189. doi:10.1021/jp400372t.

[106] N. Kuritz, T. Stein, R. Baer and L. Kronik. "Charge-Transfer-Like $\pi \rightarrow \pi^*$ Excitations in Time-Dependent Density Functional Theory: A Conundrum and Its Solution". *J. Chem. Theory Comput.*, 7 (2011) pages 2408–2415. doi:10.1021/ct2002804.

[107] ChemAxon (**2013**). Molecular structures created with Marvin 6.1.2, (`http://www.chemaxon.com`).

[108] A. I. Krylov and P. M. W. Gill. "Q-Chem: an engine for innovation". *WIREs Comput. Mol. Sci.*, 3 (2013) pages 317–326. doi:10.1002/wcms.1122.

[109] T. H. J. Dunning. "Gaussian basis sets for use in correlated molecular calculations. I. The atoms boron through neon and hydrogen". *J. Chem. Phys.*, 90 (1989) pages 1007–1023. doi:10.1063/1.456153.

[110] A. Schäfer, H. Horn and R. Ahlrichs. "Fully optimized contracted gaussian basis sets for atoms lithium to krypton". *J. Chem. Phys.*, 97 (1992) pages 2571–2577. doi:10.1063/1.463096.

[111] S. Horn, F. Plasser, T. Müller, F. Libisch, J. Burgdörfer and H. Lischka. "A comparison of singlet and triplet states for one- and two-dimensional graphene nanoribbons using multireference theory". *Theor. Chem. Acc.*, 133 (2014) page 1511. doi:10.1007/s00214-014-1511-8.

[112] F. Plasser. "Wave Function Analysis Tools" (**2013**). `http://www.iwr.uni-heidelberg.de/groups/compchem`.

[113] F. Plasser, A. Aquino, H. Lischka and D. Nachtigallova. *Electronic Excitation Processes in Single-Strand and Double-Strand DNA: A Computational Approach*. Springer (**2014**).

[114] F. Plasser, A. J. A. Aquino and H. Lischka. "The UV absorption spectrum of alternating DNA duplexes analysis of excitonic and charge transfer interactions". *J. Phys. Chem. A*, 116 (2012) pages 11151–11160. doi:10.1021/jp304725r.

[115] F. Plasser and H. Lischka. "Electronic Excitation and Structural Relaxation of the Adenine Dinucleotide in Gas Phase and Solution". *Photochem. Photobiol. Sci.*, 12 (2013) page 1440. doi:10.1039/C3PP50032B.

[116] E. G. Hohenstein and C. D. Sherrill. "Effects of Heteroatoms on Aromatic π-π Interactions: Benzene - Pyridine and Pyridine Dimer". *J. Phys. Chem. A*, 113 (2009) pages 878–886. doi:10.1021/jp809062x.

[117] B. K. Mishra and N. Sathyamurthy. "$\pi - \pi$ Interaction in Pyridine". *J. Phys. Chem. A*, 109 (2005) pages 6–8. doi:10.1021/jp045218c.

[118] P. Petelenz and B. Pac. "Is dipole moment a valid descriptor of excited state's charge-transfer character?" *J. Am. Chem. Soc.*, 135 (2013) pages 17379–86. doi:10.1021/ja407379h.

[119] Z. L. Cai and J. R. Reimers. "The Low-Lying Excited States of Pyridine". *J. Phys. Chem. A*, 104 (2000) pages 8389–8408. doi:10.1021/jp000962s.

[120] J.-L. Brédas, J. Cornil, D. Beljonne, D. A. Dos Santos and Z. Shuai. "Excited-State Electronic Structure of Conjugated Oligomers and Polymers: A Quantum Chemical Approach to Optical Phenomena". *Acc. Chem. Res.*, 32 (1999) pages 267–276. doi:10.1021/ar9800338.

[121] G. D. Scholes and G. Rumbles. "Excitons in Nanoscale Systems". *Nat. Mater.*, 5 (2006) pages 683–696. doi:10.1038/nmat1710.

[122] J.-L. Brédas, J. Cornil and H. A. J. "The Exciton Binding Energy in Luminescent Conjugated Polymers". *Adv. Mater.*, 8 (1996) pages 447–452. doi:10.1002/adma.19960080517.

[123] T. M. Clarke and J. R. Durrant. "Charge Photogeneration in Organic Solar Cells". *Chem. Rev.*, 110 (2010) pages 6736–6767. doi:10.1021/cr900271s.

[124] D. Moses, J. Wang, A. J. Heeger, A. Kirova and S. Brazovski. "Singlet exciton binding energy in poly(phenylene vinylene)". *Proc. Nat. Acad. Sci. USA*, 98 (2001) pages 13496–13500. doi:10.1073/pnas.241497098.

[125] I. H. Campbell, T. W. Hagler, D. L. Smith and J. P. Ferraris. "Direct Measurement of Conjugated Polymer Electronic Excitation Energies Using Metal/Polymer/Metal Structures". *Phys. Rev. Lett.*, 76 (1996) pages 1900–1903. doi:10.1103/PhysRevLett.76.1900.

[126] S. F. Alvarado, P. F. Seidler, D. G. Lidzey and D. D. C. Bradley. "Direct determination of the exciton binding energy of conjugated polymers using a scanning tunneling microscope". *Phys. Rev. Lett.*, 81 (1998) pages 1082–1085. doi:10.1103/PhysRevLett.81.1082.

[127] M. Chandross, S. Mazumdar, M. Liess, P. A. Lane, Z. V. Vardeny, M. Hamaguchi and K. Yoshino. "Optical absorption in substituted phenylene-based conjugated polymers - Theory and experiment". *Phys. Rev. B*, 55 (1997) pages 1486–1496. doi:10.1103/PhysRevB.55.1486.

[128] E. Zojer, P. Buchacher, F. Wudl, J. Cornil, J. P. Calbert, J. L. Brédas and G. Leising. "Excited state localization in organic molecules consisting of conjugated and nonconjugated segments". *J. Chem. Phys.*, 113 (2000) page 10002. doi:10.1063/1.1323263.

[129] M. Sun, P. Kjellberg, W. J. Beenken and T. Pullerits. "Comparison of the electronic structure of PPV and its derivative DIOXA-PPV". *Chem. Phys.*, 327 (2006) pages 474 – 484. doi:10.1016/j.chemphys.2006.05.031.

[130] I. G. Scheblykin, A. Yartsev, T. Pullerits, V. Gulbinas and V. Sundström. "Excited State and Charge Photogeneration Dynamics in Conjugated Polymers". *J. Phys. Chem. B*, 111 (2007) pages 6303–6321. doi: 10.1021/jp068864f.

[131] W. Humphrey, A. Dalke and K. Schulten. "VMD - Visual Molecular Dynamics". *J. Molec. Graphics*, 14 (1996) pages 33–38.

[132] W. Barford. "Excitons in Conjugated Polymers: A Tale of Two Particles". *J. Phys. Chem. A*, 117 (2013) pages 2665–2671. doi:10.1021/jp310110r.

[133] F. Plasser, H. Pasalic, M. H. Gerzabek, F. Libisch, R. Reiter, J. Burgdörfer, T. Müller, R. Shepard and H. Lischka. "The Multiradical Character of One- and Two-Dimensional Graphene Nanoribbons". *Angew. Chem., Int. Ed.*, 52 (2013) pages 2581–2584. doi:10.1002/anie.201207671.

[134] A. Knippenberg, J. H. Starcke, M. Wormit and A. Dreuw. "The low-lying excited states of neutral polyacenes and their radical cations: a quantum chemical study employing the algebraic diagrammatic construction scheme of second order". *Mol. Phys.*, 108 (2010) pages 2801–2813. doi: 10.1080/00268976.2010.526643.

[135] C. M. Marian and N. Gilka. "Performance of Density Functional Theory/Multireference Configuration Interaction Method on Electronic Excitation of Extended π-Systems". *J. Chem. Theory Comput.*, 4 (2008) pages 1501–1515. doi:10.1021/ct8001738.

[136] R. Korytár, D. Xenioti, P. Schmitteckert, M. Alouani and F. Evers. "Signature of the Dirac cone in the properties of linear oligoacenes." *Nat. Commun.*, 5 (2014) page 5000. doi:10.1038/ncomms6000.

[137] B. M. Wong and T. H. Hsieh. "Optoelectronic and Excitonic Properties of Oligoacenes: Substantial Improvements from Range-Separated Time-Dependent Density Functional Theory". *J. Chem. Theory Comput.*, 6 (2010) pages 3704–3712. doi:10.1021/ct100529s.

[138] S. A. Mewes, J.-M. Mewes, A. Dreuw and F. Plasser. "Excitons in poly(para phenylene vinylene): A quantum-chemical perspective based on high-level ab initio calculations". *Phys. Chem. Chem. Phys.*, 18 (2016) pages 2548–2563. doi:10.1039/C5CP07077E.

[139] A. J. Heeger. "Semiconducting and Metallic Polymers: The Fourth Generation of Polymeric Materials (Nobel Lecture)". *Angew. Chem. Int. Ed.*, 40 (2001) pages 2591–2611. doi:10.1002/1521-3773(20010716)40:14¡2591::AID-ANIE2591¿3.0.CO;2-0.

[140] J. Gierschner, J. Cornil and H.-J. Egelhaaf. "Optical Bandgaps of π-Conjugated Organic Materials at the Polymer Limit: Experiment and Theory". *Adv. Mater.*, 19 (2007) pages 173–191. doi:10.1002/adma.200600277.

[141] E. Collini and G. D. Scholes. "Coherent Intrachain Energy Migration in a Conjugated Polymer at Room Temperature". *Science*, 323 (2009) pages 369–373. doi:10.1126/science.1164016.

[142] A. O. Patil, A. J. Heeger and F. Wudl. "Optical properties of conducting polymers". *Chem. Rev.*, 88 (1988) pages 183–200. doi:10.1021/cr00083a009.

[143] W. J. D. Beenken. "Excitons in conjugated polymers: Do we need a paradigma change?" *Phys. Status Solidi A*, 206 (2009) pages 2750–2756. doi: 10.1002/pssa.200925297.

[144] S. Brazovskii and N. Kirova. "Physical theory of excitons in conducting polymers". *Chem. Soc. Rev.*, 39 (2010) pages 2453–2465. doi: 10.1039/B917724H.

[145] M. Kuik, G.-J. A. H. Wetzelaer, H. T. Nicolai, N. I. Craciun, D. M. De Leeuw and P. W. M. Blom. "25th Anniversary Article: Charge Transport and Recombination in Polymer Light-Emitting Diodes". *Adv. Mater.*, 26 (2014) pages 512–531. doi:10.1002/adma.201303393.

[146] M. Liess, S. Jeglinski, Z. V. Vardeny, M. Ozaki, K. Yoshino, Y. Ding and T. Barton. "Electroabsorption spectroscopy of luminescent and nonluminescent π-conjugated polymers". *Phys. Rev. B*, 56 (1997) pages 15712–15724. doi:10.1103/PhysRevB.56.15712.

[147] P. Gomes da Costa and E. M. Conwell. "Excitons and the band gap in poly(phenylene vinylene)". *Phys. Rev. B*, 48 (1993) pages 1993–1996. doi: 10.1103/PhysRevB.48.1993.

[148] R. Kersting, U. Lemmer, H. J. Bakker, R. F. Mahrt, H. Kurz, V. I. Arkhipov, H. Bässler and E. O. Göbel. "Ultrafast Field-Induced Dissociation of Excitons in Conjugated Polymers". *Phys. Rev. Lett.*, 73 (1994) pages 1440–1443. doi:10.1103/PhysRevLett.73.1440.

[149] T. G. Pedersen, P. M. Johansen and H. C. Pedersen. "Particle-in-a-box model of one-dimensional excitons in conjugated polymers". *Phys. Rev. B*, 61 (2000) pages 10504–10510. doi:10.1103/PhysRevB.61.10504.

[150] D. Beljonne, Z. Shuai, R. H. Friend and J.-L. Brédas. "Theoretical investigation of the lowest singlet and triplet states in poly(para phenylene vinylene) oligomers". *J. Chem. Phys.*, 102 (1995) page 2042. doi:10.1063/1.468726.

[151] C. De Leener, E. Hennebicq, J.-C. Sancho-Garcia and D. Beljonne. "Modeling the dynamics of chromophores in conjugated polymers: the case of poly(2-methoxy-5-(2'-ethylhexyl)oxy 1,4-phenylene vinylene) (MEH-PPV)." *J. Phys. Chem. B*, 113 (2009) pages 1311–1322. doi:10.1021/jp8029902.

[152] V. Lukeš, R. Šolc, M. Barbatti, H. Lischka and H.-F. Kauffmann. "Torsional Potentials and Full-Dimensional Simulation of Electronic Absorption Spectra of para-Phenylenevinylene Oligomers Using Semiempirical Hamiltonians". *J. Theor. Comput. Chem.*, 09 (2010) pages 249–263. doi: 10.1142/S0219633610005645.

[153] M. Y. Lavrentiev, W. Barford, S. J. Martin, D. H. and R. J. Bursill. "Theoretical investigation of the low-lying electronic structure of poly(p-phenylene vinylene)". *Phys. Rev. B*, 59 (1999) pages 9987–9994. doi: 10.1103/PhysRevB.59.9987.

[154] R. J. Bursill and W. Barford. "Symmetry-adapted density matrix renormalization group calculations of the primary excited states of poly(paraphenylene vinylene)". *J. Chem. Phys.*, 130 (2009) page 234302. doi: 10.1063/1.3149536.

[155] A. Pogantsch, G. Heimel and E. Zojer. "Quantitative prediction of optical excitations in conjugated organic oligomers: A density functional theory study". *J. Chem. Phys.*, 117 (2002) page 5921. doi:10.1063/1.1502244.

[156] S. Tretiak, K. Igumenshchev and V. Chernyak. "Exciton size of conducting polymers predicted by time-dependent density functional theory". *Phys. Rev. B*, 71 (2005) page 033201. doi:10.1103/PhysRevB.71.033201.

[157] M. Rohlfing and S. G. Louie. "Optical Excitations in Conjugated Polymers". *Phys. Rev. Lett.*, 82 (1999) pages 1959–1962. doi:10.1103/PhysRevLett.82.1959.

[158] T. M. Cardozo, A. J. A. Aquino, M. Barbatti, I. Borges and H. Lischka. "Absorption and Fluorescence Spectra of Poly(p-phenylenevinylene) (PPV) Oligomers: An ab Initio Simulation". *J. Phys. Chem. A*, 119 (2015) pages 1787–1795. doi:10.1021/jp508512s.

[159] B. Saha, M. Ehara and H. Nakatsuji. "Investigation of the Electronic Spectra and Excited-State Geometries of Poly(para-phenylene vinylene) (PPV) and Poly(para-phenylene) (PP) by the Symmetry-Adapted Cluster Configuration Interaction (SAC-CI) Method". *J. Phys. Chem. A*, 111 (2007) pages 5473–5481. doi:10.1021/jp068441d.

[160] T. Nelson, S. Fernandez-Alberti, V. Chernyak, A. E. Roitberg and S. Tretiak. "Nonadiabatic Excited-State Molecular Dynamics Modeling of Photoinduced Dynamics in Conjugated Molecules". *J. Phys. Chem. B*, 115 (2011) pages 5402–5414. doi:10.1021/jp109522g.

[161] R. Binder, J. Wahl, S. Römer and I. Burghardt. "Coherent exciton transport driven by torsional dynamics: a quantum dynamical study of phenylenevinylene type conjugated systems". *Faraday Discussions*, 163 (2013) page 205. doi:10.1039/c3fd20148a.

[162] S. Mukamel, S. Tretiak, T. Wagersreiter and V. Chernyak. "Electronic Coherence and Collective Optical Excitations of Conjugated Molecules". *Science*, 277 (1997) pages 781–787. doi:10.1126/science.277.5327.781.

[163] S. A. Mewes, F. Plasser and A. Dreuw. "Exciton analysis in time-dependent density functional theory: How functionals shape excited-state characters". *J. Chem. Phys.*, 143 (2015) page 171101. doi:10.1063/1.4935178.

[164] J. Quenneville and T. J. Martínez. "Ab Initio Study of Cis-Trans Photoisomerization in Stilbene and Ethylene". *J. Phys. Chem. A*, 107 (2003) pages 829–837. doi:10.1021/jp021210w.

[165] V. Molina, M. Merchán and B. O. Roos. "Theoretical Study of the Electronic Spectrum of trans-Stilbene". *J. Phys. Chem. A*, 101 (1997) pages 3478–3487. doi:10.1021/jp9624109.

[166] C. Wu, S. V. Malinin, S. Tretiak and V. Y. Chernyak. "Exciton scattering approach for branched conjugated molecules and complexes. I. Formalism." *J. Chem. Phys.*, 129 (2008) page 174111. doi:10.1063/1.3005647.

[167] D. Abramavicius, B. Palmieri, D. V. Voronine, F. Sanda and S. Mukamel. "Coherent multidimensional optical spectroscopy of excitons in molecular aggregates; quasiparticle versus supermolecule perspectives". *Chem. Rev.*, 109 (2009) pages 2350–2408. doi:10.1021/cr800268n.

[168] R. Binder, S. Römer, J. Wahl and I. Burghardt. "An analytic mapping of oligomer potential energy surfaces to an effective Frenkel model". *J. Chem. Phys.*, 141 (2014) page 014101. doi:10.1063/1.4880415.

[169] P. H. P. Harbach, M. Wormit and A. Dreuw. "The third-order algebraic diagrammatic construction method (ADC(3)) for the polarization propagator for closed-shell molecules: Efficient implementation and benchmarking". *J. Chem. Phys.*, 141 (2014) page 064113. doi:10.1063/1.4892418.

[170] J. Schirmer. "Closed-form intermediate representations of many-body propagators and resolvent matrices". *Phys. Rev. A*, 43 (1991) pages 4647–4659. doi:10.1103/PhysRevA.43.4647.

[171] "TURBOMOLE V6.4 2012, a development of University of Karlsruhe and Forschungszentrum Karlsruhe GmbH, 1989-2007, TURBOMOLE GmbH, since 2007; available from
`http://www.turbomole.com`."

[172] C. Hättig and F. Weigend. "CC2 excitation energy calculations on large molecules using the resolution of identity approximation". *J. Chem. Phys.*, 113 (2000) pages 5154–5161. doi:10.1063/1.1290013.

[173] C. Hättig and K. Hald. "Implementation of RI-CC2 triplet excitation energies with an application to trans-azobenzene". *Phys. Chem. Chem. Phys.*, 4 (2002) pages 2111–2118. doi:10.1039/B110847F.

[174] C. Hättig. "Structure optimizations for excited states with correlated second-order methods: CC2, CIS(D), and ADC(2)". *Adv. Quant. Chem.*, 50 (2005) pages 37–60. doi:10.1016/S0065-3276(05)50003-0.

[175] A. Schäfer, C. Huber and R. Ahlrichs. "Fully optimized contracted Gaussian basis sets of triple zeta valence quality for atoms Li to Kr". *J. Chem. Phys.*, 100 (1994) pages 5829–5835. doi:10.1063/1.467146.

[176] F. Plasser. "TheoDORE: a package for theoretical density, orbital relaxation, and exciton analysis; available from
`http://theodore-qc.sourceforge.net/`."

[177] E. Hennebicq, C. Deleener, J.-L. Brédas, G. D. Scholes and D. Beljonne. "Chromophores in phenylenevinylene-based conjugated polymers: Role of conformational kinks and chemical defects". *J. Chem. Phys.*, 125 (2006) page 054901. doi:10.1063/1.2221310.

[178] A. B. Trofimov, G. Stelter and J. Schirmer. "A consistent third-order propagator method for electronic excitation". *J. Chem. Phys.*, 111 (1999) pages 9982–9999. doi:10.1063/1.480352.

[179] A. B. Trofimov, G. Stelter and J. Schirmer. "Electron excitation energies using a consistent third-order propagator approach: Comparison with full configuration interaction and coupled cluster". *J. Chem. Phys.*, 117 (2002) pages 6402–6409. doi:10.1063/1.1504708.

[180] M. Albota, D. Beljonne, J.-L. Brédas, J. E. Ehrlich, J.-Y. Fu, A. A. Heikal, S. E. Hess, T. Kogej, M. D. Levin, S. R. Marder *et al.* "Design of Organic Molecules with Large Two-Photon Absorption Cross Sections". *Science*, 281 (1998) pages 1653–1656. doi:10.1126/science.281.5383.1653.

[181] D. Yamaki, Y. Kitagawa, H. Nagao, M. Nakano, Y. Yoshioka and K. Yamaguchi. "Visualization of Two-Body Electron Densities and Wave Functions of Magnetic Molecules". *Int. J. Quant. Chem.*, 75 (1999) pages 645–654. doi:10.1002/(SICI)1097-461X(1999)75:4/5¡645::AID-QUA31¿3.0.CO;2-0.

[182] J. Coe and M. Paterson. "Characterising a configuration interaction excited state using natural transition geminals". *Mol. Phys.*, 112 (2014) pages 733–739. doi:10.1080/00268976.2013.856489.

[183] A. V. Luzanov, D. Casanova, X. Feng and A. I. Krylov. "Quantifying charge resonance and multiexciton character in coupled chromophores by charge and spin cumulant analysis". *J. Chem. Phys.*, 142 (2015) page 224104. doi: 10.1063/1.4921635.

[184] G. Hohlneicher and B. Dick. "Experimental determination of the low-lying excited a states of trans-stilbene". *J. Photochem.*, 27 (1984) pages 215 – 231. doi:10.1016/0047-2670(84)85039-X.

[185] H. Woo, O. Lhost, S. Graham, D. Bradley, R. Friend, C. Quattrocchi, J. Brédas, R. Schenk and K. Müllen. "Optical spectra and excitations in phenylene vinylene oligomers". *Synth. Met.*, 59 (1993) pages 13 – 28. doi: 10.1016/0379-6779(93)91153-S.

[186] J. Gierschner, H.-G. Mack, L. Lüer and D. Oelkrug. "Fluorescence and absorption spectra of oligophenylenevinylenes: Vibronic coupling, band shapes, and solvatochromism". *J. Chem. Phys.*, 116 (2002) pages 8596–8609. doi:10.1063/1.1469612.

[187] A. Knippenberg, J. H. Starcke, M. Wormit and A. Dreuw. "How much double excitation character do the lowest excited states of linear polyenes have?" *J. Chem. Phys.*, 329 (2006) pages 39–49. doi:10.1016/j.chemphys.2006.07.020.

[188] J. H. Starcke, M. Wormit and A. Dreuw. "Nature of the lowest excited states of neutral polyenyl radicals and polyene radical cations". *J. Chem. Phys.*, 131 (2009) page 144311. doi:10.1063/1.3246350.

[189] M. Wohlgenannt, W. Graupner, R. Österbacka, G. Leising, D. Comoretto and Z. V. Vardeny. "Singlet Fission in Luminescent and Nonluminescent π-conjugated Polymers". *Synth. Met.*, 101 (1999) pages 267–268. doi:10.1016/S0379-6779(99)80002-2.

[190] M. B. Smith and J. Michl. "Singlet Fission". *Chem. Rev.*, 110 (2010) pages 6891–6936.

[191] S. Kraner, R. Scholz, F. Plasser, C. Koerner and K. Leo. "Exciton size and binding energy limitations in one-dimensional organic materials". *J. Chem. Phys.*, 143 (2015) page 244905. doi:10.1063/1.4938527.

[192] S. Martin, D. Bradley, P. Lane, H. Mellor and P. Burn. "Linear and nonlinear optical properties of the conjugated polymers PPV and MEH-PPV". *Phys. Rev. B*, 59 (1999) pages 15133–15142. doi:10.1103/PhysRevB.59.15133.

[193] E. K. Miller, D. Yoshida, C. Y. Yang and A. J. Heeger. "Polarized ultraviolet absorption of highly oriented poly(2-methoxy, 5-(2-ethyl)-hexyloxy) paraphenylene vinylene". *Phys. Rev. B*, 59 (1999) pages 4661–4664. doi: 10.1103/PhysRevB.59.4661.

[194] S. V. Frolov, Z. Bao, M. Wohlgenannt and Z. V. Vardeny. "Excited-state relaxation in π-conjugated polymers". *Phys. Rev. B*, 65 (2002) page 205209. doi:10.1103/PhysRevB.65.205209.

[195] A. Köhler and D. Beljonne. "The Singlet-Triplet Exchange Energy in Conjugated Polymers". *Adv. Funct. Mater.*, 14 (2004) pages 11–18. doi: 10.1002/adfm.200305032.

[196] A. P. Monkman, H. D. Burrows, L. J. Hartwell, L. E. Horsburgh, I. Hamblett and S. Navaratnam. "Triplet Energies of π-Conjugated Polymers". *Phys. Rev. Lett.*, 86 (2001) pages 1358–1361. doi: 10.1103/PhysRevLett.86.1358.

[197] W. Barford, R. J. Bursill and R. W. Smith. "Theoretical and computational studies of excitons in conjugated polymers". *Phys. Rev. B*, 66 (2002) page 115205. doi:10.1103/PhysRevB.66.115205.

[198] D. Halliday, P. Burn, R. Friend, D. Bradley, A. Holmes and A. Kraft. "Extended π-conjugation in poly(p-phenylenevinylene) from a chemically modified precursor polymer". *Synt. Met.*, 55 (1993) pages 954 – 959. doi: 10.1016/0379-6779(93)90181-U.

[199] J.-M. Mewes, Z.-Q. You, M. Wormit, T. Kriesche, J. M. Herbert and A. Dreuw. "Experimental Benchmark Data and Systematic Evaluation of Two a Posteriori, Polarizable-Continuum Corrections for Vertical Excitation Energies in Solution". *J. Phys. Chem. A*, 119 (2015) pages 5446–5464. doi: 10.1021/jp511163y.

[200] B. Moore, H. Sun, N. Govind, K. Kowalski and J. Autschbach. "Charge-Transfer Versus Charge-Transfer-Like Excitations Revisited". *J. Chem. Theo. Comput.*, 11 (2015) pages 3305–3320. doi:10.1021/acs.jctc.5b00335.

[201] J. P. Perdew, K. Burke and M. Ernzerhof. "Generalized Gradient Approximation Made Simple". *Phys. Rev. Lett.*, 77 (1996) pages 3865–3868. doi: 10.1103/PhysRevLett.77.3865.

[202] V. Vlček, H. R. Eisenberg, G. Steinle-Neumann, D. Neuhauser, E. Rabani and R. Baer. "Spontaneous Charge Carrier Localization in Extended One-Dimensional Systems". *Phys. Rev. Lett.*, 116 (2016) page 186401. doi: 10.1103/PhysRevLett.116.186401.

[203] W. De Roeck and F. Huveneers. "Scenario for delocalization in translation-invariant systems". *Phys. Rev. B*, 90 (2014) page 165137. doi: 10.1103/PhysRevB.90.165137.

[204] J. M. Hickey, S. Genway and J. P. Garrahan. "Signatures of many-body localisation in a system without disorder and the relation to a glass transition". *J. Stat. Mech. Theory Exp.*, (2016) page 054047. doi:10.1088/1742-5468/2016/05/054047.

[205] N. Y. Yao, C. R. Laumann, J. I. Cirac, M. D. Lukin and J. E. Moore. "Quasi Many-body Localization in Translation Invariant Systems". *arXiv:1410.7407*, (2014).

[206] M. Schiulaz, A. Silva and M. Müller. "Dynamics in many-body localized quantum systems without disorder". *Phys. Rev. B*, 91 (2015) page 184202. doi:10.1103/PhysRevB.91.184202.

[207] J. Rissler, H. Bässler, F. Gebhard and P. Schwerdtfeger. "Excited states of ladder-type poly-p-phenylene oligomers". *Phys. Rev. B*, 64 (2001) page 045122. doi:10.1103/PhysRevB.64.045122.

[208] H. S. Yu, S. L. Li and D. G. Truhlar. "Perspective : Kohn-Sham density functional theory descending a staircase". *J. Chem. Phys.*, 145 (2016) page 130901. doi:10.1063/1.4963168.

[209] C. Adamo and V. Barone. "Toward reliable density functional methods without adjustable parameters: The PBE0 model". *J. Chem. Phys.*, 110 (1999) pages 6158–6170. doi:10.1063/1.478522.

[210] Y. Zhao and D. G. Truhlar. "The M06 suite of density functionals for main group thermochemistry, thermochemical kinetics, noncovalent interactions, excited states, and transition elements: two new functionals and systematic testing of four M06-class functionals and 12 other functionals". *Theor. Chem. Acc.*, 120 (2008) pages 215–241. doi:10.1007/s00214-007-0310-x.

[211] T. M. Henderson, B. G. Janesko and G. E. Scuseria. "Generalized gradient approximation model exchange holes for range-separated hybrids". *J. Chem. Phys.*, 128 (2008). doi:10.1063/1.2921797.

[212] M. Knupfer, J. Fink, E. Zojer, G. Leising and D. Fichou. "Universal exciton size scaling in π conjugated systems". *Chem. Phys. Lett.*, 318 (2000) pages 585–589. doi:10.1016/S0009-2614(00)00033-6.

[213] K. I. Igumenshchev, S. Tretiak and V. Y. Chernyak. "Excitonic effects in a time-dependent density functional theory". *J. Chem. Phys.*, 127 (2007) page 114902. doi:10.1063/1.2773727.

[214] F. Plasser. "Entanglement entropy of electronic excitations". *J. Chem. Phys.*, 144 (2016) page 194107. doi:10.1063/1.4949535.

[215] T. Helgaker, P. Jørgensen and J. Olsen. *Molecular electronic structure theory*. Wiley & Sons (**2000**).

[216] A. Dreuw. "Quantum Chemical Methods for the Investigation of Photoinitiated Processes in Biological Systems: Theory and Applications". *ChemPhysChem*, 7 (2006) pages 2259–2274. doi:10.1002/cphc.200600064.

[217] H. Koch, O. Christiansen, P. Jørgensen and J. Olsen. "Excitation energies of BH, CH_2, and Ne in full configuration interaction and the hierarchy CCS, CC2, CCSD, and CC3 of coupled cluster models". *Chem. Phys. Lett.*, 244 (1995) pages 75–82. doi:10.1016/0009-2614(95)00914-P.

[218] M. Schreiber, M. R. Silva-Junior, S. P. A. Sauer and W. Thiel. "Benchmarks for electronically excited states: CASPT2, CC2, CCSD, and CC3". *J. Chem. Phys.*, 128 (2008) page 134110. doi:10.1063/1.2889385.

[219] D. Jacquemin, V. Wathelet, E. A. Perpète and C. Adamo. "Extensive TD-DFT Benchmark: Singlet-Excited States of Organic Molecules". *J. Chem. Theory Comput.*, 5 (2009) pages 2420–2435. doi:10.1021/ct900298e.

[220] A. D. Laurent and D. Jacquemin. "TD-DFT benchmarks: A review". *Int. J. Quant. Chem.*, 113 (2013) pages 2019–2039. doi:10.1002/qua.24438.

[221] R. Send, M. Kühn and F. Furche. "Assessing Excited State Methods by Adiabatic Excitation Energies". *J. Chem. Theory Comput.*, 7 (2011) pages 2376–2386. doi:10.1021/ct200272b.

[222] D. Kánnár and P. G. Szalay. "Benchmarking Coupled Cluster Methods on Valence Singlet Excited States". *J. Chem. Theory Comput.*, 10 (2014) pages 3757–3765. doi:10.1021/ct500495n.

[223] D. Jacquemin, B. Mennucci and C. Adamo. "Excited-state calculations with TD-DFT: from benchmarks to simulations in complex environments". *Phys. Chem. Chem. Phys.*, 13 (2011) pages 16987–16998. doi:10.1039/C1CP22144B.

[224] E. Brémond, M. Savarese, A. J. Pérez-Jiménez, J. C. Sancho-García and C. Adamo. "Speed-Up of the Excited-State Benchmarking: Double-Hybrid Density Functionals as Test Cases". *J. Chem. Theory Comput.*, 13 (2017) pages 5539–5551. doi:10.1021/acs.jctc.7b00627.

[225] M. Pastore, E. Mosconi, F. De Angelis and M. Grätzel. "A Computational Investigation of Organic Dyes for Dye-Sensitized Solar Cells: Benchmark, Strategies, and Open Issues". *J. Phys. Chem. C*, 114 (2010) pages 7205–7212. doi:10.1021/jp100713r.

[226] N. T. Maitra. "Perspective: Fundamental aspects of time-dependent density functional theory". *J. Chem. Phys.*, 144 (2016) page 220901. doi:10.1063/1.4953039.

[227] H. Reisler and A. I. Krylov. "Interacting Rydberg and valence states in radicals and molecules: experimental and theoretical studies". *Int. Rev. Phys. Chem.*, 28 (2009) pages 267–308. doi:10.1080/01442350902989170.

[228] M. Head-Gordon, A. M. Graña, D. Maurice and C. A. White. "Analysis of Electronic Transitions as the Difference of Electron Attachment and Detachment Densities". *J. Phys. Chem.*, 99 (1995) pages 14261–14270. doi:10.1021/j100039a012.

[229] B. Demoulin, M. M. T. ElTahawy, A. Nenov, M. Garavelli and T. Le Bahers. "Intramolecular photoinduced charge transfer in visual retinal chromophore mimics: electron densitybased indices at the TDDFT and postHF levels". *Theor. Chem. Acc.*, 135 (2016). doi:10.1007/s00214-016-1815-y.

[230] M. Savarese, C. A. Guido, E. Brémond, I. Ciofini and C. Adamo. "Metrics for Molecular Electronic Excitations: A Comparison between Orbital- and Density-Based Descriptors". *J. Phys. Chem. A*, 121 (2017) pages 7543–7549. doi:10.1021/acs.jpca.7b07080.

[231] F. Plasser and L. González. "Communication: Unambiguous comparison of many-electron wavefunctions through their overlaps". *J. Chem. Phys.*, 145 (2016) page 021103. doi:10.1063/1.4958462.

[232] K. Sneskov and O. Christiansen. "Excited state coupled cluster methods". *WIREs Comput. Mol. Sci.*, 2 (2012) pages 566–584. doi:10.1002/wcms.99.

[233] R. Bartlett. "Coupled-cluster theory and its equation-of-motion extensions". *WIREs Comput. Mol. Sci.*, 2 (2012) pages 126–138.

[234] A. I. Krylov. "Equation-of-Motion Coupled-Cluster Methods for Open-Shell and Electronically Excited Species: The Hitchhikers Guide to Fock Space". *Annu. Rev. Phys. Chem.*, 59 (2008) pages 433–462. doi:10.1146/annurev.physchem.59.032607.093602.

[235] H. Sekino and R. J. Bartlett. "A linear response, coupled-cluster theory for excitation energy". *Int. J. Quant. Chem.*, 26 (1984) pages 255–265. doi:10.1002/qua.560260826.

[236] J. Geertsen, M. Rittby and R. J. Bartlett. "The equation-of-motion coupled-cluster method: Excitation energies of Be and CO". *Chem. Phys. Lett.*, 164 (1989) pages 57–62. doi:10.1016/0009-2614(89)85202-9.

[237] "Jmol: an open-source Java viewer for chemical structures in 3D." Version 14.13.1., `http://www.jmol.org/` .

[238] J. Stanton and R. Bartlett. "The equation of motion coupled-cluster method. A systematic biorthogonal approach to molecular excitation energies, transition probabilities, and excited state properties". *J. Chem. Phys.*, 98 (1993) pages 7029–7039. doi:10.1063/1.464746.

[239] E. Epifanovsky, D. Zuev, X. Feng, K. Khistyaev, Y. Shao and A. I. Krylov. "General implementation of the resolution-of-the-identity and Cholesky representations of electron repulsion integrals within coupled-cluster and equation-of-motion methods: Theory and benchmarks". *J. Chem. Phys.*, 139 (2013) 134105. doi:10.1063/1.4820484.

[240] R. Kendall, T. H. J. Dunning and R. Harrison. "Electron affinities of the firstrow atoms revisited. Systematic basis sets and wave functions". *J. Chem. Phys.*, 96 (1992) page 6796. doi:10.1063/1.462569.

[241] J.-M. Mewes, J. M. Herbert and A. Dreuw. "On the accuracy of the general, state-specific polarizable-continuum model for the description of correlated ground- and excited states in solution". *Phys. Chem. Chem. Phys.*, 19 (2017) pages 1644–1654. doi:10.1039/C6CP05986D.

[242] D. R. Rehn. *Development of Quantum Chemical Methods for Excited-State and Response Properties*. Ph.D. thesis, Ruprecht-Karls University Heidelberg (**2015**). doi:10.11588/heidok.00019871.

[243] R. Mulliken. "Report on Notation for the Spectra of Polyatomic Molecules". *J. Chem. Phys.*, 23 (1955) page 1997. doi:10.1063/1.1740655.

[244] Depending on molecular orientation, symmetry labels corresponding to the same orbital or vibrational mode may be different. Q-Chem's standard molecular orientation is different from that of Mulliken[243]. For example, Q-Chem places formaldehyde molecule in the xz-plane instead of yz. Consequently, for C_{2v} symmetry, b_1 and b_2 labels are flipped. More details can be found at http://iopenshell.usc.edu/resources/howto/symmetry.

[245] A. I. Krylov, C. D. Sherrill and M. Head-Gordon. "Excited States Theory for Optimized Orbitals and Valence Optimized Orbitals Coupled-Cluster Doubles Models". *J. Chem. Phys.*, 113 (2000) pages 6509–6527. doi:10.1063/1.1311292.

[246] K. Kaufmann, W. Baumeister and M. Jungen. "Universal Gaussian basis sets for an optimum representation of Rydberg and continuum wavefunctions". *J. Phys. B*, 22 (1989) page 2223.

[247] Z. R. Grabowski, K. Rotkiewicz and W. Rettig. "Structural Changes Accompanying Intramolecular Electron Transfer: Focus on Twisted Intramolecular Charge-Transfer States and Structures". *Chem. Rev.*, 103 (2003) pages 3899–4032. doi:10.1021/cr940745l.

[248] I. Georgieva, A. J. A. Aquino, F. Plasser, N. Trendafilova, A. Köhn and H. Lischka. "Intramolecular Charge-Transfer Excited-State Processes in 4-(N,N–Dimethylamino)benzonitrile: The Role of Twisting and the $\pi\sigma^*$ State". *J. Phys. Chem. A*, 119 (2015) page 62326243. doi:10.1021/acs.jpca.5b03282.

[249] F. Plasser and A. Dreuw. "High-Level Ab Initio Computations of the Absorption Spectra of Organic Iridium Complexes". *J. Phys. Chem. A*, 119 (2015) pages 1023–1036. doi:10.1021/jp5122917.

[250] P. Kautny, F. Glöcklhofer, T. Kader, J.-M. Mewes, B. Stöger, J. Fröhlich, D. Lumpi and F. Plasser. "Charge-transfer states in triazole linked donor-acceptor materials: strong effects of chemical modification and solvation". *Phys. Chem. Chem. Phys.*, 19 (2017) pages 18055–18067. doi: 10.1039/C7CP01664F.

[251] R. Colditz, D. Grebner, M. Helbig and S. Rentsch. "Theoretical studies and spectroscopic investigations of ground and excited electronic states of thiophene oligomers". *Chem. Phys.*, 201 (1995) pages 309 – 320. doi: http://dx.doi.org/10.1016/0301-0104(95)00280-4.

[252] D. V. Lap, D. Grebner and S. Rentsch. "Femtosecond Time-Resolved Spectroscopic Studies on Thiophene Oligomers". *J. Phys. Chem. A*, 101 (1997) pages 107–112. doi:10.1021/jp961670n.

[253] E. Epifanovsky, K. Kowalski, P.-D. Fan, M. Valiev, S. Matsika and A. I. Krylov. "On the electronically excited states of uracil". *J. Phys. Chem. A*, 112 (2008) pages 9983–9992. doi:10.1021/jp803758q.

[254] C.-P. Hsu, S. Hirata and M. Head-Gordon. "Excitation Energies from Time-Dependent Density Functional Theory for Linear Polyene Oligomers: Butadiene to Decapentaene". *J. Phys. Chem. A*, 105 (2001) pages 451–458. doi: 10.1021/jp0024367.

[255] W. Barford, R. J. Bursill and M. Y. Lavrentiev. "Density-matrix renormalization-group calculations of excited states of linear polyenes". *Phys. Rev. B*, 63 (2001) page 195108. doi:10.1103/PhysRevB.63.195108.

[256] M. Dallos and H. Lischka. "A systematic theoretical investigation of the lowest valence- and Rydberg-excited singlet states of trans-butadiene. The character of the 1^1B_u (V) state revisited". *Theor. Chem. Acc.*, 112 (2004) pages 16–26. doi:10.1007/s00214-003-0557-9.

[257] M. Dierksen and S. Grimme. "Density functional calculations of the vibronic structure of electronic absorption spectra". *J. Chem. Phys.*, 120 (2004) pages 3544–3554. doi:10.1063/1.1642595.

[258] J. Catalán and J. L. G. de Paz. "On the photophysics of all-trans polyenes: Hexatriene versus octatetraene". *J. Chem. Phys.*, 124 (2006) page 034306. doi:10.1063/1.2158992.

[259] C. Angeli and M. Pastore. "The lowest singlet states of octatetraene revisited". *J. Chem. Phys.*, 134 (2011) page 184302. doi:10.1063/1.3585607.

[260] Y. Shu and D. G. Truhlar. "Doubly Excited Character or Static Correlation of the Reference State in the Controversial 2^1A_g State of trans-Butadiene?" *J. Am. Chem. Soc.*, 139 (2017) pages 13770–13778. doi:10.1021/jacs.7b06283.

[261] Y. Shao, M. Head-Gordon and A. I. Krylov. "The spin-flip approach within time-dependent density functional theory: Theory and applications to diradicals". *J. Chem. Phys.*, 118 (2003) pages 4807–4818. doi: 10.1063/1.1545679.

[262] Y. A. Bernard, Y. Shao and A. I. Krylov. "General formulation of spin-flip time-dependent density functional theory using non-collinear kernels: Theory, implementation, and benchmarks". *J. Chem. Phys.*, 136 (2012) page 204103. doi:10.1063/1.4714499.

[263] L. Edwards, D. H. Dolphin, M. Gouterman and A. D. Adler. "Porphyrins XVII. Vapor Absorption Spectra and Redox Reactions: Tetraphenylporphins and Porphin". *J. Mol. Spectrosc.*, 38 (1971) pages 16–32. doi: 10.1016/0022-2852(71)90090-7.

[264] M. Gouterman. "Spectra of porphyrins". *J. Mol. Spectr.*, 6 (1961) pages 138–163. doi:10.1016/0022-2852(61)90236-3.

[265] M. Gouterman. "Study of the Effects of Substitution on the Absorption Spectra of Porphin". *J. Chem. Phys.*, 30 (1959) pages 1139–1161. doi: 10.1063/1.1730148.

[266] M. Rubio, B. O. Roos, L. Serrano-Andrès and M. Merchán. "Theoretical study of the electronic spectrum of magnesium-porphyrin". *J. Chem. Phys.*, 110 (1999) pages 7202–7209. doi:10.1063/1.478624.

[267] F. Plasser, S. A. Mewes, A. Dreuw and L. González. "Detailed Wave Function Analysis for Multireference Methods: Implementation in the Molcas Program Package and Applications to Tetracene". *J. Chem. Theory Comput.*, 13 (2017) pages 5343–5353. doi:10.1021/acs.jctc.7b00718.

[268] D. Hirose, Y. Noguchi and O. Sugino. "Quantitative characterization of exciton from GW+Bethe-Salpeter calculation". *J. Chem. Phys.*, 146 (2017) page 044303. doi:10.1063/1.4974320.

List of Figures

List of Tables

List of Publications

1. F. Plasser, S. A. Bäppler, M. Wormit, A. Dreuw, "Visualization and systematic analysis of electronic excitations using density matrices. Part II.", *J. Chem. Phys.* 141, 2014, 024107.

2. S. A. Bäppler, F. Plasser, M. Wormit, A. Dreuw, "Exciton analysis of many-body wave functions: Bridging the gap between the quasiparticle and molecular orbital pictures", *Phys. Rev. A* 90, 2014, 052521.

3. F. Plasser, B. Thomitzni, S. A. Bäppler, J. Wenzel, D. R. Rehn, M. Wormit, A. Dreuw, "Statistical Analysis of Electronic Excitation Processes: Location, Compactness, and Electron-Hole Correlation" *J. Comp. Chem.* 36, 2015, pp. 1609−1620.

4. S. A. Mewes, F. Plasser, A. Dreuw, "Exciton analysis in time-dependent density functional theory: How functionals shape excited-state characters", *J. Chem. Phys.* 143, 2015, 171101.

5. S. A. Mewes, J.-M. Mewes, A. Dreuw, F. Plasser, "Excitons in poly(para phenylene vinylene): a quantum-chemical perspective based on high-level ab initio calculations", *Phys. Chem. Chem. Phys.* 18, 2016, pp. 2548−2563.

6. S. A. Mewes, F. Plasser, A. Dreuw, "Universal exciton size in Organic Polymers is Determined by Nonlocal Orbital Exchange in Time-Dependent Density Functional Theory", *J. Phys. Chem. Lett.* 8, 2017, pp. 1205−1210.

7. F. Plasser, S. A. Mewes, A. Dreuw, L. González "Detailed wavefunction analysis for multireference methods: Implementation in the Molcas program package and applications to tetracene", *J. Chem. Theory Comput.* 13, 2017, pp. 5343−5353.

8. S. A. Mewes, F. Plasser, A. Krylov, A. Dreuw, "Benchmarking excited-state calculations using exciton properties", *J. Chem. Theory Comput.* 14, 2018, pp. 710−725.

Danksagung

Am Ende dieser Arbeit möchte ich mich bei den Menschen bedanken, die mich auf dem Weg zur Promotion unterstüzt haben.

An erster Stelle gilt mein großer Dank meinem Doktorvater Prof. Dr. Andreas Dreuw, der meine Begeisterung für Computational Chemistry entfacht hat und mich über die letzten Jahre wissenschaftlich und persönlich in vielfältiger Weise unterstützt hat. Danke für die Bereitstellung des spannenden Forschungsthemas und den Rahmenbedingungen, die diese Arbeit möglich gemacht haben.

Dr. Markus Pernpointner danke ich für die Betreuung des Projekts als Zweitbetreuer im Rahmen des Curriculums der HGS MathComp.

Dr. Alexander Kuleff danke ich für die Begutachtung dieser Arbeit.

Dr. Felix Plasser danke ich insbesondere für die Einführung in das Themengebiet der Dichteanalyse und die inspirierende Zusammenarbeit über die letzten Jahre. Ebenfalls danke ich Benjamin Thomitzni für seinen Beitrag zu *libwfa* im Rahmen seiner Bachelorarbeit.

Ich bin dankbar für die Zeit, die ich gemeinsam mit Dr. Michael Wormit verbringen durfte. Sein Beitrag zu dieser Arbeit mit spannenden Fachgesprächen und sein Engagement *libwfa* in Q-Chem zu etablieren bedeuten mir viel.

I would like to acknowlegde Prof. Dr. Anna I. Krylov for inspiring discussions on the topic of benchmarking excited states with exciton properties.

Prof. Dr. Peter Schwerdtfeger danke ich für die Aufnahme in das New Zealand Institute for Advanced Studies, für seine immerzu aufmunternden Worte und den Arbeitsplatz in Neuseeland.

Mein Dank gilt der Arbeitsgruppe Dreuw mit Tim, Michael, Mercedes, Chong, Jie, Daniel, Maximilian, Marvin, Georg, Shirin, Tobias, Daria, Philipp, Stefan K., Stefan P., Jörg, Manuel, Adrian und allen neueren Mitgliedern. Es war immer eine schöne Zeit mit euch! I would like to acknowledge the members of CTCP and NZIAS for creating an inspiring research environment during my stay in New Zealand.

Danke an Ellen Vogel und Manfred Trunk für die organisatorische Unterstützung dieser Arbeit in Heidelberg. Thank you, Vesna, for taking care of organizational work in the NZIAS.

Für die finanzielle Unterstützung dieser Arbeit danke ich der Heidelberg Graduate School of Mathematical and Computational Methods for the Sciences (HGS MathComp) und der Landesgraduiertenföderung Baden-Württemberg.

Für das Korrekturlesen dieser Arbeit danke ich meinem Bruder Florian Bäppler und meinem Mann Dr. Jan-Michael Mewes.

Ich danke meiner Familie für ihre Unterstützung und liebevolle Begleitung auf dem Weg der Promotion.

Mein besonderer Dank gilt meinem Mann Dr. Jan-Michael Mewes, der mich immer unterstützt und an mich geglaubt hat. Ich danke ihm für seine Geduld, für die wunderbare gemeinsame Zeit, seinen positive Haltung und dafür, dass er ein so liebevoller Vater für unsere kleine Lotta-Minza ist, was nicht zuletzt zum Gelingen dieser Arbeit beigetragen hat.

Danke, liebe Lotta, dass du unser kleines Glückskind bist und mit uns deine Lebensfreude teilst.

Eidesstattliche Versicherung gemäß §8 der Promotionsordnung der Naturwissenschaftlich-Mathematischen Gesamtfakultät der Universität Heidelberg

1. Bei der eingereichten Dissertation zu dem Thema
   "Exciton analysis tools for quantum-chemical investigation of molecular photochemistry"
   handelt es sich um meine eigenständig erbrachte Leistung.

2. Ich habe nur die angegebenen Quellen und Hilfsmittel benutzt und mich keiner unzulässigen Hilfe Dritter bedient. Insbesondere habe ich wörtlich oder sinngemäß aus anderen Werken übernommene Inhalte als solche kenntlich gemacht.

3. Die Arbeit oder Teile davon habe ich bislang nicht an einer Hochschule des In- oder Auslands als Bestandteil einer Prüfungs- oder Qualifikationsleistung vorgelegt.

4. Die Richtigkeit der vorstehenden Erklärungen bestätige ich.

5. Die Bedeutung der eidesstattlichen Versicherung und die strafrechtlichen Folgen einer unrichtigen oder unvollständigen eidesstattlichen Versicherung sind mir bekannt.

Ich versichere an Eides statt, dass ich nach bestem Wissen die reine Wahrheit erklärt und nichts verschwiegen habe.

Ort/Datum Unterschrift